

**Effects of vagus nerve stimulation on ventricular
electrophysiology and nitric oxide release**

**Thesis submitted for the degree of
Doctor of Philosophy
The University of Leicester**

by

Pott Pongpaopattanakul
MEng (Biomedical Engineering)

**Department of Cardiovascular Sciences
College of Medicine, Biological Sciences and
Psychology
University of Leicester**

July 2018

Effects of vagus nerve stimulation on ventricular electrophysiology and nitric oxide release

Pott Pongpaopattanakul

Autonomic imbalance is a known hallmark of heart failure (HF). Patients are prone to a sudden cardiac death (SCD) as a result of lethal arrhythmias. Our group has previously shown that vagus nerve stimulation (VNS) protects the heart against ventricular fibrillation (VF) via a nitric oxide (NO) pathway which could be relevant in HF. Clinical studies using vagus nerve stimulators in HF have produced ambiguous outcomes and it has been questioned whether an adequate level of stimulation was actually achieved which raises the question as to the optimal stimulation parameters needed to produce relevant functional effects. In this thesis, the effects of different parameters of VNS on cardiac electrophysiology and NO release were assessed. Hearts from adult male New Zealand White rabbits were procured for dual-innervated Langendorff perfused preparations *ex vivo*. The cervical vagus was unilaterally stimulated with different voltages, frequencies, and pulse widths. Heart rate (HR), ventricular electrophysiology parameters and NO release in the left ventricle were measured. Results demonstrated an anti-arrhythmic benefit of VNS in all stimulations with involvement of NO release during VNS that protects the heart through the action potential duration restitution mechanism. Data also suggested that NO was released from the neural components within the intra-cardiac nervous system. For VNS parameters, the high amplitude voltage affected the level of HR reduction more but not the level of NO release. In contrast, high frequency VNS, even at very low voltages, alters NO release whilst causing relatively little changes in HR. This current finding confirmed the HR independent protection of VNS and also suggested an importance of stimulation frequency to cause NO release in this action. Low strength voltage with high frequency VNS was suggested as an optimal setting to be translated to the clinical use to prevent SCD in HF patients.

Acknowledgements

First of all, I would like to thank my 1st supervisor Prof G Andre Ng and my ex-supervisor Dr Kieran E Brack for offering me this PhD opportunity. This research could not have been completed without the many invaluable advices and suggestions from Prof Ng. Many thanks to Dr Brack for his constant support throughout the 1st year. I have gained lots of knowledge and skills from being a part of the research team, which would not have been possible if not for the extensive and constructive feedback given by my supervisors.

This thesis was completed under the constant support together with numerous feedbacks and advices from my 2nd supervisor, Dr Richard Rainbow. Thank you very much for instructing me on how to write a good scientific report and also for helping me finish this thesis.

I would like to thank Dr Gabriella O. Kocsis-Fodor for her experimental help and technical support during my 1st and 2nd years. Also, thanks for her friendship.

There is a fact that this research could not have been completed without the help and support from Dr Emily Allen and Dr Reshma Chauhan. Million thanks to both of them for all the things they have done for me. I am unable to explain how much it means to me but I can tell that it made me get through this PhD. Becoming a team with them is a wonderful experience.

Special thanks to my wife, who has given her full support and encouragement throughout this PhD study. Thanks for staying beside me for all the good and the bad times.

Finally, I wish to thank Naresuan University, Thailand for providing a funding to my PhD study.

With my respect to Prof John H Coote, it was my honour to have a chance to meet you. Thanks for being a brilliant role model of a good researcher. Good bye Prof, I will miss you.

Contents

Chapter 1	Introduction.....	1
1.1.	Autonomic innervation to the heart	2
1.1.1	Cardiac ganglionic plexuses (GPs).....	5
1.1.2	Vagus nerve composition	9
1.2	Autonomic modulation of cardiac function.....	13
1.2.1	Vagus nerve stimulation (VNS) and ventricular electrophysiology studies 15	
1.2.2	Low level vagus nerve stimulation (LLVS).....	18
1.2.3	Vagus nerve stimulation in human clinical study	19
1.3	Cardiac electrophysiology	23
1.3.1	Cardiac conduction system	23
1.3.2	Pacemaker cell action potential	23
1.3.3	Non-pacemaker cell action potential.....	26
1.3.4	Excitation contraction (EC) coupling.....	27
1.3.5	Intracellular response to parasympathetic neurotransmitters	28
1.4	LLVS and ventricular arrhythmias	37
1.4.1	Re-entry circuits.....	37
1.4.2	Monophasic action potential duration electrical restitution (MAPDR) 37	
1.4.3	Dispersion of repolarizations	38
1.5	Research gaps.....	39
Chapter 2	Thesis aims and layouts	42
2.1	Aims of study	42
2.2	Hypotheses	42
2.3	Thesis layouts	43
Chapter 3	General methodology	45

3.1	Background.....	45
3.2	Surgery procedures for the isolated innervated rabbit heart preparation 45	
3.3	Langendorff perfusion system.....	46
3.4	Data recording and analysis.....	48
3.5	Vagus Nerve Stimulation.....	48
3.5.1	Voltage use for VNS.....	49
3.5.2	Frequency use for VNS.....	50
3.5.3	Pulse width use for VNS.....	51
3.6	Effective Refractory Period (ERP) and Monophasic Action Potential Duration 90% Restitution (MAPDR ₉₀).....	53
3.6.1	Effective Refractory Period (ERP) protocol.....	54
3.6.2	Monophasic Action Potential Duration 90% Restitution (MAPDR ₉₀) protocol.....	54
3.7	Ventricular Fibrillation Threshold protocol.....	57
3.8	Nitric Oxide level by using a single bifurcated light guide system.....	58
3.8.1	Single bifurcated light guide system.....	58
3.8.2	Fluorescence dye for NO measurement.....	60
3.8.3	4, 5-Diaminofluorescein diacetate (DAF-2 DA) dye.....	60
3.8.4	VNS procedures for single bifurcated light guide technique.....	61
3.9	Nitric Oxide release in Ventricle by using DAF-2 DA optical mapping	62
3.9.1	Optical mapping background.....	62
3.9.2	DAF-2 optical mapping apparatus.....	63
3.9.3	DAF-2 optical mapping protocol.....	66
3.10	Statistical analysis.....	67
Chapter 4	Preliminary effects of different stimulation voltage and frequency on ventricular electrophysiology and NO release in the isolated rabbit heart...	69

4.1	Background of VNS impact on electrophysiology and an involvement of NO	69
4.2	Chapter objectives	70
4.3	VNS parameters	71
4.4	The Langendorff perfused isolated innervated rabbit heart preparation	72
4.5	Haemodynamic respond the unilateral VNS	74
4.6	Voltage and frequency configurations	76
4.6.1	Voltage response curve	76
4.6.2	Frequency respond curve	77
4.7	Effective refractory period (ERP) protocol	79
4.8	Ventricular fibrillation threshold (VFT) protocol	87
4.9	Monophasic action potential duration restitution (MAPDR)	91
4.10	Nitric oxide (NO) release in the ventricle by a single bifurcated light guided system	96
4.11	Discussion	102
4.11.1	Main findings	104
4.11.2	Next stage	105
4.11.3	Limitations	106
Chapter 5	Effects of different right vagus nerve stimulation parameters on rabbit ventricular electrophysiology	109
5.1	Introduction	109
5.2	Chapter objectives	111
5.3	VNS parameters	111
5.4	Voltage response and frequency response curves of different RVNS parameters	112
5.4.1	Low frequency stimulation	112

5.4.2	Low voltage stimulation	117
5.4.3	Low frequency low voltage stimulation	118
5.5	Effect of different RVNS parameters on left ventricular effective refractory period (ERP).....	122
5.5.1	Low frequency stimulation ERP protocol	122
5.5.2	Low voltage stimulation ERP protocol	129
5.5.3	Low frequency low voltage stimulation ERP protocol	135
5.6	Effect of different RVNS parameters on ventricular fibrillation threshold (VFT) 141	
5.6.1	VFT increase by low frequency RVNS	141
5.6.2	VFT increase by low voltage RVNS.....	145
5.6.3	VFT increase by low frequency low voltage RVNS.....	149
5.7	Effect of different RVNS parameters on monophasic action potential duration restitution (MAPDR) maximum slope.....	152
5.7.1	Effect of low frequency stimulation on MAPDR slope.....	152
5.7.2	Effect of low voltage stimulation on MAPDR slope	161
5.7.3	Effect of low frequency low voltage stimulation on MAPDR slope 168	
5.8	Discussion.....	176
5.8.1	RVNS parameters and anti – arrhythmic mechanism.....	176
5.8.2	RVNS parameters and vagal fibre recruitment	177
5.8.3	Clinical relevance	179
5.8.4	Limitations	181
5.8.5	Next stage	182
Chapter 6	Effects of different right vagus nerve stimulation parameters on nitric oxide release in rabbit ventricular	184
6.1	Introduction	184

6.2	Chapter objective	185
6.3	VNS parameters	186
6.4	Voltage response and frequency response curves of different RVNS parameters	186
6.4.1	Low frequency stimulation	186
6.4.2	Low voltage stimulation	188
6.4.3	Low frequency low voltage stimulation	189
6.5	Increase of nitric oxide fluorescence (NOFL) signal during right vagus nerve stimulation by a single bifurcated light guided system	192
6.5.1	Nitric oxide fluorescence (NOFL) signal increased by nerve stimulations	192
6.6	Changes of nitric oxide fluorescence (NOFL) signal and percentage change of other physiological parameters	200
6.7	Discussions	206
6.7.1	Response of NOFL signal to right vagus nerve stimulation	206
6.7.2	Source of nitric oxide	208
6.7.3	DAF-2 specificity	209
6.7.4	Limitations and future study	210
Chapter 7	Development of DAF-2 optical mapping technique for measuring nitric oxide release in the rabbit ventricle	213
7.1	Introduction	213
7.2	Chapter objective	214
7.3	VNS parameters	215
7.4	Voltage response and frequency response curves of different RVNS parameters	215
7.4.1	Low frequency stimulation	215
7.4.2	Low voltage stimulation	218

7.4.3	Low frequency low voltage stimulation	218
7.5	NO fluorescence by DAF-2 DA optical mapping	220
7.5.1	Optical mapping apparatus.....	220
7.5.2	Response of isolated innervated rabbit heart to the excitation - contraction uncoupler.....	221
7.5.3	Recording of NO fluorescence signal by optical mapping system 224	
7.6	Discussions.....	228
7.6.1	Technical detail of optical mapping apparatus.....	228
7.6.2	Further development of DAF-2 optical mapping	229
Chapter 8	Conclusion.....	232
Appendix	236
	Poster presentations.....	236
	Journal publication.....	236
References	237

List of tables

Table 4.1 MAPDR maximum slope value. n = 3, mean \pm SEM.	95
Table 4.2 Absolute increase of NOFL signal.	101
Table 5.1 Summary of VNS stimulation parameters used by heart failure clinical study	180
Table 6.1 Increase of nitric oxide (NOFL) signal by 3 different nerve stimulation strategies	197

List of figures

Figure 1.1 Overview of autonomic nervous system (ANS) regulates cardiac and vascular function	3
Figure 1.2 Autonomic nerves innervation to the heart.....	4
Figure 1.3 Ganglionic plexuses (GPs) of the rabbit heart.....	6
Figure 1.4 Cholinergic and nitrergic markers inside human right atrial ganglionic plexus (RAGP)	7
Figure 1.5 Immunohistochemistry of the neurons at the conus arteriosus and the root of pulmonary trunk of the rabbit ventricle	8
Figure 1.6 A) posterior view of the human atrium and origins of preganglionic vagal fibres that innervated to atrial GPs, B) posterior view of the human with GPs (red) that innervated by the preganglionic cardiac vagal neurones (CVN) (blue), and C) the projection of the cardiac parasympathetic postganglionic fibres (green).....	10
Figure 1.7 Vagal compound action potential (VCAP) by monopolar current stimulation at 5 mA pulse duration 3 ms with the distance between stimulation and recording electrode 46 mm. Arrow represented activation point. Image taken from (Tosato et al., 2006)	11
Figure 1.8 Analysis of vagal compound action potential (VCAP) as peak to peak analysis of each VCAP peak component respond to right and left electrical cervical vagus nerve stimulation. Image taken from (Tosato et al., 2006).....	12
Figure 1.9 Heart rate reduction by vagus nerve stimulation (10 Hz 20 s) of, A myelinated fibres, B both myelinated and non-myelinated fibres, and C non-myelinated fibres. Image taken from (Woolley et al., 1987)	13
Figure 1.10 Autonomic nervous system control cardiac function	14
Figure 1.11 Effective refractory period (ERP), ventricular fibrillation threshold (VFT), and monophasic action potential duration restitution (MAPDR) slopes between control and during vagus nerve stimulation	16

Figure 1.12 Increases of nitric oxide (NO) level during 5, 10, and 15 Hz vagus nerve stimulations	17
Figure 1.13 A) subcutaneous implant of CardioFit device in the treatment of HF, B) Cybertronic VNS therapy system for autonomic regulation therapy (ART) ..	22
Figure 1.14 Conduction system of the heart	23
Figure 1.15 Action potential of pacemaker cell.....	24
Figure 1.16 Alteration of heart rate by sympathetic/parasympathetic neurotransmitters	26
Figure 1.17 Action potential of ventricular cardiac myocyte and ion conductance	27
Figure 1.18 Acetylcholine (ACh) receptors: muscarinic (Musc) and nicotinic (Nic)	29
Figure 1.19 M ₂ muscarinic acetylcholine receptors responded to acetylcholine	30
Figure 1.20 Response of acetylcholine (ACh) released from right vagus nerve in sinoatrial (SA) node.....	31
Figure 1.21 Nitric oxide (NO) in cardiomyocyte.....	32
Figure 1.22 Nitric oxide (NO) signalling pathway	33
Figure 1.23 Effect of NO on cardiac ion channels	35
Figure 1.24 Roles of neuronal nitric oxide synthase (nNOS) on neurotransmitters releases from both sympathetic and parasympathetic neurons that innervate sinoatrial (SA) node	36
Figure 1.25 Role of nitric oxide (NO) in the effect of vagus nerve stimulation (VNS) on monophasic action potential duration 90% repolarisation (MAPD ₉₀) restitution (MAPDR)	38
Figure 3.1 Scheme demonstrated the isolated innervated Langendorff rabbit heart with intact dual autonomic innervation. (LA, left atrium; LV, left ventricle; RA, right atrium; RV, right ventricle; LVNS, left vagus nerve stimulation; RVNS, right vagus nerve stimulation, SNS, sympathetic nerve stimulation; RA _{EG} , right	

atrial electrogram; MAP, monophasic action potential, LVP, left ventricular pressure; PP, aortic perfusion pressure.) Image taken with permission from (Ng et al., 2001)	47
Figure 3.2 VNS parameters used for cardiac electrophysiology and ventricular NO release studies.....	52
Figure 3.3 Monophasic action potential (MAP) and pacing stimuli recorded during the S1–S2 extrastimulus effective refractory period (ERP) protocol with the analysis of standard electrical restitution.....	55
Figure 3.4 Exponential fit of a restitution curve plot and maximum slope of exponential fit.....	56
Figure 3.5 Ventricular fibrillation threshold protocol	57
Figure 3.6 Single bifurcated light guide system.....	59
Figure 3.7 4, 5-Diaminofluorescein diacetate (DAF-2 DA) dye for measuring intra-cellular NO in cardiac cell.....	61
Figure 3.8 Optical mapping system with the Langendorff heart perfusion for cardiac electrophysiology study	63
Figure 3.9 Wavelength allowance (percentage of transmission (%T)) of DAF-2 optical mapping filter system	65
Figure 4.1 The isolated innervated rabbit heart preparation.....	73
Figure 4.2 Langendorff perfusion of isolated innervated rabbit heart preparation	74
Figure 4.3 Raw tracing recording from LabChart software.....	75
Figure 4.4 Voltage response curve of strong voltage stimulation	76
Figure 4.5 Frequency response curve of strong voltage stimulation	78
Figure 4.6 Frequency response curve of high frequency stimulation	79
Figure 4.7 Raw tracing of relevant parameters during a set of an S1 – S2 extra stimuli.....	81
Figure 4.8 Raw tracing of monophasic action potential (MAP) and S1 – S2 pacing spike	82

Figure 4.9 Heart rate reduction during ERP protocol by voltage $80\% \Delta HR_{max}$ with pulse width 2 ms	83
Figure 4.10 Percentage of heart rate decrease during ERP protocol by voltage $80\% \Delta HR_{max}$ with pulse width 2 ms	84
Figure 4.11 ERP prolongation by vagal stimulation at voltage $80\% \Delta HR_{max}$ with pulse width 2 ms	85
Figure 4.12 Heart rate reduction during ERP protocol by voltage $10\% \Delta HR_{BL}$ with pulse width 0.1 ms	86
Figure 4.13 Percentage of heart rate decrease during ERP protocol by voltage $10\% \Delta HR_{BL}$ with pulse width 0.1 ms.....	86
Figure 4.14 ERP prolongation by VNS at voltage $10\% \Delta HR_{BL}$ with PW 0.1 ms	87
Figure 4.15 VF threshold test by a right ventricle (RV) rapid pacing protocol ..	88
Figure 4.16 VFT increase by stimulation at voltage $80\% \Delta HR_{max}$ with pulse width 2 ms	89
Figure 4.17 percentage increase of VFT by stimulation at voltage $80\% \Delta HR_{max}$ with pulse width 2 ms	89
Figure 4.18 VFT increase by VNS at voltage $10\% \Delta HR_{BL}$ with PW 0.1 ms.....	90
Figure 4.19 percentage increase of VFT by VNS at voltage $10\% \Delta HR_{BL}$ with PW 0.1 ms	91
Figure 4.20 example MAPs recorded during ERP protocol that was used for MAPDR analysis	92
Figure 4.21 Analysis of baseline MAPDR and VNS MAPDR	93
Figure 4.22 Assessment the maximum slope by the 1 st derivatives of both baseline and VNS restitution exponential curves	94
Figure 4.23 MAPDR slope value	96
Figure 4.24 Increase of NOFL signal in the left ventricle of isolated innervated rabbit heart preparation by VNS with voltage $80\% \Delta HR_{max}$	98
Figure 4.25 Increase of NOFL by VNS with voltage $10\% \Delta HR_{BL}$	99
Figure 4.26 NOFL signal increase by VNS compared to baseline signal	100

Figure 4.27 Scheme represented combinations of voltage, frequency, and pulse width used in VNS study	105
Figure 5.1 Voltage response curve of low frequency stimulation	115
Figure 5.2 Frequency respond curves of low frequency stimulation.....	116
Figure 5.3 frequency response curves of low voltage stimulation	120
Figure 5.4 Frequency response curve of low frequency low voltage stimulation	121
Figure 5.5 Effects of PW on HR reduction by low frequency stimulation ERP protocol.	124
Figure 5.6 Effects of PW on percentage of HR decrease by low frequency stimulation ERP protocol.....	124
Figure 5.7 Effects of frequency on HR reduction by low frequency stimulation ERP protocol.....	125
Figure 5.8 Effects of frequency on percentage of HR decrease by low frequency stimulation ERP protocol.....	125
Figure 5.9 Effects of PW on ERP prolongation by low frequency stimulation	128
Figure 5.10 Effects of frequency on ERP prolongation by low frequency stimulation.....	128
Figure 5.11 Effects of PW on HR reduction by low voltage stimulation ERP protocol.	131
Figure 5.12 Effects of PW on percentage of HR decrease by low voltage stimulation ERP protocol.....	131
Figure 5.13 Effects of frequency on HR reduction by low voltage stimulation ERP protocol.....	132
Figure 5.14 Effects of frequency on percentage of HR decrease by low voltage stimulation ERP protocol.....	132
Figure 5.15 Effects of PW on ERP prolongation by low voltage stimulation...	134
Figure 5.16 Effects of frequency on ERP prolongation by low voltage stimulation.....	134

Figure 5.17 Effects of PW on HR reduction by low frequency low voltage stimulation ERP protocol.....	137
Figure 5.18 Effects of PW on percentage of HR decrease by low frequency low voltage stimulation ERP protocol.	137
Figure 5.19 Effects of frequency on HR reduction by low frequency low voltage stimulation ERP protocol.....	138
Figure 5.20 Effects of frequency on percentage of HR decrease by low frequency low voltage stimulation ERP protocol.	138
Figure 5.21 Effects of PW on ERP prolongation by low frequency low voltage stimulation.....	140
Figure 5.22 Effects of frequency on ERP prolongation by low frequency low voltage stimulation	140
Figure 5.23 Effects of PW on VFT increase by low frequency stimulation	143
Figure 5.24 Effects of PW on percentage of VFT increase by low frequency stimulation VFT protocol.	143
Figure 5.25 Effects of frequency on VFT increase by low frequency stimulation	144
Figure 5.26 Effects of frequency on percentage of VFT increase by low frequency stimulation VFT protocol.....	144
Figure 5.27 Effects of PW on VFT increase by low voltage stimulation	147
Figure 5.28 Effects of PW on percentage of VFT increase by low voltage stimulation VFT protocol.	147
Figure 5.29 Effects of frequency on VFT increase by low voltage stimulation	148
Figure 5.30 Effects of frequency on percentage of VFT increase by low voltage stimulation VFT protocol.	148
Figure 5.31 Effects of PW on VFT increase by low frequency low voltage stimulation.....	150
Figure 5.32 Effects of PW on percentage of VFT increase by low frequency low voltage stimulation VFT protocol.	150

Figure 5.33 Effects of frequency on VFT increase by low frequency low voltage stimulation.....	151
Figure 5.34 Effects of frequency on percentage of VFT increase by low frequency low voltage stimulation VFT protocol.....	151
Figure 5.35 Analysis of MAPDR as effect of low frequency RVNS	153
Figure 5.36 Effects of frequency on apex APDR maximum slope by low frequency RVNS	154
Figure 5.37 Effects of frequency on base APDR maximum slope by low frequency RVNS	155
Figure 5.38 Effects of PW on apex APDR maximum slope by low frequency RVNS.....	158
Figure 5.39 Effects of PW on base APDR maximum slope by low frequency RVNS.....	158
Figure 5.40 Effects of PW on percentage change of apex MAPDR maximum slope by low frequency stimulation.....	159
Figure 5.41 Effects of PW on percentage change of base MAPDR maximum slope by low frequency stimulation.....	159
Figure 5.42 Effects of frequency on percentage change of apex MAPDR maximum slope by low frequency stimulation.	160
Figure 5.43 Effects of frequency on percentage change of base MAPDR maximum slope by low frequency stimulation.	160
Figure 5.44 Baseline MAPDR and low voltage RVNS MAPDR.....	161
Figure 5.45 Effects of PW on apex APDR maximum slope by low voltage RVNS	162
Figure 5.46 Effects of PW on base APDR maximum slope by low voltage RVNS	163
Figure 5.47 Effects of frequency on apex APDR maximum slope by low voltage RVNS	165

Figure 5.48 Effects of frequency on base APDR maximum slope by low voltage RVNS	165
Figure 5.49 Effects of PW on percentage change of apex MAPDR maximum slope by low voltage stimulation.....	166
Figure 5.50 Effects of PW on percentage change of base MAPDR maximum slope by low voltage stimulation.....	166
Figure 5.51 Effects of frequency on percentage change of apex MAPDR maximum slope by low voltage stimulation.	167
Figure 5.52 Effects of frequency on percentage change of base MAPDR maximum slope by low voltage stimulation.	167
Figure 5.53 Baseline MAPDR and low frequency low voltage RVNS MAPDR	168
Figure 5.54 Effects of PW on apex APDR maximum slope by low frequency low voltage RVNS.....	169
Figure 5.55 Effects of PW on base APDR maximum slope by low frequency low voltage RVNS.....	170
Figure 5.56 Effects of frequency on apex APDR maximum slope by low frequency low voltage RVNS.....	173
Figure 5.57 Effects of frequency on base APDR maximum slope by low frequency low voltage RVNS.....	173
Figure 5.58 Effects of PW on percentage change of apex MAPDR maximum slope by low frequency low voltage stimulation.....	174
Figure 5.59 Effects of PW on percentage change of base MAPDR maximum slope by low frequency low voltage stimulation.....	174
Figure 5.60 Effects of frequency on percentage change of apex MAPDR maximum slope by low frequency low voltage stimulation.	175
Figure 5.61 Effects of frequency on percentage change of base MAPDR maximum slope by low frequency low voltage stimulation.	175

Figure 6.1 Voltage response curve of low frequency stimulation for NOFL technique	190
Figure 6.2 Frequency response curves of low frequency stimulation for NOFL technique	190
Figure 6.3 Frequency response curves of low voltage stimulation for NOFL technique	191
Figure 6.4 Frequency response curves of low frequency low voltage stimulation for NOFL technique.....	191
Figure 6.5 Increase of F490 nm NOFL signal during right vagus nerve stimulation by low frequency approach. Left ventricular pressure (LVP), perfusion pressure (PP), vagus nerve stimulation (VNS), volt (V), millimeter mercury (mmHg).	193
Figure 6.6 Increase of F490 nm NOFL signal by low voltage (LV) stimulation of the right vagus nerve.....	194
Figure 6.7 Increase of F490 nm NOFL signal by low frequency low voltage (LFLV) stimulation.	194
Figure 6.8 Effect of pulse width on increase of NOFL signal.....	198
Figure 6.9 Effect of frequency on increase of NOFL signal.....	199
Figure 6.10 Increase of NOFL signal and percent heart rate reduction by low frequency stimulation (red), low voltage stimulation (green), and low frequency low voltage stimulation (blue); mean \pm SEM.	202
Figure 6.11 Increase of NOFL signal and percent ventricular fibrillation threshold increase by low frequency stimulation (red), low voltage stimulation (green), and low frequency low voltage stimulation (blue); mean \pm SEM.....	203
Figure 6.12 Increase of NOFL signal and percent maximum slope reduction of apex restitution by low frequency stimulation (red), low voltage stimulation (green), and low frequency low voltage stimulation (blue); mean \pm SEM.....	204
Figure 6.13 Increase of NOFL signal and percent maximum slope reduction of base restitution by low frequency stimulation (red), low voltage stimulation (green), and low frequency low voltage stimulation (blue); mean \pm SEM.....	205

Figure 7.1 Voltage response curve of low frequency stimulation	217
Figure 7.2 Frequency response curves of low frequency stimulation.....	217
Figure 7.3 Frequency response curves of low voltage stimulation	219
Figure 7.4 Frequency response curves of low voltage stimulation.....	219
Figure 7.5 Optical mapping apparatus for measuring NO by DAF-2 DA dye. (A) preparation tray, (B) lens, (C) dichroic mirror, (D) LED light source, (E) video camera, (F) filter, (G) 1 st photodetector, and (H) 2 nd photodetector.....	221
Figure 7.6 Response of the heart to BDM as loss of contraction represented by reduction of left ventricular pressure (LVP).	222
Figure 7.7 Left ventricular free-wall within the optimal focus length of an optical mapping system. Image was snap shot by the video camera of an optical mapping system.	223
Figure 7.8 Fluorescence signal recorded by optical mapping system from the rabbit left ventricle during the baseline stage. Data represented as 16 x 16 (256) pixels. The X axis of each pixel was a 10 seconds time and the Y axis was an amplitude of the recorded signal.....	225
Figure 7.9 Fluorescence signal recorded by optical mapping system from the rabbit left ventricle during the RVNS by frequency 20 Hz pulse width 1 ms and voltage 1 V.	226
Figure 7.10 Representation of fluorescence signal change from figure 7.8 by a colour map. A) Colour mapping at the low amplitude signal within the recording 10 seconds pixel (the lowest point of a green tracing displayed in a small box) and B) colour mapping at the peak amplitude of the 10 seconds pixel (the highest point of a green tracing).....	227
Figure 7.11 Wavelength profile of the 470 LED light head of optical system .	229

List of abbreviations

ACh; Acetylcholine
AChE; Acetylcholinesterase
AF; Atrial fibrillation
ANS; Autonomic nervous system
Ao; Aorta
APs; Action potentials
APD; Action potential duration
AVN; Atrioventricular node
bpm; Beats per minute
cAMP; Cyclic adenosine monophosphate
cGMP; Cyclic guanosine monophosphate
ChAT; Choline acetyltransferase
CICR; Calcium induced calcium release
CL; Cycle length
CNS; Central nervous system
DAD; Delayed afterdepolarisation
DI; Diastolic interval
DMNV; Dorsal motor nucleus of the vagus
DoR; Dispersion of repolarisation
EAD; Early afterdepolarisation
EC coupling; Excitation contraction coupling
eNOS; Endothelial nitric oxide synthase
ERP; Effective refractory period
GC; Guanylate cyclase
GPCR; G-protein coupled receptors
GPs; Ganglionic plexuses
HF; Heart failure
HR; Heart rate
HRV; Heart rate variability
iNOS; inducible nitric oxide synthase
IVC; Inferior vena cava
LA; left atrium

LAa; Left atrium appendage
L-Arg; L-arginine
L-NA; N^G-nitro-L-arginine
LLVS; Low level vagus nerve stimulation
LV; Left ventricle
LVEF; Left ventricular ejection fraction
LVESD; Left ventricular end systolic diameter
LVP; Left ventricular pressure
LVESV; Left ventricular end systolic volume
LVSV; Left ventricular systolic volume
mA; Milli ampere
mAChRs; Muscarinic receptors
MAP; Monophasic action potential
MAPD₉₀; Monophasic action potential duration at 90% repolarisation
MAPDR; Monophasic action potential duration restitution
NA; Nucleus ambiguus
NA; Noradrenaline
nAChRs; Nicotinic receptors
NO; Nitric oxide
nNOS; Neuronal nitric oxide synthase
NYHA; New York heart association classification
PA; Pulmonary artery
PDEs; Phosphodiesterases
PKA; Protein kinase A
PKG; Protein kinase G
PP; perfusion pressure
PVs; Pulmonary veins
RA; Right atrium
RAGP; Right atrial ganglionic plexus
RMP; Resting membrane potential
RV; Right ventricle
RVNS; Right vagus nerve stimulation
RyR; Ryanodine receptor
SAN; Sinoatrial node

SCD; Sudden cardiac death
 sGC; Soluble guanylate cyclase
 SR; Sarcoplasmic reticulum
 SVC; Superior vena cava
 TH; Tyrosine hydroxylase
 TN-I; Troponin-I
 TN-C; Troponin-C
 TRIM; 1-(2-trifluoromethylphenyl) imidazole
 VCAP; Vagal compound action potential
 VF; Ventricular fibrillation
 VFT; Ventricular fibrillation threshold
 VIP; Vasoactive intestinal peptide
 VNS; Vagus nerve stimulation

Ions, ionic channels and ionic current abbreviations

Ca^{2+} ; Calcium ions
 Cl^- ; Chloride ions
 GIRK; G-protein inwardly rectifying potassium channels
 I_{CaL} ; L-type calcium current
 I_{CaT} ; T-type calcium current
 I_f ; Funny current
 I_{K1} ; Inward rectifying potassium current
 I_{KACh} ; G-protein-gated Ach sensitive potassium current
 I_{Kr} ; Rapid activating delayed rectifier potassium current
 I_{Ks} ; Slow activating delayed rectifier potassium current
 I_{Kto} ; transient outward potassium current
 I_{Na} ; Sodium current
 I_{NCX} ; Sodium-calcium exchange current
 I_{to1} ; Transient outward current
 K^+ ; Potassium ions
 Na^+ ; Sodium ions
 $\text{Na}^+\text{-K}^+\text{-ATPase}$; Sodium-potassium ATPase pump
 NCX ; Sodium-calcium exchange

Chapter 1 Introduction

Heart failure (HF) is associated with an increased risk of a fatal arrhythmia such as ventricular fibrillation (VF), which can lead to sudden cardiac death (SCD). SCD remains an unsolved clinical problem that requires a particular focus in treatment strategies. Deranged autonomic control is hallmark feature of HF (Lymeropoulos et al., 2013). Elevated sympathetic nerve activity, and / or a reduction in parasympathetic tone, are associated with pathogenesis and disease progression (Olshansky et al., 2008, Lymeropoulos et al., 2013). Results from experimental studies demonstrate beneficial functional effects of vagus nerve stimulation (VNS) in HF animal models (Schwartz, 2011), with studies now translated into clinical trials. NECTAR-HF, ANTHEM-HF, and INOVATE-HF have demonstrated improvements of cardiac function (Premchand et al., 2014) and quality of life (Zannad et al., 2014), however, data on electrophysiological outcomes have not been reported.

Pre-clinically, from an electrophysiological point of view, our group has demonstrated the protective effects of VNS on VF initiation, i.e. measured as an increase of VF threshold (VFT) and effective refractory period (ERP) together with a reduction in electrical restitution slope in rabbit hearts (Ng et al., 2007). Brack et al. (2009) extended these findings and demonstrated for the first time that these protective effects were related to nitric oxide (NO) release in the cardiac ventricle. This anti-arrhythmic VNS-NO pathway is independent of muscarinic receptor activation and was not released from the endothelium (Brack et al., 2011). However, direct and detailed anatomical evidence of the source of VNS - NO released is lacking.

In experimental models, the vagus nerve was subjected to stimulation intensities that caused a significant heart rate change (Kawada et al., 2008, Brack et al., 2006, Kawada et al., 2006). To investigate the effects of vagal activation without the side effect of any heart rate reduction, low level vagus nerve stimulation (LLVS) was investigated (Stavrakis et al., 2015, Cho et al., 2014, Li et al., 2009). In LLVS studies, stimulation parameters were

characterised to not cause any heart rate reduction or at maximum 10% heart rate decrease from baseline and/or a prolonged atrioventricular (AV) conduction (Shinlapawittayatorn et al., 2013, Buchholz et al., 2012). Low intensity vagal stimulation demonstrated a potential effect on treatment of atrial tachyarrhythmia (Li et al., 2009, Stavrakis et al., 2015, Li et al., 2015). However, there is limited evidence regarding ventricular tachyarrhythmia prevention by VNS. Furthermore, the mechanisms by which VNS NO-release protects the heart against VF are not established and require further investigation.

This chapter aims to introduce the fundamental features related to cardiac electrophysiology and autonomic modulation of the heart. It also presents the current knowledge relevant to VNS NO-release and its potential beneficial effects on cardiac function.

1.1. Autonomic innervation to the heart

Cardiac function is controlled by the autonomic nervous system (ANS). The ANS regulates both electrical and mechanical cardiac functions with the primary objective to support sufficient blood flow to the body (Buckley et al., 2015). By using the hierarchy of the heart-brain neural axis classification, the ANS components that control the cardiac function are categorized into 3 levels; the intra-cardiac, the extra-cardiac intra-thoracic, and the central nervous system (CNS) [spinal cord, brainstem, and higher centres] (figure 1.1) (Shivkumar et al., 2016, Fukuda et al., 2015, Buckley et al., 2015). At each level, neural complexes consist of afferent, efferent, and processing neurons (Beaumont et al., 2016). The afferent neuron conveys mechanical and chemical information from heart and the vasculature to communicate with other levels. The efferent neurons transfer signal from the origin inside the higher centre of the brain to the heart and vessels. Between afferent and efferent fibres of each level, there are the local processing neurons that integrate input from the surrounding network. Therefore, regulation of the heart and vessels is initiated in the higher centre in the brain and is integrated (fine-tuned) at each level of the system until it reaches the heart via an efferent fibre.

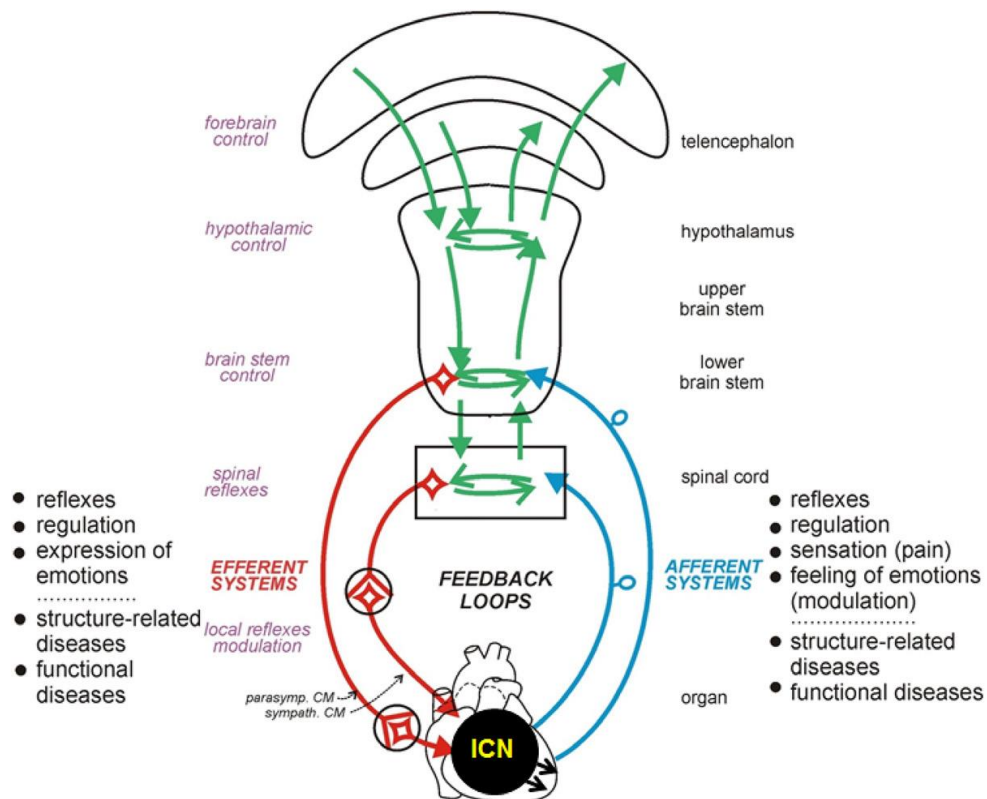


Figure 1.1 Overview of autonomic nervous system (ANS) regulates cardiac and vascular function

The ANS that regulates cardiac function is defined in 3 levels; intra-cardiac nervous (ICN) system, extra-cardiac intra-thoracic, and central nervous system (CNS). At each level, neurons are classified into afferent neurons, efferent neurons, and local processing neurons. Cardio motor (CM). Image taken from (Fukuda et al., 2015).

In addition, the ANS is also divided into two divisions according to base phenotype; sympathetic and parasympathetic divisions, and supplies nerves on the left and right side of the CNS as shown in figure 1.2. Regions of the CNS involved in autonomic control are primarily the hypothalamus, medulla, spinal cord and include pre- and post- ganglionic neurons (Chen et al., 2014, Lympelopoulos et al., 2013, Olshansky et al., 2008). Structural studies of cardiac ANS fibres utilise staining methodologies to target tyrosine hydroxylase (TH) and acetylcholinesterase (AChE) for adrenergic and cholinergic neurons respectively. Cell bodies of preganglionic parasympathetic neurons are found inside the medulla, pons, and midbrain (S2 – S4 level) (Armour, 2008). Axons of preganglionic parasympathetic neurons are distributed to the target organs

through 4 cranial nerves. The preganglionic parasympathetic neurons that innervate the heart occur via the 10th cranial nerve i.e. the vagus nerve, as shown in figure 1.2.

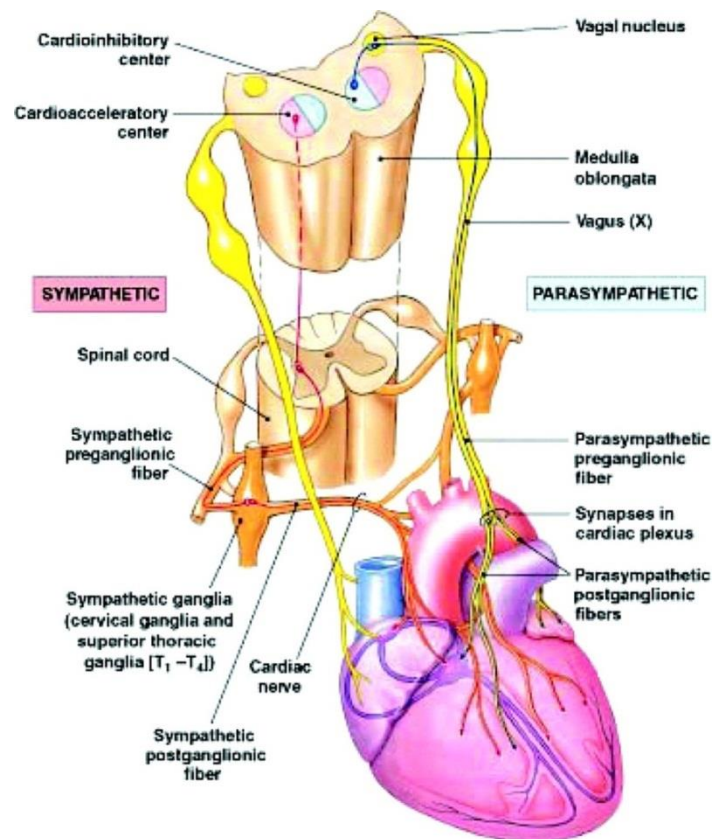


Figure 1.2 Autonomic nerves innervation to the heart

Sympathetic and parasympathetic innervations to the heart start from the hypothalamus and medulla. Preganglionic nerve fibres travel to the heart and synapse to postganglionic fibres at cervical ganglia and superior thoracic ganglia for sympathetic. Vagus nerve synapse to the postganglionic neurons at the cardiac plexus. Then, both sympathetic and parasympathetic postganglionic nerves innervate the heart. Image taken from (Olshansky et al., 2008).

Distribution of postganglionic adrenergic and cholinergic innervations is heterogeneous across the human heart. In the atrium, there are more cholinergic than adrenergic nerves (Kawano et al., 2003). In contrast, there were more TH-positive nerves than AChE-positive nerves in the ventricle. In the transmural ventricular distribution, AChE-positive nerves were more prominent in subendocardial than the subepicardial areas (Kawano et al., 2003), with both AChE-positive and TH-positive nerves more widespread in the atrium than the ventricle. Furthermore, both AChE-positive and TH-positive nerves were

expressed more at the base than the apex of the ventricle (Kawano et al., 2003). This asymmetrical distribution of adrenergic and cholinergic nerves throughout the heart, particularly in the ventricle, is thought to underpin normal cardiac function (Mantravadi et al., 2007, Kawano et al., 2003). However, it may also be a causal factor that contributes to cardiac disease, in particular the genesis of cardiac arrhythmias such as ventricular tachycardia (VT) and VF.

1.1.1 Cardiac ganglionic plexuses (GPs)

At the level of intra-cardiac hierarchy, anatomical evidence shows group of networks formed by the neuronal cell bodies and the connection of their axons lying on the epicardial surface of the heart. This local intra-cardiac nerve network is known as ganglionic plexuses (GPs) (Brack, 2015). In the human heart, GPs are found around the posterior surfaces of the atrium, i.e. the heart hilum, and superior surface of the ventricles (Armour et al., 1997). The degrees of innervation of GPs are different in each chamber (Pauza et al., 2000). The study of right atrial ganglionic plexus (RAGP) demonstrated that this GP receives preganglionic cholinergic inputs, which supports the significance of GPs in autonomic modulation of cardiac function (Hoover et al., 2009). In the rabbit heart, the species of choice for electrophysiology study (Baczkó et al., 2016), efferent nerves approach the heart via the roots of right cranial vein and innervate GPs on the heart hilum and are summarized into 7 sub-plexuses, as illustrated in figure 1.3. Between GPs in the heart, there are nerves that interconnect one cluster to another cluster, which suggests communications between GPs (Saburkina et al., 2014).

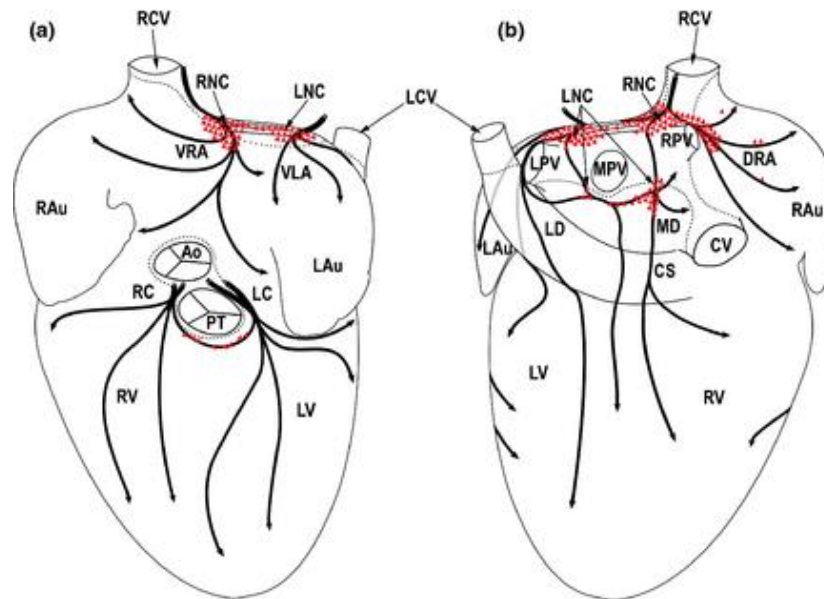


Figure 1.3 Ganglionic plexuses (GPs) of the rabbit heart

Rabbits GPs were shown in (a) ventral view (a) and (b) dorsal view. Each red triangle represented clusters of neurons. (Ao, ascending aorta; CS, coronary sinus; CV, caudal vein; DRA, dorsal right atrial subplexus; ICNs, intrinsic cardiac neurons; LAu, left auricle; LC, left coronary subplexus; LCV, left cranial vein; LD, left dorsal subplexus; LNC, left neuronal cluster; LPV, left pulmonary vein; LV, left ventricle; MD, middle dorsal subplexus; MPV, middle pulmonary vein; PT, pulmonary trunk; RAu, right auricle; RC, right coronary subplexus; RCV, right cranial vein (superior caval vein); RNC, right neuronal cluster; RPV, right pulmonary vein; RV, right ventricle; VLA, ventral left atrial subplexus; VRA, ventral right atrial subplexus). Image taken from (Saburkina et al., 2014).

Immunohistochemistry data of the intra-cardiac GPs demonstrate positive staining of choline acetyltransferase (ChAT), tyrosine hydroxylase (TH), and neuronal nitric oxide synthase (nNOS) of these neuron cell bodies and its axon (Wake and Brack, 2016, Pauziene et al., 2016). Cholinergic neurons display positive staining for ChAT while adrenergic neurons were positive for TH (human heart (figure 1.4) and rabbit heart (figure 1.5)). The cholinergic neuron positive for ChAT was also positive for neuronal nitric oxide synthase (nNOS), as shown in figure 1.4 and 1.5, demonstrating that some cardiac parasympathetic postganglionic fibres contain nNOS and are capable of producing NO. Evidence from these GPs studies reiterates a key role of the intrinsic cardiac nervous system as a final integrative station for autonomic control of the heart. Furthermore, this structural evidence of nNOS in RAGP and GP system across the heart supports our group's working hypothesis about the presence of nitrergic pathway in the heart, particularly in the ventricle (Brack et al., 2011).

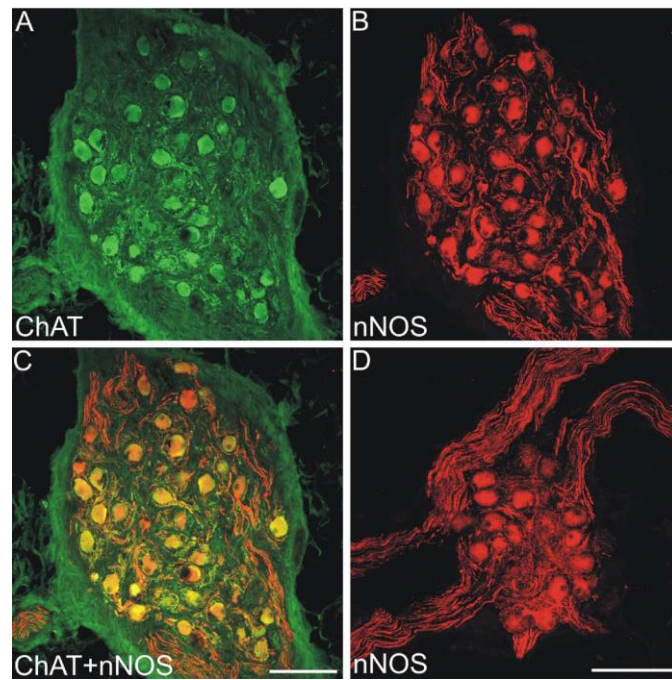


Figure 1.4 Cholinergic and nitergic markers inside human right atrial ganglionic plexus (RAGP)

Choline acetyltransferase (ChAT) -positive stained neurons, as shown green colour in (A) and (C), are also positive stained for neuronal nitric oxide synthase (nNOS), as shown in red colour in (B) and (D). Image taken from (Hoover et al., 2009).

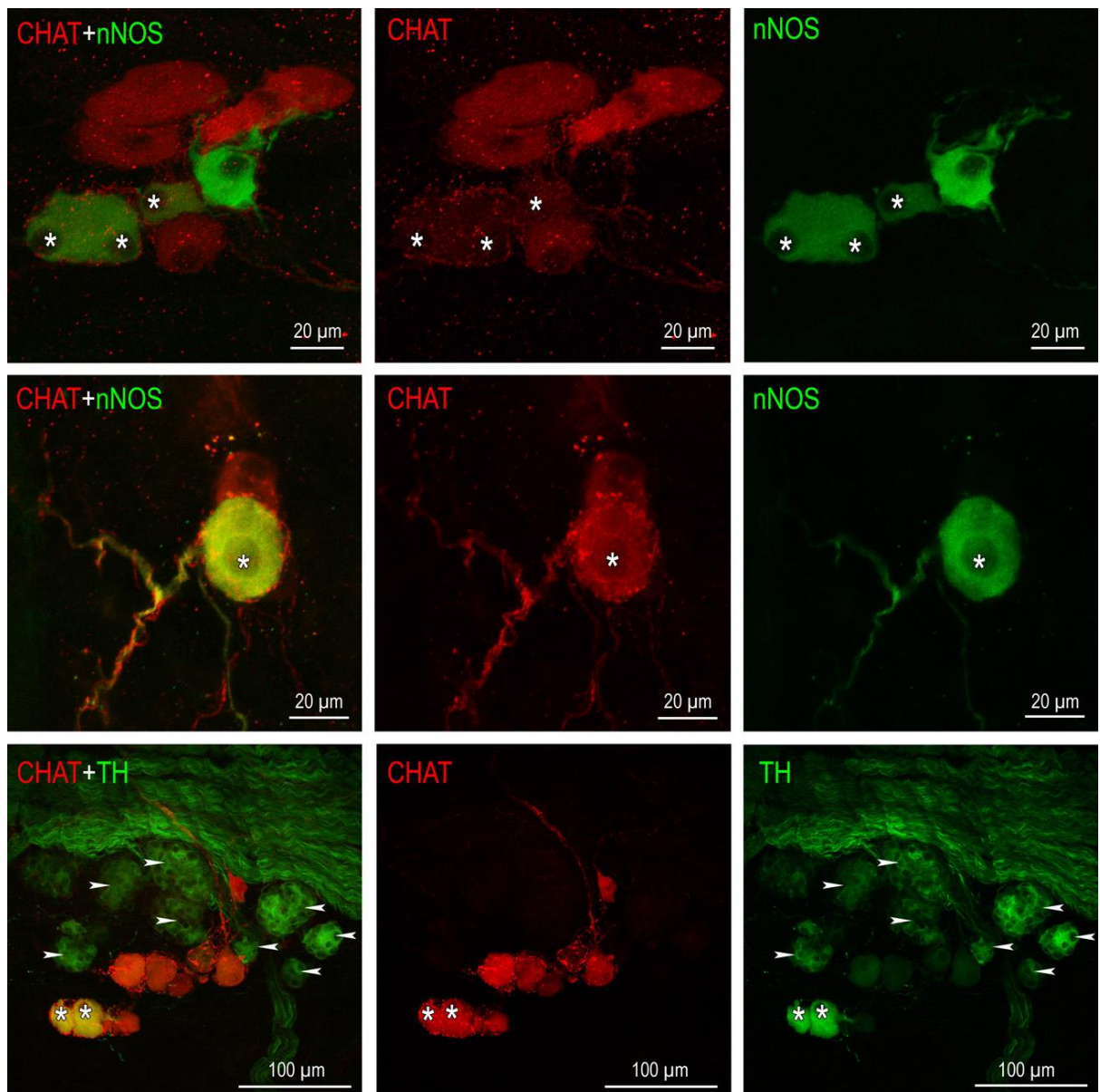


Figure 1.5 Immunohistochemistry of the neurons at the conus arteriosus and the root of pulmonary trunk of the rabbit ventricle

Choline acetyltransferase (ChAT), tyrosine hydroxylase (TH), and neuronal nitric oxide synthase (nNOS). Image taken from (Pauziene et al., 2016).

In the last decade, stimulation of the vagus nerve (each left or right) have been studied preclinically to investigate the protective effects against myocardial ischaemia (Katare et al., 2010, Uemura et al., 2010, Vanoli et al., 1991). In studies of the protective effect of VNS against ventricular arrhythmias, the role of nNOS producing NO during stimulation had been evaluated as a mechanism underpinning this effect (Brack et al., 2009). In this novel study, ventricular NO levels increased during vagus nerve stimulation (VNS). Moreover, an increased

in nNOS-derived NO released during vagus nerve activation was associated with an increased VFT (Brack et al., 2011). Unfortunately, direct evidence of nitrenergic neurons inside the ventricle is still to be detailed and is highly important in this stage.

1.1.2 Vagus nerve composition

The vagus nerve (cranial nerve 10th) contains around 80:20 percent of afferent: efferent fibres and runs parallel to the cardiopulmonary vessels and superior vena cava to synapse the intra-cardiac GPs (Hoover et al., 2008, Evans and Murray, 1954, Prechtel and Powley, 1990). The vagal-cardiac control originates from the neurones in the nucleus ambiguus (NA) of the medulla, displayed in blue and green lines in figure 1.6A. These 80% of cardiac preganglionic neurones are small myelinated fibres (B fibres) and innervate cardiac GPs at the atrial level. Another group of neurones with unmyelinated axon that project to atrial ganglia originate from the dorsal motor nucleus of the vagus (DMNV) in the medulla (Shivkumar et al., 2016, Coote, 2014). Preganglionic vagal fibres also innervate all intra-cardiac GPs (displayed as red in figure 1.6B) across the heart. Most of intra-cardiac GPs were supraventricular but one interventricular septum GP was found. With this intra-cardiac hierarchy, the parasympathetic postganglionic fibres (displayed as green in figure 1.6C) projected their axons widespread across the heart and control their regional function (Beaumont et al., 2016, Buckley et al., 2015, Coote, 2014).

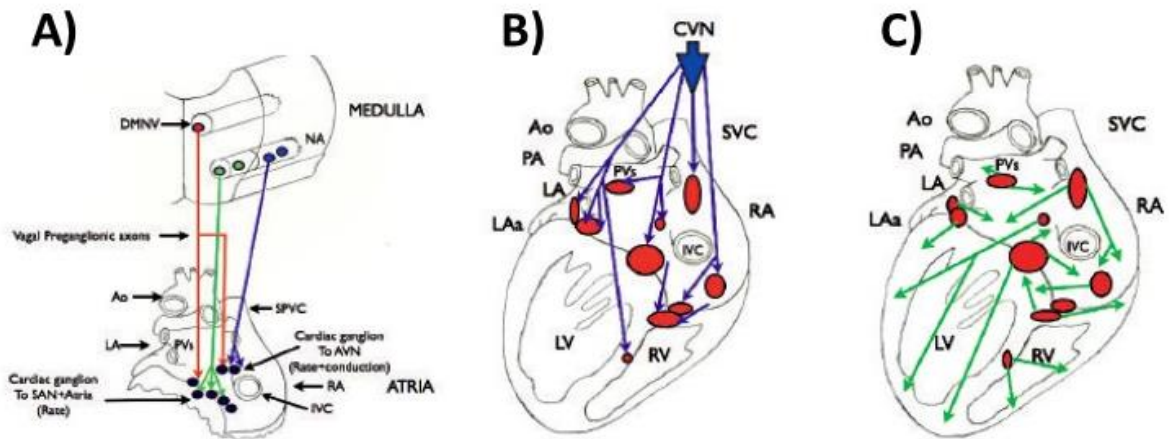


Figure 1.6 A) posterior view of the human atrium and origins of preganglionic vagal fibres that innervated to atrial GPs, B) posterior view of the human with GPs (red) that innervated by the preganglionic cardiac vagal neurones (CVN) (blue), and C) the projection of the cardiac parasympathetic postganglionic fibres (green)

Aorta (Ao), superior vena cava (SPVC), right atrium (RA), inferior vena cava (IVC), left atrium (LA), pulmonary veins (PVs), atrioventricular node (AVN), sinoatrial node (SAN), right ventricle (RV), left ventricle (LV), left atrial appendage (LAa), pulmonary artery (PA). Image taken from (Coote, 2014)

Electrical stimulation of the cervical vagus nerve would produce a vagal compound action potential (VCAP), as shown in figure 1.7. VCAP is formed by the deflection of type of vagal fibres that are activated during the electrical stimulation by the monopolar current pulse with a set of one stimulation and one recording electrode adjacent to each other (Tosato et al., 2006). From figure 1.7, VCAP showed peak of $A\beta$ and $A\gamma$ as quick response to stimulus. These fast responses from vagal A fibres resulted from large diameter (3 – 10 μm) with myelinated fibres, with a conduction velocity of 24.0 ± 4.2 m/s. The later B fibres peak had a conduction velocity of 7.5 ± 0.8 m/s, with a diameter of 1.5 – 3 μm , and were myelinated B fibres (Duclaux et al., 1976). Histological evidence suggested most of the large diameter (A) myelinated fibres, and around 40% of the small diameter myelinated (B) fibres, were efferent fibres (Evans and Murray, 1954). Changing the stimulation current caused alterations of the peak to peak amplitude of each VCAP component, which are shown in figure 1.8. From the figure, right vagus stimulation caused the saturation of $A\beta$ and $A\gamma$ peak to peak amplitude at 0.7 mA. B fibre's were recruited in a small number at low current and rapidly increased in the recruited population at

higher current (not saturated). For left vagus stimulation, the A fibres exhibited the same character as the right recruitment. The B fibres VCAP showed a saturation point around 6 – 7 mA (Tosato et al., 2006). These data demonstrated different responses of right and left cervical vagus nerves especially in the B fibres to an electrical stimulation that was widely used for pre-clinical and clinical study of the vagus nerve. Moreover, it also showed different responses to the electrical strength of different fibre population of the vagus nerve (Jones et al., 1995, Woolley et al., 1987, Middleton et al., 1950).

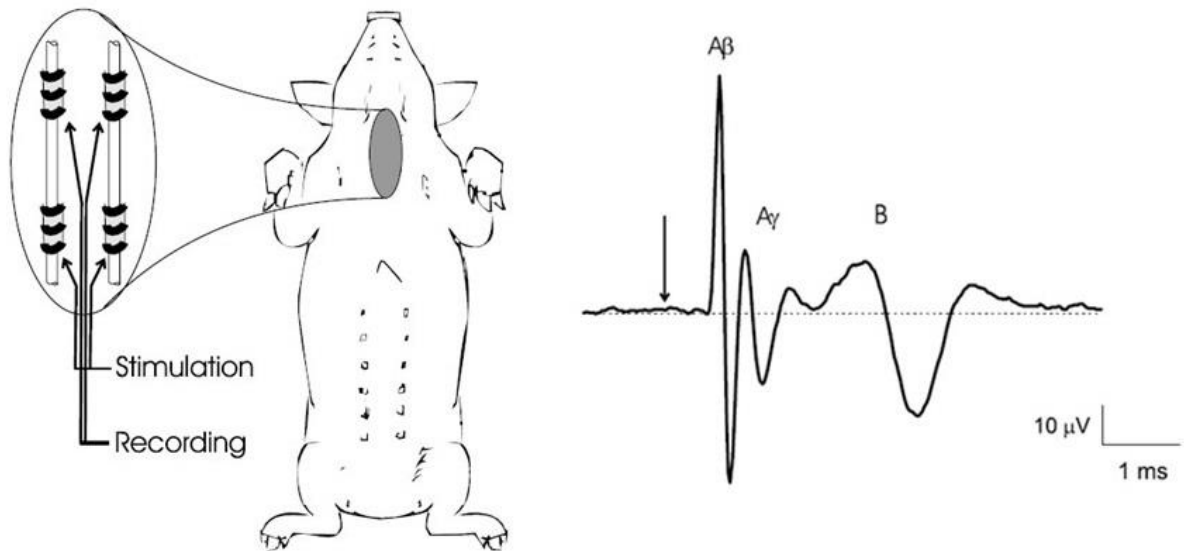


Figure 1.7 Vagal compound action potential (VCAP) by monopolar current stimulation at 5 mA pulse duration 3 ms with the distance between stimulation and recording electrode 46 mm. Arrow represented activation point. Image taken from (Tosato et al., 2006)

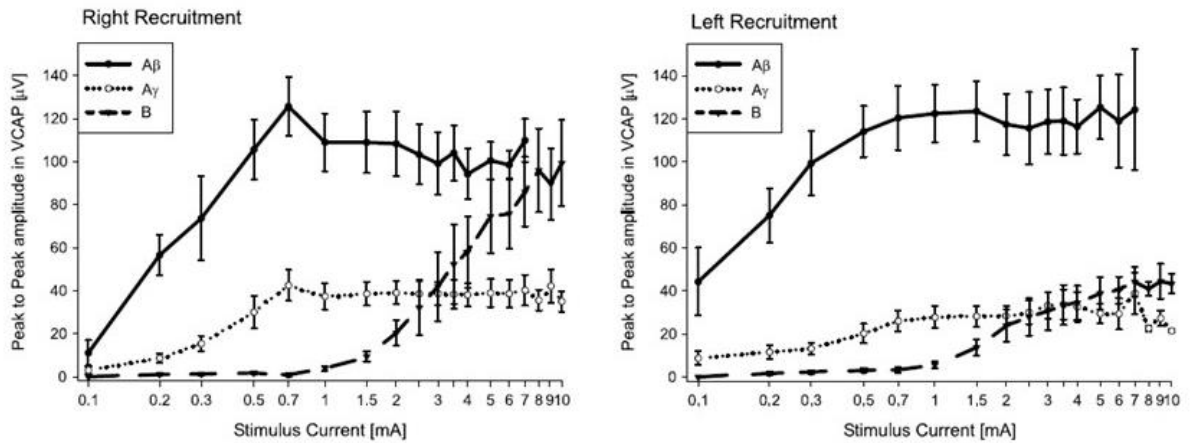


Figure 1.8 Analysis of vagal compound action potential (VCAP) as peak to peak analysis of each VCAP peak component respond to right and left electrical cervical vagus nerve stimulation. Image taken from (Tosato et al., 2006)

The last population of vagus nerve fibres was the vagal C fibre. The C fibre is diameter 0.5 – 2.0 μm non-myelinated with a conduction velocity of 1.1 ± 0.3 m/s (Duclaux et al., 1976). Stimulation of vagal C fibre required a higher amplitude of current than the A and B fibres (Middleton et al., 1950). A bradycardia effect by C fibre recruitment was smaller than the effect of myelinated fibre recruitment with the additive impact on bradycardia of the B fibre (Jones et al., 1995). Moreover, the onset of C fibre bradycardia was slow to develop unlike the rapid response by myelinated fibres recruitment (figure 1.9) (Woolley et al., 1987).

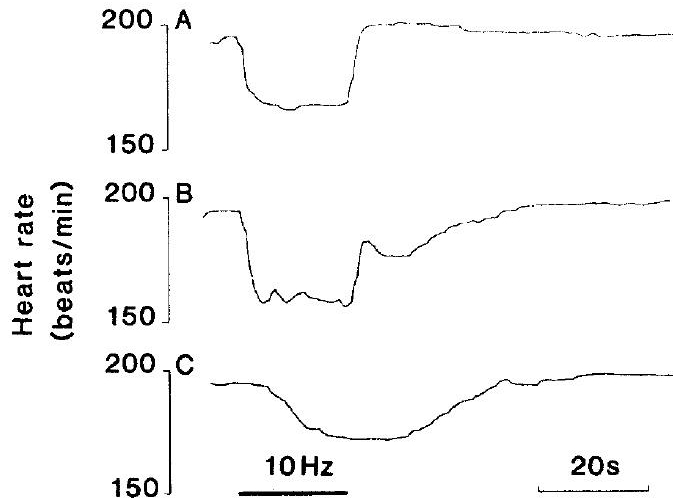


Figure 1.9 Heart rate reduction by vagus nerve stimulation (10 Hz 20 s) of, A myelinated fibres, B both myelinated and non-myelinated fibres, and C non- myelinated fibres. Image taken from (Woolley et al., 1987)

1.2 Autonomic modulation of cardiac function

The ANS directly modulates cardiac function, following the release neurotransmitters from efferent nerve fibres innervating the heart, and has effects on chronotropy (heart rate, HR), conduction (dromotropy), atrial & ventricular contractility (inotropy) and relaxation (luisitropy), as shown in figure 1.10. Autonomic neurotransmitters bind to specific receptors causing initiation of a variety of signalling cascades. These communications cause changes in ion channel physiology and calcium handling processes at a sub-cellular level, which then alters electrical activities of the heart at an organ level.

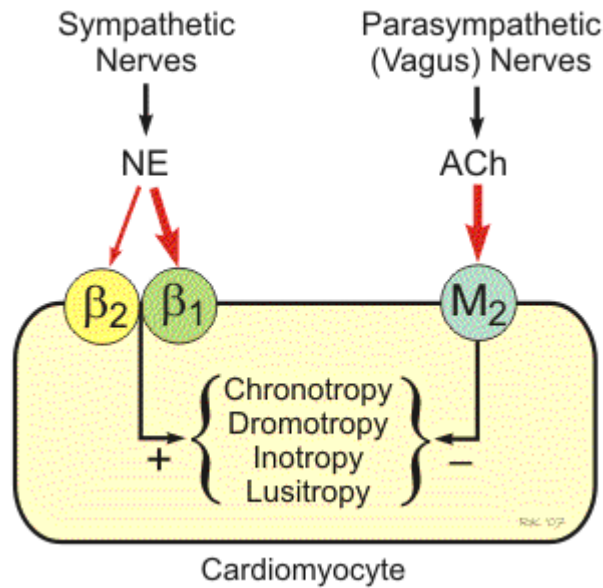


Figure 1.10 Autonomic nervous system control cardiac function

Acetylcholine (ACh), Noradrenaline (NE), adrenergic receptors (β_1 and β_2), muscarinic receptors (M_2). *Adrenergic and Cholinergic Receptors in the Heart*, n.d. image, viewed 7 June 2018. (<http://www.cvphysiology.com/Blood%20Pressure/BP010>).

The sympathetic system is also called the adrenergic nervous system because the main effects are caused by the release of catecholamines as the primary neurotransmitter. There are 2 types of catecholamines; namely noradrenaline and adrenaline. There is evidence in humans that noradrenaline released from the right stellate ganglia preferentially innervates sinoatrial (SA) and atrioventricular (AV) nodes, to increase HR and AV conduction (Lymeropoulos et al., 2013). In addition, the left stellate ganglia are suggested to preferentially innervate the left ventricle to increase LV contractility (Lymeropoulos et al., 2013).

Conversely, the parasympathetic system is commonly called the cholinergic system because parasympathetic neurons generally exert their effects by releasing acetylcholine (ACh) as its primary neurotransmitter. Acetylcholine is produced by enzyme choline acetyltransferase, from choline and acetylcoenzyme – A. The parasympathetic nervous system has both direct effects on the heart and indirect effects through inhibiting the action of sympathetic activity. The vagus nerve is reported to selectively innervate the SA and AV nodes where ACh release decreases HR and AV conduction

velocity by binding to the muscarinic 2 (M₂) receptors and causes the open of the G-protein inwardly rectifying potassium (GIRK) channels, which resulted in cell membrane hyperpolarisation (Olshansky et al., 2008). There is a suggestion that cholinergic nerves do not have any significant direct effects on left ventricular contraction (Olshansky et al., 2008), but this is contentious (Brack et al., 2010, Gauthier et al., 1998). In contrast, ACh directly decreases atrial contractility (Olshansky et al., 2008).

1.2.1 Vagus nerve stimulation (VNS) and ventricular electrophysiology studies

As mentioned previously, studies of vagus nerve stimulation on ventricular electrophysiology was performed in rabbit ventricles by our group (Brack et al., 2007). In this novel study, vagal stimulation using frequencies that induced a significant bradycardia exerted protective effects on ventricular arrhythmogenesis (increase in VFT) together with increased ERP and flattening of the slope of action potential duration restitution (MAPDR) curve, as shown in figure 1.11. The non-specific nitric oxide synthase inhibitor, N^G-nitro-L-arginine (L-NA), was used together with L-arginine (L-Arg), which is a substrate for NO, in order to investigate the role of vagal-released NO in VF protection.

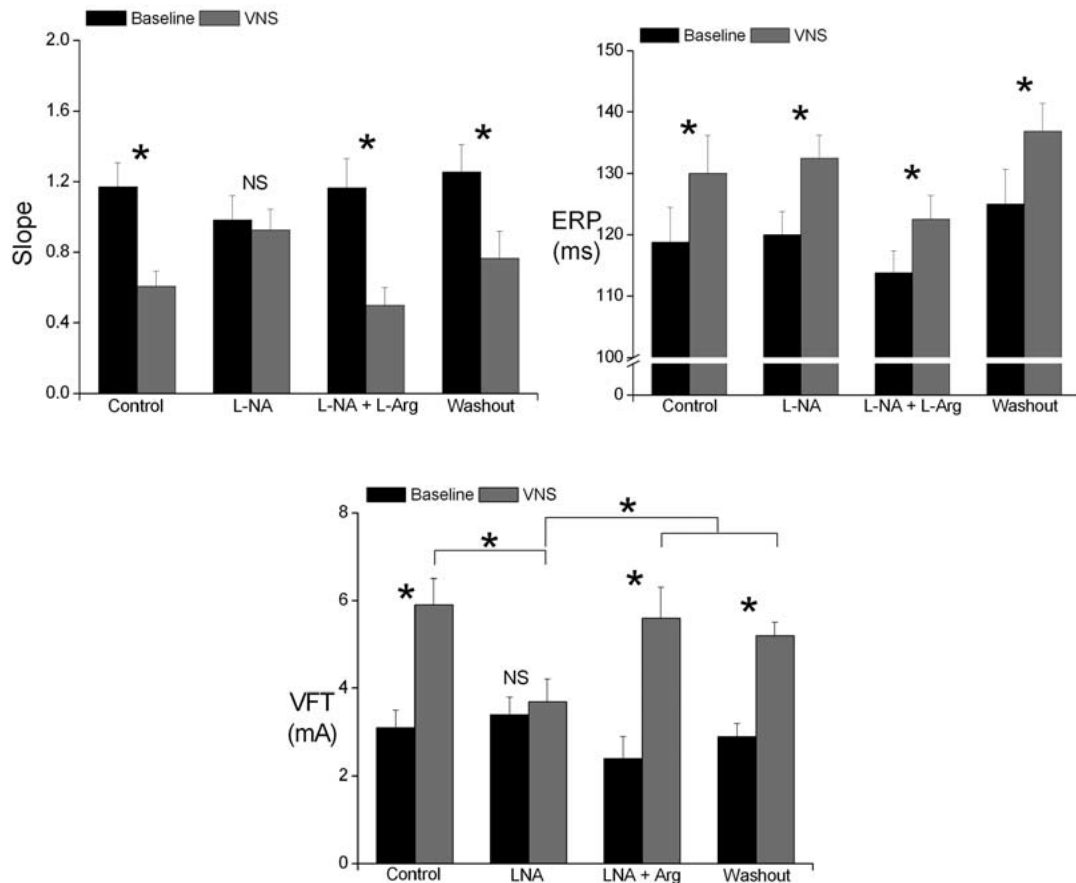


Figure 1.11 Effective refractory period (ERP), ventricular fibrillation threshold (VFT), and monophasic action potential duration restitution (MAPDR) slopes between control and during vagus nerve stimulation

Vagus nerve stimulation (VNS) flattened RT slope and also increased ERP and VFT of rabbit ventricle. N^G-nitro-L-arginine (L-NA) inhibited the stimulated effects except an increased ERP while L-arginine (L-Arg) reversed L-NA effects. Image taken with permission from (Brack et al., 2007)

To confirm that VNS causes a release of NO, these studies were extended to measure NO release in the cardiac ventricle. NO levels were measured by using the 4,5-diaminofluorescein diacetate (DAF-2 DA) with data demonstrating frequency dependent increase of NO during unilateral vagus stimulation (Brack et al., 2009), as shown in figure 1.12. The neuronal nitric oxide synthase inhibitor, 1-(2-trifluoromethylphenyl) imidazole (TRIM), abolished this NO release during vagal stimulation suggesting that NO was synthesized by the nNOS isoform. However, whether the nNOS producing this NO is from autonomic nerves or cardiac myocytes remains to be elucidated. Changes of electrophysiology parameters observed in figure 1.11 was suggested to be nNOS dependent and eNOS independent effects.

1.2.2 Low level vagus nerve stimulation (LLVS)

As decreased vagal tone, together with increased levels of sympathetic activity, are hallmark features in HF (Lympelopoulos et al., 2013) and are, more importantly, tightly associated with cardiac arrhythmogenicity (Brack et al., 2013a), methods to increase vagal tone as therapy have been investigated. These treatments have now translated from pre-clinical to clinical studies (Premchand et al., 2014, Hauptman et al., 2012, De Ferrari et al., 2011) with preliminary data from pilot studies which looked promising. Significant improvement of left ventricular ejection fraction (LVEF), left ventricular systolic volume (LVSV), and 6-minute walk test were reported (De Ferrari et al., 2011). LLVS is defined as levels of stimulation that causes minor changes in HR i.e. around a 10% HR reduction (Huang et al., 2015, Stavrakis et al., 2013).

Results from pre-clinical studies related to anti-arrhythmic effects demonstrate that LLVS can prevent and reverse atrial fibrillation (AF) (Li et al., 2009, Sheng et al., 2011, Stavrakis et al., 2013). Furthermore, LLVS prevented the loss of gap junction protein in dog atrium (Chen et al., 2015, Ando et al., 2005). Gap junctions are important for inter-cellular ion conduction and so the spread of excitation throughout the myocardium. The chronic low amplitude vagal activation (6 months) did not cause HR reduction and improved LV systolic function in the ischemic HF canine model (Hamann et al., 2013). LLVS in the ischemic swine model decreased LV infarct size and reduced VF occurrence (Shinlapawittayatorn et al., 2013). Ventricular electrophysiology changes induced by hyper-sympathetic left stellate ganglion stimulation (shortened ERP, shortened APD, and increase MAPDR slope) of canine model were reversed by LLVS (10% lower HR from sinus rate) (Huang et al., 2015). These anti-atrial and anti-ventricular fibrillation effects were involved with NO release during VNS (Kalla et al., 2016a, Stavrakis et al., 2013). At this stage, data on the impact of LLVS on ventricular electrophysiology is limited comparison to an anti-atrial arrhythmic effect. Therefore, the mechanism underlying an anti-arrhythmic effect in the ventricle of VNS requires further investigation.

1.2.3 Vagus nerve stimulation in human clinical study

The success of pre-clinical VNS led to the extension of the translation of vagus nerve stimulation to human clinical study (Schwartz, 2011). The clinical trials utilise an implanted vagus nerve stimulation device, an example being the CardioFit device (figure 1.13A), to compensate for an unbalanced vagal tone in HF cohorts (Zannad et al., 2014). With these human clinical studies, inclusion criteria were patients with New York Heart Association (NYHA) classification class II – III heart failure with left ventricular ejection fraction (LVEF) \leq 35% (Shivkumar et al., 2016).

In the first study, stimulation of the right vagus by the CardioFit device was performed in chronic HF patients (age 18 to 75 years) of NYHA functional class II – III with a follow up at 3 months and 6 months (with 1 year optional). This study was a single-arm, open label intervention in an international multicentre trial. Inclusion criteria of the study were sinus rhythm (HR 60 – 110 bpm), optimal medication without any change within 3 months, LVEF \leq 35%, and patients being capable to perform a 6-minute walk test. Exclusion criteria were detailed in (De Ferrari et al., 2011). Primary endpoint was the occurrence of adverse events that related to system and procedure. Secondary endpoints were changes at the 6-month follow-up compared to baseline data [NYHA class, quality of life, 6-minute walk test, LVEF, LV end diastolic volume (LVEDV), and LV end systolic volume (LVESV)]. Thirty-two patients were enrolled in this study. At the end of the study, VNS improved the NYHA class, 6-minute walk test, LVEF, and LV systolic volume (De Ferrari et al., 2011). The CardioFit device used the intra-cardiac lead to sense HR and then deliver the delayed stimulation between 70 – 325 ms after the R wave. The bradycardia by the device was limited at 55 bpm. The VNS device was turned on approximately 3 weeks after implantation. Maximum stimulation amplitude was 5.5 mA with average amplitude of 4.1 ± 1.2 mA being reported (Shivkumar et al., 2016, De Ferrari et al., 2011). Results from this study demonstrated safety and feasibility of using VNS in HF patients. The 32 participants of this trial was a small number, therefore further investigation in a larger sample size was required.

The second study, the Autonomic Regulation Therapy (ART) for the Improvement of Left Ventricular Function and heart Failure Symptom (ANTHEM-HF), inclusion criteria used were NYHA class II – III (age ≥ 18 years) with LVEF $\leq 40\%$, LV end diastolic diameter ≥ 50 mm and < 80 mm, QRS width ≤ 150 ms, capable to perform a 6-minute walk test (baseline distance 150 – 425 metres), and receiving optimal medication (Dicarlo et al., 2013). Exclusion criteria were described in detail in (Dicarlo et al., 2013). This study was an open-label multicentre study conducted at 10 sites in India (July 2012 – July 2013) to assess safety, feasibility, and tolerability of autonomic regulation therapy (ART). Participants who provided informed consent were randomised to either right or left cervical VNS (based on physician judgement). ART was done by implantation of the Cybertronics VNS therapy system (figure 1.13B) to 60 participants. This study stimulated either the right or left vagus nerve without HR sensing for 6 months. Stimulation parameters were frequency 10 Hz, pulse width 250 μ s, and current 2.0 ± 0.6 mA. VNS therapy was continued for 26 weeks under 2 follow-up visits (13 and 26 weeks). After 6 months of ART, ANTHEM-HF reported improvement of LVEF, LV end systolic diameter (LVESD), heart rate variability (HRV), and 6-minute walk test. A greater efficacy of the right nerve stimulation than the left nerve was reported (Shivkumar et al., 2016, Premchand et al., 2014). There were 2 VT adverse events reported during the study but these were not related to the ART system. This study demonstrated that ART system was feasible for HF patients. ART also showed the capability to restore autonomic balance. There was a suggestion of more favourable outcomes from the right VNS, which needed to be confirmed in a larger controlled study.

The third study was the Increase Of Vagal TonE in Heart Failure (INOVATE-HF) study. This study was an international, multi-centre, randomised trial. It aimed to assess safety and efficacy of VNS by the CardioFit system in symptomatic HF patients, who were receiving optimal medication (within 1 month before enrolment) (Hauptman et al., 2012). Inclusion criteria were NYHA class III, age ≥ 18 years, sinus rhythm 65 – 110 bpm, LVEF $\leq 40\%$, LVEDD 50 – 80 mm, QRS duration < 120 ms, and being capable to perform 6-minute walk test (baseline 150 – 425 metres). Exclusion criteria were fully described in

(Hauptman et al., 2012). Primary efficacy endpoint was all-cause mortality or HF hospitalisation and primary safety endpoints were > 75% free from complication regards to system and procedure (within 90 days post operation). Secondary endpoints (at 6 and 12 months) were all-cause mortality, serious adverse events, and system or procedure related complications (Hauptman et al., 2012). Patients in this study were randomised [3:2 ratio (active: control)] from 80 sites over United States and Europe. For the results, 707 patients [436: 271 patients (active: control)] were enrolled to the study. Patients in the active group received right VNS over 18 months. Follow-up was performed every 3-month interval. Among the active group, there were 132 patients from 436 who reached the primary efficacy outcome. In the control group, there were 70 patients from 271 who reached the primary efficacy outcome. Stimulation amplitude of the nerve was 3.5 – 5.5 mA. After the mean 16 month follow up, positive improvements were reported for quality of life, NYHA class, and 6-minute walking distance. Results from this large randomised clinical trial supported the safety and feasibility of using VNS in HF patients. Unfortunately, results of this study, with stimulation of the right VNS (RVNS) by the CardioFit system at 16 months follow up, did not show any positive outcome regarding improvement of risk of death and HF events (Gold et al., 2016). This data raised concern about the optimal parameters for VNS including site of stimulation, frequency, and stimulus intensity that were used for nerve stimulation in the study.

The fourth study was the NEural Cardiac TherApy foR Heart Failure (NECTAR-HF). This study was a randomised sham-controlled trial over multi-centres in Europe (27 centres). Patients with NYHA class II – III and LVEF \leq 35%, LVEDD < 55 mm, age > 18 years, who were receiving optimal medication and provided informed consent, were enrolled to the study. Exclusion criteria were fully described in (De Ferrari et al., 2014). Ninety-six patients were implanted with VNS device and stimulation electrode was placed at the right cervical vagus. Participants (n = 95) were randomised into 2:1 ratio of VNS on: VNS off [63 patients: 32 patients (treatment: control)]. RVNS was performed using the Boston Scientific device at frequency 20 Hz, and current 1.3 ± 0.8 mA for a 6-month period. All staff that were involved with end point data collection were

blinded to the randomisation. The primary efficacy endpoint was a change of LVESD from baseline to 6-month followed up. Secondary endpoints were changes from baseline to 6-month visit of LVESV, LVEF, NT-proBNP, Minnesota Living with Heart Failure Questionnaire (MLHFQ), Short Form 36 Health Survey (SF-36), and NYHA class. Results from 6-month followed-up demonstrated that only improvement on quality of life (by MLHQF), the SF-36, and NYHA class were significantly improved in the treatment group compared to control. Moreover, RVNS in this study failed to improve LVESD, LV end systolic volume (LVESV), LVEF, peak VO_2 , and NYHA class (Zannad et al., 2014).

These clinical studies in man demonstrated the safety and feasibility for using VNS in treatment of HF with the caveat of a mixture of results reported. The endpoint of all studies was to give a significant improvement of cardiac mechanical function which remains controversial (Shivkumar et al., 2016). Information pertaining to the incidence of SCD or reporting of basic cardiac electrophysiology in these patients from the three main studies performed so far [NECTAR-HF, ANTHEM-HF, and INOVATE-HF] is lacking. Information related to the effect of LLVS on ventricular electrophysiology is very important and can produce a large impact on the treatment of HF and fatal arrhythmias.

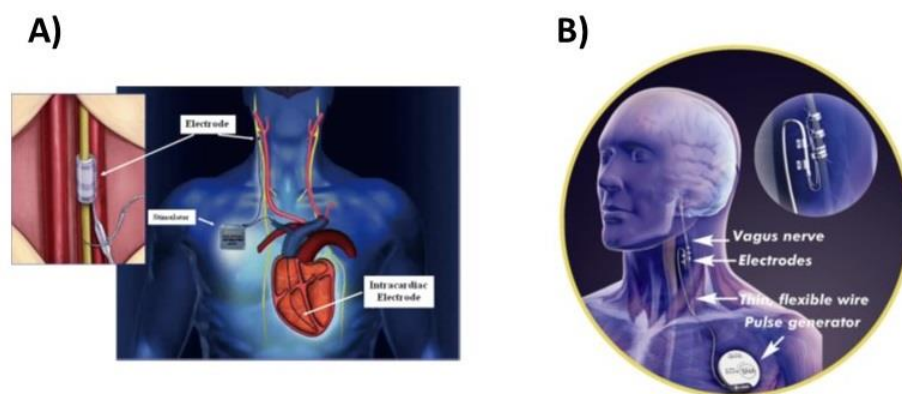


Figure 1.13 A) subcutaneous implant of CardioFit device in the treatment of HF, B) Cybertronic VNS therapy system for autonomic regulation therapy (ART)

LLVS device was implanted subcutaneously of human participants in the INcrease Of Vagal TonE in Heart Failure (INNOVATE-HF) and the Autonomic Regulation Therapy for the Improvement of Left Ventricular Function and heart Failure Symptom (ANTHEM-HF) studies. The stimulation electrode was placed to one vagus nerve and stimulated in a low intensity that did not cause any heart rate reduction or other side effects. Image taken from (Schwartz, 2011, Dicarlo et al., 2013)

1.3 Cardiac electrophysiology

1.3.1 Cardiac conduction system

Prior to mechanical contraction, the heart requires electrical activation in order to initiate excitation – contraction (EC) coupling of the non-pacemaker cardiac cells. To make a synchronous contraction, a rapid distribution of electrical impulses, or action potentials (APs), throughout the whole heart is required and requires a specific conduction system inside the heart, as shown in figure 1.14. The cardiac cycle is initiated by pacemaker cells within the sinoatrial (SA) node with APs then distributed across both atria. Consequently, the atrioventricular (AV) node receives propagated APs that travel to the lower border of the right atrium. The AV node delays and spreads these electrical impulses throughout the ventricles via Purkinje fibres; with the resulting depolarisation of the myocardium triggering the mechanical contraction.

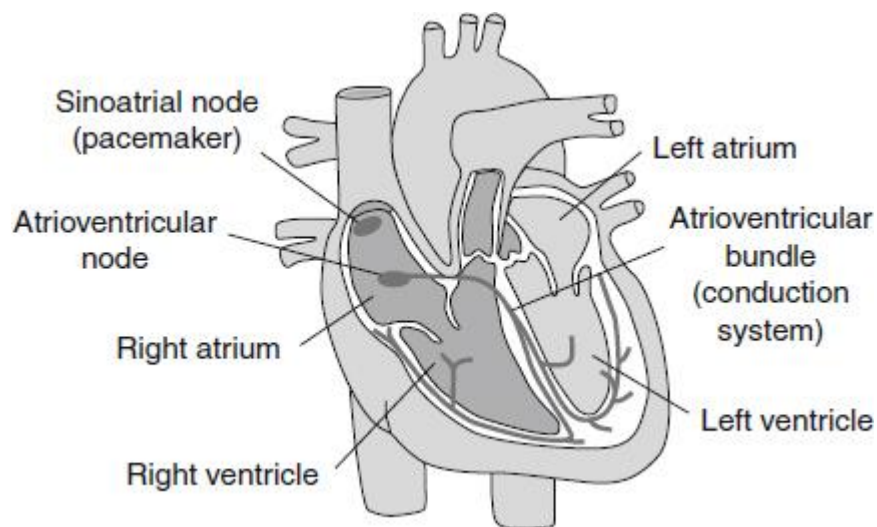


Figure 1.14 Conduction system of the heart

The electrical conduction system is displayed in purple. Action potentials (APs) are initiated inside the sinoatrial (SA) node. Then, impulses propagate to atrioventricular (AV) node and pass through the conduction system throughout the heart. Image taken from (DiFrancesco and Borner, 2007).

1.3.2 Pacemaker cell action potential

These pacemaker cell has an automaticity property to produce its own action potential, which can be modified by the ANS. The pacemaker APs in the SA

node of the right atrium consist of 3 phases - 0, 3 and 4, figure 1.15. After the hyperpolarization at the end of phase 3 (approximately -60 mV), the beginning of phase 4 starts by the flow of Na^+ ion into the cell through Na^+ channels. This inward flow is called the “funny current” (I_f) and causes a depolarization of membrane potential. Once the membrane potential reaches -50 mV, a second inward current is activated through T-type Ca^{2+} channels ($I_{\text{Ca,T}}$). This inward flow of calcium causes the membrane potential to further depolarise. When the membrane potential reaches around -40 mV, a second Ca^{2+} conductance ($I_{\text{Ca,L}}$) occurs through L-type Ca^{2+} channels. The increase in Ca^{2+} ion influx brings the membrane potential to a threshold potential, between -40 to -30 mV, and a substantial depolarisation follows i.e. phase 0. During depolarization, there are increases in inward Ca^{2+} conductance through $I_{\text{Ca,L}}$ while I_{Na} and $I_{\text{Ca,T}}$ decrease. During the depolarised state of the cell, voltage-gated K^+ channels become activated, allowing an outward K^+ current, which begins to repolarize the pacemaker cells i.e. phase 3. This increase of outward K^+ conductance, together with the reduction of inward Ca^{2+} conductance by the inactivation and closing of $I_{\text{Ca,L}}$ completes the cycle. The relationship between the pacemaker AP and the ionic fluxes that are involved is displayed in figure 1.15.

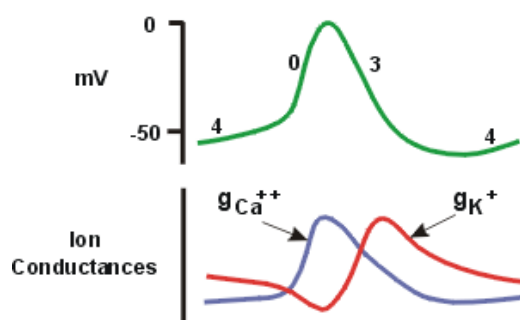


Figure 1.15 Action potential of pacemaker cell

Representative pacemaker cell action potential is displayed in the upper panel. Action potential of slow response cell consists of phase 0, 3, and 4. The main ion conductance of this cell type are calcium and potassium. Consider showing a more complete ion current illustration. *Nodal cell action potentials*, n. d. image, viewed 21 May 2015. ($g_{\text{Ca}^{++}}$, calcium conductance; g_{K^+} , potassium conductance). http://www.cvpharmacology.com/antiarrhy/cardiac_action_potentials.htm.

Due to the response during the depolarization occurs by via slow Ca^{2+} conductance, which is different from the response of non-pacemaker cardiac myocytes, this type of AP is also called “slow response action potential”. Pacemaker APs are automatically generated inside the cell but can be modified by drugs, hormones and the autonomic nervous system (Lymperopoulos et al., 2013, Olshansky et al., 2008). From figure 1.16, noradrenaline (NA) released from sympathetic nerve binds to β adrenoceptors at the SA node. Then, adenylate cyclase (AC) is activated, which then increases intracellular cAMP level. Increased of cAMP leads to increases of the I_f current that produced an increased slope of diastolic depolarisation and reduced diastolic duration, which results in increase of HR (represented in a solid green colour in figure 1.16). In contrast, acetylcholine (ACh) released from parasympathetic nerve binds to M_2 muscarinic receptors at the SA node and produces the opposite action to NA from sympathetic nerve; lowered cAMP, decreased I_f current, decreased slope of diastolic depolarisation, and increased diastolic duration (represented in a light green colour in figure 1.16), which causes a slower of HR.

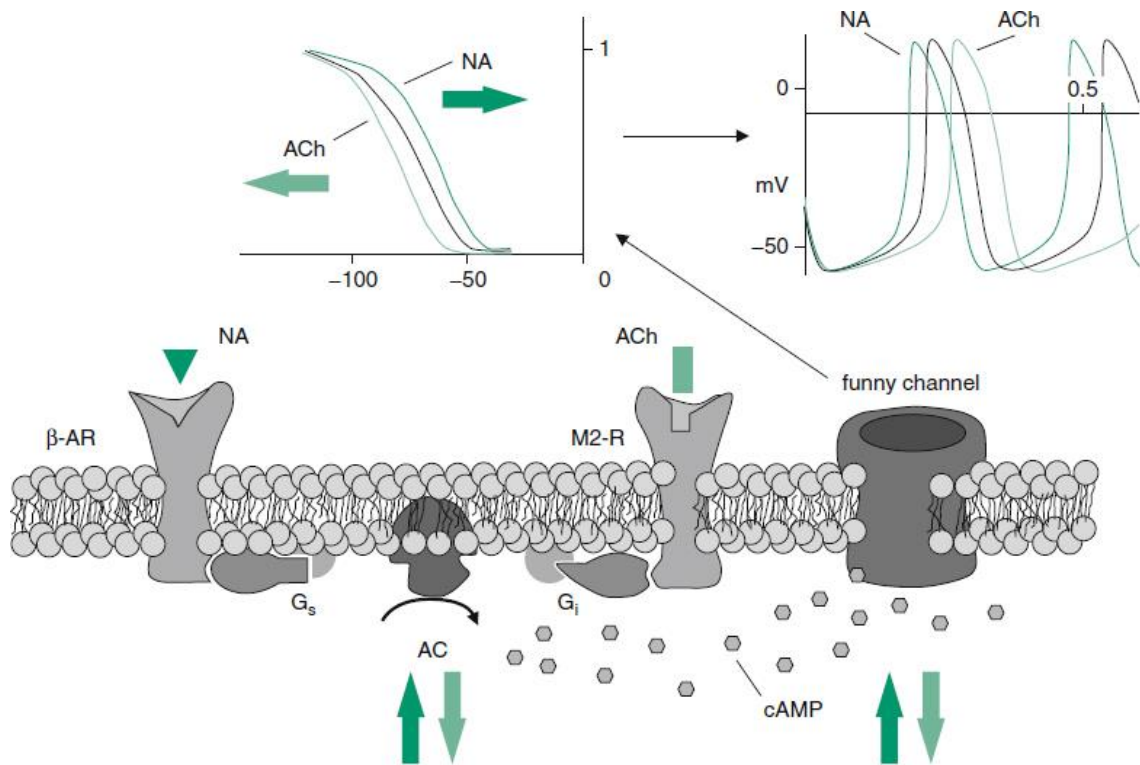


Figure 1.16 Alteration of heart rate by sympathetic/parasympathetic neurotransmitters

Acetylcholine (ACh), adenylate cyclase (AC), β -adrenoceptor receptor (β -AR), inhibitory G-protein (inhibits AC) (G_i), stimulatory G-protein (stimulates AC) (G_s), type-2 muscarinic receptor (M2-R), noradrenaline (NA). Image taken from (DiFrancesco and Borer, 2007).

1.3.3 Non-pacemaker cell action potential

APs generated from pacemaker cells passively change the membrane potential of the adjacent non-pacemaker cells i.e. ventricular myocytes. APs of non-pacemaker cells differ from APs of pacemaker cells, as shown in figure 1.17. Non-pacemaker APs consist of 5 phases; 0, 1, 2, 3 and 4 and has a stable resting membrane potential (RMP) of around -90 mV. During this stage i.e. phase 4, K^+ conductance by inward rectifier K^+ channels (I_{K1}) dominates. Na^+ channels and $I_{Ca,L}$ channels are closed. Depolarising currents pass from excited to non-excited regions by gap junctions (Rohr, 2004). After being triggered by the depolarization of the adjacent cells, the quiescent cell becomes depolarized. In phase 0 of ventricular myocytes, cells are depolarised by the activation of rapidly activating voltage-gated Na^+ channels, hence why these APs are so called "fast response AP". Following depolarisation, there is a short period of repolarization, i.e. phase 1, where K^+ efflux occurs through transient outward K^+ channels ($I_{K,to}$). During this time, L-type Ca^{2+} channels are also

opening and eventually there is a competition between inward Ca^{2+} and outward K^+ currents that results in the membrane potential remaining relatively stable. This is called the plateau phase i.e. phase 2. During this plateau phase, L-type Ca^{2+} channels are inactive, while K^+ conductance through rapidly activating rapid delayed rectifier potassium channels (I_{Kr}) and steadily activating slow delayed rectifier potassium channels (I_{Ks}) is increased. Finally, L-type Ca^{2+} channels close and the K^+ current causes complete repolarisation of the membrane potential, where these channels close allowing I_{K1} to maintain the cell in phase 4 prior to the next stimulus (Grant, 2009).

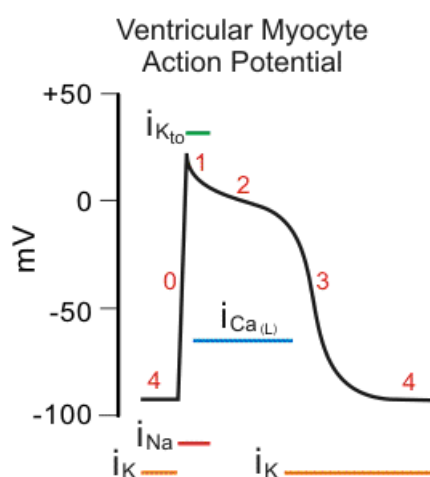


Figure 1.17 Action potential of ventricular cardiac myocyte and ion conductance

Atrial and ventricular cardiac myocytes have 0, 1, 2, 3, and 4 phases of action potential. This fast response cell has a sharp depolarization generated by a rapid influx of sodium current. Calcium influx during phase 2 is used for calcium-induced calcium release (CICR) and produces contractions. *Non-nodal cell action potential*, n. d. image, viewed 21 May 2015. (i_{K} , potassium current; i_{Na} , sodium current; i_{Kto} , potassium current through transient outward potassium channels; $i_{\text{Ca(L)}}$, calcium current through L-type calcium channels).

http://www.cvpharmacology.com/antiarrhy/cardiac_action_potentials.htm.

1.3.4 Excitation contraction (EC) coupling

EC coupling of cardiac myocytes utilizes Ca^{2+} influx during phase 2 and then triggers intracellular release of Ca^{2+} from the sarcoplasmic reticulum (SR) by intracellularly binding to ryanodine receptors (RyR) located at the SR membrane. This Ca^{2+} -induced Ca^{2+} release (CICR) promotes the accumulation of cytosolic Ca^{2+} , which is required to promote contraction. To generate the

physical movement of actin over myosin, Ca^{2+} binds to troponin-C (TN-C), which causes a conformational change of troponin-I (TN-I). When intracellular Ca^{2+} is low, TN-I binds to actin that prevents contraction from occurring. After CICR, when intracellular Ca^{2+} is high, Ca^{2+} binds to TN-C, causing a conformation change to uncover myosin binding sites on the actin filaments. Following the sliding of actin over myosin, actin binds to myosin resulting in contraction.

1.3.5 Intracellular response to parasympathetic neurotransmitters

Parasympathetic effects are mediated mainly by the neurotransmitter acetylcholine (ACh) released from postganglionic vagus nerve fibres in the cardiac tissue (Harvey and Belevych, 2003). At the preganglionic level, ACh plays a role as neurotransmitter for both sympathetic and parasympathetic divisions, as shown in figure 1.18. Inside postganglionic cholinergic neurons, choline acetyltransferase is co-localized with nNOS (Hoover et al., 2009, Pauziene et al., 2016, Pauza et al., 2013). Therefore, nNOS-derived NO can be released during vagal activation which facilitated ACh release (Herring et al., 2002).

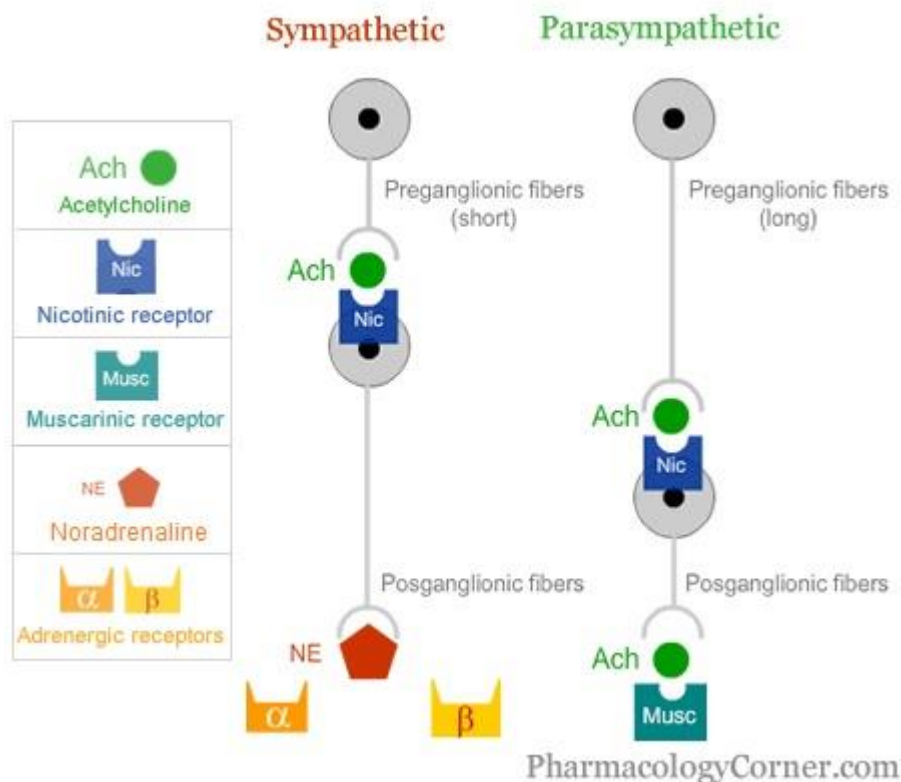


Figure 1.18 Acetylcholine (ACh) receptors: muscarinic (Musc) and nicotinic (Nic)

Scheme of ANS neurotransmitters and receptors displayed released of acetylcholine as neurotransmitter for both sympathetic and parasympathetic and bind to nicotinic receptors at preganglionic level. Then, ACh was released from postganglionic parasympathetic fibres and bind to muscarinic receptor on cardiac cell membrane. Flavio Guzman, (2015), Acetylcholine receptors: muscarinic and nicotinic, image, viewed 21 July 2015. <<http://pharmacologycorner.com/acetylcholine-receptors-muscarinic-and-nicotinic/>>.

1.3.5.1 Acetylcholine

Classically, there are 2 main parasympathetic receptors that are involved in cholinergic control; namely muscarinic receptors (mAChRs) that are G-protein coupled receptors (GPCRs) and nicotinic receptors (nAChRs) that are ligand-gated ion channels. There are 5 subtypes of muscarinic receptors - M₁ to M₅. The predominant form of muscarinic receptors in the heart of mammalian species is the M₂ subtype (Brodde and Michel, 1999). The localization of M₂ receptors are heterogeneous throughout the heart, with more M₂ receptors identified in the atria than in the ventricles (Brodde et al., 2001).

Activation of M₂ receptors on the cardiac cell, following binding with ACh, leads to a dissociation of the G-protein subunits Gβγ from Gαi. Gβγ binds to G-protein inwardly rectifying potassium (GIRK) channels and allow potassium to efflux (Harvey and Belevych, 2003). When this reaction occurs in the SA node, the resting membrane potential hyperpolarizes making it more difficult to trigger an AP and heart rate decreases. Moreover, the Gβγ subunit also activates the G-protein-gated ACh-sensitive K⁺ channel (I_{KACH}) (figure 1.19), which results in reduction of action potential duration (APD), as shown in Figure 1.20.

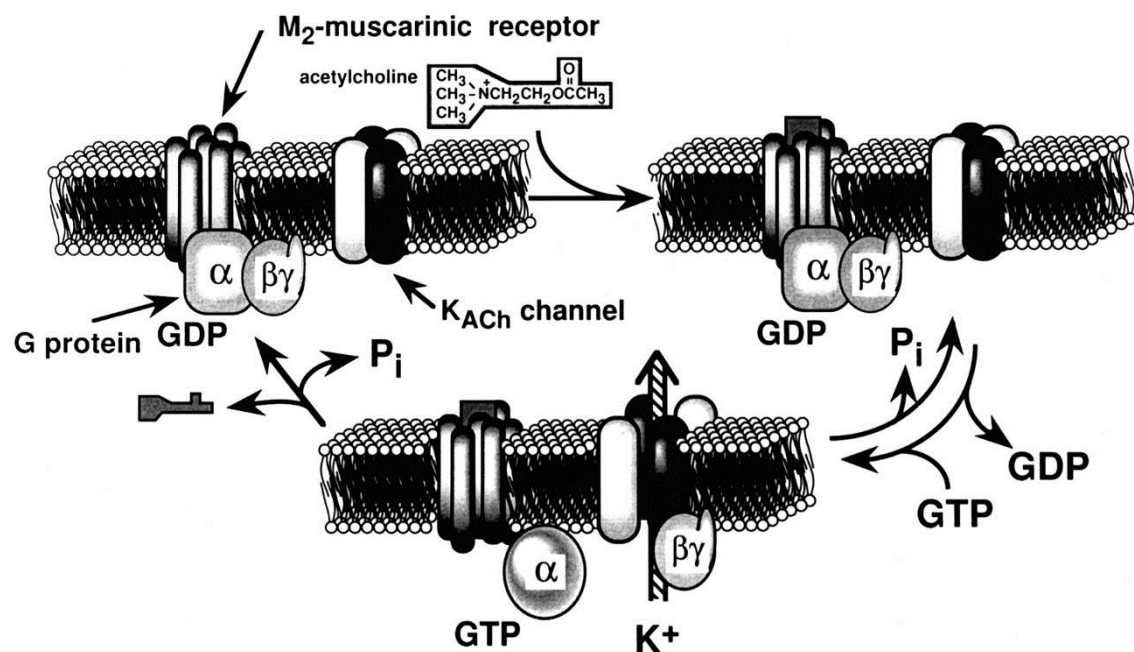


Figure 1.19 M₂ muscarinic acetylcholine receptors responded to acetylcholine

Acetylcholine binds to M₂ muscarinic receptors and activates the G-protein-gated ACh-sensitive K⁺ channel at the membrane of cardiac myocytes. Image taken from (Yamada et al., 1998).

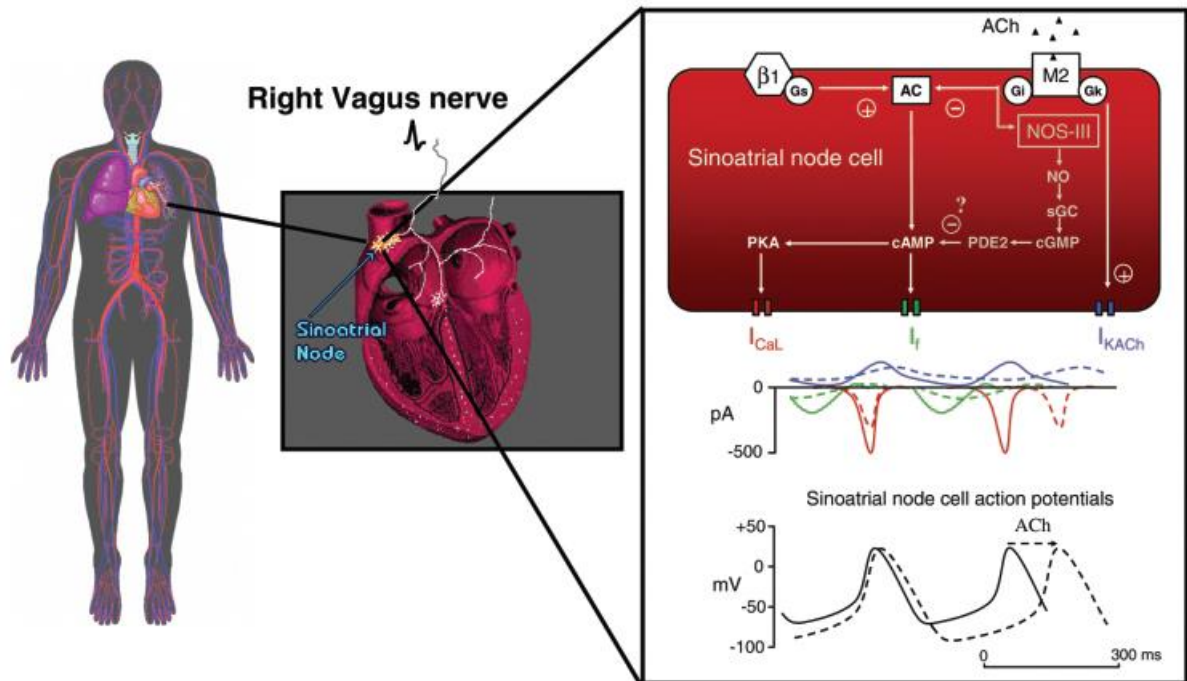


Figure 1.20 Response of acetylcholine (ACh) released from right vagus nerve in sinoatrial (SA) node

ACh released from vagus nerve bind to M_2 receptors, which subsequently regulate G protein coupled inward rectifying K^+ (GIRK). M_2 activation gated inward-rectifying potassium current (I_{KACh}) leads to shorten of action potential duration (APD). (G_i , G protein inhibition; G_k , G protein gating of inwardly rectifying potassium channels; AC, adenylyl cyclase; cAMP, cyclic adenosine monophosphate; PKA, protein kinase A; cGMP, cyclic guanosine monophosphate; I_{CaL} , L-type calcium current; I_f , funny current; sGC, soluble guanylyl cyclase; PDE, phosphodiesterase; NO, nitric oxide). Image taken from (Herring et al., 2002)

Nicotinic receptors are located on the cell bodies of both sympathetic and parasympathetic neurons specifically at neuronal ganglia i.e. at the synapse between preganglionic and postganglionic neurons, figure 1.16. This ligand-gated ion channel serves the purpose to allow Na^+ influx into the neuron and trigger excitation. Therefore, the key role of nAChRs is in signal transduction from one neuron to another. As a result, cholinergic modulation can be regulated at preganglionic and postganglionic levels.

1.3.5.2 Nitric oxide (NO)

NO is produced by the enzyme nitric oxide synthase (NOS), of which there are 3 isoforms; endothelial (eNOS, NOS III), inducible (iNOS, NOS II) and neuronal (nNOS, NOS I) (Ziolo et al., 2008). eNOS is found in blood vessels and also in

cardiomyocytes themselves (Gauthier et al., 1998) whilst nNOS is primarily expressed in autonomic nerves and intra-cardiac ganglia (Tamargo et al., 2010) with smaller amounts located inside including the SR, sarcolemma, and mitochondria (Massion et al., 2003) of cardiomyocytes, as shown in figure 1.21. iNOS is expressed in cardiomyocytes, vascular smooth muscle cell, endothelial cells, fibroblast and inflammatory cells (Ziolo et al., 2008), but is only usually involved in pathological responses.

Effects of endogenous NO in the cardiomyocyte

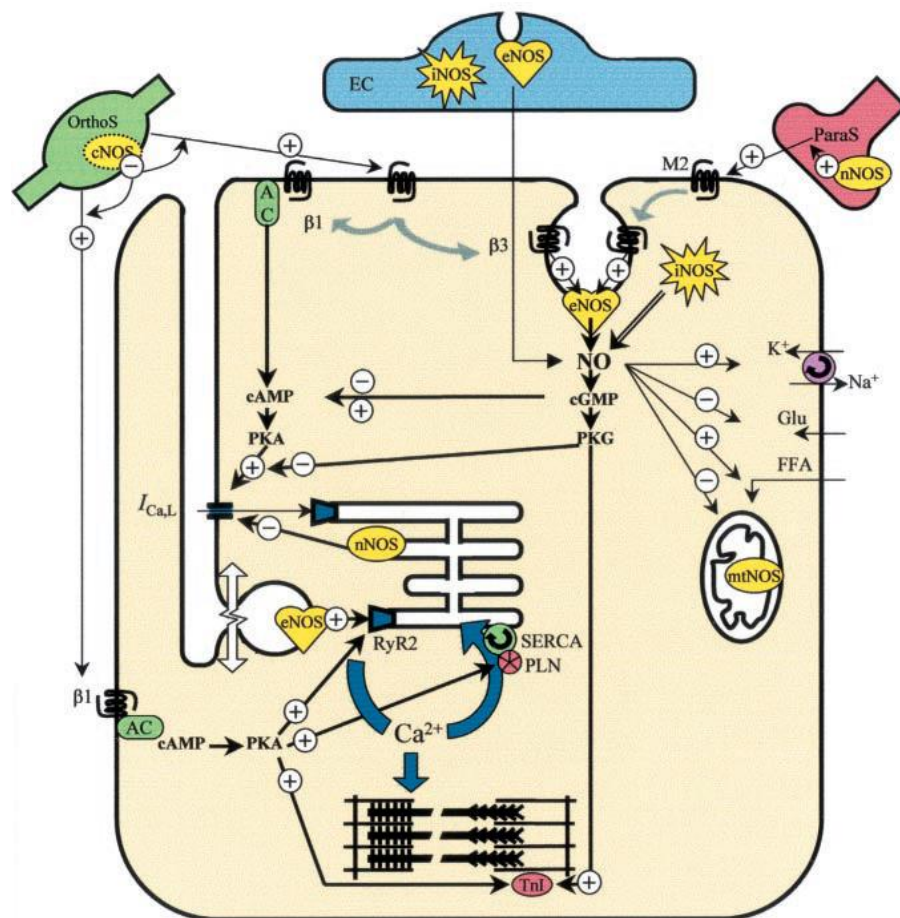


Figure 1.21 Nitric oxide (NO) in cardiomyocyte

Three nitric oxide synthase (NOS) isoforms expressed in endothelial cell (EC), sympathetic varicosities (OrthoS), postganglionic parasympathetic fibres (ParaS), and cardiomyocytes. (eNOS, endothelial nitric oxide synthase; nNOS, neuronal nitric oxide synthase; iNOS, inducible nitric oxide synthase; AC, adenylyl cyclase; cAMP, cyclic adenosine monophosphate; PKA, protein kinase A; PKG, protein kinase G; cGMP, cyclic guanosine monophosphate; PLN, phospholamban; SERCA, sarcoplasmic reticulum Ca^{2+} -ATPase; $I_{Ca,L}$, L-type calcium current; RyR, ryanodine receptor; Tnl, troponin I). Image taken from (Massion et al., 2003)

Under normal physiological conditions, NO is produced spontaneously within endothelial cells that line the coronary vasculature (eNOS) and is an action of shear stress (Pinsky et al., 1997). NO modulates the heart through a number of pathways including cyclic guanosine monophosphate (cGMP) dependent and cGMP-independent mechanisms (Ziolo et al., 2008), as show in figure 1.22A. NO is known to effect chronotropic and inotropic function of the heart in both positive and negative ways (Ziolo, 2008).

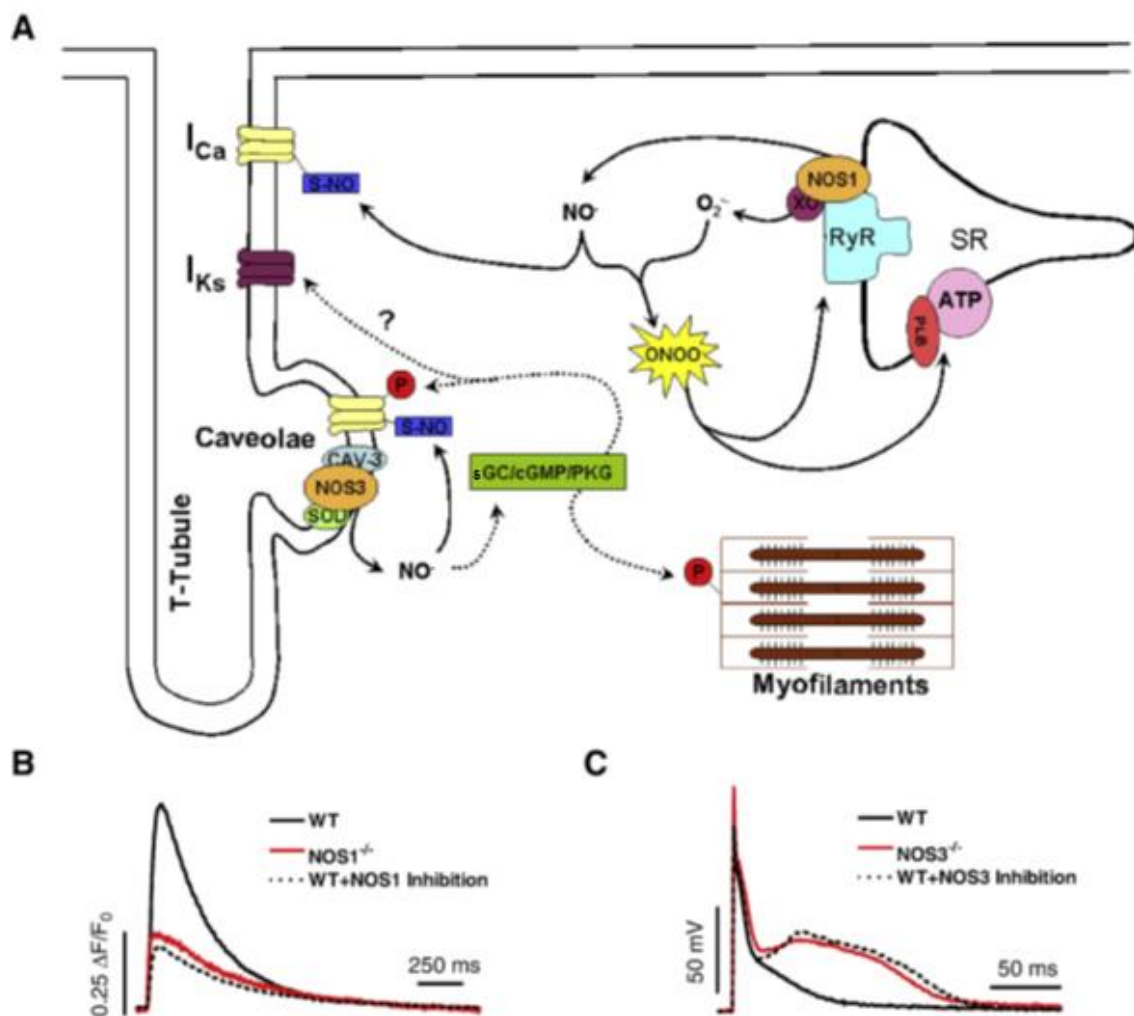


Figure 1.22 Nitric oxide (NO) signalling pathway

The cGMP-dependent signalling was presented in dash line while the cGMP-independent, S-nitrosylation, was in solid line. (NOS3, endothelial nitric oxide synthase; NOS1, neuronal nitric oxide synthase; sGC, soluble guanylyl cyclase; PKG, protein kinase G; cGMP, cyclic guanosine monophosphate; PLB, phospholamban; ATP, adenosine triphosphate; I_{Ca} , calcium current; I_{Ks} , slowly activating delayed rectifier current; RyR, ryanodine receptor; SR, sarcoplasmic reticulum; ONOO $^-$, peroxynitrite; O_2^- , superoxide). Image taken from (Ziolo et al., 2008).

1.3.5.2.1 Paracrine effects

At high concentrations, NO activates cyclic guanosine monophosphate (cGMP)-dependent protein kinase (PKG), via a stimulation of soluble guanylate cyclase (sGC). PKG decreases intra-cellular Ca^{2+} by decreasing the L-type Ca^{2+} current (I_{Ca}), which then decrease inotropic of the heart. cGMP also stimulates the cGMP-regulated phosphodiesterases (PDEs) (Tamargo et al., 2010). In rat ventricular myocytes and human atrial myocytes, cGMP stimulates PDE2 leads to hydrolysis of intra-cellular cyclic adenosine monophosphate (cAMP). Moreover, in human atrial myocytes, cGMP inhibits PDE3, which causes an increases of intra-cellular cAMP level (Rastaldo et al., 2007, Yan et al., 2007). Both PDE2 and PDE3 are able to hydrolyse cGMP and cAMP (Yan et al., 2007). On the other hand, some conditions that support NO generation induce the S-nitrosylation pathway (cGMP-independent pathway). S-nitrosylation leads to activation of the L-type Ca^{2+} channel, which increases I_{Ca} . S-nitrosylation of the ryanodine receptor (RyR) on the sarcoplasmic reticulum (SR) membrane will increase its open probability, allowing more release of Ca^{2+} from the SR (Ziolo, 2008). NO modulates the function of many ion channels of cardiomyocytes. A summary of the effect of NO on cardiac action ion channels is shown in figure 1.23.

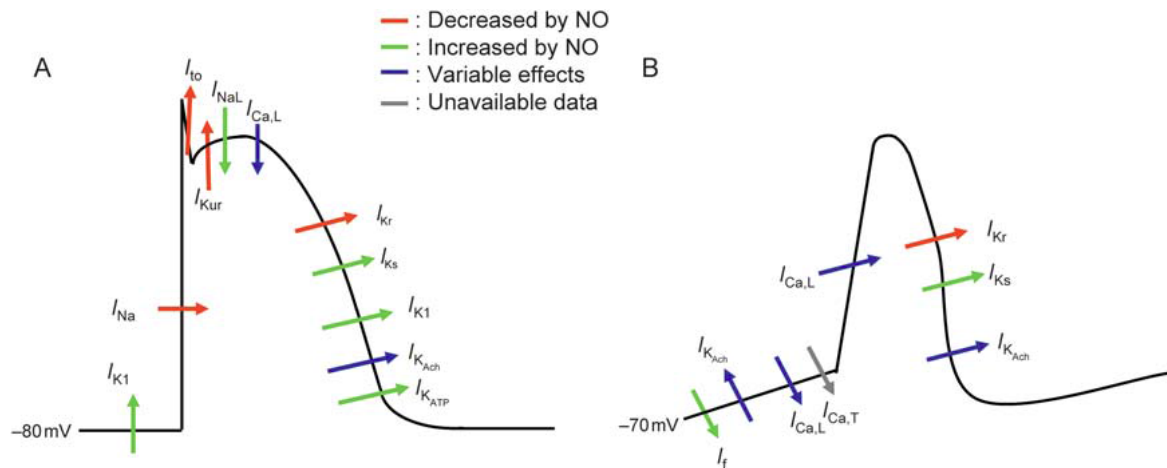


Figure 1.23 Effect of NO on cardiac ion channels

Schematic representation of action potentials from atrial/ventricular cardiomyocytes (A) and pacemaker cells with depictions of the effect of nitric oxide (NO) on specific ion channels. Arrow represents the direction of ion flow of individual ion channels. (I_{K1} , inward rectifier current; I_{Na} , inward sodium current; I_{to} , transient outward current; I_{Kur} , ultra-rapid activating delayed rectifier current; I_{NaL} , late sodium current; $I_{Ca,L}$, L-type calcium current; I_{Kr} , rapidly activating delayed rectifier current; I_{Ks} , slowly activating delayed rectifier current; I_{KACh} , acetylcholine-activated current; I_{KATP} , ATP-sensitive K1 current; I_f , pacemaker current; $I_{Ca,T}$, calcium transient). Image taken from Tamargo et al, 2010.

1.3.5.2.2 Autocrine effects

Interestingly, nNOS is also localized in the stellate ganglia of the sympathetic nervous system that innervate the SA node (Herring and Paterson, 2009), as shown in figure 1.24A. By stimulation of soluble GC (sGC) inside cholinergic neurons, nNOS-derived NO increases ACh release (Herring and Paterson, 2009). NO release pre-synaptically activates cGMP from NO-GC-cGMP pathway. The released cGMP inhibits PDE3 (via cGMP-PDE3 dependent partway). Inhibition of PDE3 causes an increase cAMP-PKA phosphorylation of N-type Ca^{2+} channels. Increase intra-cellular Ca^{2+} influx subsequently induces ACh exocytotic release from nerve ending (Herring and Paterson, 2009). Inside the sympathetic ganglia, NO stimulates PDE2 through sGC-cGMP-dependent pathway. cGMP activates PDE2 leads to increase break-down of intra-cellular cAMP. This stimulation reduces Ca^{2+} influx and then reduces noradrenaline release (Herring and Paterson, 2009). The nNOS-derived NO effects on ACh and noradrenaline releases are illustrated in figure 1.24C. An increase of ACh

level in SA node induced by nNOS-derived NO from cholinergic neuron causes bradycardia, figure 1.20E.

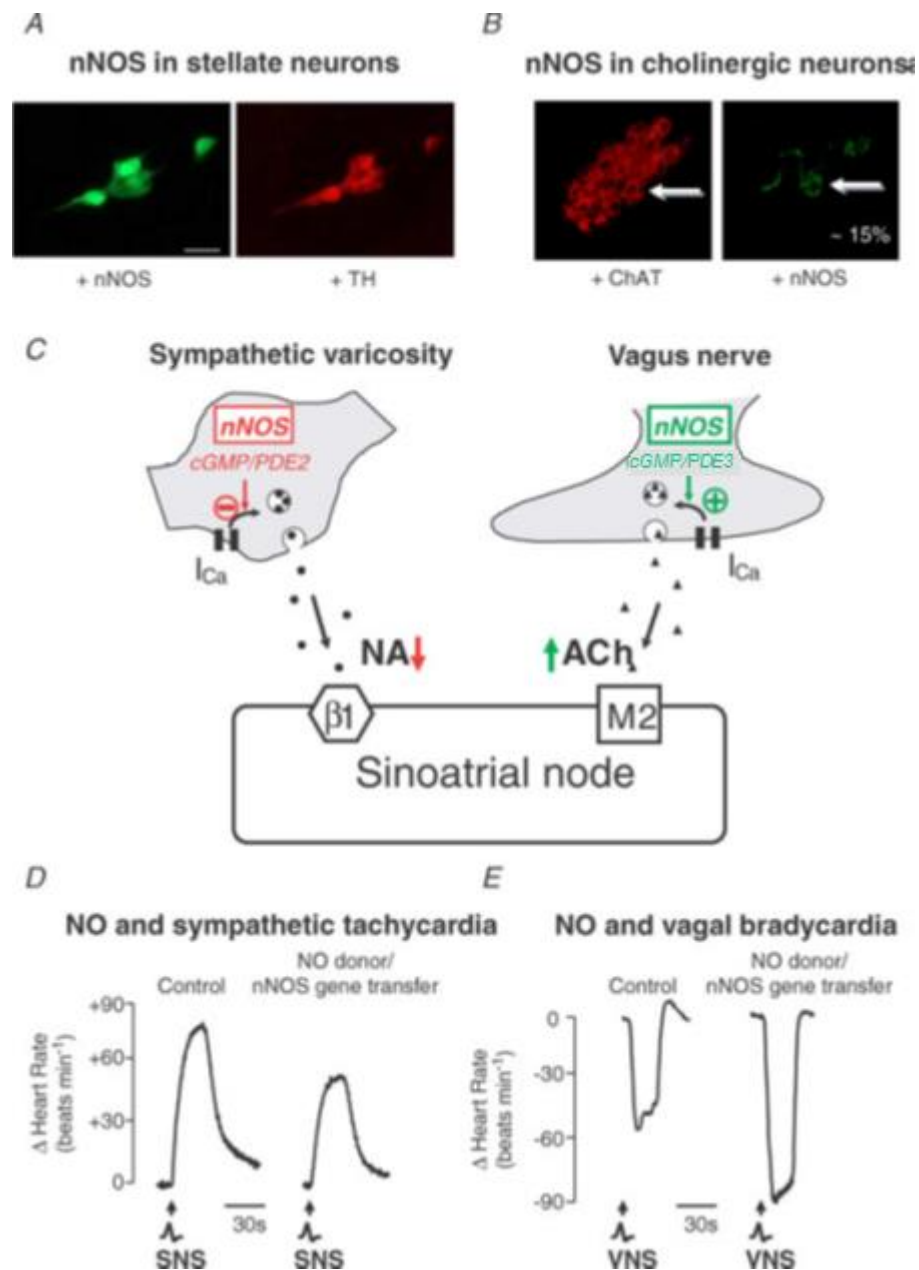


Figure 1.24 Roles of neuronal nitric oxide synthase (nNOS) on neurotransmitter releases from both sympathetic and parasympathetic neurons that innervate sinoatrial (SA) node

The nNOS-derived NO from cholinergic neurons increases acetylcholine (ACh) release to SA node. In contrast, nNOS from stellate ganglia inside sympathetic neurons decreases noradrenaline (NA) releases to SA node. Image taken from (Herring and Paterson, 2009).

1.4 LLVS and ventricular arrhythmias

Ventricular arrhythmias are dangerous cardiac rhythms that can cause death. Arrhythmogenic mechanisms of ventricular arrhythmias are related with pro-arrhythmic conditions that provide circumstances associated with initiation and maintenance of re-entry circuits inside the ventricle. Factors that provide the pro-arrhythmic substrate for ventricular (and atrial) arrhythmias can be generally grouped into 3 categories:

1.4.1 Re-entry circuits

Re-entry circuits continuously conduct electrical impulse around an anatomical or functional obstruction in the heart, also known as a ring model (Antzelevitch, 2001). This causes a focal loop of conduction and electrical excitation in the heart. To initiate and maintain focal circuits, there needs to be;

- i. Unidirectional block of impulse conduction
- ii. Impulse distributes along a specific pathway and returns to its starting point, then moving along the same pathway iteratively
- iii. Any interruption can stop the circuit movement

Asymmetrical distribution of autonomic nerve innervation, together with heterogeneous distribution of ion channels across the heart, may also predispose sources for re-entry circuits. Pathologic conditions such as HF and myocardium ischemia are also prone to develop the ring model.

1.4.2 Monophasic action potential duration electrical restitution (MAPDR)

Monophasic action potential duration electrical restitution (MAPDR) is the relationship between action potential duration 90% repolarization (APD_{90}) and diastolic interval (DI) (Franz, 1999, Garfinkel et al., 2000, Qu et al., 1999). MAPDR is analysed by the relationship between S_2 - $MAPD_{90}$, the duration from the beginning of monophasic action potential (MAP) signal to 90% repolarization, and its preceding DI, the interval between S_1 and S_2 -MAP signals minus S_1 -MAP (Ng et al., 2007). Application of MAPDR in cardiac

electrophysiology study is shown in figure 1.25. At baseline, $MAPD_{90}$ becomes shorter when DIs are shorter (< 40 ms) near the end of S_1 - S_2 standard protocol (Osadchii, 2012), which contributes to a steep RT slope. In contrast, VNS stabilised $MAPD_{90}$ at short DIs and flattened RT slope (Brack et al., 2007). Steep MAPDR curves ($MAPDR$ maximum slope ≥ 1) represent an increased risk for AP wave to break into small spiral waves, which are intimately associated with the initiation of fibrillation (Garfinkel et al., 2000). These conditions can be found to pre-exist in HF and following myocardial ischemia (Weiss et al., 2000). In contrast, shallower APD-RT slopes ($MAPDR$ maximum slope < 1) promoted wave propagation stability, which helps prevent electrical impulses to degenerate into fibrillation (Weiss et al., 2000).

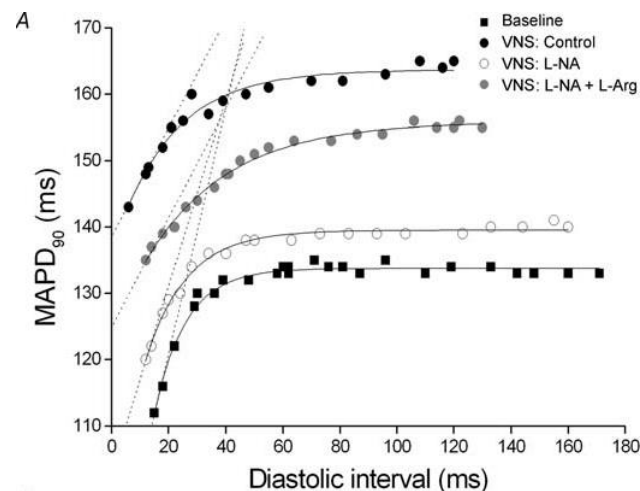


Figure 1.25 Role of nitric oxide (NO) in the effect of vagus nerve stimulation (VNS) on monophasic action potential duration 90% repolarisation ($MAPD_{90}$) restitution (MAPDR)

Electrical restitution curve during baseline shows reductions of $MAPD_{90}$ when diastolic interval (DI) lower than 40 ms and represented a steep slope. NO released by VNS flattened RT slope by maintained $MAPD_{90}$ at short DI. Maximum MAPDR slope ≥ 1 indicated high possibility of action potential to be degenerated into small spiral wave while slope < 1 showed a stable in wave propagation. (L-NA, N^G -nitro-L-arginine; L-Arg, L-arginine). Image taken with permission from Brack et al., 2007

1.4.3 Dispersion of repolarizations

Spatial dispersion of repolarization (DoR) is considered an important proarrhythmic feature (M. and WEINONG, 2002). In normal conditions, DoR has a direction from “apex \rightarrow base” of the LV (Mantravadi et al., 2007) because APD is longer at the base than the apex (Szentadrassy et al., 2005). Bilateral

sympathetic and vagus nerve activation reversed DoR from “apex -> base” to “base -> apex” while unilateral vagus stimulation did not (Mantravadi et al., 2007). These differences in regional APD are thought to be underpinned by differences in ion channel density and different nerve distribution. In canine and human heart, the expression of the channel proteins that carry I_{to} and I_{Ks} was greater in the apex than the base of LV (Szentadrassy et al., 2005). Dispersion of APD and repolarisation also exists through the LV i.e. transmurally where APD is longer at subendocardial compares to subepicardial (Antzelevitch, 2001, Antzelevitch et al., 1991). This can be explained in part due to the finding that I_{to} and I_{Ks} were more abundant in sub-epicardial than the mid-myocardial layers of human and canine LV (Szabó et al., 2005). Dense distribution of autonomic nerves and repolarization-related K^+ channels at the base of the heart contribute to the DoR in the LV (Szentadrassy et al., 2005, Kawano et al., 2003). Increased DoR can lead to dynamic instability of cardiac tissue that can degenerated into re-entrant arrhythmias that is associated with the ring model and restitution concept (Antzelevitch, 2001, Weiss et al., 2000).

1.5 Research gaps

As mentioned previously in this introduction chapter, VNS has been used pre-clinically and clinically. Much evidence supports an anti-atrial arrhythmia action of VNS in animal models. Then, our group extended the study of this vagal protective effects to ventricular arrhythmias with results demonstrating an anti-ventricular arrhythmia action together with an involvement of nNOS-derived NO in the mechanisms. However, the anti-ventricular arrhythmogenesis was accompanied by a large HR reduction during nerve stimulation, which limited potential clinical application. Then, the translation of VNS to human clinical studies were conducted by adjusting stimulation strength of nerve activation into a level that did not cause any HR reduction. After the follow up period, mixed outcomes were reported raising a question as to whether an adequate stimulation of the nerve was achieved or not. Therefore, the current study was designed to investigate primarily whether the low strength VNS use in clinical study would still protect the heart against ventricular arrhythmogenesis or not.

Furthermore, this study will also investigate what stimulation level would be adequate to produce less effect on HR while protecting the heart against arrhythmias.

Basic parameters for electrical stimulation of the vagus nerve consist of voltage, frequency, and pulse width. Data on how cardiac functions respond to different settings of these parameters are still missing. It is very important to understand how the heart responds to different voltages, frequencies, and pulse widths of electrical vagal excitation. Information about changes of HR, ventricular electrophysiology, and NO release by different stimulation parameters will help the configuration of stimulation parameters to obtain the highest effectiveness of VNS device in the future. Therefore, effects of different VNS parameters on HR, ventricular electrophysiology, and NO release will be assessed in this research project.

Chapter 2 Thesis aims and layouts

2.1 Aims of study

The main objective of this project was to investigate whether the anti-arrhythmic effect of vagus nerve stimulation, via a NO-dependent pathway, was observed using clinically relevant vagus nerve stimulation parameters. In the research group's previous preclinical research data, vagus nerve stimulation was performed using stimulation strengths that produced significant heart rate changes. In this study, the aims were to repeat these studies at stimulation strengths similar to those that are used clinically to treat heart failure.

Stimulation parameters widely used for stimulating the vagus preclinically and clinically comprise of voltage, frequency, and pulse width. Each parameter was hypothesised to have different influences on cardiac physiology. It is important to understand responses of the heart to different voltages, frequencies, and pulse widths of vagus nerve stimulation, which have currently not been reported in the literature. Therefore, another objective of this study was to investigate the different effects of different stimulation parameters on the protection against ventricular fibrillation initiation.

2.2 Hypotheses

- 1) Vagus nerve stimulation by clinical relevant stimulation strengths produces an anti-arrhythmic effect to the heart.
- 2) The anti-arrhythmic effect involves nitric oxide release in the ventricle caused by vagus nerve stimulation.
- 3) Low amplitude voltage stimulation causes different cardiac responses compare to high amplitude voltage stimulation.
- 4) Low frequency and high frequency stimulations have different effects on cardiac functions.
- 5) Different durations of stimulation pulse width cause different responses of cardiac functions.

2.3 Thesis layouts

Chapter 3 describes all experimental techniques that have been used in this research project.

Chapter 4 is a preliminary study on the effect of different stimulation parameters on heart rate reduction, ventricular electrophysiology, and nitric oxide release.

Chapter 5 summarises results of the effects of different stimulation voltages, frequencies, and pulse widths on ventricular electrophysiology.

Chapter 6 summarises results of different stimulation voltages, frequencies, and pulse widths on nitric oxide release in the left ventricle.

Chapter 7 describes the development of an optical mapping technique for measuring nitric oxide release during vagus nerve stimulation in the left ventricle.

Chapter 8 is a conclusion of this research project, summarising the results of all experimental work.

Chapter 3 General methodology

3.1 Background

In studying the properties and function of the cardiovascular system, many different animal models have been used. Of the rodents, the rabbit is known to be the model that most closely represents the human due to the similarity of electrophysiological and structural characteristics with human (Baczkó et al., 2016). To investigate how the central nervous system (CNS) controls electrophysiology function, Ng et al. (2001) developed a novel *ex-vivo* rabbit heart preparation with both sympathetic and parasympathetic nerve fibres preserved, which supported an assessment the effect of ANS regulation on ventricular electrophysiology.

All procedures were undertaken following local Ethics approval at the University of Leicester and were carried out in accordance with the UK Animals (Scientific Procedures) Act 1986 (2012 amendment) and the Guide for the Care and Use of Laboratory Animals Published by the US National Institutes of Health (NIH Publication No. 85-23, revised 2011).

3.2 Surgery procedures for the isolated innervated rabbit heart preparation

First part of all experiment was the surgery to prepare the isolated innervated rabbit heart preparation. Male New Zealand White (NZW) rabbits weighing between 2.0 – 2.5 Kg were used. Surgical procedures were performed following the protocol described by Ng et al (2001). Animals were pre-medicated with subcutaneous medetomidine hydrochloride (Sedator) (0.2 mg/kg), ketamine (Ketaset) (10 mg/kg), and butorphanol (Torbugesic) (0.05mg/kg) mixture and then anesthetized with Propofol (1mg/kg) via an ear vein. Surgical anaesthetic depth was confirmed with the lack of pedal and corneal reflexes. A midline incision from cervical to abdominal was made at the ventral side of an animal.

After the trachea was identified, the animal was intubated with a 5 mm plastic tube, which was secured by silk sutures. The animals were ventilated (60 breaths/min) with air via a small animal ventilator (Harvard Apparatus Ltd, Edenbridge, Kent, UK). Level of anaesthesia was maintained with intra-venous propofol (as required) for the remainder of surgery. Then, the common carotid arteries were identified and isolated with silk sutures. The pectoral muscles and the all major blood vessels leading to and from the rib cage were dissected and tied off with silk sutures on both sides. Thereafter, both cervical vagi were isolated and cut. At this stage, for the NOFL DAF2 and optical mapping DAF2 experiments, the right common carotid artery was cannulated and secured with the silk suture for the DAF2-DA fluorescence dye delivery. The rabbits were sacrificed by an overdose of pentobarbitone sodium (Sagatal) (111 mg/kg) with 1000 IU heparin i.v via the marginal ear vein. The incisions of the thoracic cavity were made on both sides to opened and removed the anterior portion of the ribcage. An ice-cold Tyrode solution were immediately applied to the surface of the heart and mediastinal contents to lower temperature and metabolic rate. Then, the pericardium was cut. The descending thoracic aorta was identified and cannulated with a 5 mm diameter plastic tube, which was then secured with silk suture. The pulmonary artery was cut to allow the fluid to flow out of the right heart follow by a rapid injection of ice-cold Tyrode solution through cannulated aorta from the previous step. The whole part from the neck to the thorax of the rabbit was dissected and separated from the surrounding tissues. The whole preparation was then removed and placed on the Langendorff perfusion system.

3.3 Langendorff perfusion system

The preparation was then connected to the Langendorff perfusion system. The cannula that was attached to the descending aorta was then connected to the modified Langedorff system and was perfused with Tyrode solution of the following composition (mM): Na 138.0, K 4.0, Ca 1.8, Mg 1.0, HCO₃ 24.0, H₂PO₄ 0.4, Cl 121.0, glucose 11.0. This solution was bubbled with 95%O₂/5%CO₂ to maintain a pH of around 7.4 and heated to 37 – 38 °C.

Perfusion of the whole preparation was achieved through the descending aorta at a rate 100 ml/min using a Gilson Minipuls 3 peristaltic pump (Gilson Inc., Ohio, USA), as shown in figure 3.1. Venous effluent was drained through a catheter placed at the left ventricular apex. Left ventricular pressure (LVP) was monitored with a fluid-filled latex balloon connected to a pressure transducer (MTL0380, ADInstruments Ltd, Oxford, UK) and inserted into the left ventricle via the left atrium. Left ventricular end diastolic pressure was adjusted to zero. Perfusion pressure (PP) was monitored with a second pressure transducer connected in a series with the aortic cannula. A pair of platinum electrodes (Grass Instruments, Astro-Medical Inc., Slough, UK) was inserted into the right atrial appendage for recording atrial electrograms. Electrocardiogram (ECG) was recorded by using another pair of platinum electrodes (Grass Instruments, Astro-Medical Inc., Slough, UK) inserted into the preparation in a vector of bipolar limb lead II.

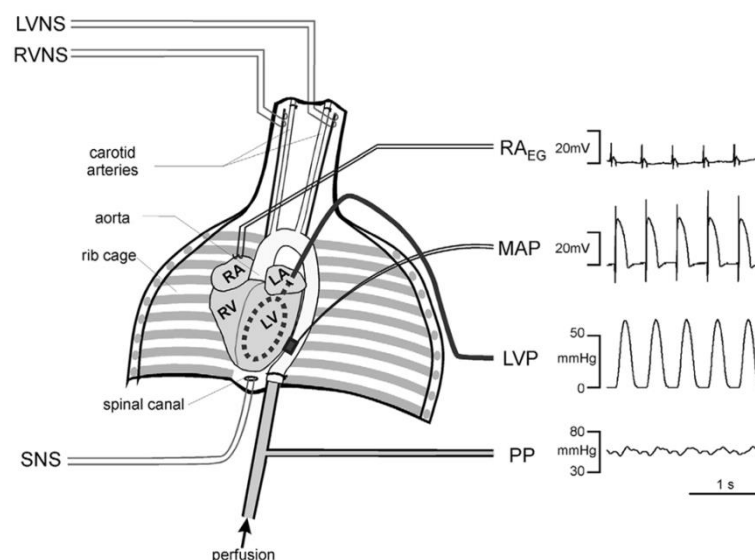


Figure 3.1 Scheme demonstrated the isolated innervated Langendorff rabbit heart with intact dual autonomic innervation. (LA, left atrium; LV, left ventricle; RA, right atrium; RV, right ventricle; LVNS, left vagus nerve stimulation; RVNS, right vagus nerve stimulation, SNS, sympathetic nerve stimulation; RA_{EG}, right atrial electrogram; MAP, monophasic action potential, LVP, left ventricular pressure; PP, aortic perfusion pressure.) Image taken with permission from (Ng et al., 2001)

After starting perfusion with Tyrode's solution, a resting period (around 5 – 10 minutes) was allowed to stabilise the preparation. Stable HR above 150 bpm and stable LV developing pressure above 30 mmHg were used as the preparation inclusion criteria before commencing an experiment. Then, unilateral VNS was tested. If VNS did not lower the HR from baseline, the preparation was terminated and excluded from data analysis.

3.4 Data recording and analysis

All signals obtained from the preparation were recorded using LabChart7 software (v7.3.7, ADInstruments Ltd, Oxford, UK) with a PowerLab 800/s system (ADInstruments Ltd, UK) at a sampling rate 2 kHz/s. Data were stored on a Microsoft Window personal computer with data analysed offline using Chart Software and Microsoft Excel (v2010, Microsoft Corporation, Reading, UK). Data processing and presentation were done by using GraphPad Prism 7 software (v7.03, GraphPad, CA, USA).

3.5 Vagus Nerve Stimulation

Vagus nerve was unilaterally stimulated by using the custom made bi-polar silver electrodes connected to a constant voltage square pulse stimulator (SD9, Grass Instruments, Astro-Med Inc., USA). Overall, the stimulation frequencies were 1, 2, 3, 5, 10, 20, and 30 Hz and the stimulation pulse widths were 0.1, 1, and 2 ms. For voltages, stimulation strengths were i) the 80% of the maximum HR reduction voltage from voltage curve protocol ($80\% \Delta HR_{max}$) and ii) the voltage that reduced HR less than 10% from baseline heart rate ($10\% \Delta HR_{BL}$). To investigate the effect of different aspect of stimulation parameters, frequency, pulse width (PW), and voltage were selectively grouped into a different stimulation set, displayed in figure 3.2. As the vagus nerve is comprised of many types of nerve fibres, different voltage, frequency, and PW may activate different group of nerve fibres, which may give different electrophysiology responses. The first step of all stimulation strategies started

with the configuration of the stimulation voltages, both $80\%\Delta HR_{\max}$ and $10\%\Delta HR_{\text{BL}}$. Vagus nerve was placed on the custom made bi-polar electrodes. Direction of electrical signal between each electrode was tested by selecting between normal or reverse polar on the control panel of the constant voltage square pulse stimulator. With the same strength, the direction that gave the larger HR reduction was selected and used throughout an experiment. Tyrode's solution was intermittently applied to the vagus nerves to maintain the condition of the nerves. The vagal stimulus signals were recorded using the same system to record the on – off timing and duration of the nerve stimuli.

3.5.1 Voltage use for VNS

3.5.1.1 High amplitude voltage

Voltage played role as an activation strength of each stimulation spike. The high voltage can reach to and recruit large population of nerve fibres inside the vagus. In the previous study using the isolated innervated rabbit heart preparation, the submaximal response stimulus strength was used (Brack et al., 2011, Brack et al., 2010, Ng et al., 2007, Brack et al., 2006, Brack et al., 2004, Ng et al., 2001). To find an optimal strength, vagus nerve was stimulated at the fix PW and fix 5 Hz frequency with 1, 2, 3, 5, 7, 10, 15, and 20 V. Voltage dependent HR reductions were measured. The HR drop related to different voltages were plotted as a voltage response curve. The maximum reduction level was defined. The HR drop at 80% of the maximum value was calculated. The voltage that produced the nearest HR drop to the calculated value was used as an $80\%\Delta HR_{\max}$ voltage. Then, this voltage was used with different frequencies to stimulate the nerve. Changing of HR associated with each frequency were plotted as a frequency respond curve.

3.5.1.2 Low amplitude voltage

As VNS clinical trial tried minimize HR reduction by nerve activation, titration of strength into level that does not cause any HR change or drop the HR 10%

from baseline was achieved (Chen et al., 2015, Li et al., 2015, Stavrakis et al., 2015, Shinlapawittayatorn et al., 2013, Schwartz, 2011). This low stimulation strength was tested with the isolated innervated rabbit heart preparation for the first time in this study. To find the voltage that dropped HR less than 10% from baseline ($10\%\Delta HR_{BL}$), vagus nerve was stimulated at the fix PW with the fix 5 Hz and 20 Hz frequencies. The amplitude was titrated to produce a lowering of HR to the level less than 10% of the baseline value. The $10\%\Delta HR_{BL}$ voltage from 5 Hz was used with the low frequency stimulations while the $10\%\Delta HR_{BL}$ voltage from 20 Hz was used with the high frequency stimulations. These two low amplitude stimulation patterns expanded an investigation to cover a full range of frequency that were used in both preclinical and clinical vagal studies (Joyner, 2016, Huang et al., 2015, Stavrakis et al., 2015, Winter et al., 2014, Zannad et al., 2014, Premchand et al., 2014, He et al., 2013b, Shinlapawittayatorn et al., 2013, Dicarolo et al., 2013).

3.5.2 Frequency use for VNS

Another stimulation parameter, frequency, referred to the number of stimulation spikes in one second. A wide range of frequencies were used for the VNS study (Zhang et al., 2016, Gold et al., 2016, Huang et al., 2015, Chen et al., 2015, Li et al., 2015, Stavrakis et al., 2015). The combination of voltage, frequency, and pulse width was displayed in figure 3.2. At the early stage, parameters were designed to investigate effects of strong voltage with long duration ($80\%\Delta HR_{max}$ with 2 ms at 1, 2, 3, and 5 Hz) compare to effects of high frequency with short duration (10, 20, and 30 Hz by $10\%\Delta HR_{BL}$ with 0.1 ms) stimulations. Both right and left vagi were stimulated in this examination. Then, the stimulation was focused only on the right VNS, as it had been previously used in a clinical study (Gold et al., 2016, Zannad et al., 2014, Dicarolo et al., 2013, Hauptman et al., 2012, Schwartz, 2011). Stimulation frequencies were redefined as (1, 2, and 3 Hz) low frequency and (5, 10, and 20 Hz) high frequency. The 30 Hz frequency was cut off in this stage.

3.5.3 Pulse width use for VNS

Pulse width refers to the duration of the stimulation spike. Previous studies on the isolated innervated rabbit heart preparation utilised only 2 ms pulse width to stimulate the nerve (Brack et al., 2011, Brack et al., 2010, Brack et al., 2009, Patel et al., 2008, Ng et al., 2007, Mantravadi et al., 2007, Brack et al., 2006, Brack et al., 2004, Ng et al., 2001). Other durations, for example 0.1 and 1 ms, were used for stimulate vagus with protective effect against arrhythmias reported (Chen et al., 2015, He et al., 2013b). In this research, differences between longest pulse width, 2 ms, and shortest pulse width, 0.1 ms, was studied at the early stage. Then, to study a complete range of stimulation pulse width; short, moderate, and long duration (0.1, 1, and 2 ms) were applied.

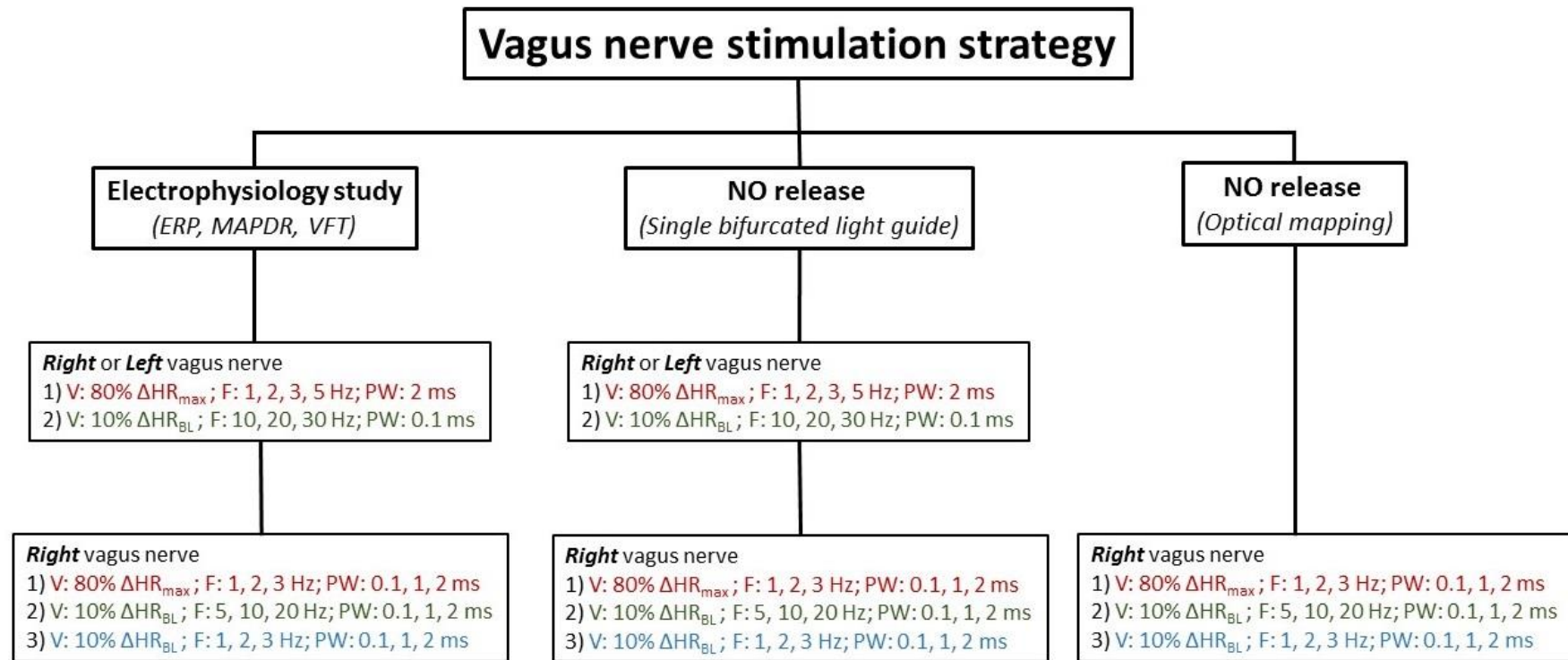


Figure 3.2 VNS parameters used for cardiac electrophysiology and ventricular NO release studies

Combinations of voltage (V), frequency (F), and pulse width (PW) used for unilateral VNS in electrophysiology and nitric oxide (NO) release studies. Voltages were 80% of maximum heart rate reduction ($80\% \Delta HR_{max}$) by the voltage curve protocol and 10% of heart rate reduction from the baseline ($10\% \Delta HR_{BL}$).

3.6 Effective Refractory Period (ERP) and Monophasic Action Potential Duration 90% Restitution (MAPDR₉₀)

The LV electrophysiological parameters of interest in this project were ERP, MAPDR₉₀, and VFT. To study the ERP and MAPDR₉₀ protocols, right ventricular pacing was required. The pacing catheter was inserted into the right ventricle via the hole at the right ventricular outflow tract and was connected to a PC-controlled constant current stimulator (DS7A, Digitimer, Welwyn Garden City, UK). The tip of the catheter was located at the right ventricular apex. The pacing Cycle Length (CL) was set to 300 ms, producing a HR of 200 bpm. To find the threshold, pacing current was started at 0.0 mA and gradually increased by 0.01 mA until the heart captured the pacing signal and beating at 200 bpm. This pacing strength that captured the heart was called the diastolic threshold (DT). The strength of this threshold was set to be lower than 0.5 mA. In case of DT over that 0.5 mA, the tip of the pacing catheter was required a re-location and the DT was repeated again. Then, the DT was double the value to ensure that the pacing of the heart was maintained throughout the ERP and MAPDR₉₀ protocols (Ng et al., 2007).

Two recording silver electrodes were placed on an epicardial surface of the LV free wall, one at the base and one at the apex. Then, electrodes were connected to a DC-coupled high input impedance differential amplifier to record the monophasic action potential (MAP), displayed in figure 3.3. MAP duration was measured by using a custom written program (Francis Burton, Glasgow University, UK). MAP duration was measured from the start of signal to 90% of repolarisation (MAPD₉₀). The amplitude of the MAP was measured from the peak to the isoelectric line (Ng et al., 2007).

3.6.1 Effective Refractory Period (ERP) protocol

The ERP and MAPDR₉₀ protocols were performed by using right ventricular pacing with a 20 beats of the S1 drive train at a cycle length (CL) of 300 ms followed by an extra - stimulus S2 (S1–S2 extrastimulus method) (Osadchii, 2012, Brack et al., 2011), show in Figure 3.3. The S1 - S2 durations were progressively shortened by 10 ms, from CL 300 – 200 ms, and by 5 ms, from 200 ms until S2 stimulus not produce any capture by lacked of an S2 - MAP. ERP was defined as the longest S1 – S2 interval that failed to capture the ventricles (Ng et al., 2007). ERPs were examined between baseline and during VNSs.

3.6.2 Monophasic Action Potential Duration 90% Restitution (MAPDR₉₀) protocol

The MAPDR₉₀ is analysis of the relationship between S2 - MAPD₉₀ and preceding diastolic intervals (DI) (Ng et al., 2007), displayed in figure 3.3. MAP and pacing stimulation time recorded from the ERP protocol were measured by using a custom written program (Francis Burton, Glasgow University, UK) and then used to calculate the MAPD₉₀ and DI (Kettlewell et al., 2004). The DI was defined as the interval between the S1 and S2 MAP signals minus the S1 MAPD₉₀. Data were plotted as DI was an X axis and corresponding MAPDR₉₀ was a Y axis. An exponential curve was fitted to the data using Microcal Origin (v6.1, Origin, San Diego, CA, USA), as displayed in figure 3.4A. Then, the maximum slope of restitution was measured by analysing the first derivative of the fitted curve, showed in figure 3.4B.

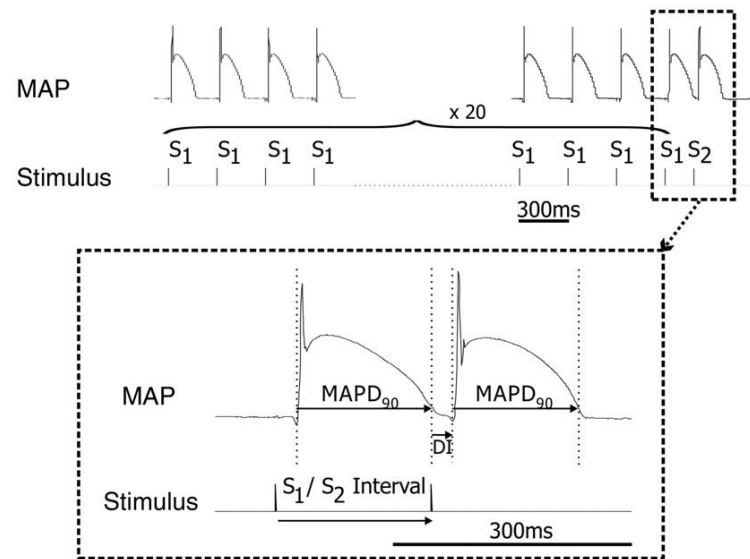


Figure 3.3 Monophasic action potential (MAP) and pacing stimuli recorded during the S1–S2 extrastimulus effective refractory period (ERP) protocol with the analysis of standard electrical restitution

Monophasic action potentials (MAP) and right ventricular pacing stimulus used for the determination of ERP and standard electrical restitution with 20 stimuli delivered during the drive train (S1) at 300 ms cycle length and an extra stimulus (S2). Lower Panel: Expanded section from Upper Panel showing the calculation of diastolic interval (DI) and measurement of MAP duration at 90% repolarization (MAPD₉₀). Image taken with permission from Ng et al, 2007.

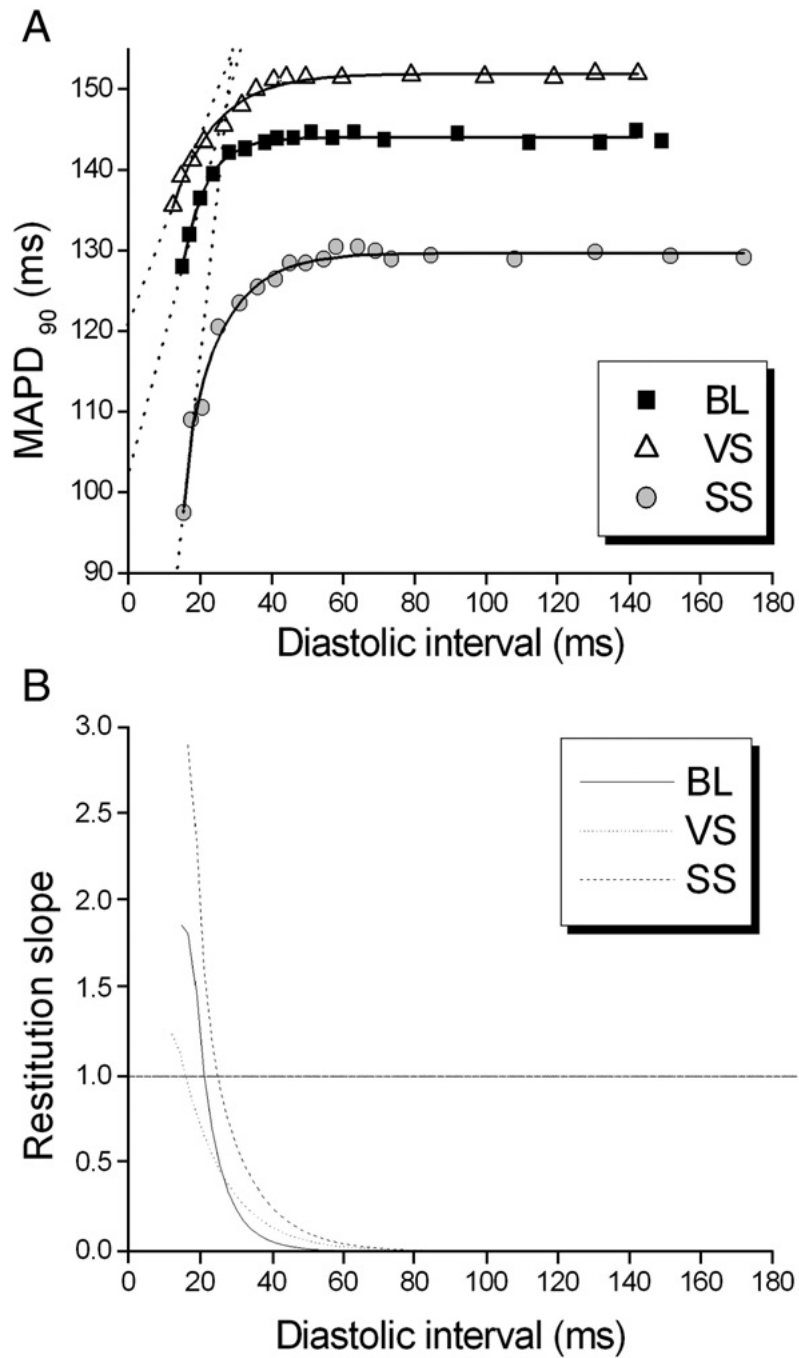


Figure 3.4 Exponential fit of a restitution curve plot and maximum slope of exponential fit
Example plotting and fitting of restitution analysis of baseline (BL), vagal stimulation (VS), and sympathetic stimulation (SS). B) Maximum slope of exponential fit of BL, VS, and SS. Image taken with permission from Ng et al, 2007

3.7 Ventricular Fibrillation Threshold protocol

Another electrophysiological parameter, Ventricular Fibrillation Threshold (VFT), was performed by a different protocol (Ng et al., 2007). VFT was obtained with right ventricular pacing using a rapid pacing protocol. The DT was checked prior the protocol to guarantee the heart was captured at lower than 0.5 mA. Protocol used a train of 20 stimuli drive train (CL 300 ms) spanning the refractory period of MAPs followed by a train of 30 stimuli (30 ms interval) at the end. A 500 milliseconds break was allowed between the next set of pacing train if no VF was induced by the current stimuli. The strength of RV pacing current was started at 0.5 mA and progressively increased by 0.5 mA step in each round until it caused sustained VF (VFT), as displayed in figure 3.5. VFT was defined as the minimum current required to produce sustained VF, which can be monitored by ECG and MAP channels from LabChart. Hearts were cardioverted from VF to normal sinus rhythm with a bolus injection of KCl. After that, a minimum resting time 10 minutes was required before starting a new VFT test. In case that increasing of VFT to 30 mA was unable to induce a sustain VF under the baseline condition, the protocol was terminated and data was excluded. One set of electrophysiology parameters (ERP, MAPDR₉₀, and VFT) were obtained from the same preparation.

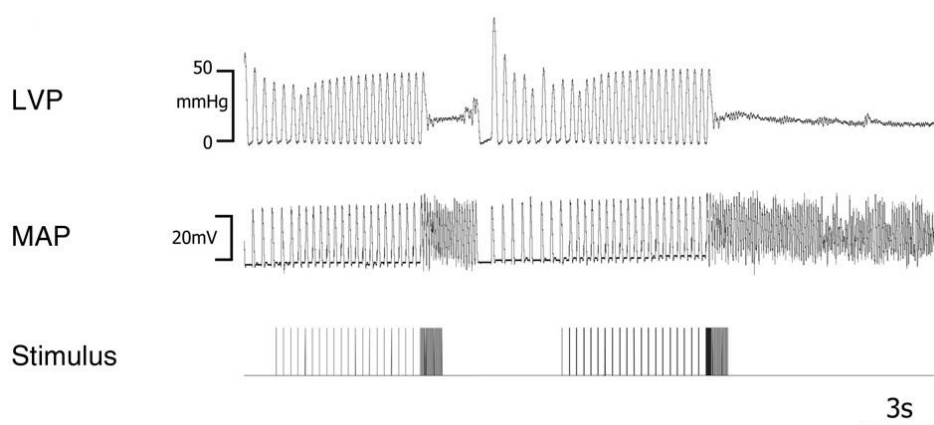


Figure 3.5 Ventricular fibrillation threshold protocol

Left ventricular (LV) pressure, monophasic action potentials (MAP) and ventricular pacing stimulus during the determination of ventricular fibrillation (VF) threshold. Stimulus train comprises of the first run of 20 beats at 300 ms cycle length followed by 30 stimuli (30 ms interval). Image taken with permission from Ng et al, 2007

3.8 Nitric Oxide level by using a single bifurcated light guide system

Nitric Oxide (NO) release in the LV is known to modify ion channels function, which results in alteration of the MAP at the organ level. Therefore, NO release was indirectly measured in this study to investigate whether there was a correlation between the NO changes and the changes in electrophysiological parameters. Real-time NO monitoring in a beating heart was carried out using a single bifurcated light guide system together with the NO sensitive fluorescent indicator, DAF-2 DA (Patel et al., 2008). This system measured an NO-dependent fluorescence signal from the LV epicardia. The NO fluorescence (NOFL) experiments were studied separately from an electrophysiology experiment.

3.8.1 Single bifurcated light guide system

The Optoscan spectrophotometer modular system (Cairn Research Ltd, Faversham, UK) was used, as shown in figure 3.6. The light was generated by the high stability 75W Xenon arc lamp from the light source unit and was transmitted to the Monochromator. Then, the light was separated into 4 bandwidths by the Monochromator: 470 ± 10 nm (F470), 480 ± 10 nm (F480), 490 ± 10 nm (F490), and 500 ± 10 nm (F500). All excitation lights were transmitted to the tip of bifurcated light guide probe through the optic fibre cable. At the tip, there were two concentrically arranged sets of fibres. The central set was used to radiate the excitation light to heart while the peripheral set was used to collect emitted fluorescence from the heart. The light guide was placed on the left ventricular free wall with a positioned perpendicular to the epicardial surface. Epicardial fluorescence at 470 nm, 480 nm, 490 nm, and 500 nm were measured for 20, 20, 8 and 2 ms, respectively. With the fixed gain settings, these measure durations were selected to correct for the fluorescence levels at the specified wavelengths so that the signals could be recorded in a comparable scale. Emission wavelengths were collected at 535 nm with a 50-nm bandpass filter and were processed through the photomultiplier (PMT). PMT measured the light signal and then converted into electrical signal before sending to the display unit. The PMT voltage gain settings was adjusted before

each experimental protocol to optimise the fluorescence levels and was maintained at the same level throughout each manoeuvre. From 4 recording wavelengths, the signal from the F490 channel was quantitatively largest and most representative of changes in NO (Brack et al., 2009, Patel et al., 2008).

Before loading the dye, background auto fluorescence from the tissue was measured. The DT of the RV pacing was achieved. The heart was paced at double the DT with 300 ms CL. Baseline auto fluorescence were measured and optimised to the maximum comparable scales by increasing the PMT value.

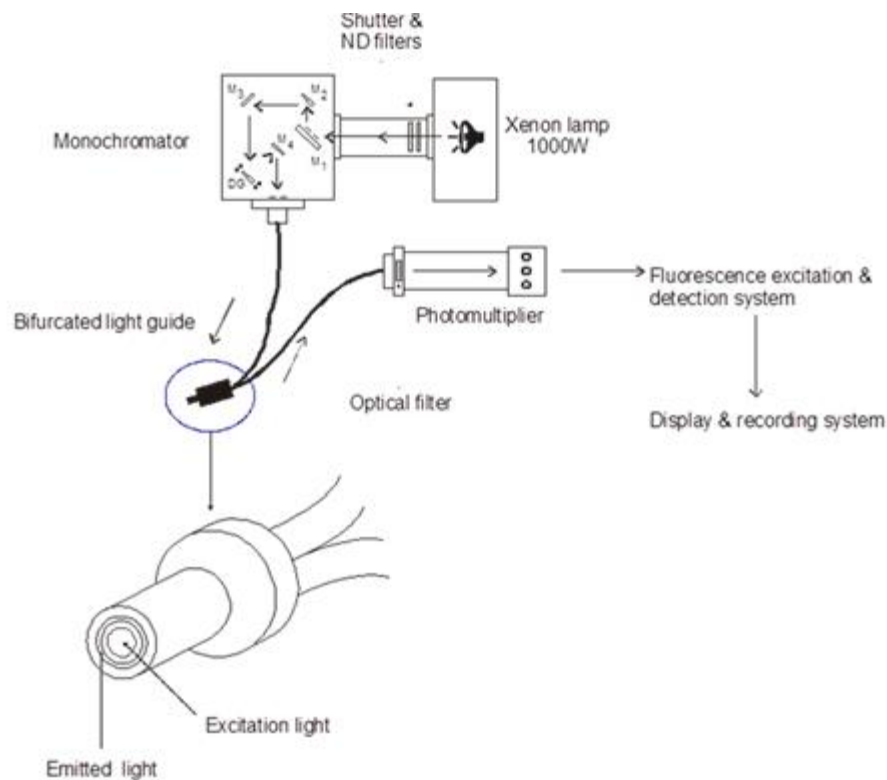


Figure 3.6 Single bifurcated light guide system

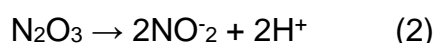
Light was generated inside the Xenon arc lamp. Monochromator separated the light into bandwidths and passed through the heart via probe. Emitted wavelength was measured by the same probe but with a different set of fibres. Photomultiplier optimised the recorded signal into a comparable scale on the display unit.

3.8.2 Fluorescence dye for NO measurement

Level of NO release in the LV was investigated by the 4, 5-diaminofluorescein diacetate (DAF-2 DA) fluorescence dye (Brack et al., 2009, Patel et al., 2008, von Bohlen und Halbach, 2003). Firstly, heart was perfused with Tyrode containing 0.3 mM probenecid (Sigma-Aldrich, Dorset, UK) before loading with DAF-2 DA. This agent prevented intracellular leakage of fluorescence indicators. After probenecid stable (at least 30 minutes), DAF-2 DA (150–250 μ l, 1 μ M; Calbiochem c/o Merck, Nottingham, UK) was injected into the right carotid artery cannula as a single bolus injection and flushed with 5 ml warmed Tyrode solution. This fluorescent dyes is a membrane permeant (von Bohlen und Halbach, 2003). DAF-2 DA was in an inactive form outside the cell. Therefore, a period of 60 min was allowed for intracellular esterases to cleave DAF-2 DA into its active form (von Bohlen und Halbach, 2003). During this waiting period, signals were recorded intermittently until the DAF-2 signal reached equilibrium and baseline fluorescence was stable.

3.8.3 4, 5-Diaminofluorescein diacetate (DAF-2 DA) dye

The Diaminofluorescein (DAF) dye was broadly used for NO fluorescence. The membrane-permeable DAF-2 diacetate (DAF-2 DA) was loaded into cells. Then, the intracellular esterases hydrolyse the ester bonds, which transform to the free DAF-2 (Figure 3.7). DAF-2 was suggested not directly react with the NO. The chemical transformation from 4,5-diaminofluorescein (DAF-2) to highly green-fluorescent triazole form, DAF-2T, is based on the reactivity of DAF-2 with Nitrous Anhydride (N_2O_3) in the presence of dioxygen (Planchet and Kaiser, 2006).



Fluorescence signal inside the cells increased as a NO concentration - dependent manner, which based on NO production and NO oxidation (Planchet

and Kaiser, 2006). DAF-2T molecules was excited at the wavelength around 495 nm and emitted the green light at 515 nm (von Bohlen und Halbach, 2003).

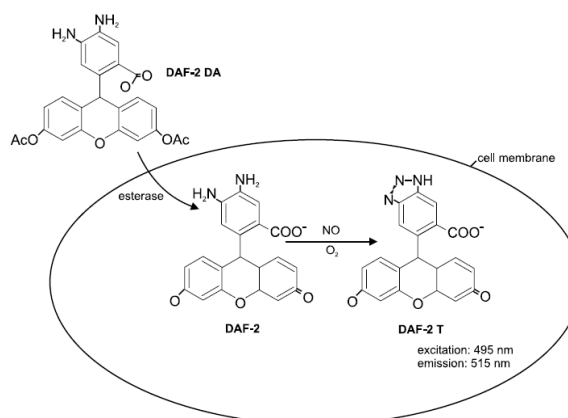


Figure 3.7 4, 5-Diaminofluorescein diacetate (DAF-2 DA) dye for measuring intra-cellular NO in cardiac cell

DAF-2 DA molecule enter into the cell. The intra-cellular esterase hydrolysed the molecules to DAF-2. DAF-2 reacts with intra-cellular NO and transform to fluorescence active form DAF-2T. Image taken from (von Bohlen und Halbach, 2003).

3.8.4 VNS procedures for single bifurcated light guide technique

After baseline NO fluorescence signal under the constant pacing was stable, the light guide probe was placed on the epicardium of LV free wall. PMT was optimised to obtain measurable signals for the 470, 480, 490, and 500 nm channels on LabChart and was maintained to the end of protocol. VNS response signal from recording site was tested by high strength stimulation parameters, for example 10 V 10 Hz 2 ms. If the respond signal increased during VNS, experiment protocol was started. VNS was stimulated from high strength to low strength, for example from 5 Hz to 1 Hz. Stimulation was on 20 seconds and off 30 seconds. Constant pacing was off and the nerve was removed from the stimulation electrodes during a pause time between each sub-protocol. At the same time, warm Tyrode`s solution was applied to the vagus nerve to sustain its viability. In case that respond signal from recording site was not increased by VNS, the probe was re-positioned to another spot on LV free wall.

3.9 Nitric Oxide release in Ventricle by using DAF-2 DA optical mapping

3.9.1 Optical mapping background

Optical mapping is a tool for studying cardiac electrophysiology and arrhythmias (Arora et al., 2003). The Optic system briefly consisted of voltage sensitive dye, light source, filters, and photodetector, displayed in figure 3.8. The voltage sensitive dye was perfused directly into the heart where it bound to the cardiomyocyte cell membrane with high affinity. The light source delivered the excitation light onto the heart, which then excited the molecules of the voltage sensitive dye. The excited dye molecules then emitted light at a different wavelength to the light from the excitation light corresponding to the membrane voltage. A dichroic mirror reflected the excitation light to the cardiac surface whereas the emission filter allowed the emitted wavelength of light from the heart to pass to the detector and blocked other lights. The fluorescence signal was recorded by the detector, which transformed the light into a measureable electrical signal.

Optical mapping system with di-4-ANEPPS, a voltage sensitive dye, enabled the study of activation, repolarization, and propagation of electrical signal on the surface of the heart (Attin and Clusin, 2009). For an electrophysiology study, the excitation – contraction uncoupler (2,3-butanedione monoxime (BDM)) was required as it was important for the reduction of the motion artefact (Attin and Clusin, 2009). Signals that represent voltage changes by this technique were not absolute values and so the reported signal were either change in fluorescence (ΔF) or normalised fluorescence change ($\Delta F/F$) (Attin and Clusin, 2009).

Optical mapping technique was capable of evaluating changes of fluorescence signal from the wide area of the heart. In contrast, measurement of NOFL by single bifurcated light guide system was able to monitor signal from one small area of the heart. Therefore, the optical mapping of DAF-2 DA dye to investigate change of NO level in the ventricular free wall was first applied in this study.

Optical mapping setting, as used for study cardiac electrophysiology, was used in conjunction with the DAF-2 DA dye to measure the level and characteristic of NO release in rabbit ventricle. Light source, dichroic mirror, and filters of the optic system were adjusted to make the system compatible with the DAF-2 DA dye.

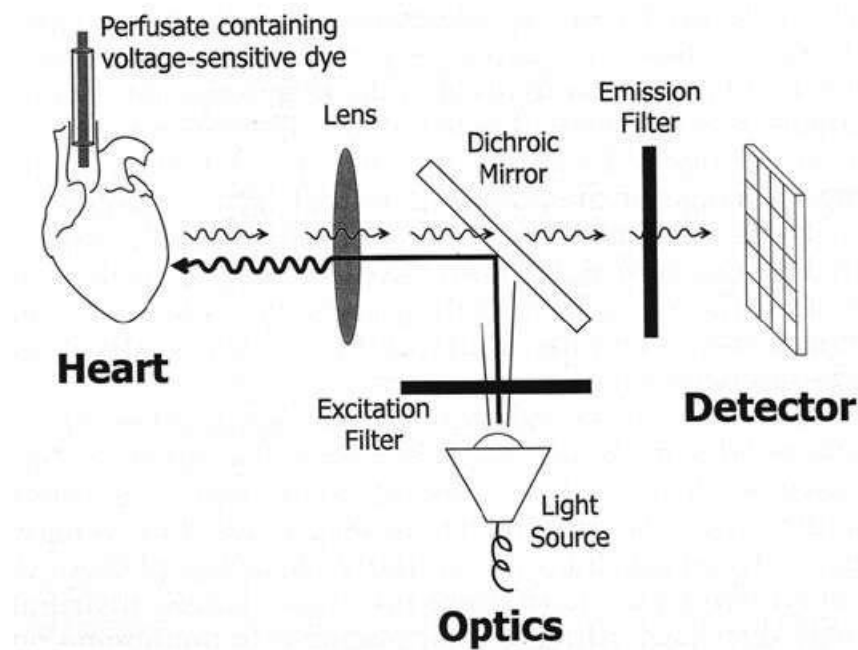


Figure 3.8 Optical mapping system with the Langendorff heart perfusion for cardiac electrophysiology study

Optical mapping scheme for studying cardiac electrophysiology. Light source provided an excitation light that was selectively reflected at a specific wavelength to deliver to the heart. Excited voltage sensitive dye molecules at cell membrane emitted different wavelength light that were filtered before measuring by the detector. Image taken from (Arora et al., 2003).

3.9.2 DAF-2 optical mapping apparatus

Optical mapping systems used for studying ventricular NO level comprised a light source, DAF-2 DA dye, filters, detectors, and excitation-contraction uncoupler.

3.9.2.1 Light source

The light source used for excitation light was the OptoLED, the light-emitting diode (LED), with a wavelength of 470 nm (Cairn Research Ltd, Faversham, UK). This LED light source provided a high intensity light with a stable wavelength.

3.9.2.2 4, 5-Diaminofluorescein diacetate (DAF-2 DA) dye

DAF-2 DA dye administration was performed using the same technique as single bifurcated light guide technique.

3.9.2.3 Filter systems

Filter systems consisted of dichroic mirror and 535/50m bandpass filter (Chroma Technology Corporation, Vermont, USA). The dichroic mirror reflects all of the 470 nm light from the LED light source to the heart. The 470 nm light excited the DAF-2T molecules, which then emitted the 535 nm light in a direction towards the dichroic mirror. The dichroic mirror allowed only wavelengths longer than 510 nm to pass through the filter and so on to the detector, respectively. After that, the 535/50m bandpass filter allowed the wavelength from 510 – 560 nm to pass through the photodetector. Emitted light signal from the heart that passed the dichroic mirror was displayed in the black line in figure 3.9 and signal that was filtered by the bandpass filter was shown in a red line in figure 3.9.

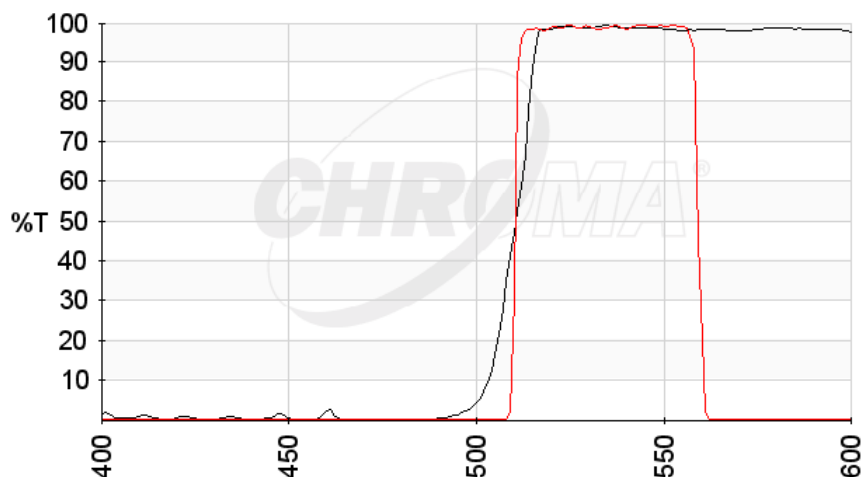


Figure 3.9 Wavelength allowance (percentage of transmission (%T)) of DAF-2 optical mapping filter system

Emitted light from the heart was cut off by dichroic mirror at 510 nm. Wavelengths longer than 510 nm were passed through dichroic mirror (black line). Then, the light was filtered to allow wavelength from 510 to 560 nm (red line) to reach the photodetector. Image taken from (<https://www.chroma.com/products/sets/49011-et-fitc-alexa-fluor-488-fluo3-oregon-green>).

3.9.2.4 Detectors

The 16 × 16 (256) element photodiode array detector (C4675-102, Hamamatsu Photonics UK Limited, Hertfordshire, UK) was used as a photodetector in this setting. This 2 dimensional arrays continuously transduced the light photon into an electrical signal (Arora et al., 2003). Signal was transmitted to the NI PXI-8110 processing module (National Instruments Corporation, Texas, USA). Recording and analysis were done by QRecord software.

3.9.2.5 Excitation - contraction uncoupler

The photodetector array measures fluorescence signals from a single area of the heart. A beating heart can alter the quality of the recorded signal, known as motion artefact. Therefore, an excitation – contraction (E-C) uncoupler was applied to the Langendorff perfused heart in order to stop the heart from beating while preserving all other electrical activities. For cardiac

electrophysiological investigation, blebbistatin is widely used (Attin and Clusin, 2009, Fedorov et al., 2007). Blebbistatin targets the interaction between actin – myosin of cardiac cells. In Langendorff-perfused rabbit hearts, blebbistatin prolonged MAP duration and increased MAPDR slope. VFT was also increased by perfusion of this E-C uncoupler (Brack et al., 2013b). Moreover, this agent was not cost – effective. Another E-C uncoupler that frequently used for optical study was 2, 3 – butanedione monoxime (BDM). Although, BDM was a cost – effective agent, it was not suitable for electrophysiology study because it reduced an action potential duration and attenuated calcium current (Attin and Clusin, 2009). As DAF-2 optic technique focused on changing of NO level in ventricle with less attention on cardiac electrophysiology, a low cost agent, the BDM, was used as an E-C uncoupler in this optic experiment.

3.9.3 DAF-2 optical mapping protocol

DAF-2 optical mapping of isolated innervated rabbit heart preparation utilised a similar protocol to NO fluorescence by bifurcated light guided system. The main limitation of NO by single light guide was it records signal at a small area of the LV while optical mapping records NO release across the LV free wall at one time. Optical experiments were started with a voltage and frequency response curve. Unlike single light guided technique, the constant pacing was not required in this protocol. This technique was done under normal sinus rhythm. However, NO by optical mapping also required probenecid to prevent an intra-cellular leakage of the DAF-2T, an active fluorescence form of DAF-2 DA dye, out from the cell. Probenecid 0.3 mM (Sigma-Aldrich, Dorset, UK) was perfused to the heart through the aortic cannula 30 minutes before dye loading. Once probenecid stable, DAF-2 DA dye (150–250 μ l, 1 μ M; Calbiochem c/o Merck, Nottingham, UK) loading was intermittently injected with 5 ml Tyrode`s solution through the cannula attached to the right common carotid artery and 60 minutes waiting time needed for stabilise the dye. BDM (20 mM, Sigma-Aldrich), mechanical un – couple agent, was perfused through the heart by mixed with Tyrode`s solution.

After the heart stopped beating, the isolated innervated rabbit heart preparation was repositioned to locate the LV anterior wall on a recording field. The focal area was adjusted by changing the distance between the heart and the photodetector, which was monitored by the Watec monochrome camera (WAT-902B, Camtronics BV, Eindhoven, Netherlands). Once the LV anterior wall was in focus, LED 470 nm light was turned on. The LED intensity was maximised by increasing current from light source power supply.

The fluorescence signals were recorded under basal and VNS conditions. VNS was started from high strength to low strength. Stimulation was on approximately 30 seconds at a time with at least 30 seconds break between each stimulation. Vagus nerve was rested for around 2 minutes between each sub – protocol and Tyrode`s applied.

3.10 Statistical analysis

Experimental data collected included, voltage used (V), HR change (bpm), ERP (ms), VFT (mA), MAPDR₉₀ maximum slope, and fractional change of fluorescence signal ($\Delta F/F$). The measured parameters were continuous variables. Absolute change and percentage change from baseline were calculated. Data were presented as mean \pm SEM and analysed using two way ANOVA with Bonferroni post hoc test, unless indicated in the text. $P < 0.05$ was considered significant and reported as * $P < 0.05$, ** $P < 0.01$, *** $P < 0.001$, and **** $P < 0.0001$. Differences between baseline and VNS were compared. Comparisons between different stimulation frequencies and pulse widths were investigated.

Chapter 4 Preliminary effects of different stimulation voltage and frequency on ventricular electrophysiology and NO release in the isolated rabbit heart

4.1 Background of VNS impact on electrophysiology and an involvement of NO

In many cardiac electrophysiology studies, the vagus nerve was stimulated to protect the heart against arrhythmias. As a result, vagus nerve stimulation (VNS) showed anti-atrial fibrillation and prevent loss of Connexin43 (Li et al., 2009, Ando et al., 2005). Ventricular arrhythmia was also suppressed by VNS in the literature (Zhang et al., 2016). Stimulation frequency ranging from 5 to 20 Hz were employed within these studies while variety of pulse widths (PW), from 0.1 to 3 ms, were used (Chen et al., 2015, He et al., 2013b, Shen et al., 2013, Kawada et al., 2008). Regarding voltage strength, some studies employed a fixed voltage stimulation (Uemura et al., 2010, Kawada et al., 2008, Takei et al., 2001). On the other hand, some studies utilized an flexible voltage that correlated to physiological responses such as percent heart rate (HR) reduction or AV conduction prolongation (Shinlapawittayatorn et al., 2013, Sheng et al., 2011, Shen et al., 2011, Li et al., 2009). A 10% heart rate reduction from a resting baseline value was mainly used as a reference point for adjusting the voltage amplitude, called low level vagus nerve stimulation (LLVS) (Stavrakis et al., 2015, Shinlapawittayatorn et al., 2013). From these studies, there were a variety of stimulation parameters (voltage, frequency, and pulse width) that were set for recruiting the neuron fibres within the vagus nerve. As the vagus nerve is comprised of many group of nerve fibres, different activation combinations would recruit different groups of neuron and therefore have a different impact on cardiac function.

To focus on an anti-ventricular arrhythmia effects, a rabbit model was utilized as it represents a well characterized animal model that is considered as a good model for representing human cardiac repolarization (Baczko et al., 2016). To

study an anti – arrhythmic mechanism of vagus nerve, previous work on the VNS of the isolated innervated rabbit heart used the voltage that produced 80% of the maximum heart rate reduction. The maximum level of heart rate drop was defined from unilateral stimulation of the nerve by frequency 5 Hz and voltage from 1 V to 20 V with pulse width 2 ms (Brack et al., 2011, Ng et al., 2007). Average frequency used for this study was 10.8 ± 2.4 Hz. Prolongation of effective refractory period (ERP), flattened monophasic action potential duration restitution (MAPDR) slope, increased ventricular fibrillation threshold (VFT), and increased ventricular nitric (NO) level in the left ventricle by unilateral VNS have been previously reported (Brack et al., 2011). The anti - arrhythmic protection acted through the post-ganglionic efferent fibres of rabbit vagus. Despite protecting the heart against ventricular arrhythmia, VNS by these high amplitude voltages and high frequencies are accompanied by large heart rate (HR) changes, which would not be appropriate to be used clinically.

Most of this current study was focused on the protective effects of vagal stimulation on the heart against arrhythmias. It is clear that there is further need to establish what is the optimal activation of the vagal nerve or what is the appropriate approach of vagal fibre recruitment. It is important to investigate the effects of stimulation voltage and stimulation frequency used to excite vagus nerve in the preclinical stage in order to provide an essential understanding of stimulation parameters and its effect on cardiac function for the potential clinical translation.

4.2 Chapter objectives

- 1) To investigate ventricular electrophysiological responses to electrical cervical vagus nerve stimulation by a high amplitude voltage
- 2) To evaluate effects of high frequency electrical cervical vagus nerve stimulation on ventricular electrophysiology
- 3) To assess nitric oxide release in rabbit left ventricle in response to the high amplitude voltage and high frequency stimulations

4.3 VNS parameters

In this chapter, parameters were designed to assess the effect of voltage and frequency on HR change and ventricular electrophysiology. Firstly, voltage response curve was performed by using unilateral (left or right) VNS by frequency 5 Hz, pulse width 2 ms, and voltages from 1 to 20 V in order to identify the maximum HR reduction level. Then, HR reduction at 80% of the maximum value was calculated and was used as a reference value. From voltage response curve, a voltage that lowers HR close to the 80% of maximum HR reduction was defined as high amplitude voltage and was used for stimulating the nerve with frequency of 1, 2, 3, or 5 Hz and pulse width 2 ms. This parameter set was aimed to test effects of a high amplitude voltage stimulation on cardiac functions.

Additionally, another set of VNS parameter was designed to test effects of high frequency stimulation on the heart. In this stimulation, voltage that reduced HR less than 10% from baseline value during unilateral (left or right) VNS by frequency 20 Hz and pulse width 0.1 ms was configured. Then, this low amplitude voltage was used with high frequencies 10, 20, and 30 Hz and pulse width 0.1 ms to activate vagus nerve.

The heart rate change, effective refractory period (ERP), ventricular fibrillation threshold (VFT), and monophasic action potential duration restitution (MAPDR) were evaluated together with nitric oxide (NO) release by DAF-2 NOFL assessment.

Stimulation aspect	Voltage (V)	Frequency (Hz)	Pulse width (ms)
Strong voltage	80% ΔHR_{\max}	1, 2, 3, and 5	2
High frequency	10% $\Delta HR_{\text{baseline}}$	10, 20, and 30	0.1

4.4 The Langendorff perfused isolated innervated rabbit heart preparation

The isolated innervated rabbit heart preparation was connected to the Langendorff perfusion circuit as shown in figure 4.1. Tyrode's solution was perfused into the preparation at rate 100 ml/min through an aortic cannula attached to descending thoracic aorta, as shown in A in figure 4.1. Both sides of pulmonary arteries and lungs were tied off and cut. Circulation to the lung was not necessary as Tyrode's was already bubbled by Carbogen gas. Then, left ventricular (LV) vent, showed as B in figure 4.1, were inserted into LV apex through a small hole created on left atrium. During this stage, flow rate was reduce to 50% of target flowrate and ice cold Tyrode's was applied to the preparation in order to reduce the contraction and metabolism rate. After that, LV balloon, displayed as C in figure 4.1, was inserted into LV and secured in position by silk suture tied at the left atrium. Then, flow rate was turned back to full flow and ECG leads, shown as D, in figure 4.1, was attached to the preparation in a direction of bipolar limb lead II. Resting period about 5 to 10 minutes was given until all recording signals were stable. Solution was not re-circulated. Effluent fluid was drained out from the preparation through a hole created on pulmonary artery at the level of the right ventricular outflow tract (RVOT). After that, the vagus nerve was placed on a custom made bipolar silver electrode, displayed as E in figure 4.1, and protocol started.

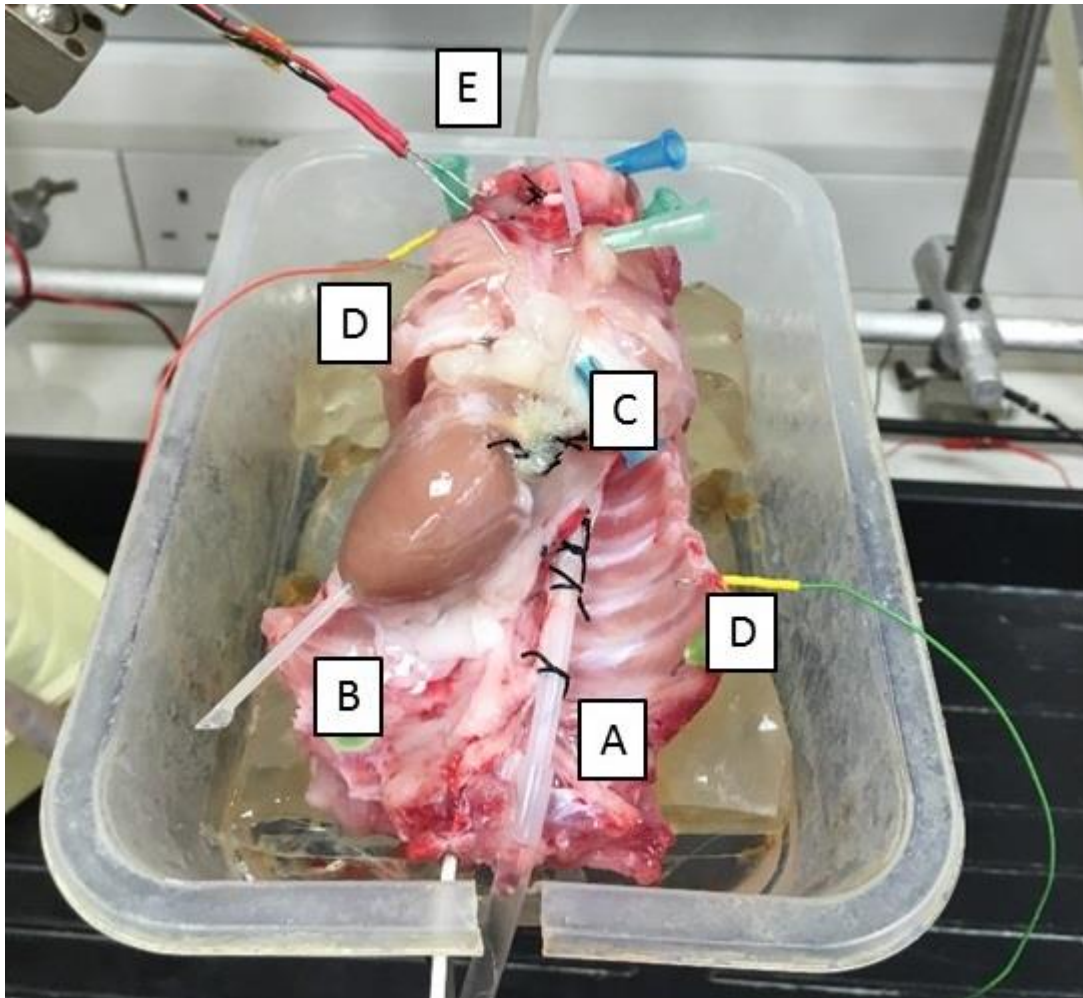


Figure 4.1 The isolated innervated rabbit heart preparation

A) aortic cannula for perfusion of Tyrode's solution attached to the descending thoracic aorta, B) LV vent for draining of excessive fluid, C) LV balloon inserted through the left atrium, D) ECG leads attached to the preparation in a vector of bi-polar limb lead II, and E) a custom made bipolar silver electrode for unilateral stimulation of vagus nerve.

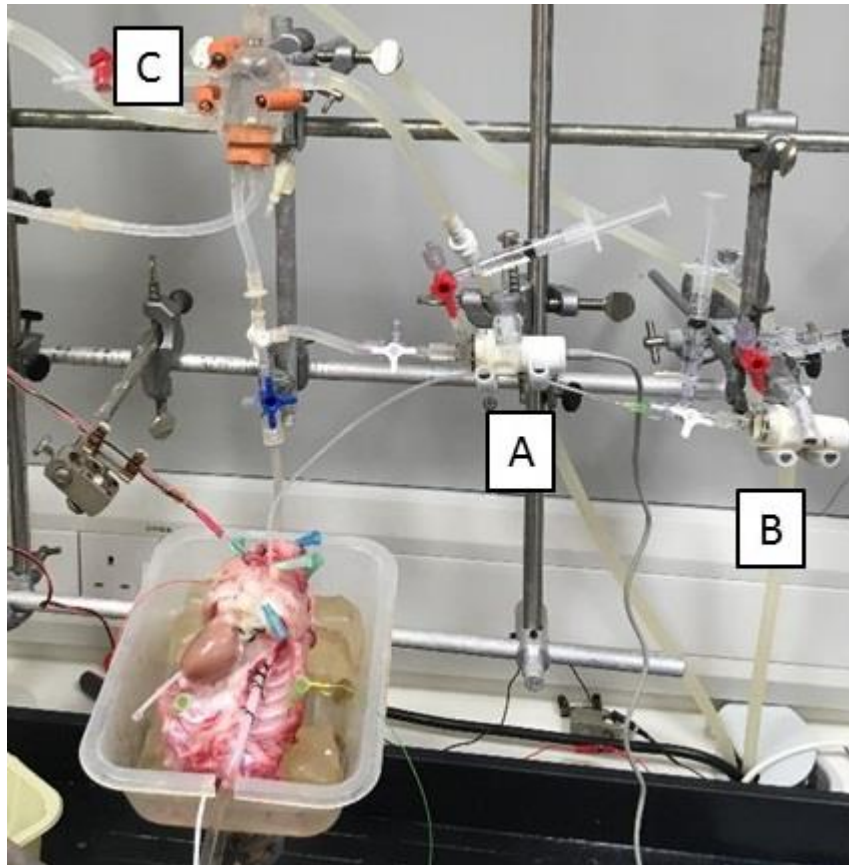


Figure 4.2 Langendorff perfusion of isolated innervated rabbit heart preparation

A) monitoring of perfusion pressure during an experiment by a pressure transducer side connected to aortic cannula, B) monitoring of developed LV pressure by a pressure transducer connected to a custom made rubber balloon inserted into LV, C) bubble trap use for prevention of air emboli to the preparation.

4.5 Haemodynamic respond the unilateral VNS

Recording of haemodynamic parameters from the preparation is shown in figure 4.3. Vagus nerve was electrical activated. From figure 4.3A, stimulation by the 80% HR_{max} (high amplitude) voltage lowered HR during VNSs and also caused decreases of LVP. A decreased in left ventricular pressure (LVP) by this stimulation was not a direct lusitropy effect but was a secondary outcome of the negative chronotropic impact of VNS (Brack et al., 2006). Perfusion pressure (PP) remained constant throughout the experiment.

For another stimulation aspect, the 10%HR_{baseline} (low amplitude) voltage VNSs produced HR reduction and decreases of LVP similar to the previous high amplitude stimulation, as displayed in figure 4.3B. However, HR reductions by this low strength voltage stimuli were smaller than HR reduction by the 80%HR_{max} voltage. Decrease of LVP was a result of the negative chronotropic and PP was stable similar to the response of high amplitude voltage in figure 4.3A.

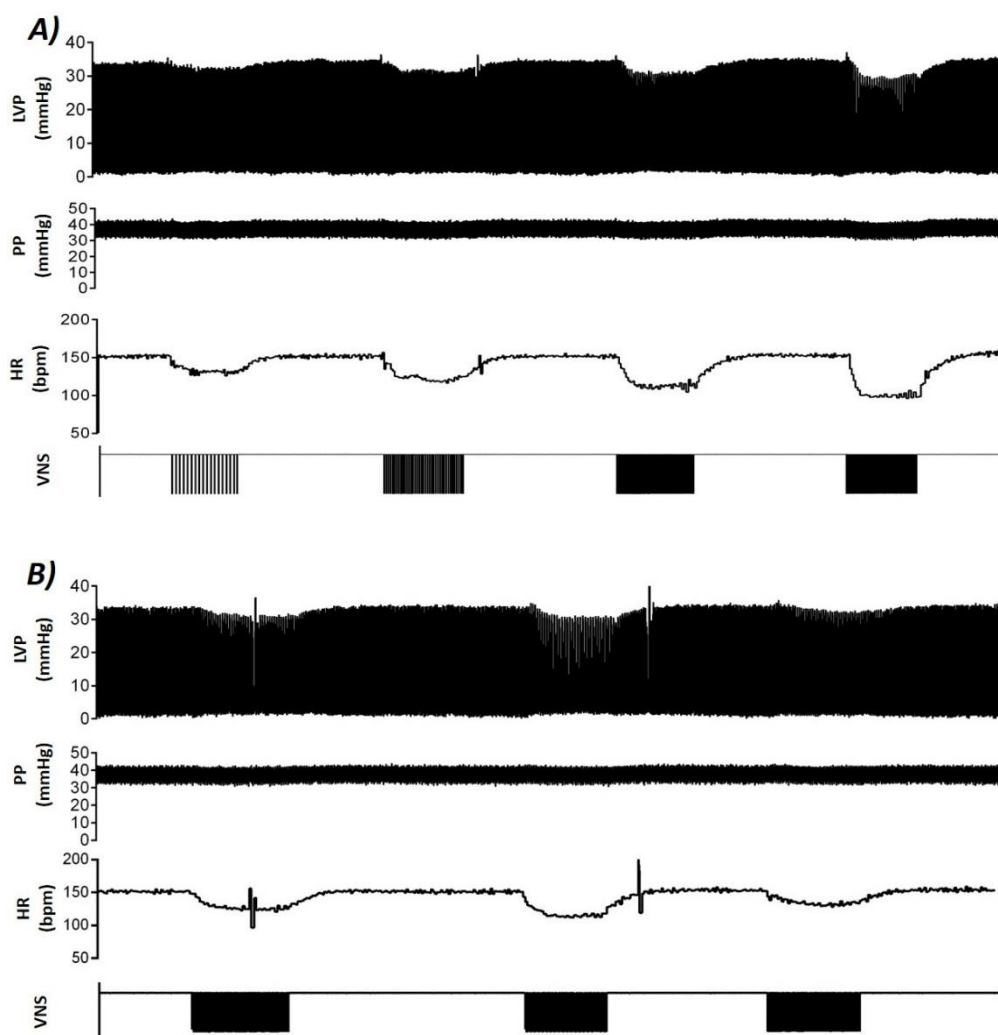


Figure 4.3 Raw tracing recording from LabChart software

Haemodynamic responds of an isolated innervated rabbit heart preparation to the unilateral VNS by A) strong voltage protocol and B) high frequency protocol. Left ventricular pressure (LVP), Perfusion pressure (PP), Heart rate (HR), and Vagus nerve stimulation (VNS).

4.6 Voltage and frequency configurations

4.6.1 Voltage response curve

Firstly, a voltage response curve was carried out (sequences from 1 V to 20 V) to establish the voltage that produced the maximum heart rate reduction. Either right or left vagus nerve was unilaterally stimulated by a stimulus at 5 Hz 2 ms. Heart rate response to the voltage curve is shown in figure 4.4. In this voltage curve, VNS significantly reduced heart rate in all stimulus strengths. Baseline heart rate was ranging between 159.3 ± 5.5 bpm to 159.8 ± 5.4 bpm and there was no significant difference between baseline heart rate at all stimulation voltages. The 1 volt stimulus significantly dropped HR from 159.8 ± 5.4 bpm to 139.4 ± 9.6 bpm ($P < 0.0001$). A significant difference between heart rate reductions by nerve activation was found between 1 V and 2 V stimuli (139.4 ± 9.6 bpm vs 113.7 ± 11.3 bpm, $P < 0.0001$). There was no significant difference in heart rate reduction by vagus activation from 2 V to 20 V stimuli.

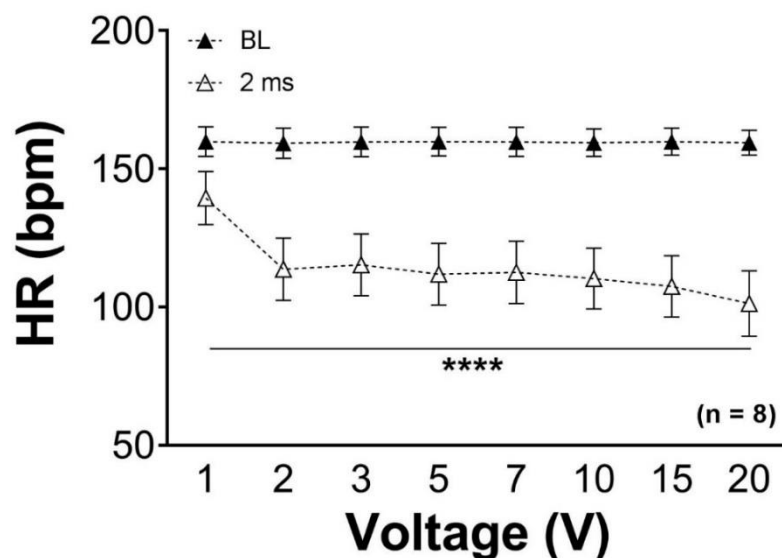


Figure 4.4 Voltage response curve of strong voltage stimulation

Unilateral (mixtures of left and right) VNS at frequency 5 Hz with PW 2 ms from voltage 1 to 20 stimuli. Heart rate (HR), baseline (BL), beat per min (bpm), volt (V); $n = 8$, mean \pm SEM., Two-way ANOVA with Bonferroni post test, **** $P < 0.0001$.

4.6.2 Frequency response curve

4.6.2.1 Low frequency response curve

The maximum heart rate reduction was identified in figure 4.4. Then, the reduction at 80% of the maximum value was calculated. An associated voltage to this 80% value was used for the following protocols. This 80% ΔHR_{max} voltage was used to stimulate the vagus at frequency 1, 2, 3, and 5 Hz. This high amplitude voltage was used under an assumption that a high amplitude voltage stimulus may recruit large fibres inside the vagus. The 80% ΔHR_{max} (5.63 ± 1.22 V, $n = 8$) significantly reduced heart rate at all frequencies, as shown in figure 4.5. The degree of heart rate reduction by the high amplitude voltage was found to be frequency dependent as a higher frequency stimulus significantly decreased heart rate more than a lower frequency; 1 Hz (151.9 ± 5.6 bpm to 137.0 ± 5.8 bpm, $P < 0.01$), 2 Hz (151.5 ± 5.6 bpm to 125.0 ± 8.6 bpm, $P < 0.0001$), 3 Hz (151.7 ± 5.8 bpm to 116.1 ± 8.3 bpm, $P < 0.0001$), and 5 Hz (153.1 ± 5.9 bpm to 105.3 ± 8.8 bpm, $P < 0.0001$). The baseline heart rate was stable. The 2 Hz stimulus significantly lowered heart rate more than the 1 Hz stimulus (125.0 ± 8.6 bpm vs 137.0 ± 5.8 bpm, $P < 0.05$) and 5 Hz was also significantly reduced heart rate more than the 3 Hz (105.3 ± 8.8 bpm vs 116.1 ± 8.3 bpm, $P < 0.05$). There was no significant difference between 2 Hz and 3 Hz heart rate reduction.

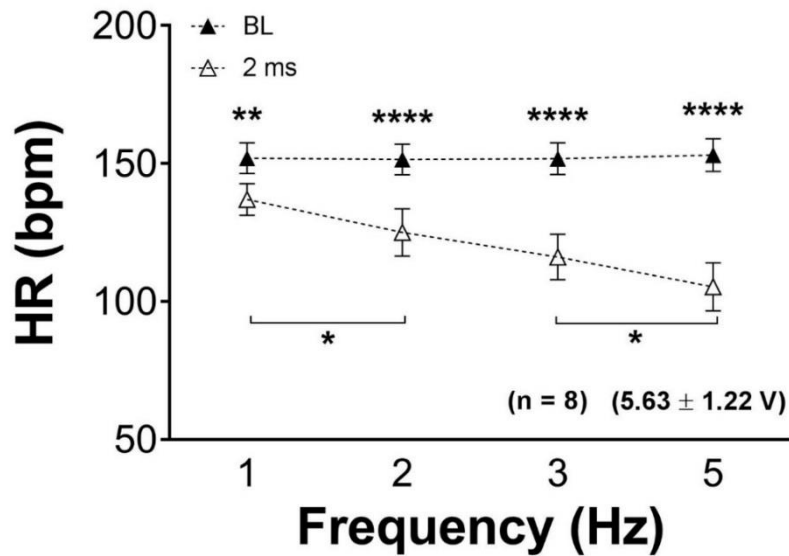


Figure 4.5 Frequency response curve of strong voltage stimulation

Unilateral (mixtures of left and right) VNS at voltage $80\% \Delta HR_{\max}$ (5.63 ± 1.22 V) with PW 2 ms for frequency 1, 2, 3, and 5 Hz stimuli. Heart rate (HR), baseline (BL), beat per min (bpm), volt (V); $n = 8$, mean \pm SEM., Two-way ANOVA with Bonferroni post test, * $P < 0.05$, ** $P < 0.01$, **** $P < 0.0001$.

4.6.2.2 High frequency response curve

The high frequency stimulation was designed to target a different group of nerve fibres (a small diameter fibres) inside the vagus. A small voltage that reduced heart rate from baseline value less than 10% was used instead of a high amplitude voltage (the voltage $80\% \Delta HR_{\max}$). Instead of using a low frequency, high frequencies (10 Hz, 20 Hz, and 30 Hz) were applied with this low amplitude voltage, which enabled an investigation of effect of stimulation frequency on heart rate reduction and ventricular electrophysiology. To find an optimal voltage, vagus was unilateral activated at frequency 20 Hz with a pulse width 0.1 ms. Voltage was gradually titrated until it produced a stable heart rate reduction at a level less than 10% from baseline value.

For frequency response curve, a low strength voltage (1.79 ± 0.46 V, $n = 5$) reduced heart rate from 165.2 ± 11.3 bpm to 152.7 ± 11.6 bpm (ns) for 10 Hz, from 163.4 ± 11.6 bpm to 147.0 ± 12.9 bpm (ns) for 20 Hz, and from $165.5 \pm$

12.1 bpm to 158.9 ± 15.1 bpm (ns) for 30 Hz stimulation. The baseline heart rate was stable for all stimulation. The 30 Hz stimulation did not produce a significant reduction.

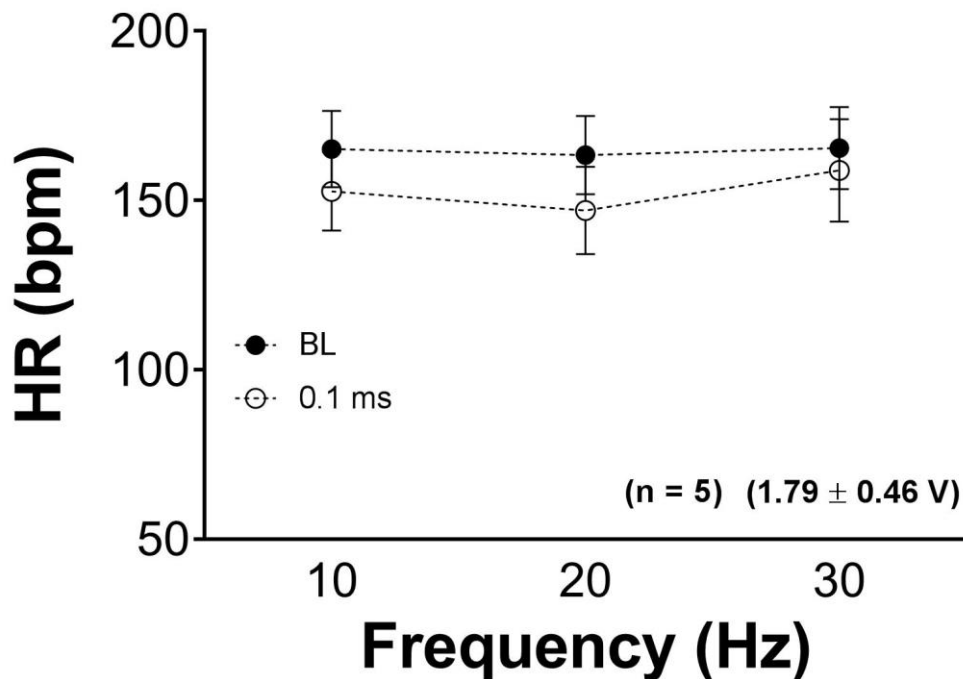


Figure 4.6 Frequency response curve of high frequency stimulation

Unilateral (mixtures of left and right) VNS at voltage $10\% \Delta HR_{BL}$ (1.79 ± 0.46 V) with PW 0.1 ms for frequency 10, 20, and 30 Hz stimuli. Heart rate (HR), baseline (BL), beat per min (bpm), volt (V); $n = 8$, mean \pm SEM.

4.7 Effective refractory period (ERP) protocol

An investigation of ERP of the left ventricle by the S1 – S2 extra stimulus protocol was performed. Relevant parameters of an ERP protocol from one iteration are displayed in figure 4.7. In this figure, pacing stimulus was set at cycle length (CL) 300 ms, which resulted in heart rate 200 bpm during pacing. Nerve stimulation was started prior to the pacing stimuli and caused heart rate to drop to around 100 bpm. Monophasic action potential was recorded from an epicardial surface of the left ventricle by contact electrodes. Figure 4.7 was selected from the end of one stimulus set at the point of S2 stimulus that failed

to produce a capture. For this S1 – S2 extra stimulus protocol, duration between S1 and S2 was progressively shortened. Figure 4.8A showed an example of capturing of S2 pacing spike, which caused an S2 – MAP and a contraction of left ventricle. ERP was defined as a longest S1 – S2 duration that S2 failed to produce any monophasic action potential (MAP) and/or any contraction, as displayed in figure 4.8B.

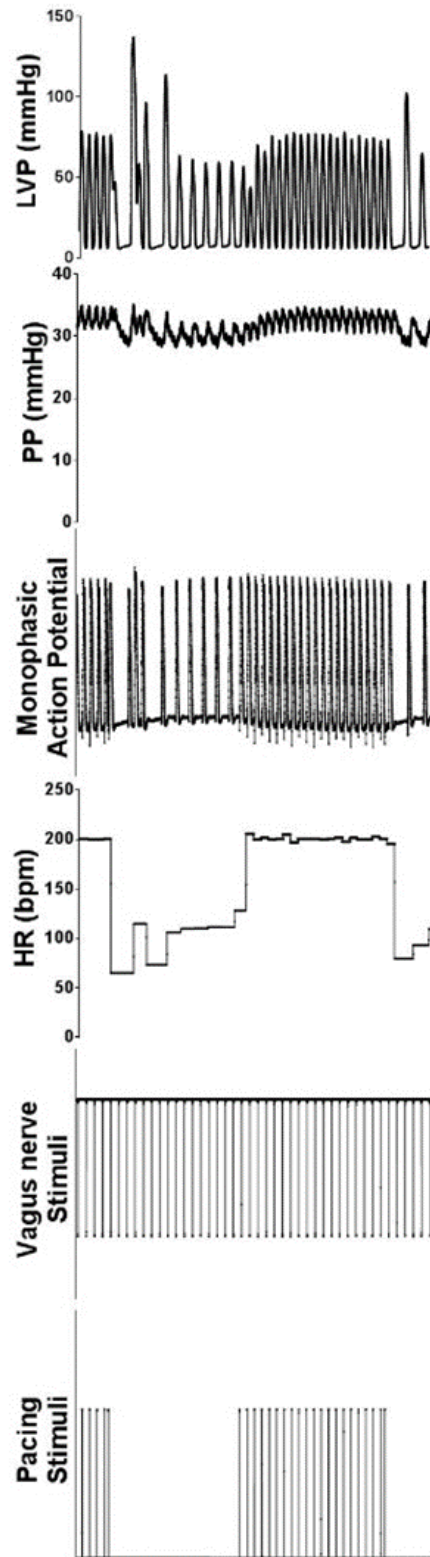


Figure 4.7 Raw tracing of relevant parameters during a set of an S1 – S2 extra stimuli
 Cycle length (CL) of S1 stimuli was 300 ms (HR 200 bpm). Left ventricular pressure (LVP), perfusion pressure (PP), heart rate (HR), beat per min (bpm).

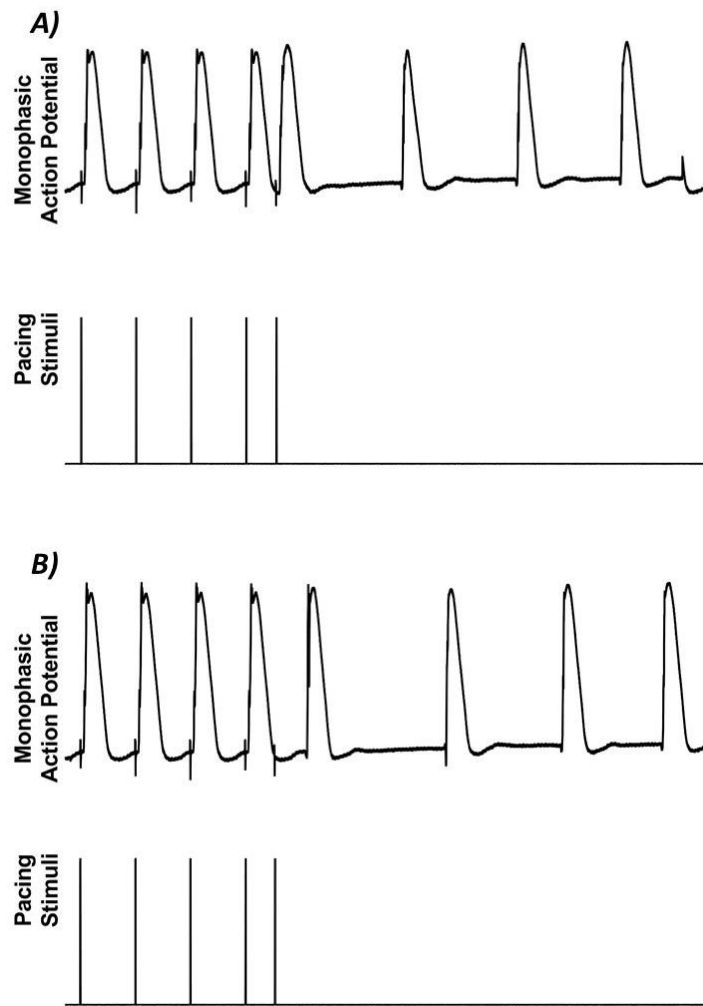


Figure 4.8 Raw tracing of monophasic action potential (MAP) and S1 – S2 pacing spike

A) Capture of S2 pacing spike produced a following MAP and B) failed to capture of S2 pacing spike.

Heart rate reduction during ERP protocol by a high strength voltage was shown in figure 4.9. The $80\% \Delta HR_{max}$ voltage decreased heart rate from 155.0 ± 11.3 bpm to 143.4 ± 10.9 bpm (ns), 164.0 ± 10.1 bpm to 148.3 ± 9.8 bpm (ns), 166.0 ± 9.1 bpm to 131.9 ± 9.6 bpm ($P < 0.001$), and 164.2 ± 8.9 bpm to 117.3 ± 7.7 bpm ($P < 0.001$), for 1, 2, 3, and 5Hz ERP, respectively. There was no significant difference between each baseline heart rate. The 5 Hz stimulation significantly lowered heart rate more than 1 Hz ($P < 0.01$) and 2 Hz ($P < 0.001$)

stimuli. Percentage change of the heart rate was calculated and displayed in figure 4.10. Stimulation by 1 and 2 Hz dropped heart rate by under 10% ($7.6 \pm 1.6\%$ and $8.9 \pm 4.6\%$) while 3 and 5 Hz stimulations caused reduction of $20.2 \pm 4.6\%$ and $26.7 \pm 6.7\%$ from the baseline heart rate. The 5 Hz ERP lowered heart rate more significantly than 1 Hz ERP ($26.7 \pm 6.7\%$ vs $7.6 \pm 1.6\%$, $P < 0.01$) and 2 Hz ERP ($26.7 \pm 6.7\%$ vs $8.9 \pm 4.6\%$, $P < 0.01$).

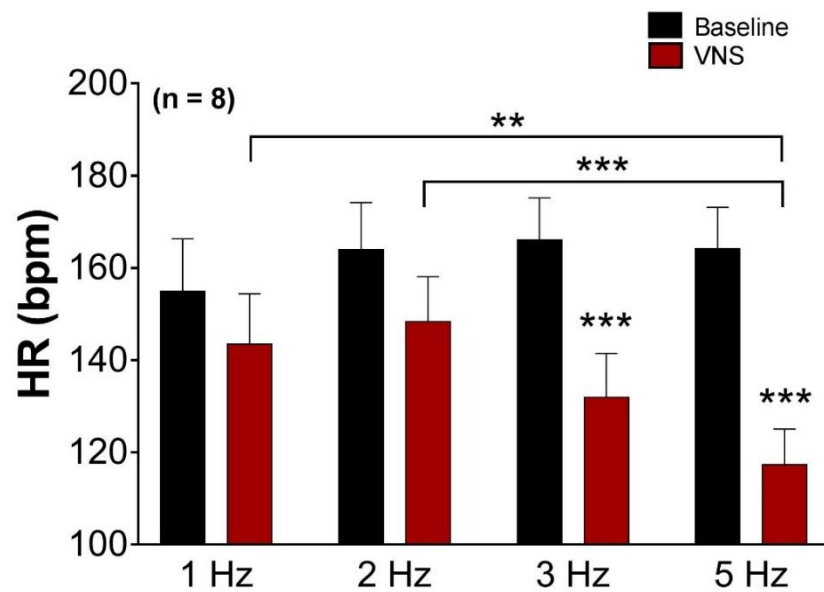


Figure 4.9 Heart rate reduction during ERP protocol by voltage $80\% \Delta HR_{max}$ with pulse width 2 ms

Heart rate (HR), beat per min (bpm); $n = 8$, mean \pm SEM., Two-way ANOVA with Bonferroni post test, ** $P < 0.01$, *** $P < 0.001$.

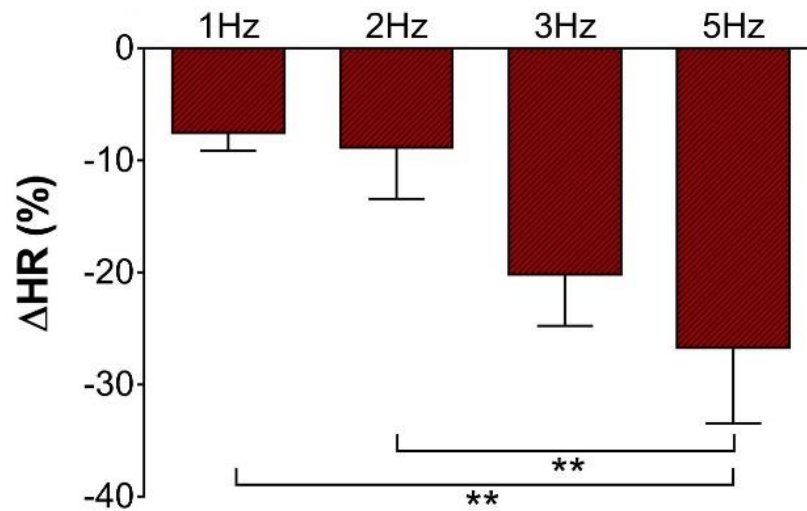


Figure 4.10 Percentage of heart rate decrease during ERP protocol by voltage $80\% \Delta HR_{max}$ with pulse width 2 ms

Heart rate (HR); $n = 8$, mean \pm SEM., One-way ANOVA, ** $P < 0.01$.

For ERP results, stimulation by voltage $80\% \Delta HR_{max}$ prolonged ERP in all stimulation frequencies when compare to baseline, as shown in figure 4.11. The prolongation of ERP displayed a trend of frequency dependent effect; 1 Hz prolonged ERP from 140.6 ± 5.3 ms to 147.5 ± 5.8 ms ($P < 0.05$), 2 Hz prolonged ERP from 143.8 ± 5.8 ms to 149.4 ± 5.3 ms (ns), 3 Hz prolonged ERP from 145.0 ± 5.7 ms to 154.4 ± 4.5 ms ($P < 0.01$), and 5 Hz prolonged ERP from 148.1 ± 5.1 ms to 157.5 ± 4.0 ms ($P < 0.01$). The 5 Hz VNS significantly prolonged ERP more than 1 Hz ($P < 0.01$) and 2 Hz ($P < 0.05$).

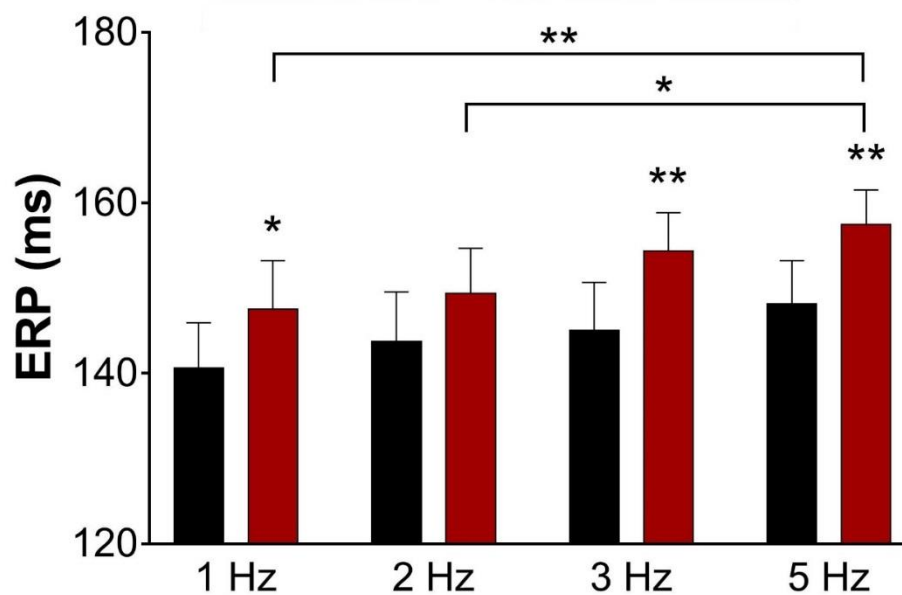


Figure 4.11 ERP prolongation by vagal stimulation at voltage $80\%\Delta HR_{max}$ with pulse width 2 ms

Effective refractory period (ERP), millisecond (ms); $n = 8$, mean \pm SEM., Two-way ANOVA with Bonferroni post test, * $P < 0.05$, ** $P < 0.01$.

For an evaluation of stimulation frequency on ERP response, stimulation by voltage $10\%\Delta HR_{BL}$ ($n = 5$) significantly decreased heart rate by 10 Hz (170.1 ± 11.9 bpm to 148.4 ± 9.8 bpm, $P < 0.05$) and 20 Hz (170.4 ± 11.0 bpm to 145.7 ± 9.7 bpm, $P < 0.01$) stimulations, as displayed in figure 4.12. Furthermore, frequency 30 Hz decreased heart from 176.3 ± 12.0 bpm to 156.4 ± 8.2 bpm (ns). Baseline heart rates were stable for all frequency and there was no significant difference in VNS heart rate reduction by all frequency. Percentages of heart rate change were 11.5 ± 7.2 %, 15.1 ± 7.3 %, and 10.2 ± 5.8 % for 10 Hz, 20 Hz, and 30 Hz respectively (figure 4.13). There was no significant difference between percent heart rate decreases between 3 stimulation frequencies.

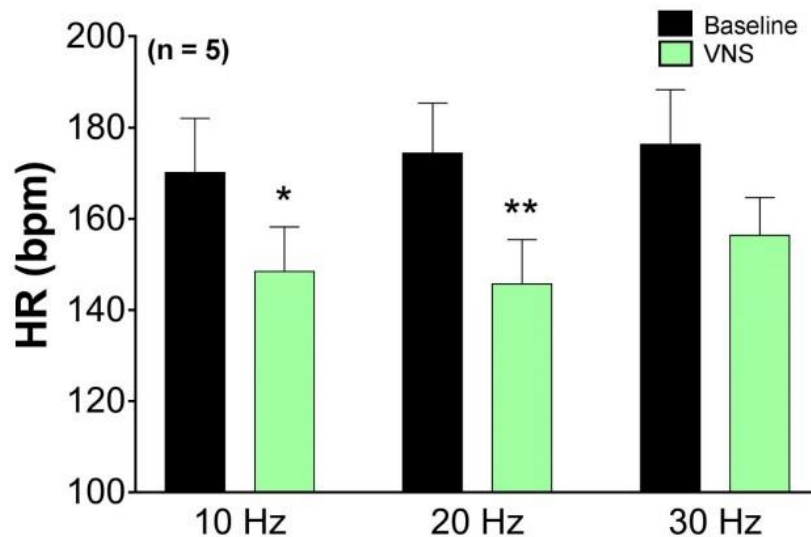


Figure 4.12 Heart rate reduction during ERP protocol by voltage $10\% \Delta HR_{BL}$ with pulse width 0.1 ms

Heart rate (HR), beat per min (bpm); $n = 5$, mean \pm SEM., Two-way ANOVA with Bonferroni post test, * $P < 0.05$, ** $P < 0.01$.

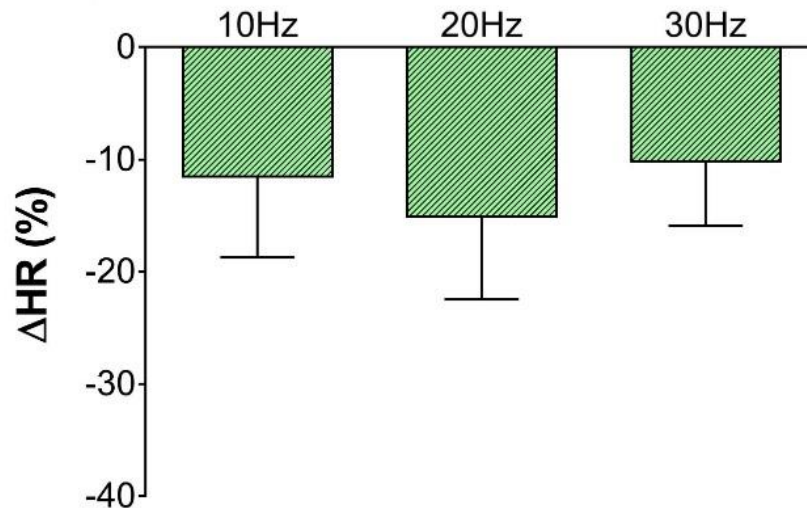


Figure 4.13 Percentage of heart rate decrease during ERP protocol by voltage $10\% \Delta HR_{BL}$ with pulse width 0.1 ms

Effective refractory period (ERP); $n = 5$, mean \pm SEM.

Stimulation by voltage $10\% \Delta HR_{BL}$ prolonged ERP from 137.0 ± 3.4 ms to 144.0 ± 2.9 ms (ns) by 10 Hz stimulation, from 136.0 ± 4.0 ms to 146.0 ± 4.0 ms ($P < 0.05$) by 20 Hz stimulation, and from 135.5 ± 5.0 ms to 137.0 ± 5.0 ms (ns) by 30 Hz stimulation, as shown in figure 4.14. Baseline ERP remained stable

throughout the protocol. Stimulation at 30 Hz appeared to have no effect on ERP prolongation compared to 20 Hz (137.0 ± 5.0 ms vs 146.0 ± 4.0 ms, $P < 0.05$).

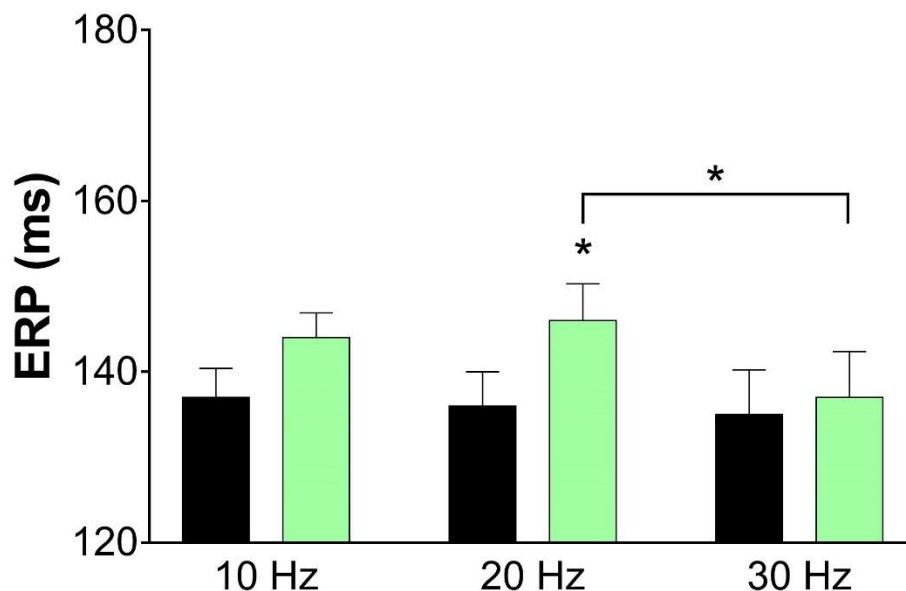


Figure 4.14 ERP prolongation by VNS at voltage $10\% \Delta HR_{BL}$ with PW 0.1 ms

Heart rate (HR), beat per min (bpm); $n = 5$, mean \pm SEM., Two-way ANOVA with Bonferroni post hoc test, * $P < 0.05$.

4.8 Ventricular fibrillation threshold (VFT) protocol

Another interesting parameter for ventricular physiology associated with arrhythmias protection in this study was ventricular fibrillation threshold (VFT). An example of VFT test by a right ventricle (RV) rapid pacing protocol is shown in figure 4.15. The 20 stimuli drive train (CL 300 ms) produced monophasic action potentials and contraction. Then, a train of 30 stimuli (CL 30 ms) induced an onset of ventricular fibrillation. With sufficient pacing current, this stimuli train induced a sustain ventricular fibrillation, which requires cardioversion by KCl. During an onset of ventricular fibrillation, there was no synchronous contraction of ventricle, as seen from left ventricular pressure in figure 4.15. Distribution

of electrical signal across the heart was not uniform, which was unable to produce any defined monophasic action potential.

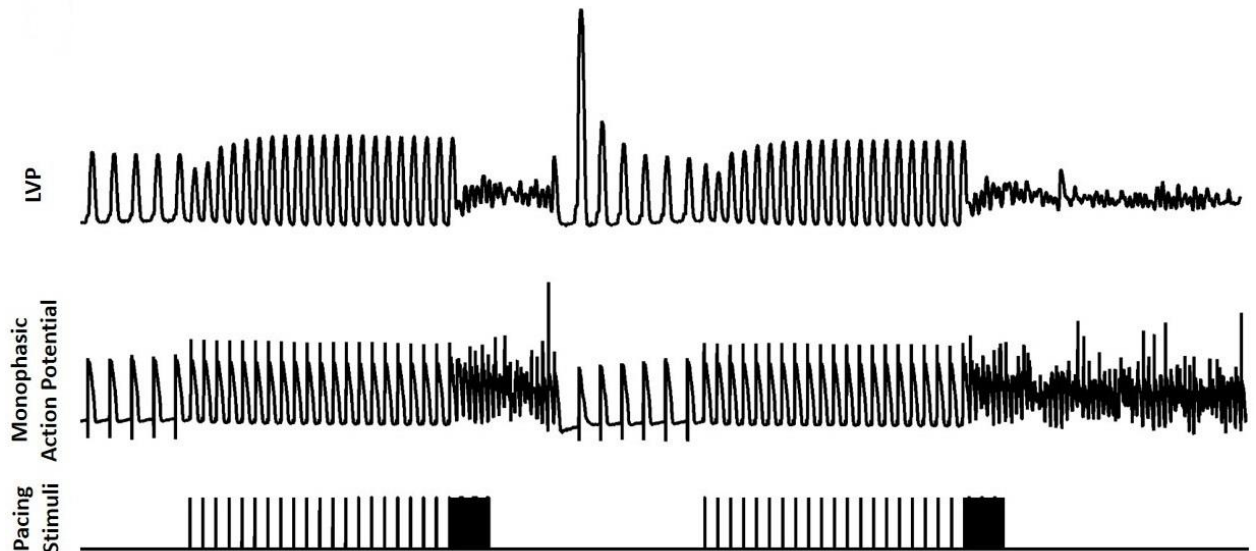


Figure 4.15 VF threshold test by a right ventricle (RV) rapid pacing protocol

For the 1st set stimuli, VF was not sustained and automatic reversed back to normal rhythm. By increased current 0.5 mA from the 1st stimuli, the 2nd set stimuli caused a sustained VF. Left ventricular pressure (LVP).

Stimulation by voltage $80\% \Delta HR_{max}$ with pulse width 2 ms increased VF threshold at all stimulation frequencies [1 Hz (2.4 ± 0.8 mA to 5.1 ± 1.2 mA, ns); 2 Hz (3.0 ± 0.7 mA to 6.1 ± 1.9 mA, ns); 3 Hz (4.1 ± 0.8 mA to 8.0 ± 2.5 mA, $P < 0.05$); 5 Hz (4.4 ± 0.8 mA to 9.0 ± 2.9 mA, $P < 0.01$)], as shown in figure 4.16. Percentage increase of VFT showed that high amplitude voltage stimulation increased threshold 113.2 ± 24.3 %, 104.2 ± 27 %, 93.9 ± 51.2 %, and 102.8 ± 54.2 % for stimulation at 1 Hz, 2 Hz, 3 Hz, and 5 Hz respectively (figure 4.17). There were no significant difference between percentage increases between the frequencies.

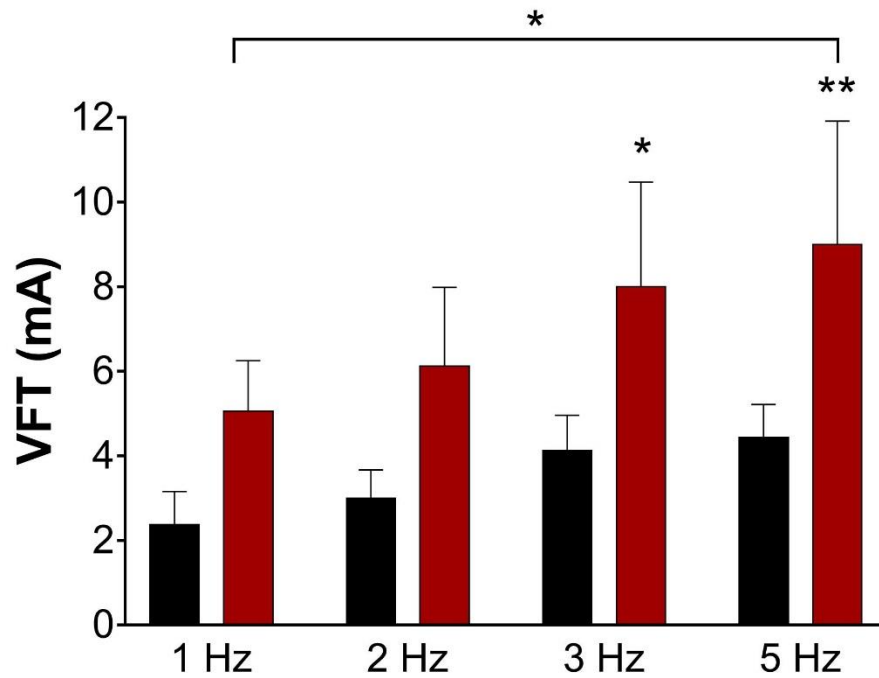


Figure 4.16 VFT increase by stimulation at voltage $80\%\Delta HR_{\max}$ with pulse width 2 ms
 Ventricular fibrillation threshold (VFT), milliampere (mA); $n = 8$, mean \pm SEM., Two-way ANOVA with Bonferroni post test, * $P < 0.05$, ** $P < 0.01$.

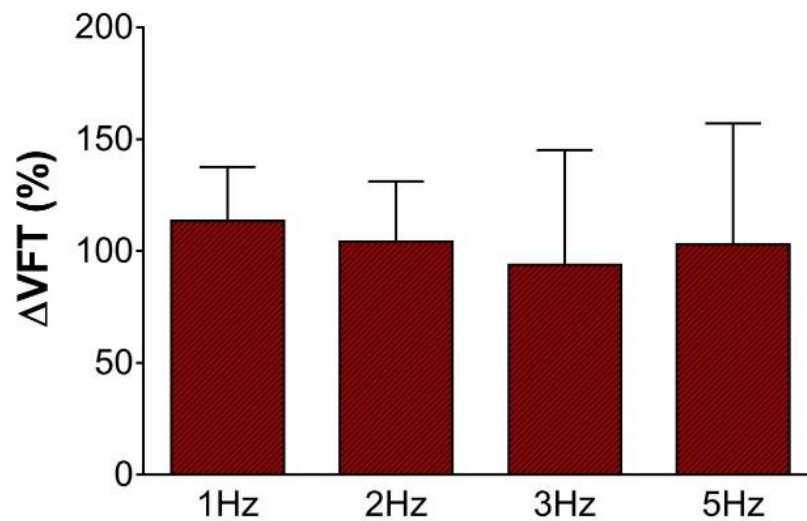


Figure 4.17 percentage increase of VFT by stimulation at voltage $80\%\Delta HR_{\max}$ with pulse width 2 ms

Ventricular fibrillation threshold (VFT); $n = 8$, mean \pm SEM.

VFT increase in response to high frequency stimulation is shown in figure 4.18. High frequency stimulation with voltage $10\% \Delta HR_{BL}$ and pulse width 0.1 ms significantly increased threshold in all stimuli [10 Hz (2.9 ± 0.6 mA to 5.5 ± 1.3 mA, $P < 0.01$); 20 Hz (2.9 ± 0.7 mA to 4.4 ± 1.0 mA, $P < 0.05$); 30 Hz (2.7 ± 0.8 mA to 4.5 ± 1.2 mA, $P < 0.01$)]. However, conversion to percentage increase of VFT, as displayed in figure 4.19, demonstrated that only 10 Hz stimulation increased VFT to 89.2 ± 25.8 %. The 20 and 30 Hz increased VFT by 30.7 ± 11.4 % and 23.3 ± 23.1 %, which was significantly lower than 10 Hz stimulation.

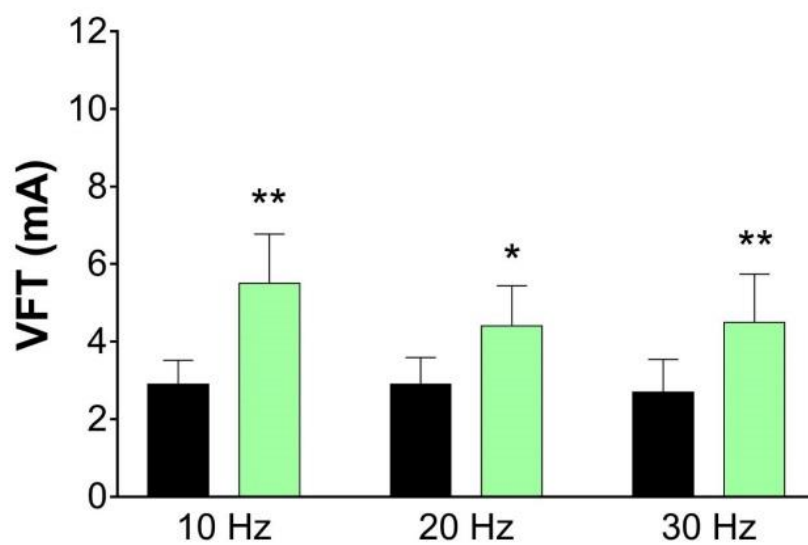


Figure 4.18 VFT increase by VNS at voltage $10\% \Delta HR_{BL}$ with PW 0.1 ms

Ventricular fibrillation threshold (VFT), milliampere (mA); $n = 5$, mean \pm SEM., Two-way ANOVA with Bonferroni post test, * $P < 0.05$, ** $P < 0.01$.

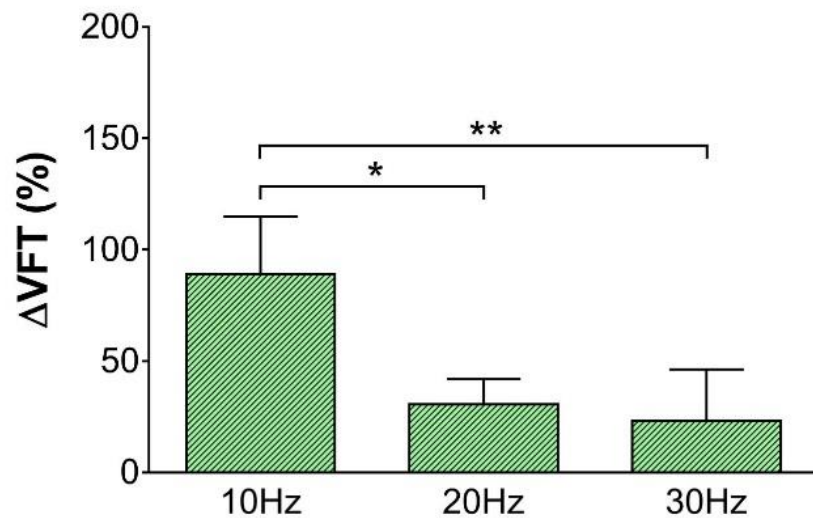


Figure 4.19 percentage increase of VFT by VNS at voltage $10\% \Delta HR_{BL}$ with PW 0.1 ms
Ventricular fibrillation threshold (VFT); n = 5, mean \pm SEM., One-way ANOVA, * P < 0.05,
**** P < 0.01.**

4.9 Monophasic action potential duration restitution (MAPDR)

Monophasic action potential recorded during the ERP protocol was then used for evaluation of the MAPDR. At the end of each iteration of S1 – S2 stimuli, the duration of MAP of the last S1 and the S2 were measured, displayed in figure 4.20A. The 90% of repolarization of both S1 and S2 was measured and shown in figure 4.20B and 4.20C, respectively. Data from this analysis were then used to plot a relationship between monophasic action potential duration 90% (MAPD90%) and diastolic interval (DI) as displayed in figure 4.21.

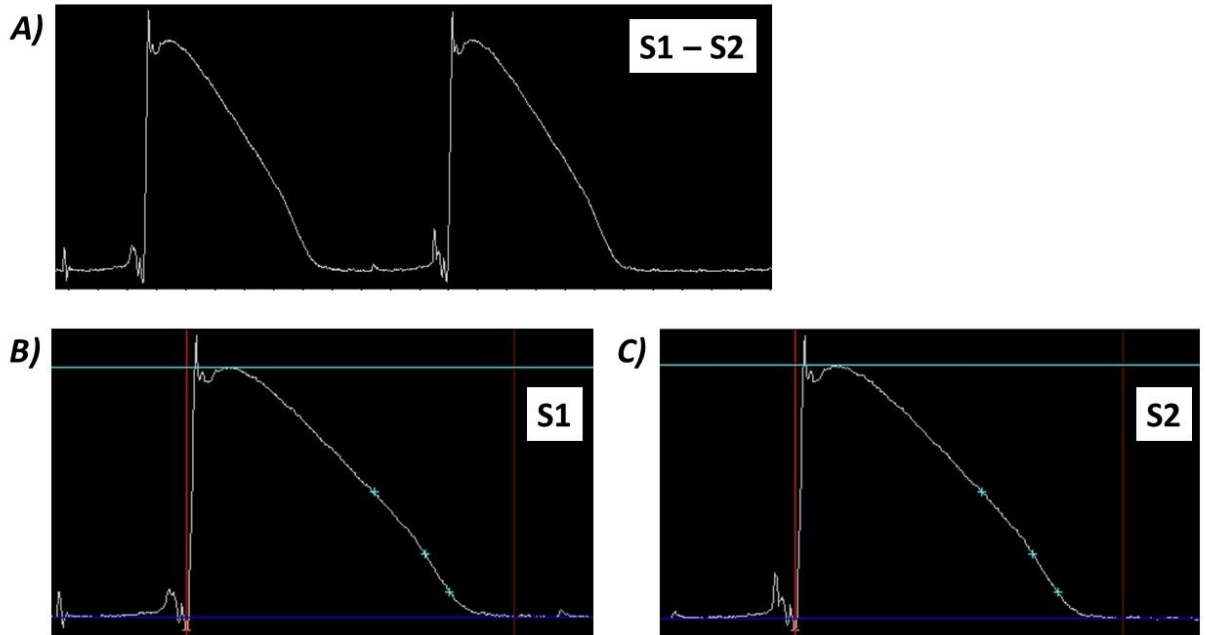


Figure 4.20 example MAPs recorded during ERP protocol that was used for MAPDR analysis

A) the last S1 and S2 MAP from the end of each S1 – S2 stimuli, **B)** selection of starting point and 90% of repolarization of an S1 MAP, and **C)** selection of starting point and 90% of repolarization of an S2 MAP. From B) and C) the left red vertical line defined the starting of the MAP and the right red line defined the end of repolarization. The blue horizontal line indicated the plateau of an MAP. Three blue + signs represent the 50%, 75%, and 90% of repolarization, respectively.

The MAPDR dataset from the previous step was then plot from the long diastolic interval to short diastolic interval between baseline conditions, showed in black dots in figure 4.21, compared to VNS conditions, displayed in red dots in figure 4.21. Exponential fit of each dataset was done, shown in black and red dash lines in figure 4.21, and followed by 1st derivative of this exponential in order to evaluate the maximum slope of each exponential curve, figure 4.22.

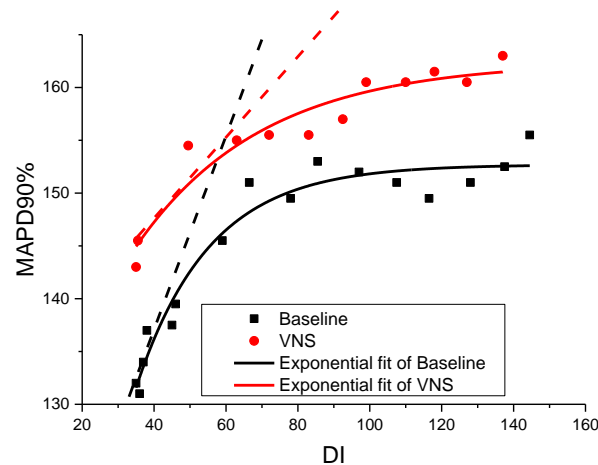


Figure 4.21 Analysis of baseline MAPDR and VNS MAPDR

Baseline MAPDR was plotted by black dots with the black dash line represented an exponential fit of this dataset. VNS MAPDR was plotted by red dots and then exponential fitted by showed in red dash line. VNS MAPDR curve was flattener than baseline MAPDR; monophasic action potential duration at 90% repolarization (MAPDR90%), diastolic interval (DI), and vagus nerve stimulation (VNS).

When compared to baseline restitution, VNS shifted a restitution curve upward. VNS MAPDR started with a longer MAPD90% (around 160 ms) than baseline (around 150 ms) at the long diastolic interval (around 140 ms). At the diastolic interval around 60 ms, the baseline MAPD90% was rapidly shortened while the VNS MAPD90% was gradually shortened. Baseline MAPD90% ended around 130 ms at ERP whereas the VNS MAPD90% was around 145 ms.

Exponential fits of both baseline and VNS restitutions in figure 4.21 displayed a flatter slope of VNS restitution (red dash line) than baseline (black dash line). Evaluation of maximum slope of both exponential curves was done by using the 1st derivative of exponential curve. From figure 4.22, maximum slopes of baseline restitution were 1.03 (black solid line) and 0.49 for the VNS restitution (red solid line).

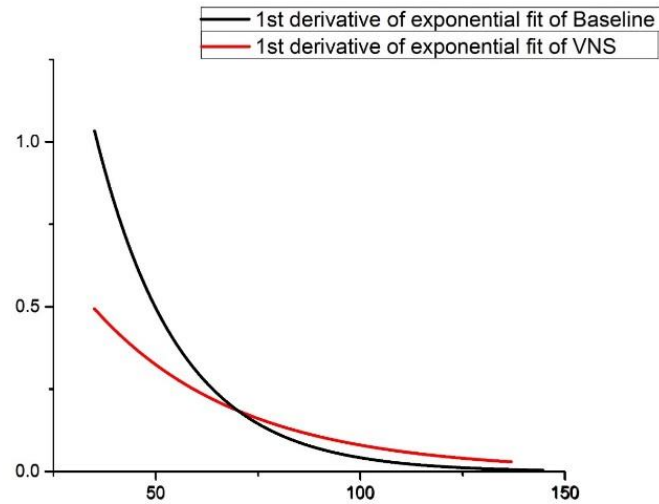


Figure 4.22 Assessment the maximum slope by the 1st derivatives of both baseline and VNS restitution exponential curves

Restitution slope value was summarized in table 4.1. Overall, baseline values were close to 1.0. Nerve stimulation by both 80% ΔHR_{max} and 10% ΔHR_{BL} reduced the restitution slope value in all stimulations. Statistical analysis was not performed due to a small data number ($n = 3$), which was a result of poor signal to noise ratio of monophasic action potential signal recording during ERP protocols.

Table 4.1 MAPDR maximum slope value. n = 3, mean \pm SEM.

<i>Apex MAPDR</i>						
Frequency	Baseline			VNS		
	Mean		SEM	Mean		SEM
1 Hz	0.71	\pm	0.05	0.52	\pm	0.22
2 Hz	0.83	\pm	0.06	0.53	\pm	0.12
3 Hz	0.84	\pm	0.06	0.31	\pm	0.11
5 Hz	0.82	\pm	0.20	0.42	\pm	0.16
10 Hz	1.12	\pm	0.17	0.61	\pm	0.12
20 Hz	1.12	\pm	0.17	0.55	\pm	0.20
30 Hz	1.11	\pm	0.18	0.55	\pm	0.12

<i>Base MAPDR</i>						
Frequency	Baseline			VNS		
	Mean		SEM	Mean		SEM
1 Hz	0.89	\pm	0.16	0.51	\pm	0.27
2 Hz	1.07	\pm	0.14	0.29	\pm	0.07
3 Hz	1.07	\pm	0.25	0.40	\pm	0.10
5 Hz	1.16	\pm	0.28	0.63	\pm	0.17
10 Hz	0.96	\pm	0.14	0.42	\pm	0.15
20 Hz	0.96	\pm	0.14	0.42	\pm	0.09
30 Hz	0.75	\pm	0.19	0.62	\pm	0.23

Data from table 4.1 was displayed in figure 4.23. Effect of VNS by voltage 80% ΔHR_{max} and pulse width 2 ms on restitution was displayed in figure 4.23A for the base restitution and 4.23B for the apex restitution. High frequency stimulation with voltage 10% ΔHR_{BL} (pulse width 0.1 ms) also flattened restitution maximum slope at ventricular base, figure 4.23C, and apex, figure 4.23D.

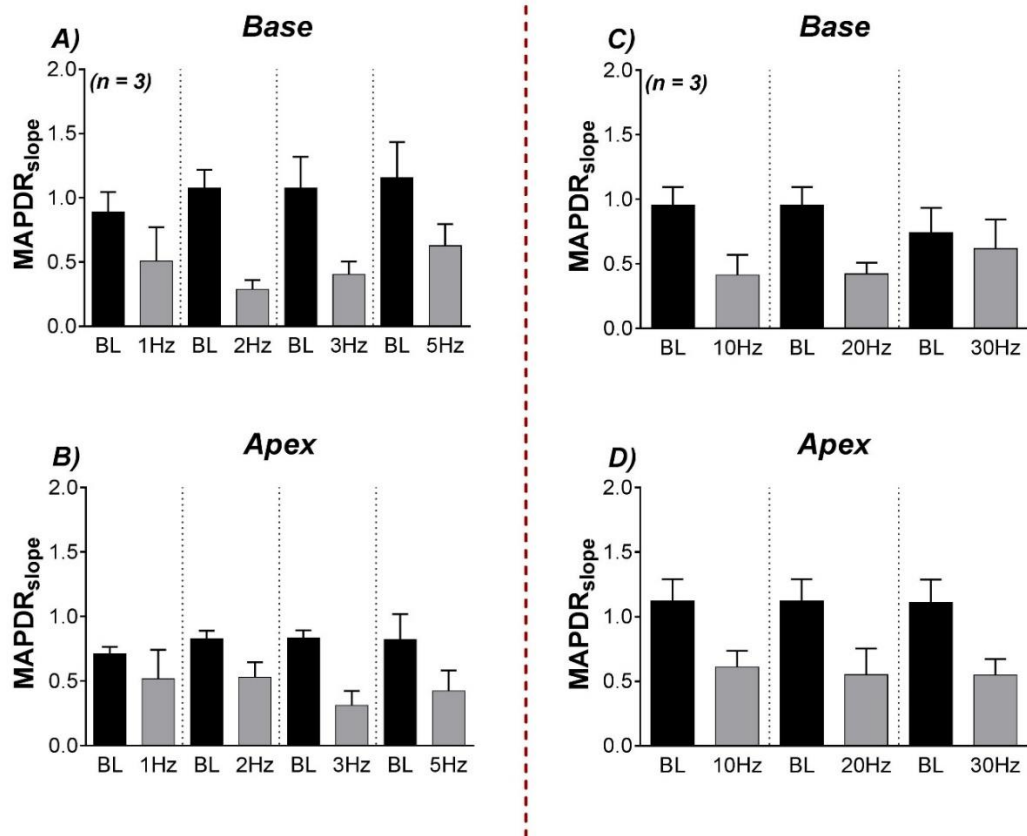


Figure 4.23 MAPDR slope value

A) High amplitude voltage VNS base restitution. B) High amplitude voltage apex restitution. C) High frequency base restitution. D) High frequency stimulation apex restitution. $n = 3$, mean \pm SEM.

4.10 Nitric oxide (NO) release in the ventricle by a single bifurcated light guided system

Nitric oxide has been shown to be involved with protective effect against ventricular arrhythmias of vagus nerve stimulation. Real time measurement of NO release in the left ventricle was measured by using DAF-2 DA fluorescence indicator together with the single bifurcated light guide system (Patel et al., 2008). To assess the effect of voltage and frequency of vagus nerve stimulation on nitric oxide release, NO fluorescence (NOFL) by the DAF-2 DA technique was utilized in this study. Increase in fluorescence signal corresponding to vagal activation with voltage $80\% \Delta HR_{max}$ is shown in figure 4.24. From figure,

vagal stimulation increased NOFL signal from baseline fluorescence level in all recording channels (470 nm, 480 nm, 490 nm, and 500 nm) similar to results from Patel et al. (2008). Wavelengths 470 nm to 500 nm (4 channels) were used as they covered excitation (495 nm) and emission (515 nm) wavelengths of DAF-2 DA dye. Recording of NOFL signal was done under a right ventricle constant pacing, which produced constant left ventricular pressure and pulse pressure as displayed in figure 4.24.

In addition, NOFL signal increase in response to high frequency stimulation is shown in figure 4.25. Left ventricular pressure and pulse pressure during this protocol was displayed in figure 4.25. Mean value of NOFL signal was analysed and displayed as absolute change from the baseline NOFL in figure 4.26.

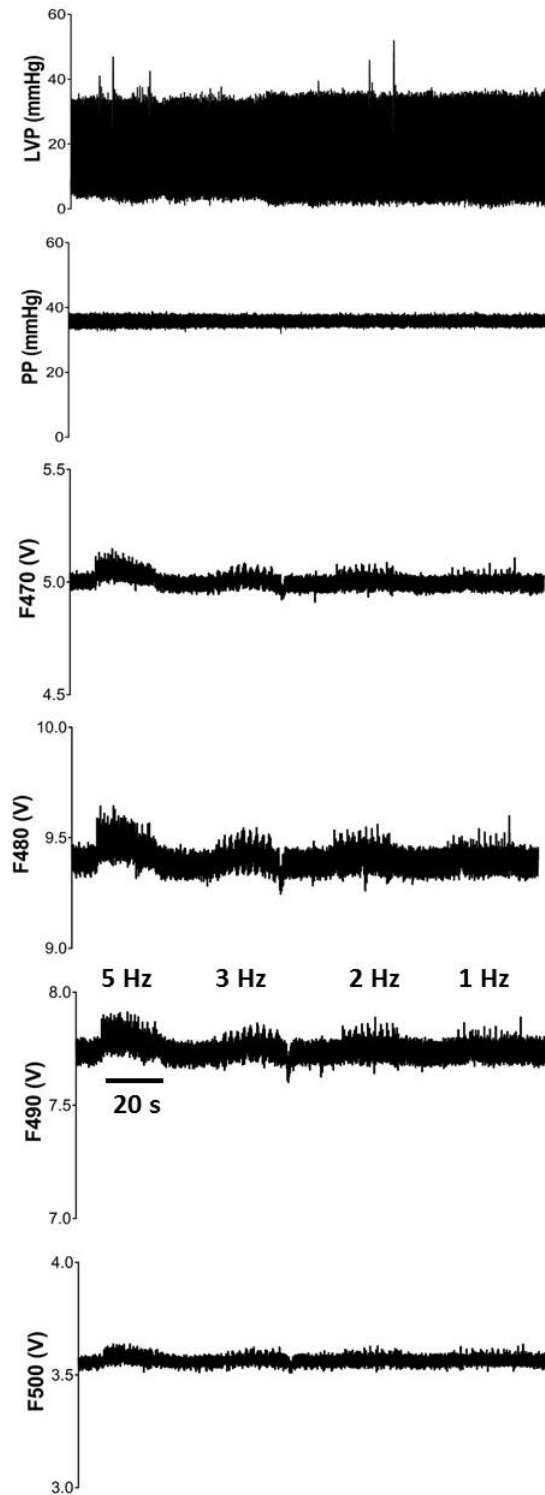


Figure 4.24 Increase of NOFL signal in the left ventricle of isolated innervated rabbit heart preparation by VNS with voltage $80\% \Delta HR_{max}$

A) NO signal increase in associate with stimulation frequency record with 470, 480, 490, and 500 nm channels. **B)** Stable LVP and PP during an RV constant pacing between NOFL protocols; left ventricular pressure (LVP), perfusion pressure (PP), volt (V), millimeter mercury (mmHg).

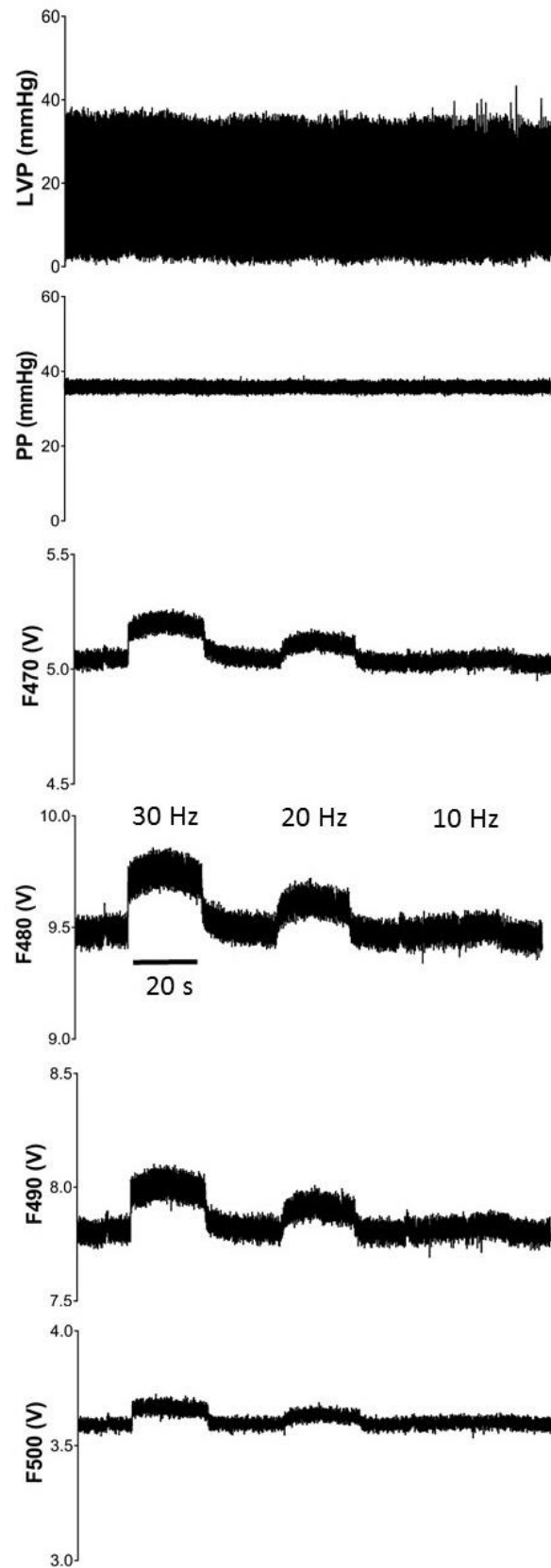


Figure 4.25 Increase of NOFL by VNS with voltage $10\% \Delta HR_{BL}$

A) NOFL signal increase B) LVP and PP during NOFL protocols; left ventricular pressure (LVP), perfusion pressure (PP), volt (V), millimeter mercury (mmHg).

NOFL experiments were done in a separate group of animal. Both high amplitude voltage and high frequency techniques were performed in the same heart. Voltage used for the $80\% \Delta HR_{max}$ was 4.60 ± 1.44 V and for the $10\% \Delta HR_{BL}$ was 1.28 ± 0.10 V. NOFL signal was increased from baseline by VNS in all recording channels, as shown figure 4.26. The noticeable changes of NOFL signal were observed in 480 and 490 nm channels. However, as seen in all channels, the high frequency stimulation (green) increased NOFL signal level more than the strong voltage stimulation (red). The 20 and 30 Hz stimuli significantly increased NOFL signal in 470, 480, and 490 nm channels. Absolute NOFL increases were summarized in table 4.2.

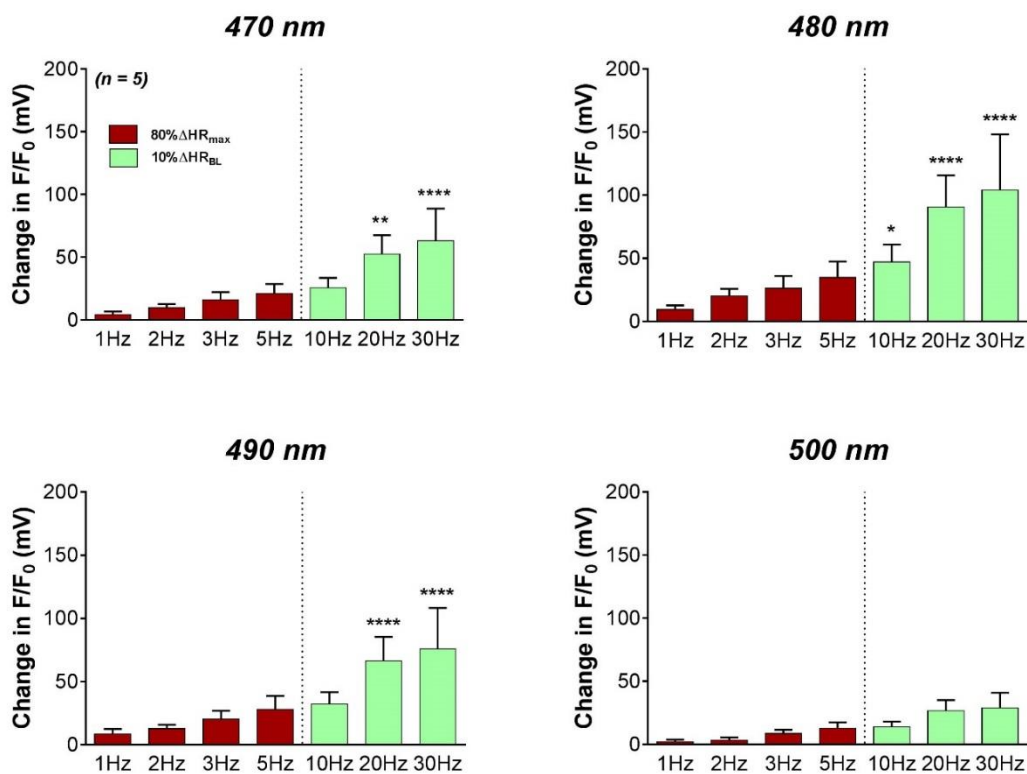


Figure 4.26 NOFL signal increase by VNS compared to baseline signal

Fluorescence (F), baseline fluorescence (F₀), nanometer (nm), millivolt (mV); n = 5, mean \pm SEM., Two-way ANOVA with Bonferroni post test, * P < 0.05, ** P < 0.01, **** P < 0.0001.

Table 4.2 Absolute increase of NOFL signal.

n = 5, mean \pm SEM., Two-way ANOVA with Bonferroni post test, * P < 0.05, ** P < 0.01, ** P < 0.0001**

	470 nm (mV)	480 nm (mV)	490 nm (mV)	500 nm (mV)
1 Hz	4.4 \pm 2.4	9.4 \pm 3.4	8.4 \pm 4.1	2.5 \pm 1.5
2 Hz	9.9 \pm 2.9	20.3 \pm 5.6	12.6 \pm 3.3	3.6 \pm 2.1
3 Hz	16.0 \pm 6.2	26.2 \pm 9.8	20.3 \pm 6.6	8.7 \pm 3.0
5 Hz	21.1 \pm 7.6	34.7 \pm 12.8	28.0 \pm 10.7	13.0 \pm 4.6
10 Hz	25.7 \pm 7.9	47.2 \pm 13.8*	32.3 \pm 9.4	14.0 \pm 4.2
20 Hz	52.7 \pm 14.9**	90.5 \pm 25.2****	66.4 \pm 19.0****	26.7 \pm 8.6
30 Hz	63.1 \pm 25.7****	104.0 \pm 44.1****	75.9 \pm 32.4****	29.2 \pm 11.9

4.11 Discussion

Results from this chapter confirmed the protective effects of unilateral vagus nerve stimulation against arrhythmogenesis (Schwartz, 2011). Recruitment of cervical vagal fibres by electrical stimulation, pre-clinically suppressed atrial fibrillation and reduced occurrence of ventricular arrhythmia episodes (Huang et al., 2015, Li et al., 2009). Reported mechanisms involved with this anti-arrhythmic effect, such as prolongation of ventricular ERP, increase of VF threshold, and flattening of MAP restitution slope, were observed in this study even with the lower stimulation intensity than seen in previous studies (Huang et al., 2015, Brack et al., 2011). The mechanism was hypothesized to involve NO release by VNS and had been confirmed using a novel fluorescence technique (Patel et al., 2008). Results of the extended stimulation intensity in this study provided evidence to support the previous findings, as VNS displayed both a ventricular protective mechanism and increased NO fluorescence signal.

In the literature regarding VNS for reducing sudden cardiac death of heart failure patients, most studies focused on the electrophysiological change by vagal activation compared to the baseline condition (De Ferrari et al., 2011). Questions remained regarding the appropriate procedures as a therapy, such as what were the optimal stimulation parameters? This had been largely ignored by most studies in the literature. In one study, the parameter selection was based on the Food and Drug Administration approval for epilepsy treatment Shinlapawittayatorn et al. (2013) (3.5 mA, 20 Hz, and 300 μ s). This selection criteria raises questions regarding the appropriateness of these parameters as stimulation of the nerves to target the brain or the heart would require recruitment of different types of vagal fibres. Treatment of epilepsy targeted afferent fibre of the vagus while anti-arrhythmia required recruitment of vagal efferent fibres (Yamakawa et al., 2015, Boon et al., 2001). However, what is an optimum stimulation parameter for cardio protective action is a challenging question (Gold et al., 2016, Shivkumar et al., 2016). To the best of our knowledge, this study was the first study that investigated responses of cardiac function to different vagal stimulation parameters. Understanding the fundamental effects of voltage, frequency, and pulse width on cardiac

electrophysiology and other relevant cardiac parameters will construct a solid background for clinical use of nerve stimulator devices.

In this study, vagal stimulation by voltage $80\% \Delta HR_{max}$ produced smaller heart rate reduction compare to those identified in a previous study from the group Brack et al. (2007). The voltage used in this study was lower than the voltage used by Brack et al. (2007). Despite this lower intensity, stimulation by these parameters still provided protective effect against ventricular arrhythmias. In contrast, a new set of parameters with low amplitude voltage and high frequency, which was studied for the first time with the innovated rabbit heart preparation, displayed a dominant impact on nitric oxide release, rather than causing a significant heart rate reduction. However, a very high frequency, 30 Hz, produced less response than other frequencies. One possible explanation was the adaptation of neural structures related to an aggressive stimulation (Shinlapawittayatorn et al., 2013). Therefore, this frequency was not used for further stimulation experiments.

Comparison between methods was only carried out in NOFL results. Responses of NO release to vagal stimulation in this study confirmed the characteristics of frequency-dependent release of NO from previous study (Brack et al., 2009). High frequencies, at 20 Hz and 30 Hz, significantly increased NOFL signal in F₄₈₀ and F₄₉₀ channels even with a short duration pulse width and low amplitude voltage used. However, the maximum increase of NOFL by this protocol was much lower than a previous study (Brack et al., 2011). At 10 Hz stimulation, F₄₉₀ of this study showed an increase of 32.3 ± 9.4 mV by 1.28 ± 0.10 V and 0.1 ms while an increase of around 200 mV from Brack et al. (2011) was generated by 10.0 ± 2.2 V, 2 ms, and 10.8 ± 2.4 Hz. As frequency used in this study were close to the previous study, NOFL increase revealed a primary effect of stimulation frequency on the level of nitric oxide increase. In addition, lower NOFL signal in current study, at the same frequency, might be impacted by lower voltage and shorter duration of this study.

Unilateral VNS in this chapter prolonged ventricular ERP and increased VFT by both high voltage amplitude and high frequency stimulations. Moreover, VNS

also flattened maximum slope of the ventricular MAPDR, however more N numbers are required to consolidate this effect as N = 3 of this dataset was small. However, ventricular electrophysiology data from this chapter confirmed the primary hypothesis that the low strength VNS protects the heart against ventricular arrhythmias. Furthermore, results of this chapter also support the secondary hypothesis that voltage and frequency of unilateral VNS are having different effects on cardiac function. The NO released during VNS was thought to be involved in the protective effect against ventricular arrhythmogenesis (Kalla et al., 2016b). Results in this chapter primarily provide evidence of NO released together with prolonged ERP, increased VFT, and flattened MAPDR during VNS by both stimulation parameter sets.

4.11.1 Main findings

4.11.1.1 High amplitude voltage stimulation

At an adequate voltage, increasing the frequency of stimulation resulted in a frequency-dependent decrease in heart rate. High amplitude voltage recruited large vagal fibres, which act through muscarinic receptor on the right atrium, particularly at the SA node (Coote, 2013, Ford and McWilliam, 1986). Therefore, large amplitude voltage strongly affected heart rate changes at the atrial level but not much effect on nitric oxide release at the ventricle level.

4.11.1.2 High frequency stimulation

For low amplitude voltage stimulation, increasing frequency did not produce further heart rate reduction even at high frequencies. However, high frequency, even at low intensity voltage, effected a release of nitric oxide in the ventricle level and has been shown to be independent from muscarinic receptor activation (Brack et al., 2011).

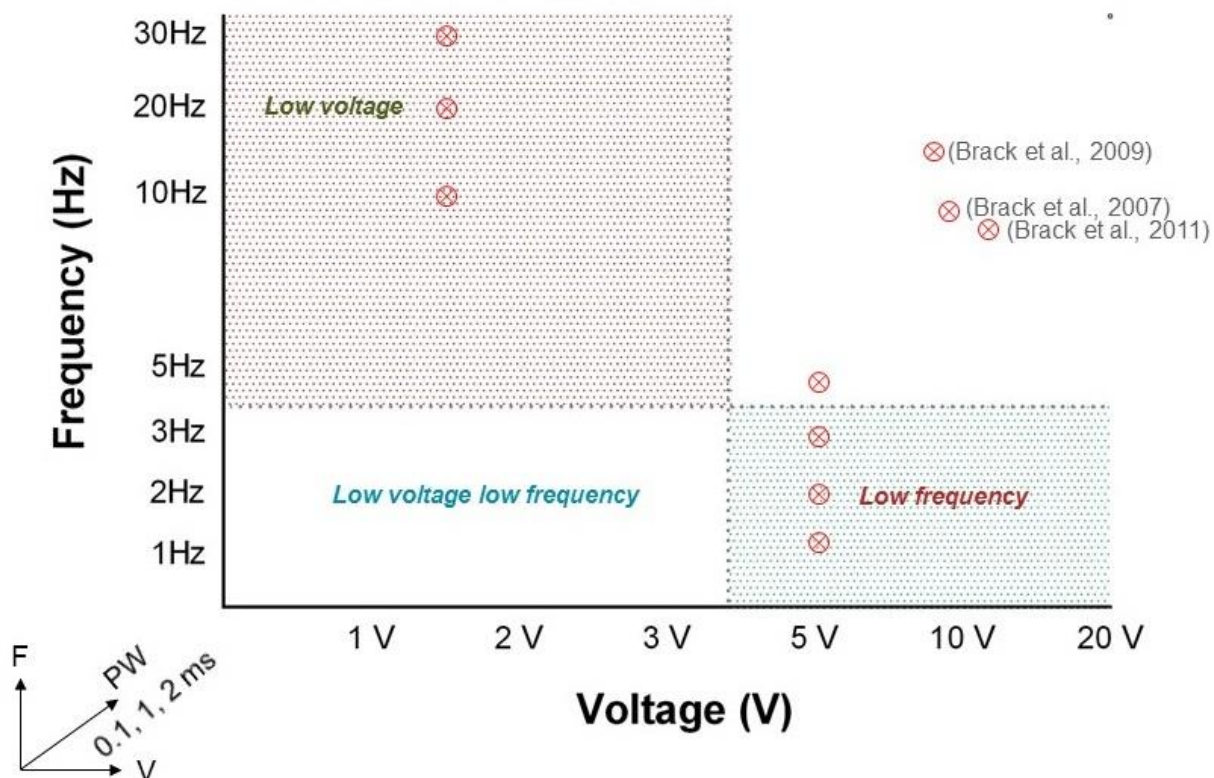


Figure 4.27 Scheme represented combinations of voltage, frequency, and pulse width used in VNS study

Previous study investigated effects of high voltage and high frequency stimulation (displayed as red circles on upper right quadrant). This chapter assessed effects of high voltage at low frequencies (lower right quadrant) and low voltage at high frequencies (upper left quadrant). Next chapter will study effects of low voltage low frequency stimulation (lower left quadrant) and effects of different stimulation pulse widths.

4.11.2 Next stage

In this early stage study, a variety of voltage, frequency, and pulse width were combined together for recruitment of vagal fibre with the aim of imparting cardio protection from arrhythmias. The aim was to identify a series of stimulation parameters to alter ventricular electrophysiology and protect the heart from arrhythmogenesis. Previous work of our group utilized high strength voltages and high frequencies to excite vagus nerve (Brack et al., 2011, Brack et al., 2009, Brack et al., 2007). In this preliminary chapter, stimulation parameters were separated into high amplitude voltage with low frequency and low amplitude voltage with high frequency. This combination produced data that

displayed distinct effect of stimulation voltage on heart rate reduction and effect of stimulation frequency on nitric oxide increase in the ventricle. Categorization of an overall nerve stimulation parameter was displayed in figure 4.27. This scheme consist of voltage as X axis and frequency as Y axis. The strength used by our previous work was classified as high amplitude voltage and high frequency (upper right quadrant). Then, this 1st step examination investigated area of low frequency stimulation (lower right quadrant) and the low amplitude voltage stimulation (upper left quadrant). For the next evaluation, exploration of low amplitude voltage low frequency region (lower left quadrant) will be performed.

In addition, considering an axis of stimulation pulse width (the Z axis), there was only 2 ms duration that was used in the high amplitude voltage with high frequency and the high amplitude voltage with low frequency regions. Also, results from the low amplitude voltage quadrant was produced only by pulse width 0.1 ms. Therefore, next step of the study will investigate effect of different pulse width on ventricular electrophysiology and nitric oxide fluorescence signal. The long duration (2 ms) and short duration (0.1 ms) will be studied by combining with different voltage and frequency. Furthermore, a moderate duration such a pulse width 1 ms will be included in the study. Results from this plan will provide information that cover different combinations of stimulation parameters.

4.11.3 Limitations

Small N number of restitution data was affected by a high level of noise that emerged with MAP recording in some experiments. MAP morphology change within protocol and the 90% of repolarization value was not consistent, which resulted in an error in the restitution curve.

There was no statistical comparison of Δ HR, ERP, VFT, and MAPDR between strong voltage and high frequency methods because data were not collected from the same preparations.

The NO measurement technique in this research project utilised changes of fluorescence signal associated with changes of intra-cellular NO level. This method is unable to deduce the precise concentration of NO release during nerve activation, which is one of the limitations of this technique. Measurement of the nitrate/nitrite level from coronary effluent fluid and correlation to the level of fluorescence signal changes would be suggested as a future study. In addition, the single-bifurcated light guided measured fluorescence signals from the epicardium of the LV. It is a possibility that NO was transmurally released and then caused an accumulation of fluorescence signals at an epicardial surface. This can cause an over estimation of the fluorescence signal. However, the single bifurcated light guided system provided a real time monitoring of NO-related fluorescence signal from a beating heart during VNS compared to the baseline.

Chapter 5 Effects of different right vagus nerve stimulation parameters on rabbit ventricular electrophysiology

5.1 Introduction

Results from the previous chapter displayed different effects between stimulation voltage and frequency of vagus stimulation on cardiac electrophysiology and nitric oxide (NO) activity. Adequate stimulus of the vagus nerve has a dominant effect causing a reduction in heart rate (HR) in a muscarinic receptor-dependent mechanism at the level of the atria. In contrast, a high frequency stimulation caused an increase in nitric oxide in the ventricle; a mechanism shown to be independent of muscarinic receptor activation from previous work. From these preliminary outcomes, more work is needed to fully investigate the effects of vagus nerve stimulation (VNS). The specific parameters used to stimulate the nerve will be investigated to provide fundamental information for parameter configuration which could be useful in a clinical study.

In this chapter, stimulation parameters were modified from the previous chapter. Parameters were reassigned into 3 groups to fully cover the frequency range from 1 Hz to 20 Hz. The maximum frequency that was reported to be used in both pre-clinical (Chen et al., 2015, Zhang et al., 2014, He et al., 2013b) and clinical studies (Stavrakis et al., 2015, Zannad et al., 2014, Dicarolo et al., 2013, Hauptman et al., 2012) was 20 Hz. In addition, the frequency 30 Hz was not continued from stimulation scheme because it seemed to provide less of a protective effect than 20 Hz. From previous results, the frequency 20 Hz increased the ventricular fibrillation threshold (VFT) but caused a longer prolongation of ERP than 30 Hz. Therefore, the frequency 30 Hz was removed, and the highest frequency was changed to 20 Hz. As a result, the high frequencies use in the new stimulation scheme were 5 Hz, 10 Hz, and 20 Hz and low frequency were moved down to 1 Hz, 2 Hz, and 3 Hz. Voltage strengths were the $80\% \Delta HR_{max}$, as used in VNS effect on ventricular electrophysiology study (Brack et al., 2013a), and $10\% \Delta HR_{BL}$, as used by other

models for pre-clinical vagal stimulation study (Chen et al., 2015, Shen et al., 2013, Li et al., 2009).

In addition, an evaluation of the pulse width (PW) effect was included to the study. Previous finding utilized a pulse width of 2 ms for high voltage low frequency and a pulse width of 0.1 ms for low voltage high frequency. There was a large gap of the results between 2 ms and 0.1 ms as a long duration (2 ms) was used only in low frequency, while a short duration (0.1 ms) was used only in high frequency. In this chapter, the moderate duration pulse width was added into the stimulation pulse width axis (the Z axis) to study the middle duration between 0.1 ms and 2 ms (Chen et al., 2015, Uemura et al., 2010). As a result, short, moderate, and long stimulation duration (0.1 ms, 1 ms, and 2 ms) were studied in all voltages and frequencies. Combination of parameters in this chapter allowed a comprehensive evaluation of stimulation parameters in 3 axes.

For human clinical studies, stimulation of vagus nerve was performed in heart failure (HF) patients in order to treat an autonomic imbalance between sympathetic and parasympathetic tone (Zannad et al., 2014, Dicarlo et al., 2013, Hauptman et al., 2012). The main objective of these clinical studies was to stimulate vagus in order to balance the sympathetic and the parasympathetic tones. Chronic elevation of sympathetic tone and withdrawal of parasympathetic tone was one of the main cause of heart failure (Lymeropoulos et al., 2013). There were 3 main clinical heart failure studies that stimulated the vagus nerve by using an implanted device; INNOVATE-HF, ANTHEM-HF, and NECTAR-HF. The INNOVATE-HF study stimulated only the right cervical vagus nerve by the CardioFit device (Gold et al., 2016, Hauptman et al., 2012, Schwartz, 2011). No detail about stimulation parameters was provided in this study. For the ANTHEM-HF study, either left or right cervical vagus was randomly selected for unilateral electrical activation. Parameter setting started from a current of 0.25 mA, frequency 10 Hz, and PW 130 μ s and was titrated for 10 weeks to current 1.5 – 3.0 mA, frequency 10 Hz, and pulse width 250 μ s (Dicarlo et al., 2013). For the last study, the NECTAR-HF stimulated only right cervical vagus nerve with current amplitude 4.0 mA

maximum, frequency 20 Hz, and PW 300 μ s (Zannad et al., 2014). As seen from these studies, right vagus nerve at the cervical level was the main target for an electrical activation. Therefore, investigation of vagus nerve stimulation effect on ventricular electrophysiology in this chapter focussed on the right vagus nerve stimulation (RVNS).

5.2 Chapter objectives

- 1) To investigate effects of right vagus nerve stimulation by different stimulation voltage on ventricular electrophysiology
- 2) To investigate effects of right vagus nerve stimulation by different stimulation frequency on ventricular electrophysiology
- 3) To investigate effects of right vagus nerve stimulation by different stimulation pulse width on ventricular electrophysiology

5.3 VNS parameters

In this chapter, experiments were designed to assess effect of voltage, frequency, and pulse width on heart rate and ventricular electrophysiology. Parameter combinations were classified into i) low frequency stimulation, ii) low voltage stimulation, and iii) low frequency low voltage stimulation. Details of voltage, frequency, and pulse width of each parameter set are summarised in table below.

Changes of heart rate (HR), effective refractory period (ERP), ventricular fibrillation threshold (VFT), and monophasic action potential duration restitution (MAPDR) were measured and compared between baseline and right vagus nerve stimulation (RVNS).

Stimulation aspect	Voltage (V)	Frequency (Hz)	Pulse width (ms)
<i>Low frequency</i>	80% ΔHR_{max}	1, 2, and 3	0.1, 1, and 2
<i>Low voltage</i>	10% ΔHR_{BL}	5, 10, and 20	0.1, 1, and 2
<i>Low frequency low voltage</i>	10% ΔHR_{BL}	1, 2, and 3	0.1, 1, and 2

5.4 Voltage response and frequency response curves of different RVNS parameters

In order to stimulate the right vagus nerve, the optimal voltages were identified as the first step. As mentioned previously, voltages used in this study were high amplitude voltage (voltage $80\% \Delta HR_{max}$) and low amplitude voltage (voltage $10\% \Delta HR_{BL}$). Therefore, the first protocol of all experiments was the voltage configuration.

5.4.1 Low frequency stimulation

5.4.1.1 Voltage response curves

Voltage response curves was carried out to assess the maximum HR reduction within the 1 V – 20 V stimuli. Right vagus nerve was stimulated at frequency 5 Hz together with 3 different PWs (0.1 ms, 1 ms, and 2 ms). Lowest HR value of each PW was defined and was used to calculate the $80\% \Delta HR_{max}$ voltage of each PW. These high amplitude voltages were then used by the low frequency stimulation method with the aim to recruit vagal neuron fibres during an activation.

For results, the low frequency stimulation at a pulse width of 0.1 ms significantly reduced heart rate from 2 V to 20 V, displayed in figure 5.1A. Baseline heart rate was stable, ranging from 146.8 ± 6.2 bpm to 153.7 ± 7.7 bpm. The 2 V stimulation caused a significantly greater reduction in heart rate than 1 V

stimulation ($P < 0.0001$). Similarly, the 3 V caused a significantly greater reduction in 2 V ($P < 0.0001$). Heart rate reduction by pulse width 0.1 ms stimulation reached saturation at 5 V stimulus with lowest HR 99.7 ± 8.6 bpm from baseline 151.9 ± 8.0 bpm (at 7 V).

With the moderate pulse width of 1 ms, a significant reduction of heart rate by RVNS was observed from 1 V to 20 V, figure 5.1B. There was a voltage-dependent reduction in heart rate with no further reduction after 10 V. There was no significant reduction between 10 V, 15 V, and 20 V stimuli. No difference was observed between baseline heart rate of this 1 ms RVNS.

The 2 ms RVNS voltage response curve exhibited the same characteristic as 1 ms voltage curve, figure 5.1C. HR was significantly reduced in a voltage dependent manner from 1 V to 10 V. No statistical difference was seen between 10 V, 15 V, and 20 V. Baseline heart rate was stable throughout the protocol (from 152.4 ± 4.5 bpm to 154.3 ± 5.8 bpm). The lowest heart rate was 78.4 ± 5.1 bpm at 15 V stimulus.

For the results, the maximum HR reduction by PW 1 ms was in the same level of minimum HR by PW 2 ms. However, the 1 ms stimuli required a higher amplitude of voltage to produce the same level of HR drop. Of the 3 PWs, the PW 0.1 ms required lowest voltage amplitude. However, the maximum HR reduction by PW 0.1 ms was smaller than the maximum reduction produced by PWs 1 ms and 2 ms. These results suggested that stimulation voltage and PW were the main determinant parameters that influenced HR change by vagal stimulation. Voltage is required as stimulus strength for recruitment while PW is required as stimulus duration for recruitment of nerve fibre in each activation spike. It was obvious that to produce to same level of HR change, a short duration (1 ms) required a higher amplitude of voltage than a long duration (2 ms). Moreover, a very short duration (0.1 ms) had a limited capability to recruit vagal fibres, which resulted in smaller amount of HR change when compared to longer PW. Therefore, as an effect of PW on HR change, an optimum duration of PW was required to provide a sufficient time for the voltage to recruit nerve fibre.

5.4.1.2 Frequency response curves

After obtaining target voltages of each PW, frequency response curves were tested by using the results of the voltages from the previous step together with a set of low frequencies (1 Hz, 2 Hz, and 3 Hz). This investigation allowed an observation effects of a combination between high amplitude voltage and low frequencies on HR reduction, which was the primary effect of VNS. Stimulation with 0.1 ms and 6.00 ± 1.84 V significantly reduced heart rate at all frequencies, figure 5.2A. The reduction displayed a frequency dependent characteristic with lowest heart rate 117.5 ± 10.5 bpm from baseline 151.9 ± 9.8 bpm at 3 Hz activation. The 1 ms and 2 ms RVNS produced significant frequency-dependent heart rate reduction similar to 0.1 ms RVNS. Voltages used were 8.17 ± 1.56 V and 7.67 ± 0.80 V, for 1 ms and 2 ms respectively. The lowest heart rate of 1 ms frequency curve was 116.6 ± 9.4 bpm from baseline 154.0 ± 9.5 bpm at 3 Hz stimulus (figure 5.2B). The lowest heart rate of 2 ms stimulus was 109.9 ± 9.8 bpm from baseline 153.6 ± 9.5 bpm at 3 Hz stimulation, figure 5.2C.

The voltages, frequencies, and PWs from this configuration step were then used to stimulate the right vagus nerve. HR changes and ventricular electrophysiology (EP) responses to this low frequency (with high amplitude voltage) stimulation were recorded. Results of this VNS investigation extended information on stimulation parameters from the previous work into lower frequencies and range of stimulation PWs used for nerve stimulation.

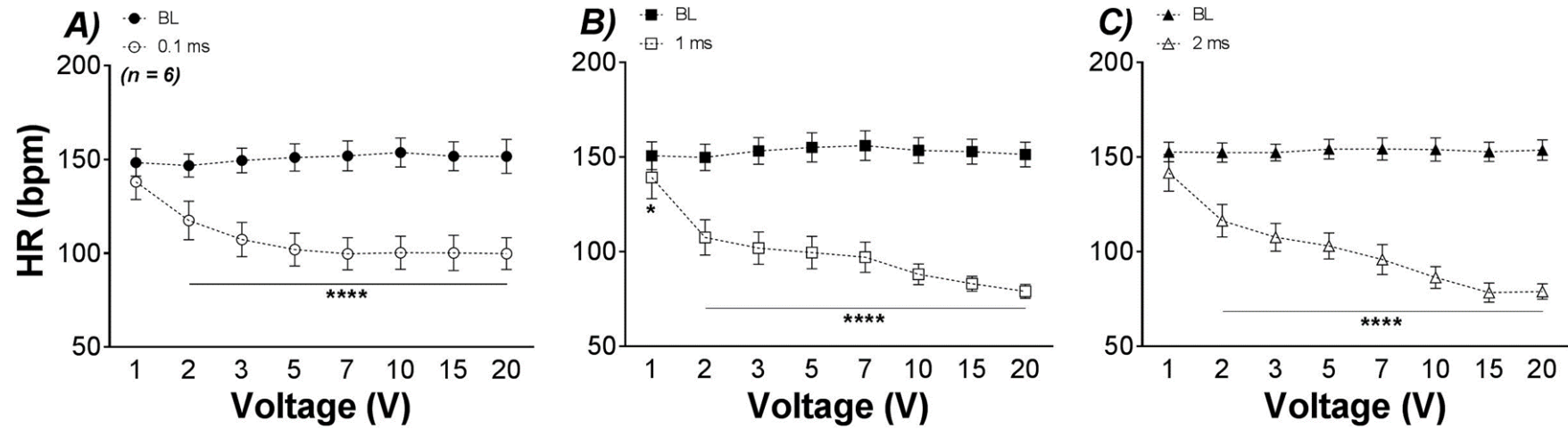


Figure 5.1 Voltage response curve of low frequency stimulation

Voltage response curves of low frequency RVNS by PW 0.1 ms, 1 ms, and 2 ms at 5 Hz. Heart rate (HR), baseline (BL), beat per min (bpm), volt (V); n = 6, mean ± SEM., Two-way ANOVA with Bonferroni post hoc test, * P < 0.05, **** P < 0.0001.

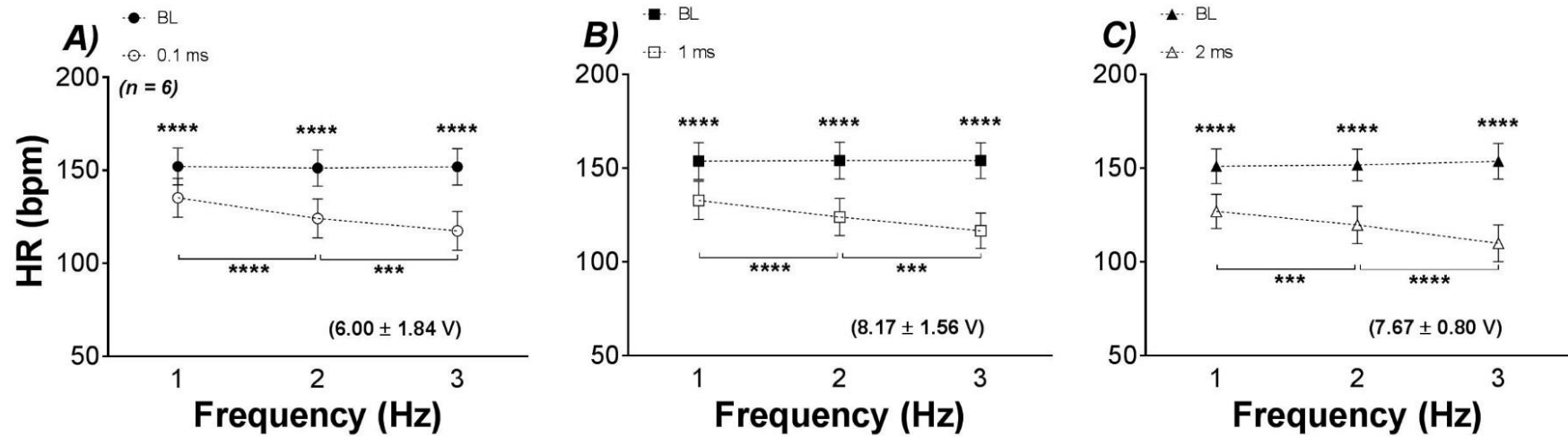


Figure 5.2 Frequency response curves of low frequency stimulation

Frequency response curves of RVNS low frequency stimulation ($80\% \Delta HR_{max}$ V with 1 Hz, 2 Hz, and 3 Hz) by PW 0.1 ms, 1 ms, and 2 ms. Heart rate (HR), baseline (BL), beat per min (bpm), volt (V); n = 6, mean \pm SEM., Two-way ANOVA with Bonferroni post hoc test, *** P < 0.001, **** P < 0.0001.

5.4.2 Low voltage stimulation

5.4.2.1 Voltage use

In this study, the new concept of vagal stimulation voltage was introduced to an isolated innervated rabbit heart preparation. This low amplitude voltage was mainly used in the low level vagus nerve stimulation (LLVS) and the human clinical studies. The main purpose was to minimize HR reduction effect but hopefully preserve anti-arrhythmic effect of vagal excitation. In the current study, the voltage that caused HR to drop less than 10% from baseline was selected and defined as the low amplitude voltage. To configure a voltage for this low voltage stimulation scheme, frequency 20 Hz was used with all 3 PWs. Voltages that reduced heart rate less than 10% from were 2.42 ± 0.26 V for 0.1 ms, 1.58 ± 0.11 V for 1 ms, and 1.54 ± 0.12 V for 2 ms.

5.4.2.2 Frequency response curve

Low amplitude voltages from section 5.2.1 were combined with high frequencies (5 Hz, 10 Hz, and 20 Hz). This combination allowed an assessment the impact of high frequency used of VNS on ventricular EP. Results by the low voltage stimulation showed the reduction of heart rate was less than that with low frequency stimulation (high voltage). Frequency response curves of the low voltage stimulation were displayed in figure 5.3A – C. From the figures, baseline HR of all frequencies and PWs were stable without any significant differences observed. Baseline HR were between 164.2 ± 5.1 bpm to 160.6 ± 5.2 bpm. RVNS reduced HR at all stimuli (ns) (figure 5.3A). Overall frequency response curves by this stimulation scheme showed less HR effect than the responses of the high amplitude voltage of the low frequency approach (figure 5.2). This low amplitude voltage with high frequency RNVS highlighted the significant impact of the high frequency use for nerve stimulation on cardiac function, particularly ventricular EP changes.

The low voltage stimulation reduced HR to a smaller extent than the low frequency stimulation similar to results from previous chapter. The low amplitude voltage used in this method reduced HR to a same level by all stimulations. Voltages used by a moderate PW was at the same level as a long PW. To produce the same amount of reduction, a very short PW required a higher amplitude of voltage when compared to moderate and long PWs. With the low amplitude voltage even with the very high frequency, the capability to decrease HR of vagal stimulation was limited. The results of low frequency stimulation together with results of this low voltage stimulation confirmed an important role of stimulation voltage on HR reduction.

5.4.3 Low frequency low voltage stimulation

5.4.3.1 Voltage use

The last voltage configuration was done under the same low level voltage configuration as section 4.2.1 but performed by frequency 5 Hz. As a result, amplitudes were 3.25 ± 0.68 V, 1.72 ± 0.25 V, and 1.38 ± 0.19 V for 0.1 ms, 1 ms, and 2 ms respectively. These voltages were combined with low frequencies (1 Hz, 2 Hz, and 3 Hz) in order to explore area of a truly low strength stimulation (low amplitude voltage and low frequency), which has not been studied before, in particular on the innervated rabbit heart preparation.

5.4.3.2 Frequency response curve

Frequency response of this low frequency low voltage method displayed less HR decrease when compare to the previous 2 methods. Baseline HRs were stable throughout the protocols, which varied between 163.0 ± 8.6 bpm to 158.9 ± 8.8 bpm. Maximum reduction level was at frequency 3 Hz and PW 2 ms (from 160.2 ± 9.2 bpm to 154.7 ± 9.7 bpm (ns)) (figure 5.4C). These low strength combinations were then applied to study ventricular EP in the rabbit heart.

The low frequency low voltage strategy was a truly low-level stimulation and had been used to stimulate the nerve first time in this study. Comparison of this technique to low voltage (high frequency) technique revealed differences between the effects of low frequency and high frequency used for vagal stimulation. Low frequency and low voltage uses a higher voltage amplitude than low voltage stimulation at the same PW and caused lesser HR reduction. A frequency dependent HR reduction within a fixed PW found in low frequency stimulation was also seen in this stimulation arrangement. Together with low voltage HR result, a low amplitude voltage started to cause a significant reduction in all PWs from frequency 3 Hz to 20 Hz. Even a significant HR reduction was produced by these frequencies, all decreases were less than 10% from the baseline value. This result suggested a small effect of stimulation frequency on HR and confirmed a large effect of voltage of vagus stimulation on HR reduction.

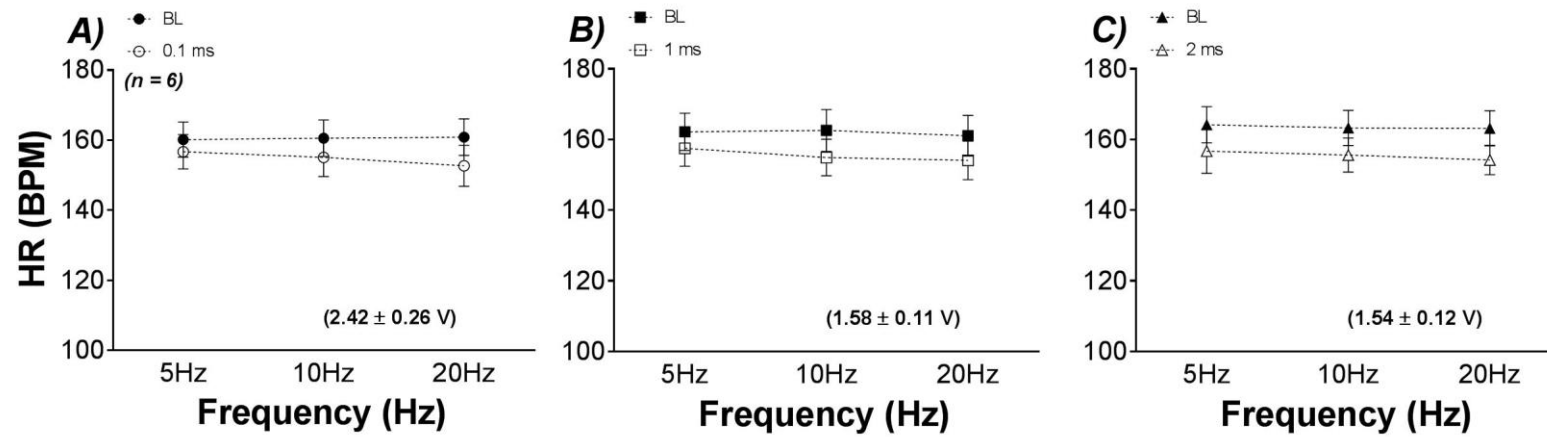


Figure 5.3 frequency response curves of low voltage stimulation

Frequency response curves of RVNS low voltage stimulation ($10\% \Delta HR_{BL}$ V with 5 Hz, 10 Hz, and 20 Hz) by PW 0.1 ms, 1 ms, and 2 ms. Heart rate (HR), baseline (BL), beat per min (bpm), volt (V); $n = 6$, mean \pm SEM.

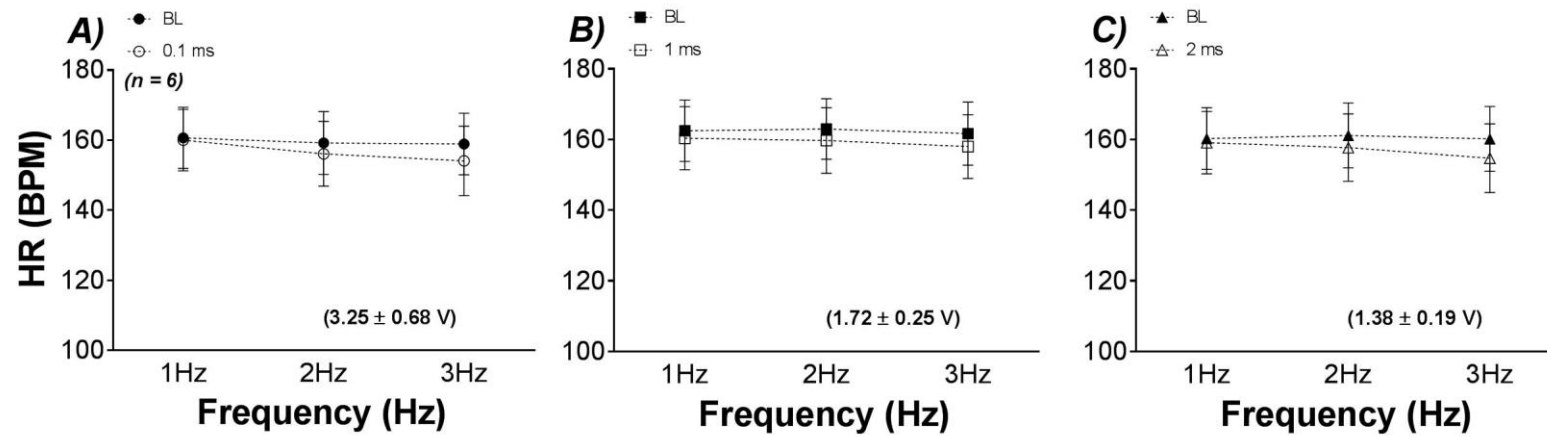


Figure 5.4 Frequency response curve of low frequency low voltage stimulation

Frequency response curves of RVNS low frequency low voltage stimulation ($10\% \Delta HR_{BL}$ V with 1 Hz, 2 Hz, and 3 Hz) by PW 0.1 ms, 1 ms, and 2 ms. Heart rate (HR), baseline (BL), beat per min (bpm), volt (V); $n = 6$, mean \pm SEM.

5.5 Effect of different RVNS parameters on left ventricular effective refractory period (ERP)

5.5.1 Low frequency stimulation ERP protocol

5.5.1.1 Heart rate reduction by low frequency RVNS during ERP protocol

RVNS during an ERP protocol produced 2 main effects on cardiac function. The first effect was via muscarinic receptor activation at the atrial level (SA node), which caused HR reduction. The second effect was a prolongation of ventricular ERP. From these experimental results, low frequency RVNS significantly lowered HR in all frequencies except stimulation at 0.1 ms and 1 Hz. Comparison between the effects of 3 different PWs within stimulation frequency was shown in figure 5.5. The PW 1 ms reduced HR the most (121.8 ± 10.7 bpm) when compared to 0.1 ms (130.3 ± 9.9 bpm) and 2 ms (125.9 ± 10.6 bpm) at 1 Hz frequency (figure 5.5A). The 1 ms pulse width produced the smallest reduction (117.5 ± 10.3 bpm) in the 2 Hz stimulation (figure 5.5B), (115.6 ± 5.7 bpm for 0.1 ms and 114.4 ± 11.2 bpm for 2 ms). At the 3 Hz stimuli, RVNS showed reduction in a pulse width dependent manner (110.2 ± 7.5 bpm for 0.1 ms, 105.3 ± 7.3 bpm for 1 ms, and 99.6 ± 8.6 bpm for 2 ms), displayed in figure 5.5C. There were no significant differences between all baselines (from 146.8 ± 11.2 bpm to 138.2 ± 9.1 bpm).

Values of absolute reduction from figure 5.5 were converted into percentage of reduction, shown in figure 5.6. Heart rate decreases by 1 Hz stimuli showed no significant difference between 1 and 2 ms duration, 1 ms (16.9 ± 3.5 %) reduced HR more than 0.1 ms (7.4 ± 1.7 %, $P < 0.01$) and 2 ms (14.4 ± 1.1 %, ns), figure 5.6A. However, the 2 Hz and 3 Hz stimuli decreased HR in a PW dependent manner as level of percent were larger from short duration to long duration; for 2 Hz stimulation [16.0 ± 1.8 % for 0.1 ms, 16.3 ± 2.7 % for 1 ms, 19.0 ± 3.4 % for 2 ms], for 3 Hz stimulation [20.6 ± 3.3 % for 0.1 ms, 25.7 ± 3.0 % for 1 ms, 30.5 ± 3.0 % for 2 ms], (figure 5.6B and C).

HR reduction data by low frequency stimuli were regrouped in order to observe the effect of different frequencies as shown in figure 5.7. Within the same PW, RVNS significantly decreased HR in a frequency dependent reduction. Then, percentage HR reductions were displayed in figure 5.8. Higher frequency

caused higher percentage of HR reduction. However, for PW 1 ms stimuli, frequency 1 Hz dropped HR to the same percentage as 2 Hz frequency ($16.9 \pm 3.5\%$ vs $16.0 \pm 1.8\%$, respectively), figure 5.8B. The high amplitude used by this stimulation scheme caused large HR reduction (overall more than 10%) even with low frequencies, which confirmed the dominant impact of voltage on the vagal HR effect.

Investigation of the effect of stimulation frequency during frequency response curve and HR reduction during ERP protocol displayed a pattern of reduction in a frequency dependent manner within the same PW. These responses were similar to the responses of low frequency stimulation from the previous chapter. Looking at the effect of PW within a fixed frequency, the PW dependent HR reduction was observed at frequency 3 Hz. The 2 Hz stimuli produced the same level of HR decrease in all PWs. With frequency 1 Hz, HR change was not consistent as PW 1 ms produced the largest change compared to 0.1 ms and 2 ms. These data suggested that stimulation frequency was a parameter that promoted effects of high amplitude voltage and PW on vagal fibre recruitment.

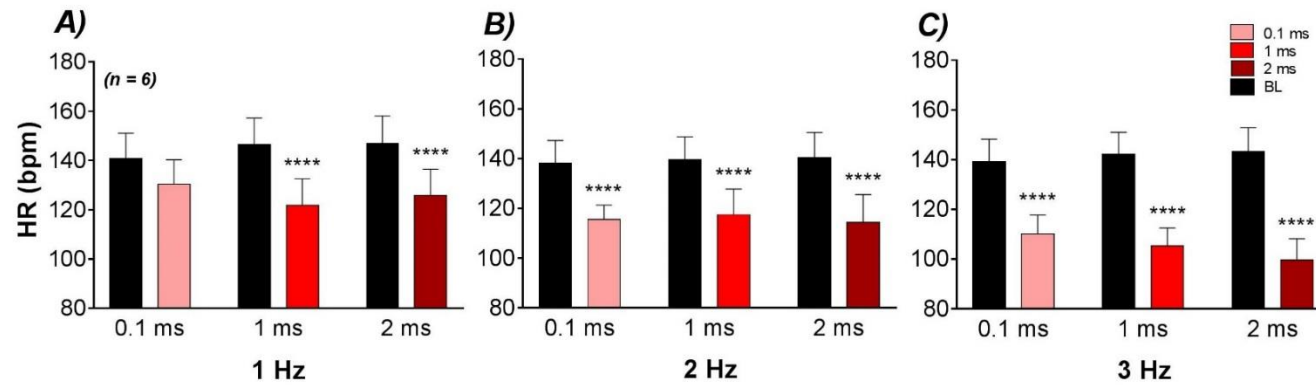


Figure 5.5 Effects of PW on HR reduction by low frequency stimulation ERP protocol.

Heart rate (HR), beat per min (bpm); $n = 6$, mean \pm SEM., Two-way ANOVA with Bonferroni post hoc test, **** $P < 0.0001$.

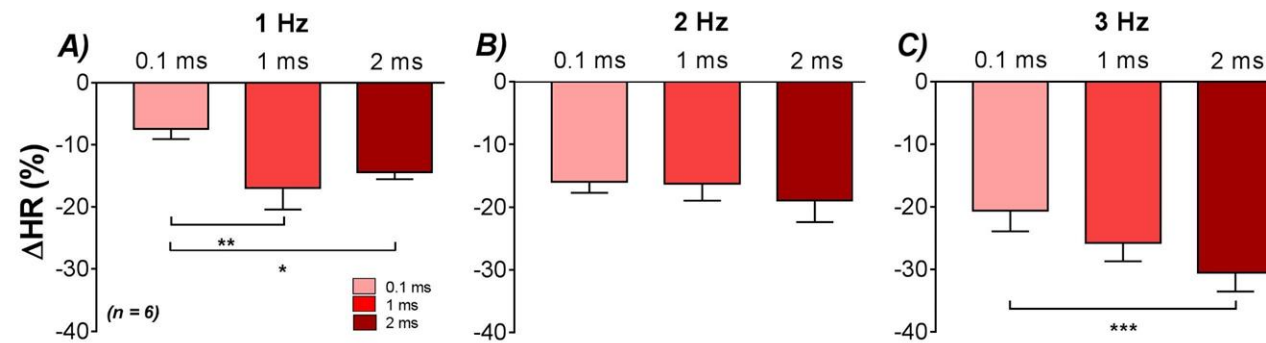


Figure 5.6 Effects of PW on percentage of HR decrease by low frequency stimulation ERP protocol.

Heart rate (HR); $n = 6$, mean \pm SEM., Two-way ANOVA with Bonferroni post hoc test, * $P < 0.05$, ** $P < 0.01$, *** $P < 0.001$.

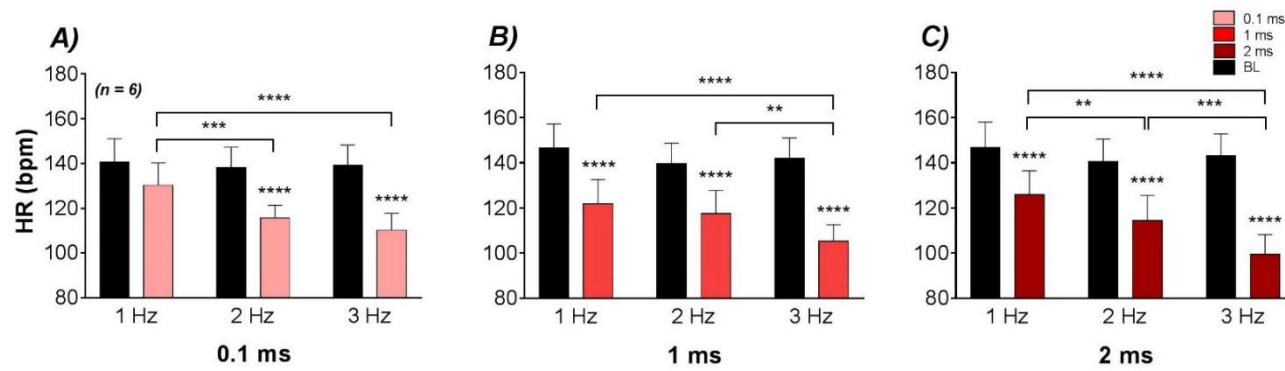


Figure 5.7 Effects of frequency on HR reduction by low frequency stimulation ERP protocol.

Heart rate (HR), beat per min (bpm); $n = 6$, mean \pm SEM., Two-way ANOVA with Bonferroni post hoc test, ** $P < 0.01$, *** $P < 0.001$, **** $P < 0.0001$.

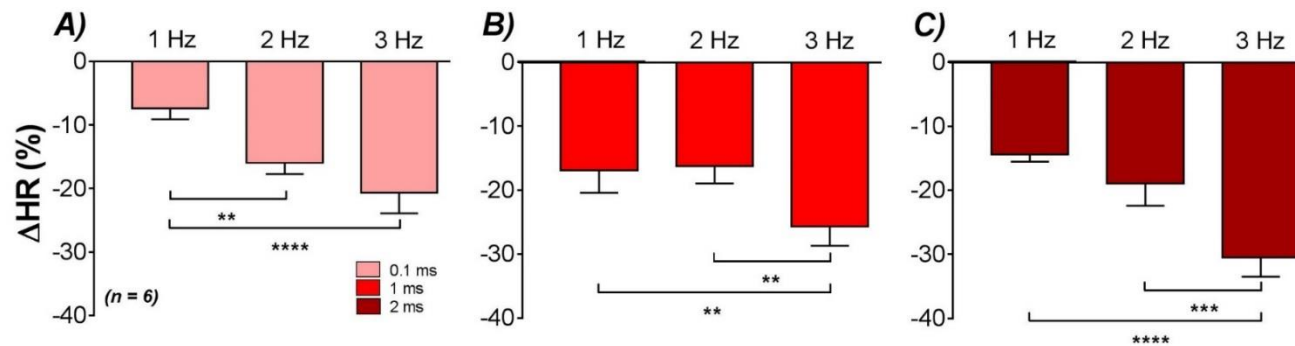


Figure 5.8 Effects of frequency on percentage of HR decrease by low frequency stimulation ERP protocol.

Heart rate (HR); $n = 6$, mean \pm SEM., Two-way ANOVA with Bonferroni post hoc test, ** $P < 0.01$, *** $P < 0.001$, **** $P < 0.0001$.

5.5.1.2 ERP prolongation by low frequency RVNS

The first ventricular EP parameter investigated was effective refractory period (ERP) that represented the refractoriness of the heart. The effects of low frequency stimulation on ERP prolongation is displayed in figure 5.9. At 1 Hz, there was no significant prolongation by RVNS in any PW (figure 5.9A). For 2 Hz frequency, a significant prolongation were observed at 0.1 ms (from 148.3 ± 7.6 ms to 156.7 ± 7.6 ms, $P < 0.01$) and 1 ms (from 148.3 ± 7.6 ms to 156.7 ± 7.6 ms, $P < 0.01$), displayed in figure 5.9B. Stimulations by frequency 3 Hz prolonged ERP in all PWs [PW 0.1 ms (149.2 ± 6.9 ms to 160.0 ± 6.1 ms, $P < 0.0001$), PW 1 ms (149.2 ± 6.9 ms to 157.5 ± 6.7 ms, $P < 0.01$), and PW 2 ms (149.2 ± 6.9 ms to 155.8 ± 7.0 ms $P < 0.05$), figure 5.9C].

Effect of stimulation frequency on ERP prolongation with the same PW is displayed in figure 5.10. At PW 0.1 ms, frequency 2 Hz significantly prolonged ERP more than 1 Hz (156.7 ± 7.6 ms vs 148.3 ± 7.7 ms, $P < 0.001$) and 3 Hz ERP was also significantly longer than the 1 Hz (160.0 ± 6.1 ms vs 148.3 ± 7.7 ms, $P < 0.0001$), figure 5.10A. There was no difference between 2 Hz and 3 Hz ERPs. RVNS by 1 ms showed the same response characteristic to 0.1 ms ERP results. The frequencies 2 Hz and 3 Hz significantly prolonged ERP more than 1 Hz; 2Hz vs 1 Hz (156.7 ± 7.6 ms vs 147.5 ± 8.5 ms, $P < 0.001$), 3 Hz vs 1 Hz (157.5 ± 6.7 ms vs 147.5 ± 8.5 ms, $P < 0.0001$), figure 5.10B. For RVNS by 2 ms, ERP at 2 Hz was significantly longer than 1 Hz (154.2 ± 6.2 ms vs 148.3 ± 9.8 ms, $P < 0.05$). Also, 3 Hz ERP was significantly longer than 1 Hz (155.8 ± 7.0 ms vs 148.3 ± 9.8 ms, $P < 0.01$). Response of ERP to stimulation frequency showed a frequency dependent prolongation as a higher frequency prolonged ERP more than a lower frequency.

Results from this section demonstrated that ERP prolongation at low frequency stimulation were found at frequencies 2 Hz and 3 Hz. Frequency 1 Hz did not produce any significant prolongation. Considered with HR reduction results, RVNS by low frequency was seemed to provide a significant prolongation at frequencies 2 Hz and above. Compared between effect of stimulation PW and stimulation frequency on ERP result, there was only an effect of different stimulation frequency on ERP prolongation as data showed a frequency

dependent prolongation pattern. There was no effect of different PW on prolongation by low frequency stimulation. In addition, the high amplitude voltage ($80\% \Delta HR_{max}$) used in this low frequency approach seemed to elevate ERP, which was similar to the effect of low frequency stimulation from the previous chapter.

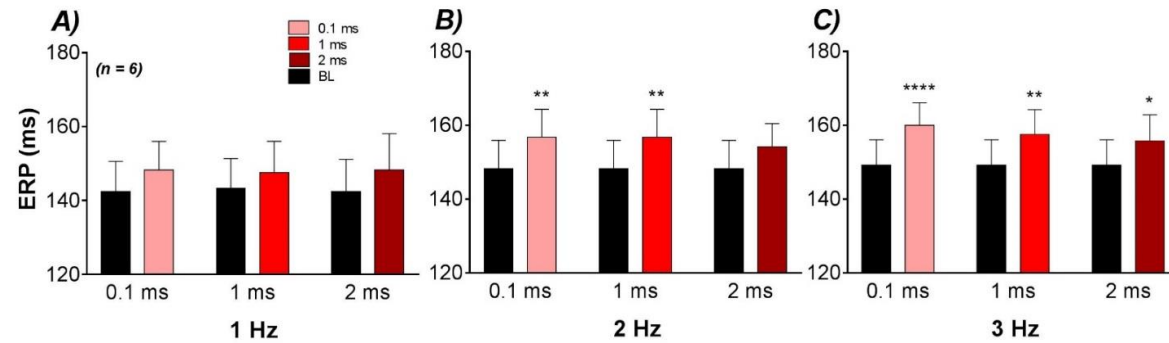


Figure 5.9 Effects of PW on ERP prolongation by low frequency stimulation

Effective refractory period (ERP), millisecond (ms); $n = 6$, mean \pm SEM., Two-way ANOVA with Bonferroni post hoc test, * $P < 0.05$, ** $P < 0.01$, **** $P < 0.0001$.

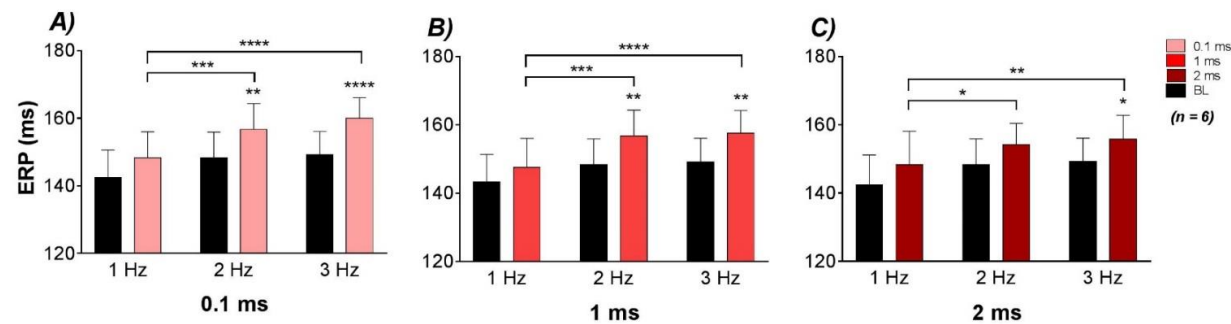


Figure 5.10 Effects of frequency on ERP prolongation by low frequency stimulation

Effective refractory period (ERP), millisecond (ms); $n = 6$, mean \pm SEM., Two-way ANOVA with Bonferroni post hoc test, * $P < 0.05$, ** $P < 0.01$, **** $P < 0.0001$.

5.5.2 Low voltage stimulation ERP protocol

5.5.2.1 Heart rate reduction by low voltage RVNS during ERP protocol

Then, the voltage strength that caused a $10\% \Delta HR_{BL}$ with a frequencies 5 Hz, 10 Hz, and 20 Hz were applied to the right vagus. This parameter set aimed to minimize the vagal HR effect by reducing voltage strength to the level of clinically used. Responses of HR and ERP prolongation to these stimulation approach revealed the effects from the high frequency used.

The effects of stimulation pulse width on HR reduction was shown in figure 5.11. At 5 Hz, RVNS significantly reduced HR from 147.6 ± 4.7 bpm to 140.5 ± 4.2 bpm by 1 ms ($P < 0.01$) and from 147.5 ± 4.7 bpm to 141.6 ± 5.1 bpm by 2 ms ($P < 0.05$) (figure 5.11A). RVNS at 10 Hz significantly lowered HR in all stimulation PWs [0.1 ms (from 148.4 ± 5.8 bpm to 139.2 ± 6.0 bpm, $P < 0.001$), 1 ms (from 148.6 ± 5.6 bpm to 142.1 ± 4.7 bpm, $P < 0.05$), and 2 ms (from 148.3 ± 5.4 bpm to 140.5 ± 4.6 bpm, $P < 0.01$); figure 5.11B]. The 20 Hz stimuli showed a significant reduction in all PWs, as demonstrated in figure 5.11C. The PW 0.1 ms reduced HR from 149.8 ± 8.0 bpm to 143.9 ± 7.4 bpm ($P < 0.05$). The 1 ms decreased HR from 149.2 ± 7.1 to 138.5 ± 7.7 bpm ($P < 0.0001$) and 2 ms reduced from 147.3 ± 5.4 bpm to 141.1 ± 6.6 bpm ($P < 0.05$).

Percent HR reductions associated with this low voltage stimulation were calculated and displayed in figure 5.12. By frequency 5 Hz, reductions were 3.9 ± 0.5 %, 4.7 ± 1.6 %, and 4.0 ± 1.2 %, for 0.1 ms, 1 ms, and 2 ms respectively (figure 5.12A). Frequency 10 Hz reduced HR 6.2 ± 1.6 % for 0.1 ms, 4.3 ± 1.2 % for 1 ms, and 5.2 ± 1.1 % for 2 ms (figure 5.12B). For 20 Hz, percent drop were 4.1 ± 1.5 %, 7.3 ± 2.0 %, and 4.4 ± 1.1 %, for 0.1 ms, 1 ms, and 2 ms respectively (figure 5.12C).

Heart rate reduction during ERP protocol in response to stimulation frequency is displayed in figure 5.13 and associated percentage of heart rate changes is displayed in figure 5.14. From these results, there was no differences of heart rate reduction and percent heart rate changes between stimulation frequencies of low voltage RVNS. Overall HR reduction by this parameter set was smaller

than 10% suggesting a relatively small effect of high frequency (low voltage) on vagal HR changes.

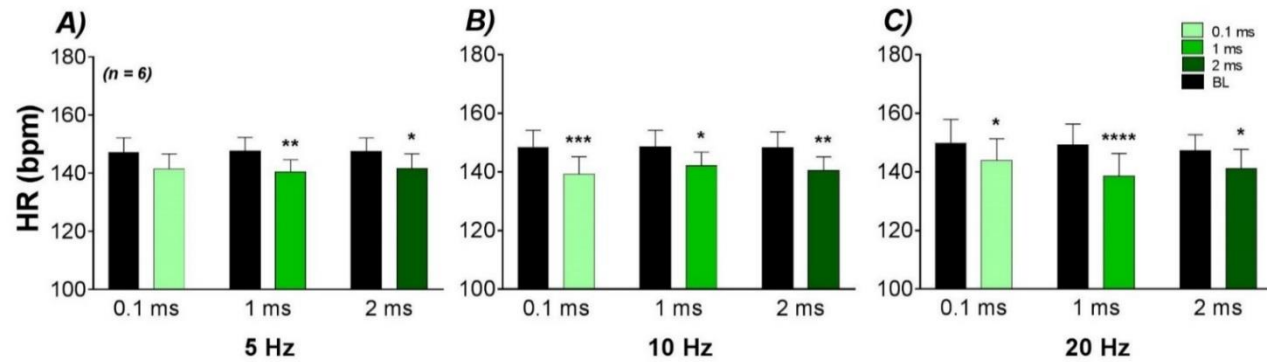


Figure 5.11 Effects of PW on HR reduction by low voltage stimulation ERP protocol.

Heart rate (HR), beat per min (bpm); n = 6, mean \pm SEM., Two-way ANOVA with Bonferroni post hoc test, * P < 0.05, ** P < 0.01, *** P < 0.001, **** P < 0.0001

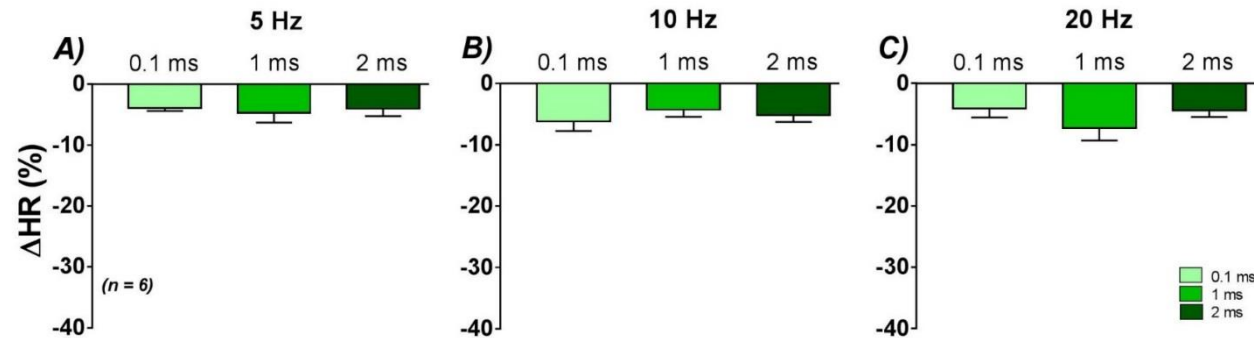


Figure 5.12 Effects of PW on percentage of HR decrease by low voltage stimulation ERP protocol.

Heart rate (HR); n = 6, mean \pm SEM.

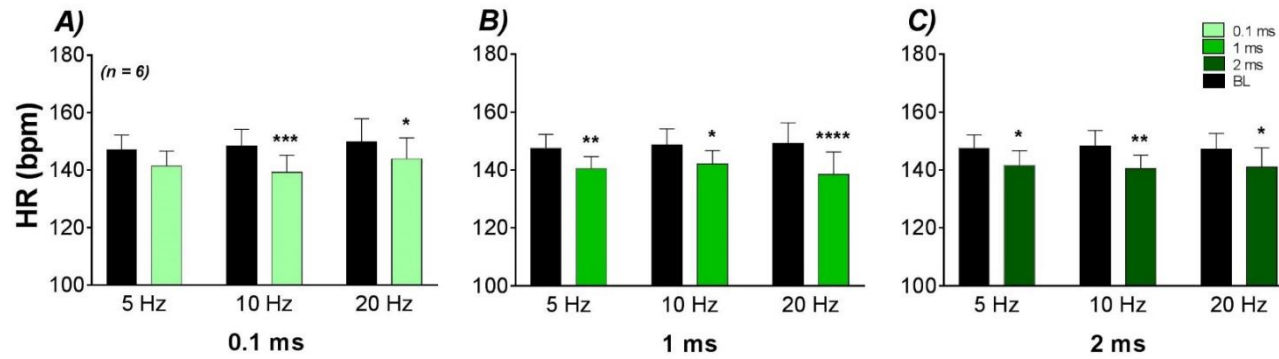


Figure 5.13 Effects of frequency on HR reduction by low voltage stimulation ERP protocol.

Heart rate (HR), beat per min (bpm); $n = 6$, mean \pm SEM., Two-way ANOVA with Bonferroni post hoc test, * $P < 0.05$, ** $P < 0.01$, *** $P < 0.001$, **** $P < 0.0001$.

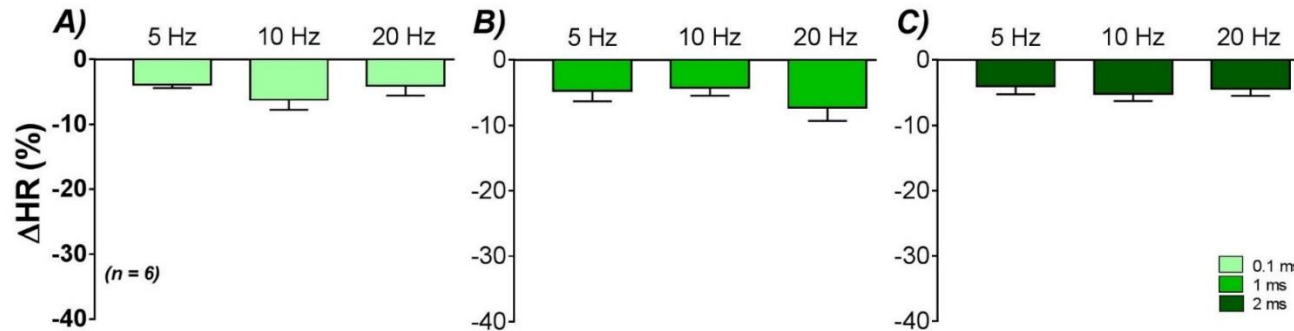


Figure 5.14 Effects of frequency on percentage of HR decrease by low voltage stimulation ERP protocol.

Heart rate (HR); $n = 6$, mean \pm SEM.

5.5.2.2 ERP prolongation by low voltage RVNS

Effect of low voltage stimulation on ERP prolongation was performed in order to investigate the response to low amplitude voltage and high frequency used by this method. The low voltage RVNS produced prolongations of ERP in all PWs and all frequencies but all prolongations did not reach statistical significance. For 5 Hz stimulation (figure 5.15A), PW 0.1 ms prolonged ERP from 140.0 ± 6.8 ms to 149.2 ± 4.4 ms (ns). The 1 ms prolonged ERP from baseline 140.0 ± 7.3 ms to 147.5 ± 5.6 ms (ns) and the 2 ms prolonged ERP from 137.5 ± 7.8 ms to 141.7 ± 8.7 ms (ns). With 10 Hz frequency (figure 5.15B), baseline 140.0 ± 7.1 ms was prolonged to 145.8 ± 8.6 ms by 0.1 ms (ns). The 1 ms caused ERP prolongation from 140.0 ± 5.2 ms to 145.8 ± 6.2 ms (ns) while 2 ms prolonged ERP from 142.5 ± 4.4 ms to 148.3 ± 5.9 ms (ns). With 20 Hz stimulation (figure 5.15C), RVNS 0.1 ms prolonged ERP from 139.2 ± 7.8 ms to 141.7 ± 7.9 ms (ns). The 1 ms and 2 ms prolonged ERP from 140.8 ± 7.0 ms to 150.0 ± 7.4 ms (ns) and from 141.7 ± 5.7 ms to 148.3 ± 6.0 ms (ns), respectively. There was no significant difference between baseline ERP of all frequencies and all PWs. Effect of stimulation frequency on ERP prolongation by low voltage stimulation was regrouped and displayed in figure 5.16. From the figure, there was no significant prolongation of ERP by RVNS at any frequency.

Results from this section demonstrated a lack of ERP prolongation effect of RVNS as observed in the low frequency (high voltage) stimulation. The low amplitude voltage used in this stimulation failed to prolong an ERP even with high frequency. High frequency stimulation did not drive a significant HR effect and also seemed to have a small impact on ERP prolongation. In addition, combined with low voltage results from previous chapter, frequency 20 Hz seemed to be a maximum frequency that is suitable to use for stimulating vagus nerve as frequency 30 Hz did not cause any HR reduction and did not prolong ERP. Low frequency (high voltage) stimulation prolonged ERP in all stimuli but the level of prolongation was not statistical significant. These findings suggested the requirement of a high amplitude voltage used by low frequency stimulation to contribute towards an elevation of ERP.

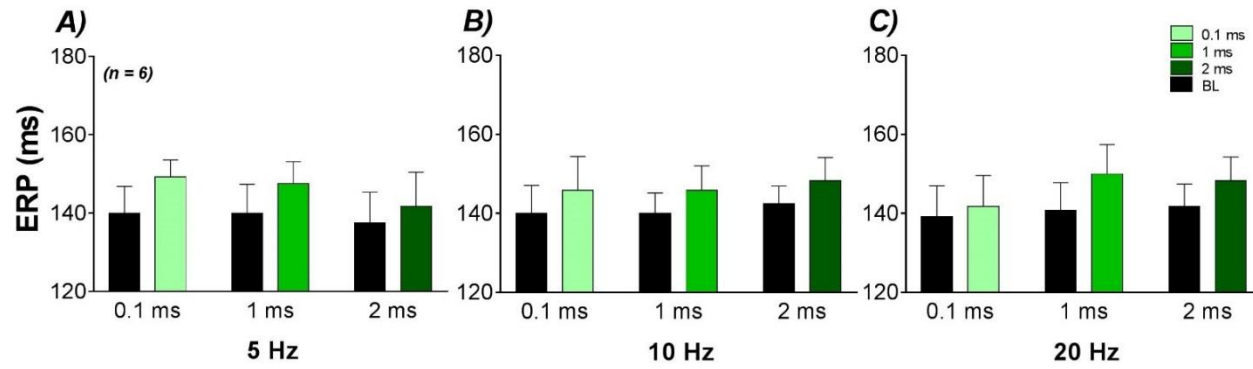


Figure 5.15 Effects of PW on ERP prolongation by low voltage stimulation

Effective refractory period (ERP), millisecond (ms); n = 6, mean \pm SEM.

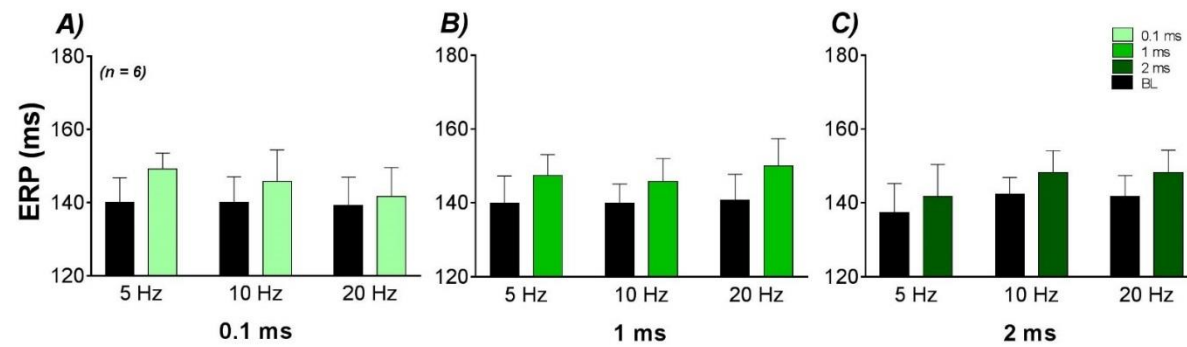


Figure 5.16 Effects of frequency on ERP prolongation by low voltage stimulation

Effective refractory period (ERP), millisecond (ms); n = 6, mean \pm SEM.

5.5.3 Low frequency low voltage stimulation ERP protocol

5.5.3.1 Heart rate reduction by low frequency low voltage RVNS during ERP protocol

From the previous 2 stimulation approaches, effects of high amplitude voltage and high frequency on HR reduction and ERP prolongation were separately investigated. With the last stimulation scheme, low amplitude voltage and low frequency were combined together and applied to the right vagus in order to assess an effect of the very low strength parameters.

HR decrease of the low frequency low voltage stimulation was shown in figure 5.17. There was no significant decrease of HR by frequency 1 Hz and 2 Hz stimuli. However, at frequency 2 Hz, PW 2 ms significantly reduced HR from 153.7 ± 10.2 bpm to 145.0 ± 9.5 bpm ($P < 0.001$) (figure 5.17B). Frequency 3 Hz significantly reduced HR from 150.1 ± 7.5 bpm to 141.6 ± 5.5 bpm ($P < 0.001$) by PW 0.1 ms. PW 1 ms also significantly decreased HR from 150.4 ± 9.8 bpm to 142.3 ± 7.5 bpm ($P < 0.01$). For frequency 3 Hz, a significantly lower of HR was found by RVNS with PW 2 ms (150.9 ± 8.5 bpm to 143.1 ± 8.4 bpm, $P < 0.01$), figure 5.17C.

Then, the heart rate reduction in figure 5.17 was analysed as percent changes and displayed in figure 5.18. Overall, all percent heart rate changes were less than 10%. The 1 Hz simulation reduced heart rate by 2.0 ± 0.6 %, 2.6 ± 1.0 %, and 1.8 ± 0.9 % for 0.1 ms, 1 ms, and 2 ms respectively (figure 5.18A). Frequency 2 Hz decreased heart rate 3.9 ± 1.1 % for 0.1 ms, 3.5 ± 0.5 % for 1 ms, and 5.6 ± 1.8 % for 2 ms (figure 5.18B). Lastly, 3 Hz low frequency low voltage ERP reduced heart rate 5.4 ± 1.2 %, 5.0 ± 1.9 %, and 5.2 ± 1.0 % by 0.1 ms, 1 ms, and 2 ms pulse widths, respectively (figure 5.18C).

Effect of frequency on HR reduction during low frequency low voltage ERP protocol is displayed in figure 5.19. Within PW 0.1 ms, frequency 2 Hz significantly lowered HR more than 1 Hz ($P < 0.05$) and 3 Hz also significantly reduced more than 1 Hz ($P < 0.001$), (figure 5.19A). For PW 1 ms, there was a significant difference in the reduction between 3 Hz and 1 Hz ($P < 0.001$) (figure 5.19B). Similarly, with PW 2 ms a significant difference in HR reduction is seen

between 3 Hz and 1 Hz ($P < 0.001$), figure 5.19C. About percent HR changes, significant difference was observed only between frequencies 1 Hz and 2 Hz at PW 2 ms ($P < 0.05$), figure 5.20C.

The HR response of this section displayed same level of HR reduction to the low voltage stimulation. All HR changes were less than 10% as influenced by low amplitude voltage. The significant reductions were found mainly at the highest frequency used (3 Hz).

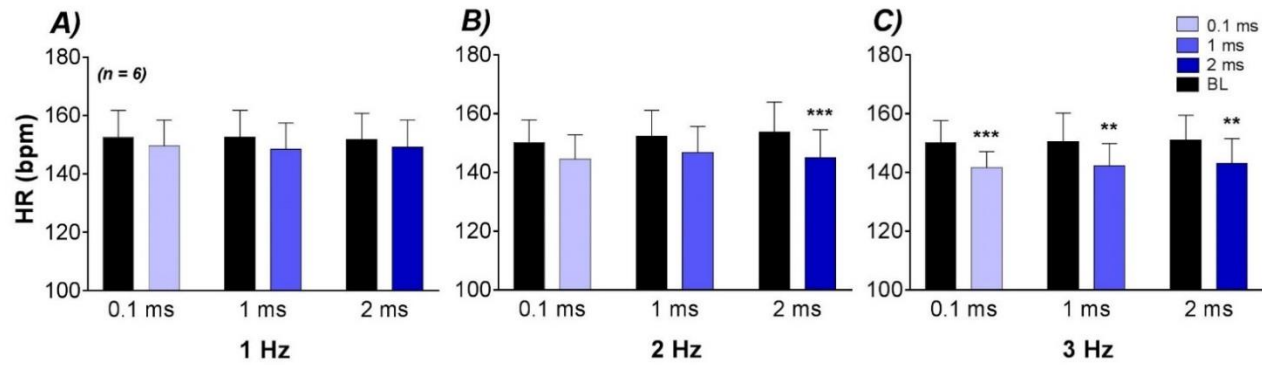


Figure 5.17 Effects of PW on HR reduction by low frequency low voltage stimulation ERP protocol.

Heart rate (HR), beat per min (bpm); n = 6, mean \pm SEM., Two-way ANOVA with Bonferroni post hoc test, ** P < 0.01, *** P < 0.001.

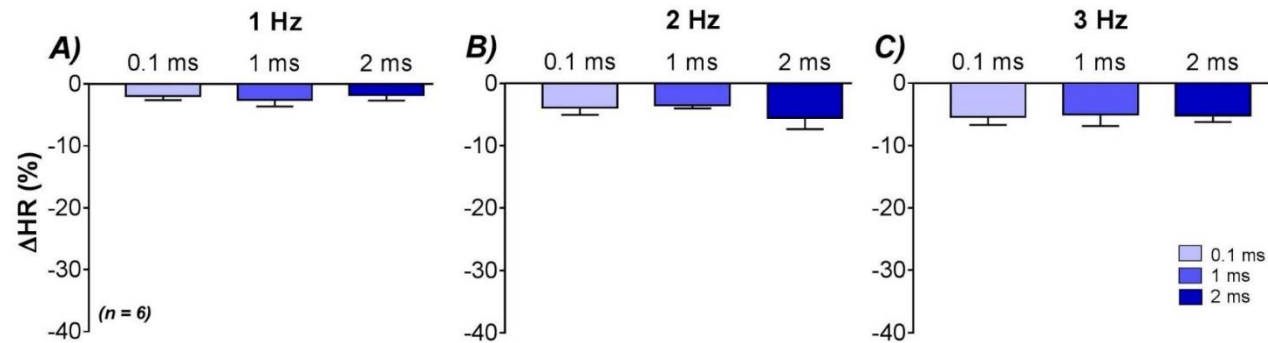


Figure 5.18 Effects of PW on percentage of HR decrease by low frequency low voltage stimulation ERP protocol.

Heart rate (HR); n = 6, mean \pm SEM.

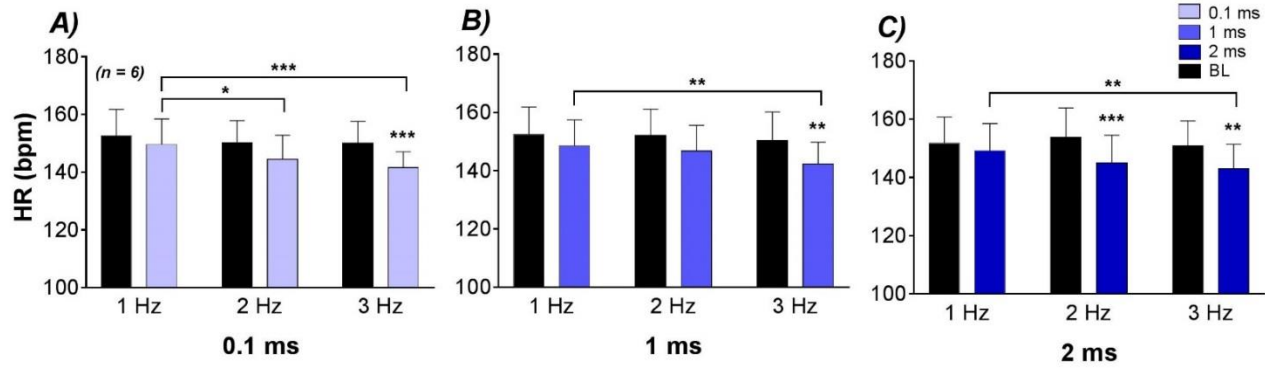


Figure 5.19 Effects of frequency on HR reduction by low frequency low voltage stimulation ERP protocol.

Heart rate (HR), beat per min (bpm); n = 6, mean ± SEM., Two-way ANOVA with Bonferroni post hoc test, * P < 0.05, ** P < 0.01, *** P < 0.001.

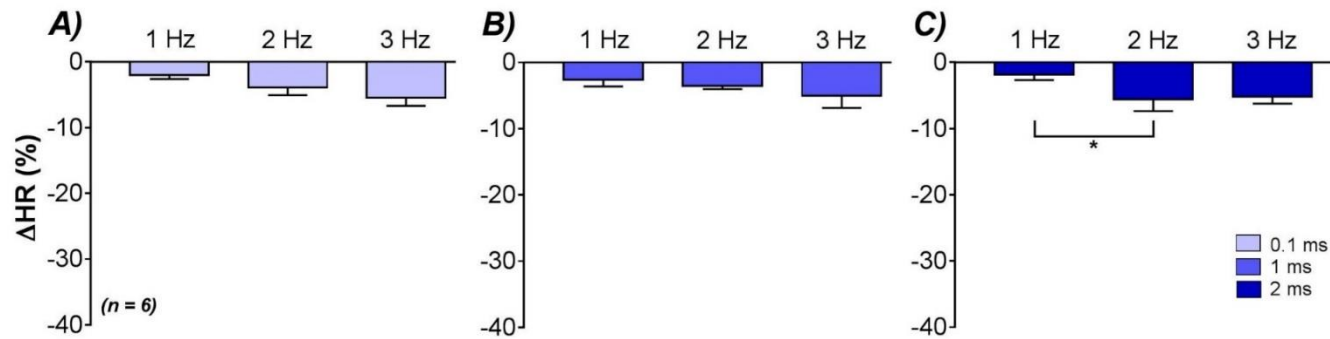


Figure 5.20 Effects of frequency on percentage of HR decrease by low frequency low voltage stimulation ERP protocol.

Heart rate (HR); n = 6, mean ± SEM.

5.5.3.2 ERP prolongation by low frequency low voltage RVNS

The ERP response to low voltage strength and low frequency was studied to provide results of this very low strength stimulation. The low frequency low voltage displayed prolongation of ERP in all PWs and all frequencies. However, the prolongation by 1 Hz and 2 Hz were not significant. For 3 Hz, ERP prolongation were from 144.2 ± 3.5 ms to 149.2 ± 3.0 ms by 0.1 ms ($P < 0.05$). Significant prolongation was also seen at 1 ms stimulation, from 144.2 ± 3.5 ms to 150.0 ± 3.4 ms ($P < 0.01$). The PW 2 ms prolonged ERP from 144.2 ± 3.5 ms to 146.7 ± 2.5 ms (ns), figure 5.21C.

The effects of stimulation frequency on ERP prolongation are shown in figure 5.22. With 0.1 ms pulse width, 3 Hz stimulation significantly prolonged ERP more than 2 Hz ($P < 0.01$), figure 5.22A. Significant prolongation between 3 Hz and 2 Hz was also observed in the 1 ms pulse width ($P < 0.001$), figure 5.22B. No differences was observed within the 2 ms stimulation. There was no change of baseline ERP by this low frequency low voltage RVNS.

The low frequency low voltage stimulation displayed ERP prolongation only at frequency 3 Hz. Frequencies 1 Hz and 2 Hz also showed small changes of ERP from baseline but this changes were not statistical significance. Together with HR reduction data from the previous section, the low frequency low voltage stimulation had a small effect on HR decrease and ERP increase. Even significant prolongations of ERP was observed at 3 Hz with 0.1 ms and 1 ms stimuli, level of prolongation by this small amplitude voltage with low frequency stimulation were very small. Compared to ERP results by low voltage (high frequency) method, level of prolongation by low frequency low voltage technique was smaller. This data confirmed a prominent effect of stimulation voltage over frequency and pulse width on prolongation of effective refractory period.

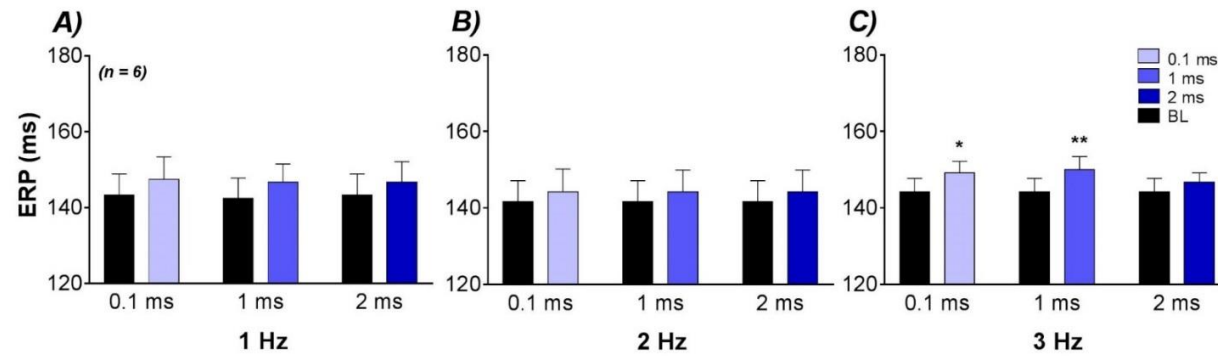


Figure 5.21 Effects of PW on ERP prolongation by low frequency low voltage stimulation

Effective refractory period (ERP), millisecond (ms); $n = 6$, mean \pm SEM., Two-way ANOVA with Bonferroni post hoc test, * $P < 0.05$, ** $P < 0.01$.

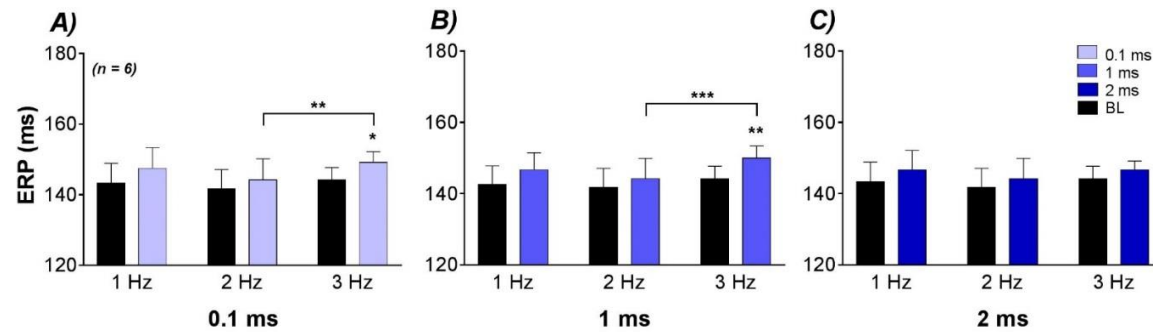


Figure 5.22 Effects of frequency on ERP prolongation by low frequency low voltage stimulation

Effective refractory period (ERP), millisecond (ms); $n = 6$, mean \pm SEM., Two-way ANOVA with Bonferroni post hoc test, * $P < 0.05$, ** $P < 0.01$, *** $P < 0.001$.

5.6 Effect of different RVNS parameters on ventricular fibrillation threshold (VFT)

5.6.1 VFT increase by low frequency RVNS

Moving to the 2nd ventricular EP parameter, VFT was studied to measure the difficulty of ventricular fibrillation (VF) induction. VNS was known to increase this threshold when compared to the baseline condition (Ng et al., 2001). In this study, the range of VNS parameters were tested and the VFT responses to these combinations were measured.

Firstly, the effect of high voltage strength ($80\% \Delta HR_{max}$) with low frequency was studied. RVNS by this low frequency scheme significantly increased VFT in all PWs of frequency 1 Hz. The PW 0.1 ms increased VFT from 2.8 ± 0.4 mA to 5.0 ± 1.2 mA ($P < 0.05$). VFT was increased from 2.8 ± 0.5 mA to 4.9 ± 0.8 mA ($P < 0.05$) by 1 ms stimulus. For PW 2 ms, VFT was increased from 2.8 ± 0.5 mA to 4.8 ± 0.9 mA ($P < 0.05$), (figure 5.23A). With frequency 2 Hz, PW 0.1 ms significantly increased VFT from 3.3 ± 0.5 mA to 6.3 ± 1.5 mA ($P < 0.001$). The 1 ms pulse width increased VFT from 3.3 ± 0.6 mA to 4.8 ± 0.5 mA (ns) and the 2 ms increased it from 2.9 ± 0.4 mA to 5.3 ± 0.6 mA ($P < 0.01$), figure 5.23B. With frequency 3 Hz stimulation, 0.1 ms increased VFT from 3.6 ± 0.4 mA to 5.0 ± 0.4 mA (ns) while 1 ms increased threshold from 3.8 ± 0.4 mA to 4.8 ± 0.6 mA (ns), figure 5.23C. Finally, PW 2 ms increased VFT from 3.9 ± 0.5 mA to 5.5 ± 0.5 mA (ns). There was no difference between effects of PW on VFT increase within all 3 frequencies.

VFT increase by low frequency stimulation was then calculated as percentage change and is shown in figure 5.24. Frequency 1 Hz increased VFT 76.0 ± 23.6 %, 79.1 ± 22.6 %, and 69.4 ± 24.8 % for PWs 0.1 ms, 1 ms, and 2 ms, respectively (figure 5.24A). VFT was increased 80.3 ± 19.8 %, 64.4 ± 25.6 %, and 94.0 ± 24.9 % for PWs 0.1 ms, 1 ms, and 2 ms at 2 Hz frequency (figure 5.24B). For the 3 Hz frequency (figure 5.24C), RVNS increased VFT 46.2 ± 17.1 % by 0.1 ms PW, 31.3 ± 21.8 % by 1 ms PW, and 48.3 ± 17.6 % by PW 2 ms. Effect of stimulation frequency on VFT increase is displayed in figure 5.25. There was no difference between effects of stimulation frequency on VFT

increase within the same PW. In addition, no difference in percentage VFT increase was observed in a comparison of frequency effect (figure 5.26).

Results of the low frequency stimulation on VFT increase demonstrated a protective effect of VNS as values were increased from baseline in all stimuli. Responses of VFT to low frequency stimulation displayed a random increase. At 0.1 ms stimuli, data showed an inconsistent increase of threshold in response to frequencies. With moderate 1 ms duration, vagal stimulation increased thresholds in the same level by all 3 frequencies. Then, the long duration PW displayed a level of threshold increase in proportion to stimulation frequency, similar to ventricular fibrillation threshold results from the previous chapter.

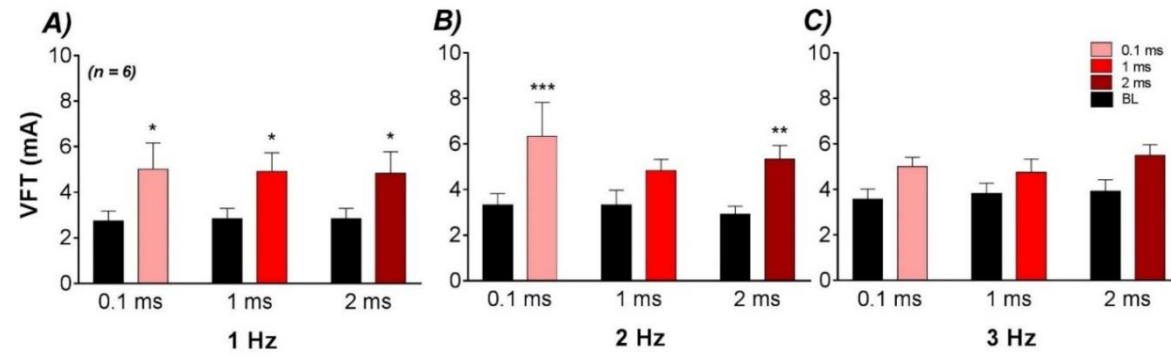


Figure 5.23 Effects of PW on VFT increase by low frequency stimulation

Ventricular fibrillation threshold (VFT), milliampere (mA); $n = 6$, mean \pm SEM., Two-way ANOVA with Bonferroni post hoc test, * $P < 0.05$, ** $P < 0.01$, *** $P < 0.001$.

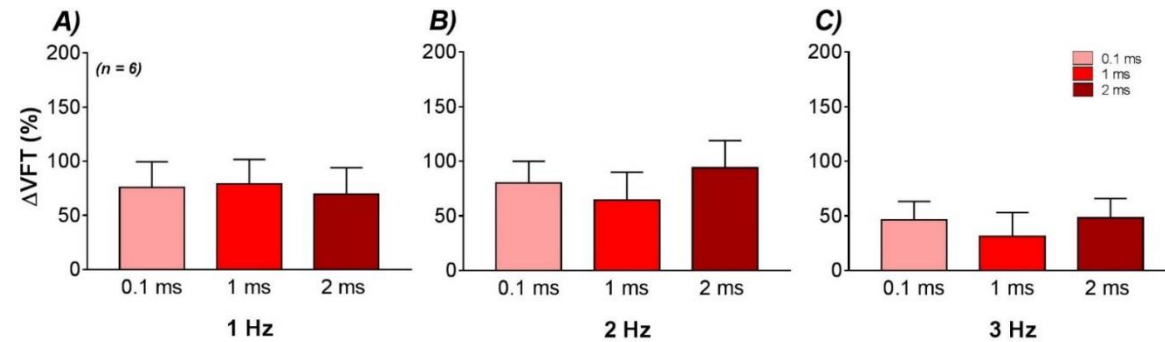


Figure 5.24 Effects of PW on percentage of VFT increase by low frequency stimulation VFT protocol.

Ventricular fibrillation threshold (VFT); $n = 6$, mean \pm SEM.

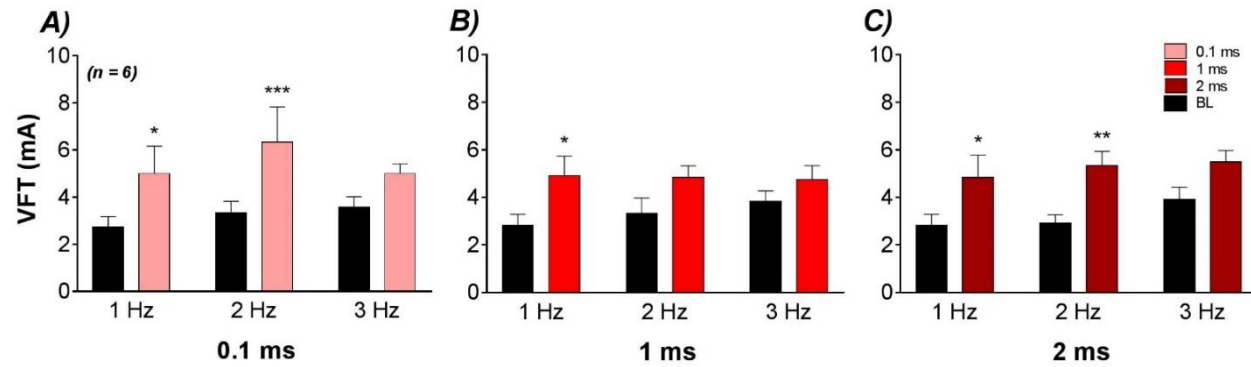


Figure 5.25 Effects of frequency on VFT increase by low frequency stimulation

Ventricular fibrillation threshold (VFT), milliamper (mA); $n = 6$, mean \pm SEM., Two-way ANOVA with Bonferroni post hoc test, * $P < 0.05$, ** $P < 0.01$, *** $P < 0.001$.

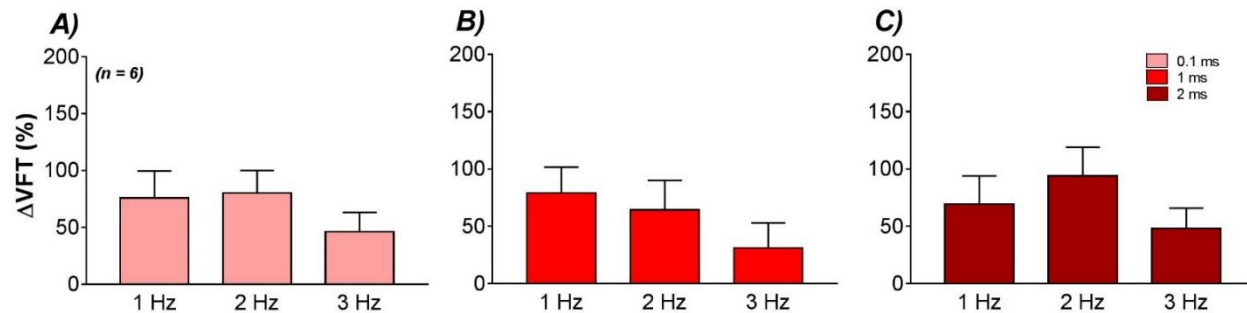


Figure 5.26 Effects of frequency on percentage of VFT increase by low frequency stimulation VFT protocol.

Ventricular fibrillation threshold (VFT); $n = 6$, mean \pm SEM.

5.6.2 VFT increase by low voltage RVNS

A high frequency approach to vagus nerve was tested with a lower voltage strength than the previous parameter set. This VFT tested by the low voltage stimulation scheme aimed to observe the effect of high frequency RVNS on the threshold increase. Effects of low voltage stimulation on VFT increase is shown in figure 5.27. With the frequency 5 Hz, 0.1 ms significantly increased VFT from 2.8 ± 0.6 mA to 5.1 ± 0.9 mA ($P < 0.05$). PW 1 ms increased threshold from 2.6 ± 0.6 mA to 5.0 ± 0.7 mA ($P < 0.01$). The 2 ms increased VFT from 2.5 ± 0.5 mA to 3.7 ± 0.6 mA (ns), figure 5.27A. At 10 Hz stimulation, 0.1 ms increased VFT from 3.3 ± 0.7 mA to 5.1 ± 0.7 mA (ns) and 1 ms increased from 3.1 ± 0.5 mA to 4.8 ± 1.0 mA (ns). The 2 ms significantly increased VFT from 3.0 ± 0.6 mA to 5.3 ± 1.2 mA ($P < 0.05$), figure 5.27B. There was no significant increase of threshold by the 20 Hz stimulation (figure 5.27C) [0.1 ms, (2.8 ± 0.6 mA to 4.3 ± 0.7 mA (ns)); 1 ms (2.9 ± 0.7 mA to 4.1 ± 0.6 mA (ns)); 2 ms (3.3 ± 0.5 mA to 5.1 ± 0.6 mA (ns))].

For percentage increase of VFT, 5 Hz stimulation increased threshold 114.8 ± 50.8 %, 127.8 ± 39.9 %, and 77.3 ± 54.9 % for 0.1 ms, 1 ms, and 2 ms respectively (figure 5.28A). Frequency 10 Hz increased threshold 98.2 ± 52.3 %, 58.6 ± 18.2 %, and 91.0 ± 38.6 % for 0.1 ms, 1 ms, and 2 ms stimuli, figure 5.28B. Finally, the 20 Hz stimulation increased threshold about 65.1 ± 14.4 % for 0.1 ms, 104.2 ± 64.4 % for 1 ms, and 70.8 ± 26.8 % for 2 ms, figure 5.28C. There was a significant difference between the effect of stimulation frequency on VFT between 5 Hz and 10 Hz frequencies within the 2 ms pulse width ($P < 0.05$), figure 5.29C. There was no difference in effect of frequency on percent VFT increase.

The low voltage stimulation exhibited the overall increased of VFT similar to the low frequency results. The high frequency displayed a potential to elevate the threshold level in all stimuli. Ventricular fibrillation threshold was increased by low voltage stimulation with all stimulations. However, most of the increase were not statistical significance. There was no effect of different frequency or PW on threshold increase by low voltage stimulation. Percentages increase of

the threshold by this technique were higher than increases with low frequency stimulation.

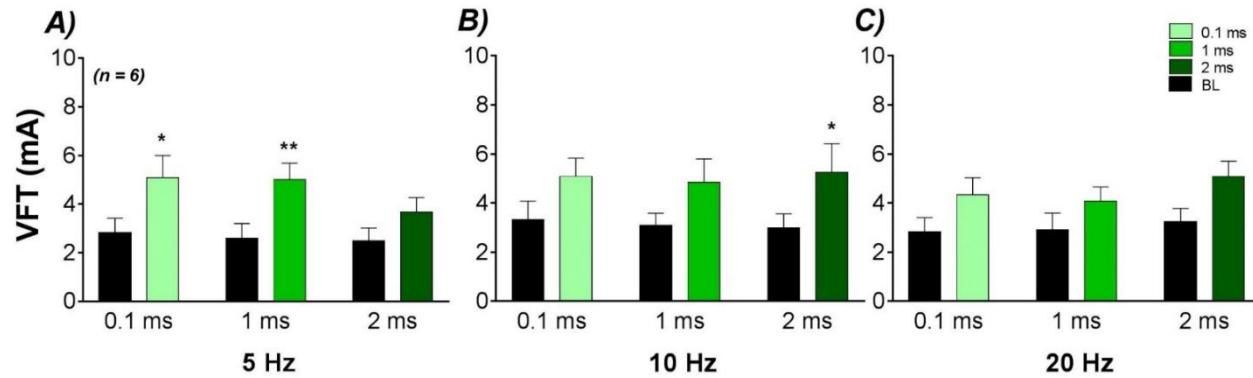


Figure 5.27 Effects of PW on VFT increase by low voltage stimulation

Ventricular fibrillation threshold (VFT), milliampere (mA); $n = 6$, mean \pm SEM., Two-way ANOVA with Bonferroni post hoc test, * $P < 0.05$, ** $P < 0.01$.

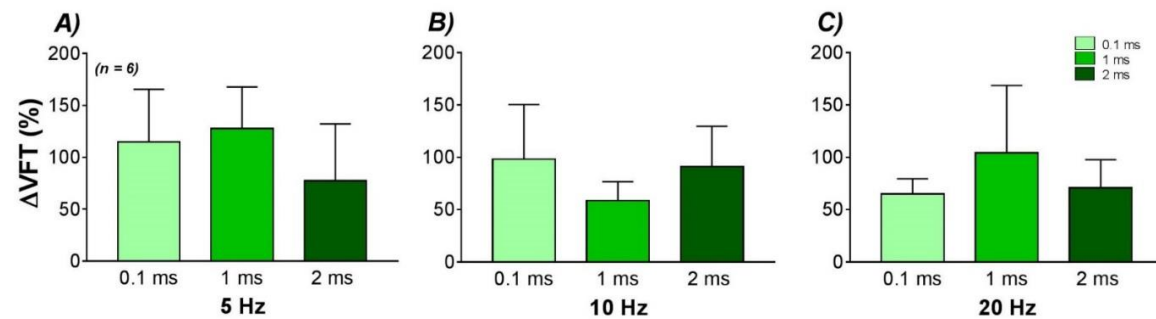


Figure 5.28 Effects of PW on percentage of VFT increase by low voltage stimulation VFT protocol.

Ventricular fibrillation threshold (VFT); $n = 6$, mean \pm SEM.

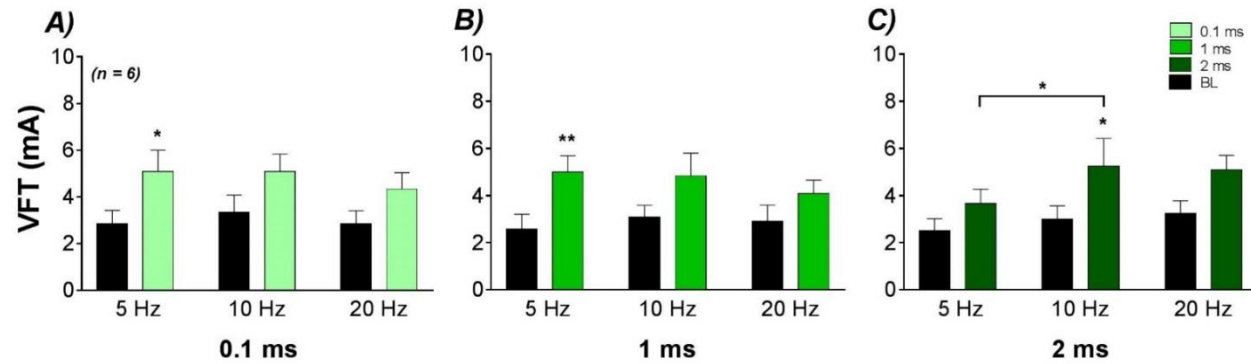


Figure 5.29 Effects of frequency on VFT increase by low voltage stimulation

Ventricular fibrillation threshold (VFT), milliampere (mA); $n = 6$, mean \pm SEM., Two-way ANOVA with Bonferroni post hoc test, * $P < 0.05$, ** $P < 0.01$.

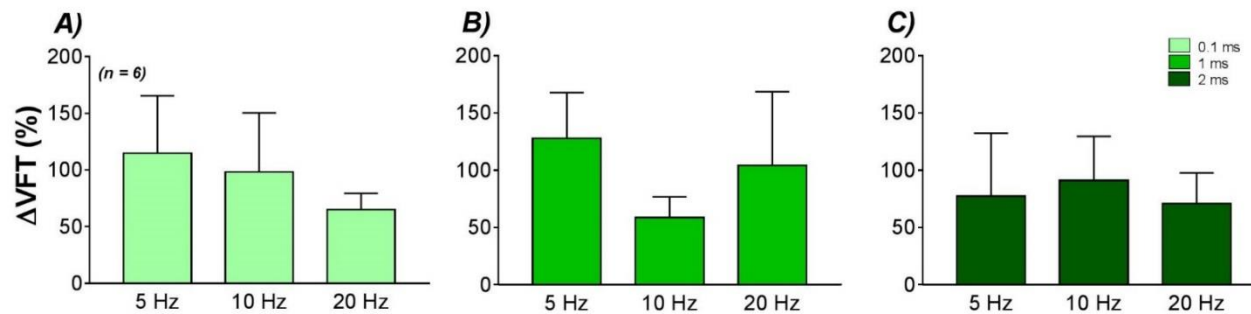


Figure 5.30 Effects of frequency on percentage of VFT increase by low voltage stimulation VFT protocol.

Ventricular fibrillation threshold (VFT); $n = 6$, mean \pm SEM.

5.6.3 VFT increase by low frequency low voltage RVNS

For the last VFT experiment - the low frequency low voltage approach - VFT response to both low voltage amplitude and low frequency was studied. For results, the low frequency low voltage stimulation at 1 Hz increased VFT in all pulse widths but not statistically significant [0.1 ms, (4.3 ± 0.8 mA to 6.2 ± 0.9 mA (ns)); 1 ms, (4.3 ± 0.8 mA to 6.3 ± 1.0 mA (ns)); 2 ms, (4.3 ± 0.8 mA to 5.9 ± 0.5 mA (ns))] (figure 5.31A). For frequency 2 Hz (figure 5.31B), PW 0.1 ms significantly increased VFT from 4.3 ± 0.6 mA to 6.5 ± 0.8 mA ($P < 0.05$). The 1 ms also significant increased threshold from 4.3 ± 0.6 mA to 6.8 ± 0.9 mA ($P < 0.01$). VFT of the 2 ms was significantly increased from 4.3 ± 0.6 mA to 6.8 ± 0.9 mA ($P < 0.01$). The 3 Hz stimulation with 0.1 ms and 1 ms pulse widths significantly increased threshold from 5.2 ± 0.9 mA to 7.9 ± 1.0 mA ($P < 0.01$) and from 4.8 ± 0.8 mA to 7.8 ± 1.2 mA ($P < 0.001$), respectively. At pulse width 2 ms VFT increased from 4.8 ± 0.8 mA to 6.6 ± 0.9 mA (ns), figure 5.31C.

Percentage increase of VFT by 1 Hz frequency were 57.5 ± 27.2 % for 0.1 ms, 57.8 ± 24.2 % for 1 ms, and 58.1 ± 27.5 % for 2 ms (figure 5.32A). Frequency 2 Hz increased threshold 54.6 ± 20.1 %, 65.9 ± 19.3 %, and 59.8 ± 17.6 % by PW 0.1 ms, 1 ms, and 2 ms respectively (figure 5.32B). For 3 Hz VFT increase, 0.1 ms increased 62.2 ± 19.6 %, 1 ms increased 66.7 ± 25.6 %, and 2 ms increased 41.0 ± 13.9 % (figure 5.32C). Difference of VFT increase as an effect of stimulation frequency was found only in PW 0.1 ms (figure 5.33A). Frequency 3 Hz significantly increased VFT more than the 1 Hz ($P < 0.05$).

Low frequency low voltage stimulation increased VFT around 50 % by all stimuli. Comparing VFT response by this technique to other 2 stimulation techniques, there was no effect of different voltage, frequency, or PW on threshold increase. An increase of threshold was inconsistent and even a lowest stimulation strength such as a combination of voltage 10% Δ HR_{BL} 0.1 ms 1 Hz was still associated with an increased threshold.

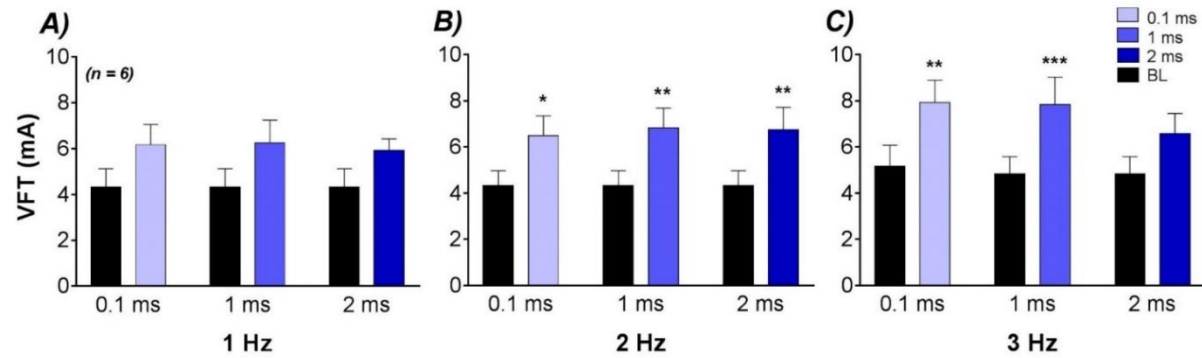


Figure 5.31 Effects of PW on VFT increase by low frequency low voltage stimulation

Ventricular fibrillation threshold (VFT), milliampere (mA); $n = 6$, mean \pm SEM., Two-way ANOVA with Bonferroni post hoc test, * $P < 0.05$, ** $P < 0.01$, *** $P < 0.001$.

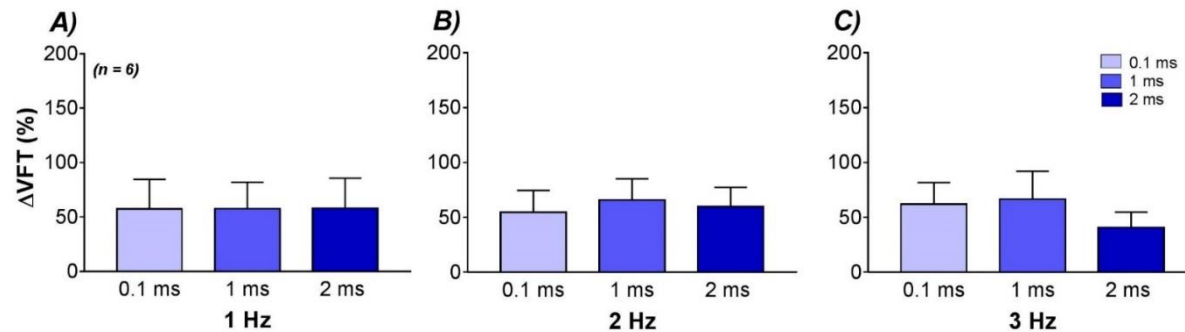


Figure 5.32 Effects of PW on percentage of VFT increase by low frequency low voltage stimulation VFT protocol.

Ventricular fibrillation threshold (VFT); $n = 6$, mean \pm SEM.

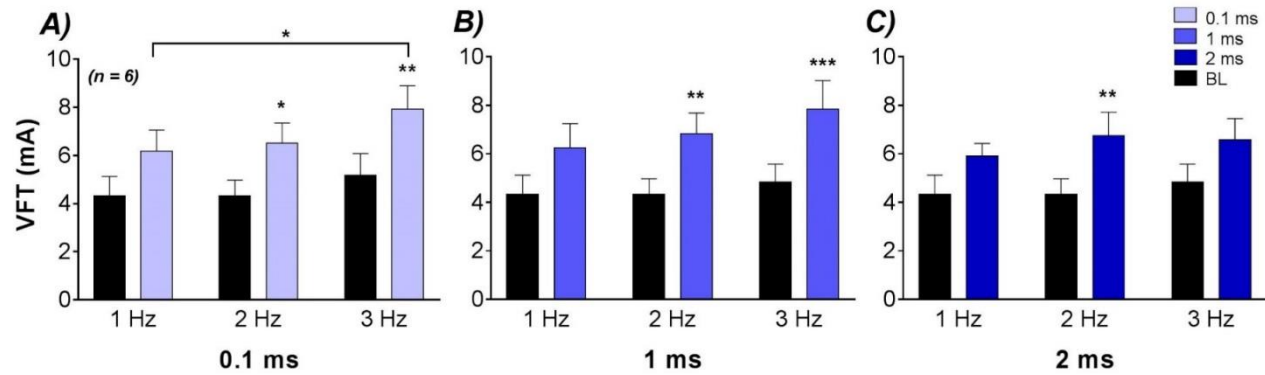


Figure 5.33 Effects of frequency on VFT increase by low frequency low voltage stimulation

Ventricular fibrillation threshold (VFT), milliampere (mA); $n = 6$, mean \pm SEM., Two-way ANOVA with Bonferroni post hoc test, * $P < 0.05$, ** $P < 0.01$, *** $P < 0.001$.

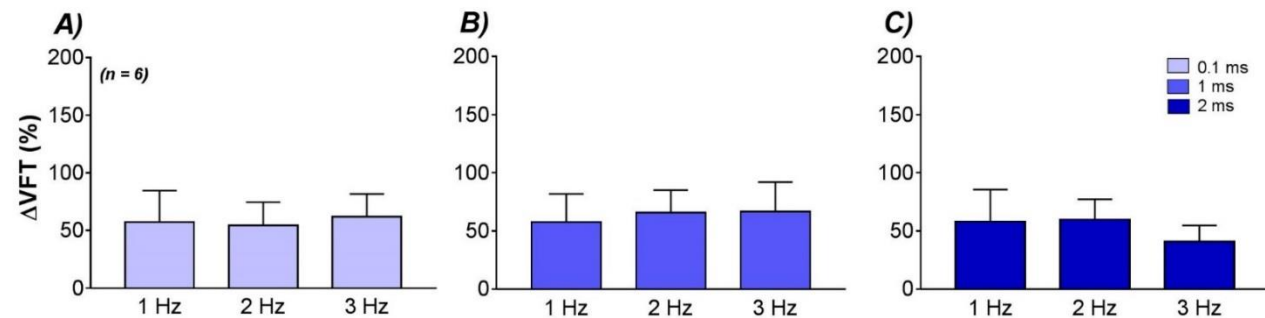


Figure 5.34 Effects of frequency on percentage of VFT increase by low frequency low voltage stimulation VFT protocol.

Ventricular fibrillation threshold (VFT); $n = 6$, mean \pm SEM.

5.7 Effect of different RVNS parameters on monophasic action potential duration restitution (MAPDR) maximum slope

5.7.1 Effect of low frequency stimulation on MAPDR slope

The final ventricular EP parameter, MAPDR was studied in association with a range of vagal stimulation parameters. In this study, MAPDRs were recorded from both apex and base of left ventricle, which allowed comparison of base – apex differences. The monophasic action potential duration restitution (MAPDR) is a relationship between preceding diastolic interval (DI) and the S2 at 90% repolarization ($MAPD_{90\%}$) from effective refractory period (ERP) protocol. For the S1-S2 extra stimulus protocol, first 20 stimuli were applied to the heart and produced 20 monophasic action potentials (MAPs). Then, the 20 MAP of that S1 was followed by one stimulus, which produced the S2 MAP. Details of DI and S2 90% repolarization recording and measurements were fully described in chapter 3. From published work, VNS protected the heart against ventricular arrhythmias by flattened the maximum slope of restitution (Huang et al., 2015, Brack et al., 2013a). In this chapter, RVNS was stimulated and MAPDR restitution analysis was performed. An example of restitution analysis of baseline and RVNS by low frequency stimulation is shown in figure 5.35. From the figure, RVNS shifted the curve up from baseline. First derivative of exponential fit revealed a smaller value of RVNS restitution maximum slope when compared to baseline maximum slope.

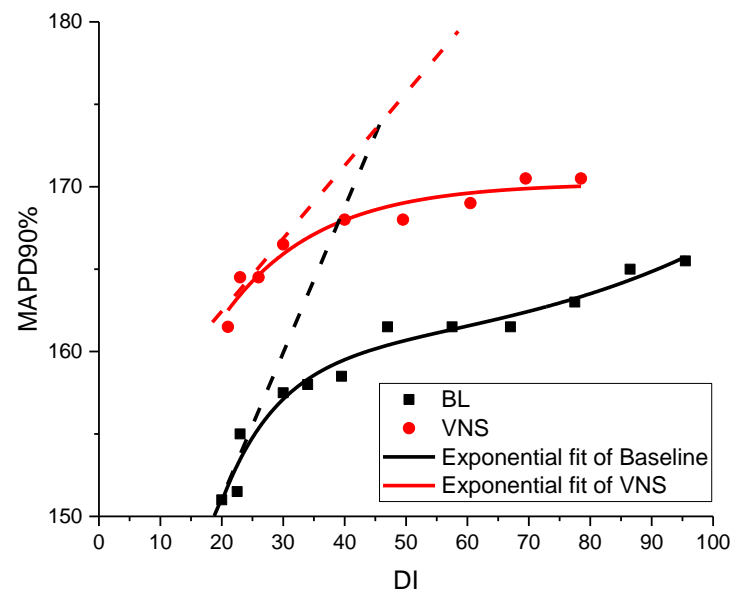


Figure 5.35 Analysis of MAPDR as effect of low frequency RVNS

Baseline MAPDR was displayed by black dots with the black line represented an exponential fit. RVNS MAPDR was plotted by red dots and exponential fitted as shown in red line. RVNS MAPDR curve was flatter than baseline MAPDR; baseline (BL), monophasic action potential duration at 90% repolarization (MAPDR90%), diastolic interval (DI), and vagus nerve stimulation (VNS).

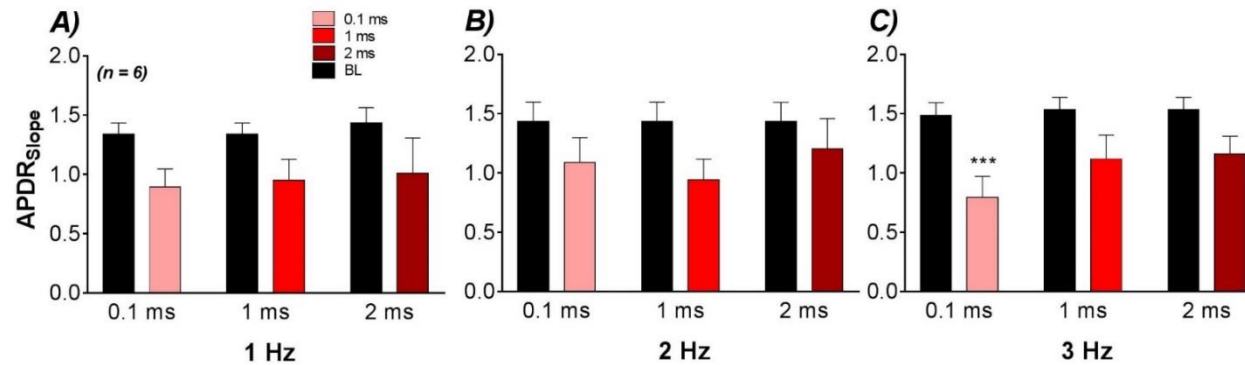


Figure 5.36 Effects of frequency on apex APDR maximum slope by low frequency RVNS

Action potential duration restitution (APDR), milliseconds (ms); n = 6, mean ± SEM., Two-way ANOVA with Bonferroni post hoc test, * P < 0.001.**

Low frequency MAPDR from LV apex results are shown in figure 5.36 and results from LV base are shown in figure 5.37. From the figures, effect of PW on MAPDR was displayed within the same frequency. With 1 Hz, 0.1 ms flattened maximum slope at the apex from 1.3 ± 0.1 to 0.9 ± 0.2 (ns). Slope value was reduced from 1.3 ± 0.1 to 0.9 ± 0.2 (ns) by 1 ms. In addition, the 2 ms caused the decrease from 1.4 ± 0.1 to 1.0 ± 0.3 (figure 5.36A). For 2 Hz (figure 5.36B), 0.1 ms flattened the slope from 1.4 ± 0.2 to 1.1 ± 0.2 (ns), 1 ms flattened from 1.4 ± 0.2 to 0.9 ± 0.2 (ns), and 2 ms flattened from 1.4 ± 0.2 to 1.2 ± 0.3 (ns). By frequency 3 Hz (figure 5.36C), 0.1 ms significantly reduced the maximum slope from 1.5 ± 0.1 to 0.8 ± 0.2 (P < 0.001). PW 1 ms flattened restitution from 1.5 ± 0.1 to 1.1 ± 0.2 (ns) and 2 ms flattened the slope from 1.5 ± 0.1 to 1.2 ± 0.1 (ns). This data demonstrated effects of high amplitude voltage on reduction of restitution maximum slope. With the same level of amplitude to the previous used by Ng et al. (2007), the lower frequency of this study still impacted on restitution curve.

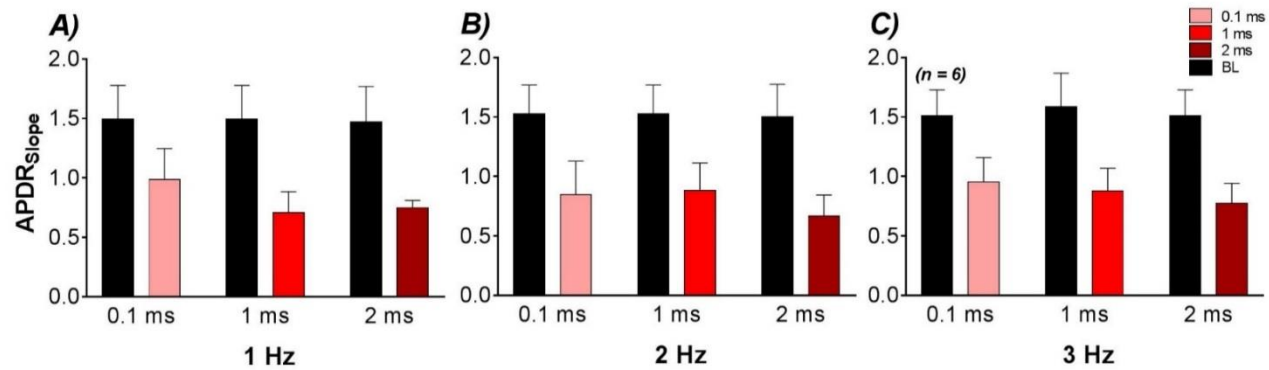


Figure 5.37 Effects of frequency on base APDR maximum slope by low frequency RVNS

Action potential duration restitution (APDR), milliseconds (ms); n = 6, mean ± SEM.

For the base restitution, stimulation by frequency 1 Hz with 0.1 ms reduced the slope from 1.5 ± 0.3 to 1.0 ± 0.3 (ns). With pulse width 1 ms, restitution slope was reduced from 1.5 ± 0.3 to 0.7 ± 0.2 (ns). The 2 ms decreased maximum slope from 1.5 ± 0.3 to 0.7 ± 0.1 (ns), as shown in figure 5.37A. Frequency 2 Hz flattened base restitution; from 1.5 ± 0.2 to 0.8 ± 0.3 (ns) by 0.1 ms, from 1.5 ± 0.2 to 0.9 ± 0.2 (ns) by 1 ms, and from 1.5 ± 0.3 to 0.7 ± 0.2 (ns) by 2 ms (figure 5.37B). Frequency 3 Hz, figure 5.37C, decreased maximum slope from 1.5 ± 0.2 to 1.0 ± 0.2 (ns) by 0.1 ms and from 1.6 ± 0.3 to 0.9 ± 0.2 (ns) by 1 ms and from 1.5 ± 0.2 to 0.8 ± 0.2 (ns) by 2 ms. From figure 5.36 and 5.37, both apex and base baseline restitutions were stable and there was no difference between response of different stimulation pulse width on a restitution slope flattening.

Next, effect of stimulation frequency on changes of apex and base restitution maximum slopes were investigated, and are shown in figure 5.38 and figure 5.39, respectively. As seen in these figures, there was no difference between effects of stimulation frequency on the restitution slope. When compared between apex and base MAPDR, low frequency RVNS caused a larger decrease of the maximum restitution slope at the LV base than the apex.

The percentage changes of both apex and base restitutions were calculated and are displayed in figure 5.40 for percent change of apex restitution as an effect of frequency and in figure 5.41 for percent changes of base restitution. At the apex, the frequency 1 Hz reduced restitution 34.0 ± 11.3 % for 0.1 ms, 29.9 ± 11.7 % for 1 ms, and 33.0 ± 14.7 % for 2 ms (figure 5.40A). For 2 Hz stimulation (figure 5.40B), RVNS flattened restitution 26.5 ± 6.5 % at 0.1 ms, 36.8 ± 10.9 % at 1 ms, and 21.5 ± 14.2 % at 2 ms. Finally, frequency 3 Hz flattened the slope 45.9 ± 10.8 % at 0.1 ms, 26.6 ± 11.8 % at 1 ms, and 22.7 ± 12.3 % at 2 ms stimuli (figure 5.40C). For percent change of base restitution, frequency 1 Hz reduced maximum slope 31.1 ± 18.1 % at 0.1 ms, 39.5 ± 15.9 % at 1 ms, and 37.6 ± 13.3 % at 2ms (figure 5.41A). The 2 Hz flattened restitution slope 46.5 ± 14.1 % at 0.1 ms, 34.9 ± 25.8 % at 1 ms, and 48.6 ± 15.2 % at 2 ms (figure 5.41B). Frequency 3 Hz caused flattening 38.4 ± 9.3 % at 0.1 ms, 33.6 ± 24.1 % at 1 ms, and 47.0 ± 10.2 % at 2 ms (figure 5.41C). Compared within stimulation frequency, there was no difference between the effects of different stimulation PW on reduction of restitution maximum slope. The percent changes of restitution were regrouped in order to observe the effect of different stimulation frequency within the same pulse width on the level of slope change, which are showed in figure 5.42 for apex and 5.43 for base. From these figures, within the same PW, there was no difference between effects of different stimulation frequency on the level of percent restitution maximum slope reduction.

This low frequency (high amplitude voltage) stimulation RVNS flattened the restitution slope at both apex and base, percent reduction of the maximum slope of the base restitution was larger than the changes of the apex restitution. This result displayed an anti-arrhythmic effect of VNS, even with the low

frequency, as restitution slope became less than 1.0 representing a stabilisation of the dynamics of the ventricle from wave break (Weiss et al., 2000).

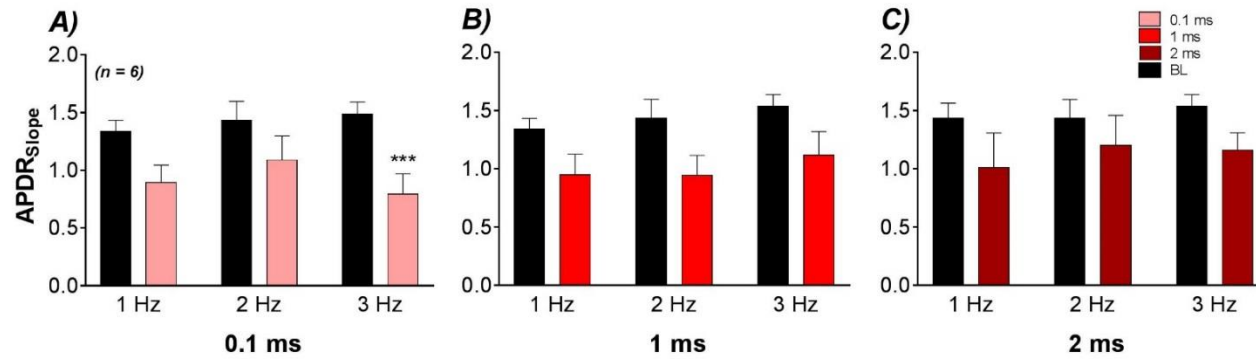


Figure 5.38 Effects of PW on apex APDR maximum slope by low frequency RVNS

Action potential duration restitution (APDR), milliseconds (ms); $n = 6$, mean \pm SEM., Two-way ANOVA with Bonferroni post hoc test, *** $P < 0.001$.

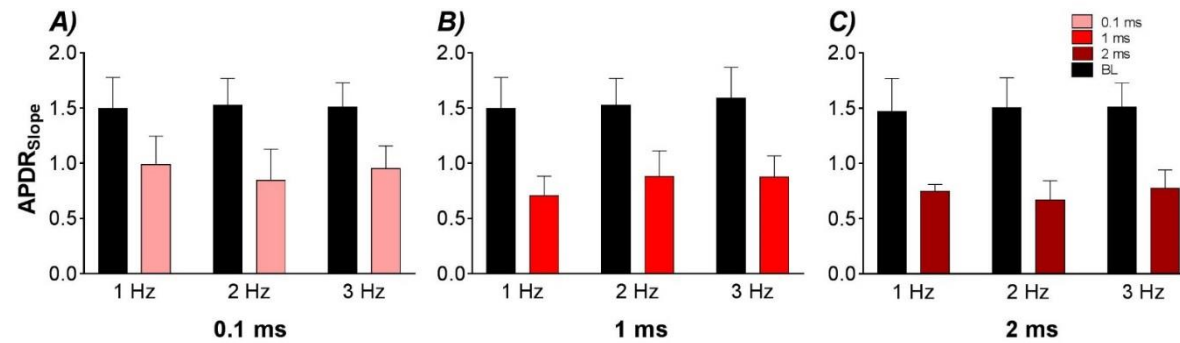


Figure 5.39 Effects of PW on base APDR maximum slope by low frequency RVNS

Action potential duration restitution (APDR), milliseconds (ms); $n = 6$, mean \pm SEM.

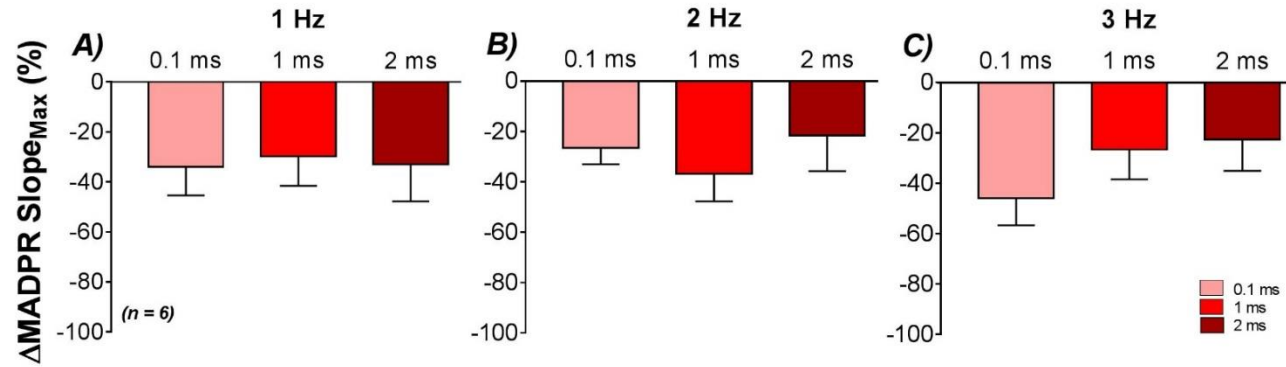


Figure 5.40 Effects of PW on percentage change of apex MAPDR maximum slope by low frequency stimulation.

Monophasic action potential duration restitution maximum slope (MAPDR Slope_{Max}); $n = 6$, mean \pm SEM.

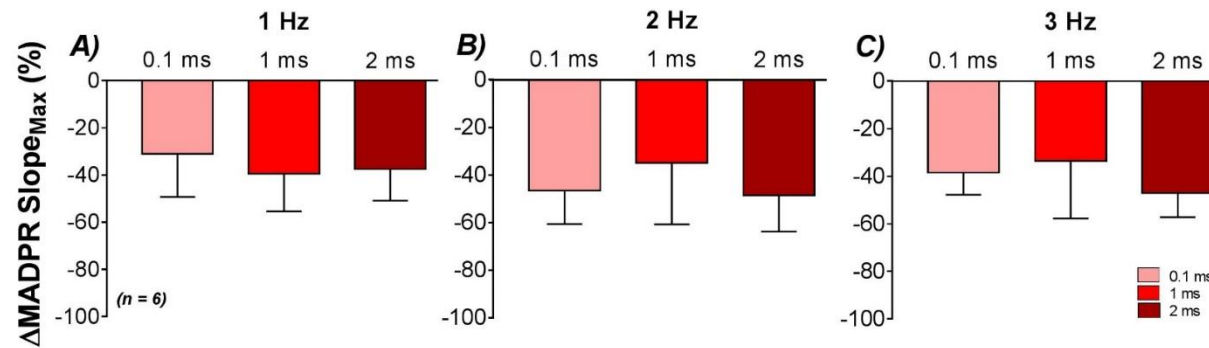


Figure 5.41 Effects of PW on percentage change of base MAPDR maximum slope by low frequency stimulation.

Monophasic action potential duration restitution maximum slope (MAPDR Slope_{Max}); $n = 6$, mean \pm SEM.

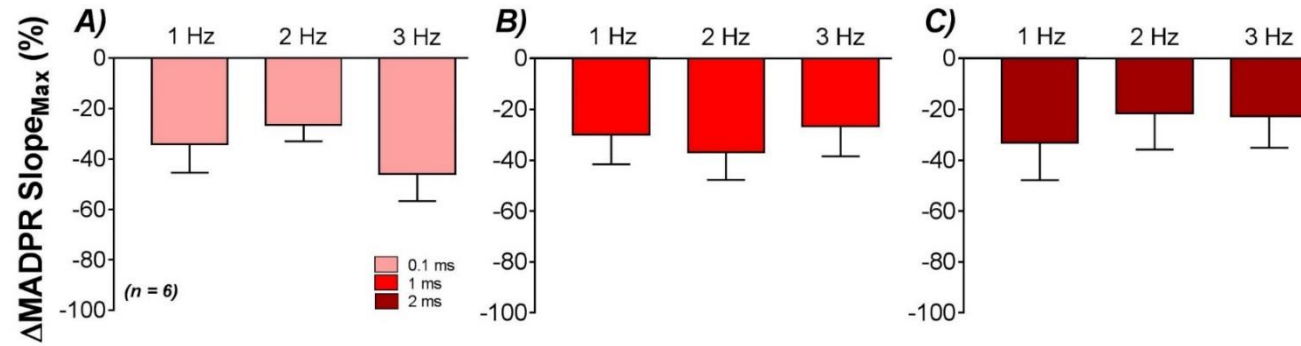


Figure 5.42 Effects of frequency on percentage change of apex MAPDR maximum slope by low frequency stimulation.

Monophasic action potential duration restitution maximum slope (MAPDR Slope_{Max}); $n = 6$, mean \pm SEM.

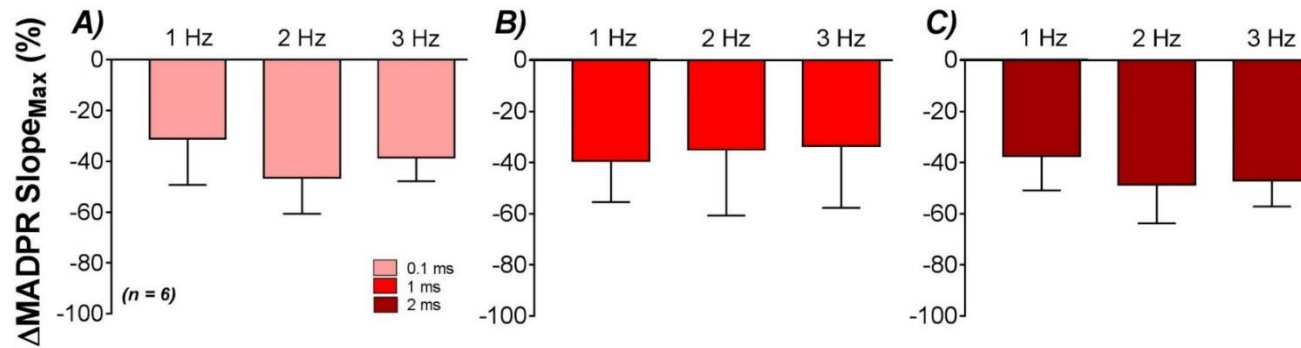


Figure 5.43 Effects of frequency on percentage change of base MAPDR maximum slope by low frequency stimulation.

Monophasic action potential duration restitution maximum slope (MAPDR Slope_{Max}); $n = 6$, mean \pm SEM.

5.7.2 Effect of low voltage stimulation on MAPDR slope

Next, low amplitude voltage was used to stimulate the right vagus instead of the high strength voltage from previous technique. Frequencies were changed from low (1 Hz, 2 Hz, and 3 Hz) to high (5 Hz, 10 Hz, and 20 Hz) in order to extend an investigate from voltage effect to frequency effect on restitution. Low frequency RVNS shifted the restitution curve up when compared to the baseline curve, which was similar to the result from low frequency stimulation.

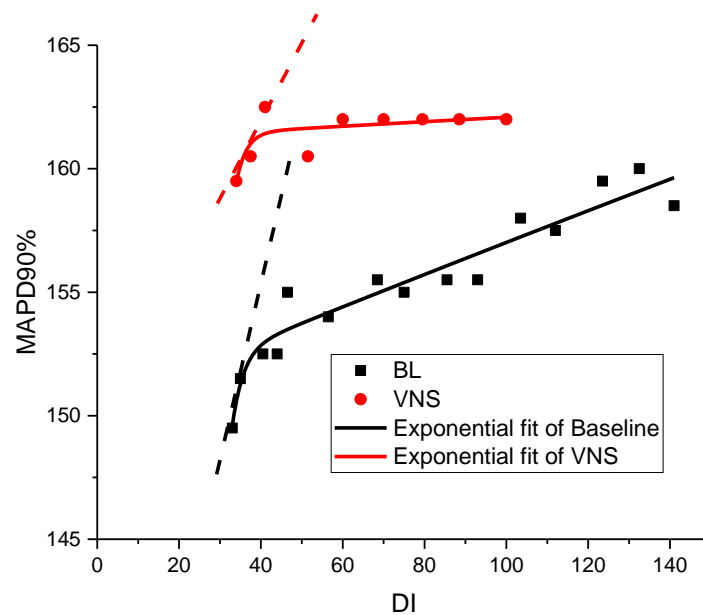


Figure 5.44 Baseline MAPDR and low voltage RVNS MAPDR

Baseline MAPDR was displayed in black and RVNS MAPDR was displayed in red. Baseline (BL), monophasic action potential duration at 90% repolarization (MAPDR90%), diastolic interval (DI), and vagus nerve stimulation (VNS).

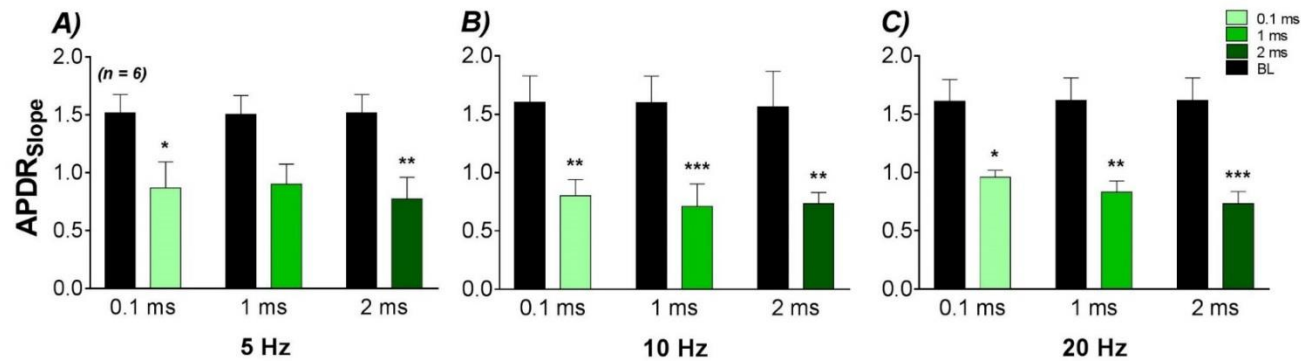


Figure 5.45 Effects of PW on apex APDR maximum slope by low voltage RVNS

Action potential duration restitution (APDR), milliseconds (ms); n = 6, mean ± SEM., Two-way ANOVA with Bonferroni post hoc test, * P < 0.05, ** P < 0.01, * P < 0.001.**

As show in figure 5.45, low voltage RVNS produced significant flattening of apex restitution maximum slope in all frequencies. With a frequency of 5 Hz, a pulse width of 0.1 ms flattened the slope from 1.5 ± 0.2 to 0.9 ± 0.2 ($P < 0.05$), a pulse width of 1 ms decreased slope from 1.5 ± 0.2 to 0.9 ± 0.2 (ns), and a pulse width of 2 ms reduced slope from 1.5 ± 0.2 to 0.8 ± 0.2 ($P < 0.01$), shown in figure 5.45A. With 10 Hz stimuli, 0.1 ms reduced slope from 1.6 ± 0.2 to 0.8 ± 0.1 ($P < 0.01$), 1 ms reduced max slope from 1.6 ± 0.2 to 0.7 ± 0.2 ($P < 0.001$), and 2 ms flattened apex restitution from 1.6 ± 0.3 to 0.7 ± 0.1 ($P < 0.01$) (figure 5.45B). For frequency 20 Hz in figure 5.45C, restitution slope was reduced from 1.6 ± 0.2 to 1.0 ± 0.1 ($P < 0.05$) by PW 0.1 ms, from 1.6 ± 0.2 to 0.8 ± 0.1 ($P < 0.01$) by PW 1 ms, and from 1.6 ± 0.2 to 0.7 ± 0.1 ($P < 0.001$) by PW 2 ms. From these results, the low voltage stimulation produced statistical flattening of apex MAPDR. Changes as impact of the high were more than effect of high amplitude voltage from the previous stimulation method.

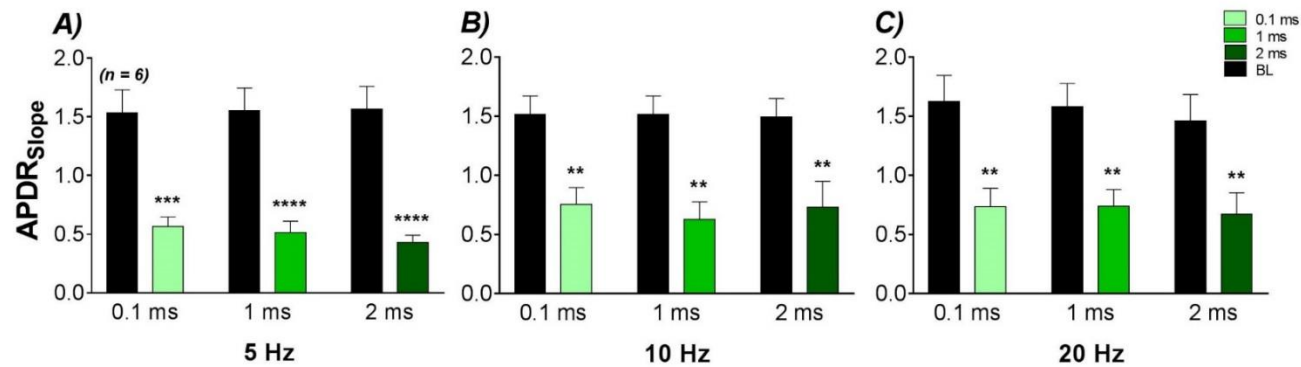


Figure 5.46 Effects of PW on base APDR maximum slope by low voltage RVNS

Action potential duration restitution (APDR), milliseconds (ms); n = 6, mean \pm SEM., Two-way ANOVA with Bonferroni post hoc test, ** P < 0.01, * P < 0.001, **** P < 0.0001.**

For the base restitution, the results of low voltage stimulation on base restitution maximum slope was displayed in figure 5.46. With frequency 5 Hz stimuli (figure 5.46A), 0.1 ms flattened base restitution from 1.5 ± 0.2 to 0.6 ± 0.1 ($P < 0.0001$). The pulse width 1 ms reduced the maximum slope from 1.6 ± 0.2 to 0.5 ± 0.1 ($P < 0.0001$) and pulse width 2 ms decreased maximum slope from 1.6 ± 0.2 to 0.4 ± 0.1 ($P < 0.0001$). Frequency 10 Hz reduced base restitution from 1.5 ± 0.2 to 0.8 ± 0.1 ($P < 0.01$) by 0.1 ms, from 1.5 ± 0.2 to 0.6 ± 0.1 ($P < 0.01$) by 1 ms, and from 1.5 ± 0.2 to 0.7 ± 0.2 ($P < 0.01$) by 2 ms, as displayed in figure 5.46B. For 20 Hz stimuli (figure 5.46C), 0.1 ms reduced maximum slope from 1.6 ± 0.2 to 0.7 ± 0.2 ($P < 0.01$). Pulse width 1 ms decreased slope from 1.6 ± 0.2 to 0.7 ± 0.1 ($P < 0.01$) and pulse width 2 ms decreased from 1.5 ± 0.2 to 0.7 ± 0.2 ($P < 0.01$). There was no difference effect of different stimulation pulse width on both apex and base maximum slope changes. Response of base MAPDR demonstrated the same characteristic to the apex data as high frequency statistical flattened MAPDR slope in all stimuli. In addition, level of reductions were higher at the base than the apex.

To investigate the effects of different stimulation frequency of low voltage RVNS on restitution maximum slope, data from figure 5.45 and 5.46 were regrouped and displayed in figure 5.47 (apex MADPR) and figure 5.48 (base MAPDR). From the figures, there was no difference between the responses of stimulation frequency on slope flattening by low voltage RVNS.

Percent change of effect of frequency on apex restitution was calculated and displayed in figure 5.49. The 5 Hz produced 40.2 ± 17.4 % drop by 0.1 ms, 38.2 ± 12.8 % drop by 1 ms, and 44.7 ± 14.7 % by 2 ms (figure 5.49A). With 10 Hz, apex restitution was flattened 45.8 ± 9.3 % by 0.1 ms, 45.5 ± 16.8 % by 1 ms, and 44.3 ± 11.3 % by 2 ms (showed in figure 5.49B). Figure 5.49C illustrated percent apex restitution flattening by 20 Hz stimuli, which were 36.2 ± 9.2 % for 0.1 ms, 44.0 ± 9.8 % for 1 ms, and 51.9 ± 8.1 % for 2 ms. For the percent change of base restitution, 5 Hz decreased the maximum slope 62.5 ± 4.4 % by 0.1 ms, 64.0 ± 7.0 % by 1 ms, and 69.7 ± 6.0 % by 2 ms (figure 5.50A). Frequency 10 Hz reduced slope value 47.5 ± 10.7 % (0.1 ms), 53.1 ± 12.2 % (1 ms), and 54.1 ± 9.2 % (2 ms), as displayed in figure 5.50B. Finally, the 20 Hz stimuli flattened slope 49.5 ± 11.8 % with 0.1 ms, 51.5 ± 10.0 % with 1 ms, and 54.4 ± 8.0 % with 2 ms (figure 5.50C). No difference between percentage reductions of restitution maximum slope in response to stimulation pulse width was observed.

Percent changes of restitution are presented as effect of different stimulation frequency within the same PW in figure 5.51 (apex) and figure 5.52 (base). From the figures, there was no difference between effects of different stimulation frequencies on restitution maximum slope reduction. Similar to the response characteristics of low frequency stimulation, low voltage RVNS produced a larger slope flattening at the base of the left ventricle more than the apex. However, the low voltage RVNS overall decreased restitution maximum slope in a larger percentage than the low frequency RVNS.

The high frequency used by this low voltage stimulation method seemed to have significant impact on the reduction of MAPDR slope at both apex and base. Changes were seen larger at the base than the apex without any differences of PW. Moreover, there was no further response to the higher frequency as frequency 5 Hz, 10 Hz, and 20 Hz produced the same amount of changes.

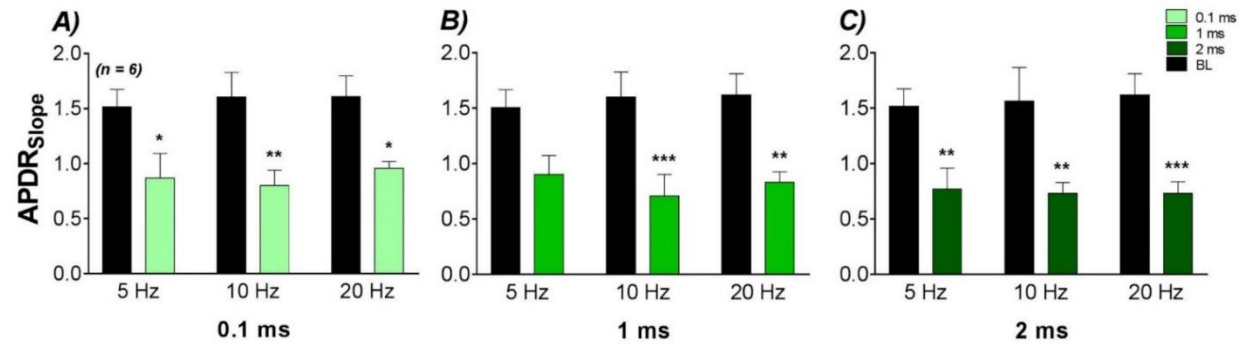


Figure 5.47 Effects of frequency on apex APDR maximum slope by low voltage RVNS

Action potential duration restitution (APDR), milliseconds (ms); $n = 6$, mean \pm SEM., Two-way ANOVA with Bonferroni post hoc test, * $P < 0.05$, ** $P < 0.01$, *** $P < 0.001$.

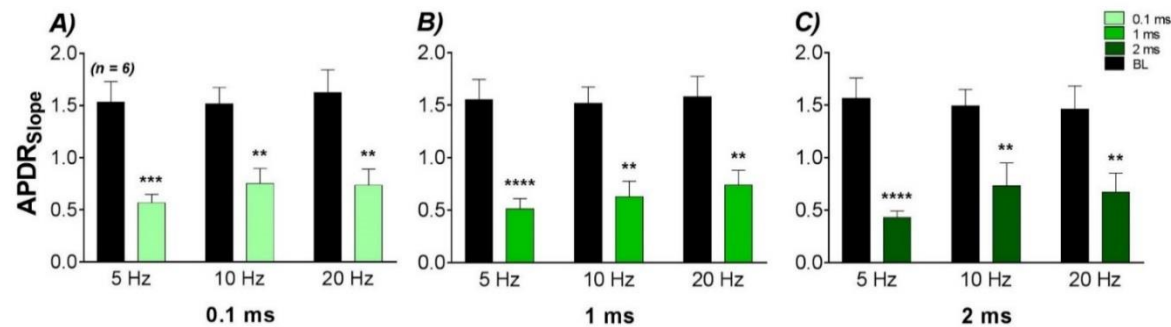


Figure 5.48 Effects of frequency on base APDR maximum slope by low voltage RVNS

Action potential duration restitution (APDR), milliseconds (ms); $n = 6$, mean \pm SEM., Two-way ANOVA with Bonferroni post hoc test, ** $P < 0.01$, *** $P < 0.001$, **** $P < 0.0001$.

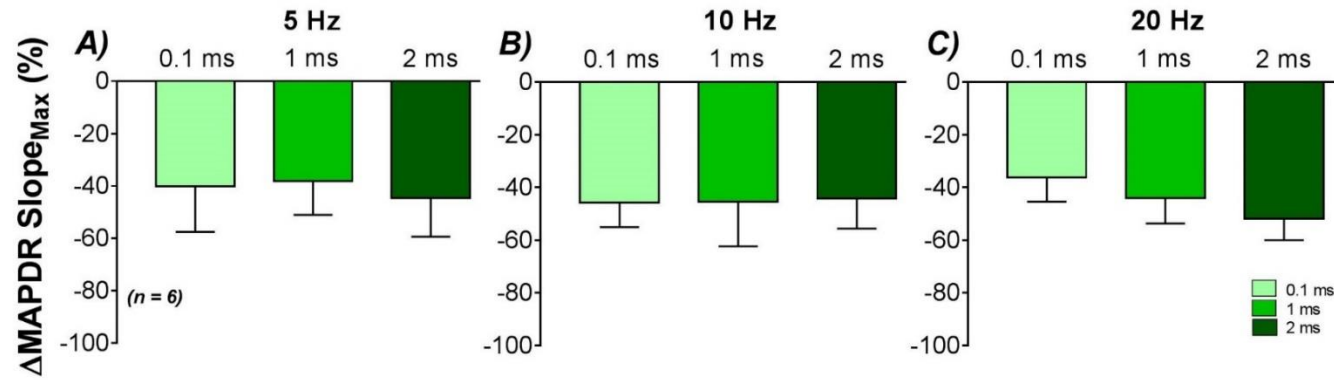


Figure 5.49 Effects of PW on percentage change of apex MAPDR maximum slope by low voltage stimulation.

Monophasic action potential duration restitution maximum slope (MAPDR Slope_{Max}); n = 6, mean \pm SEM.

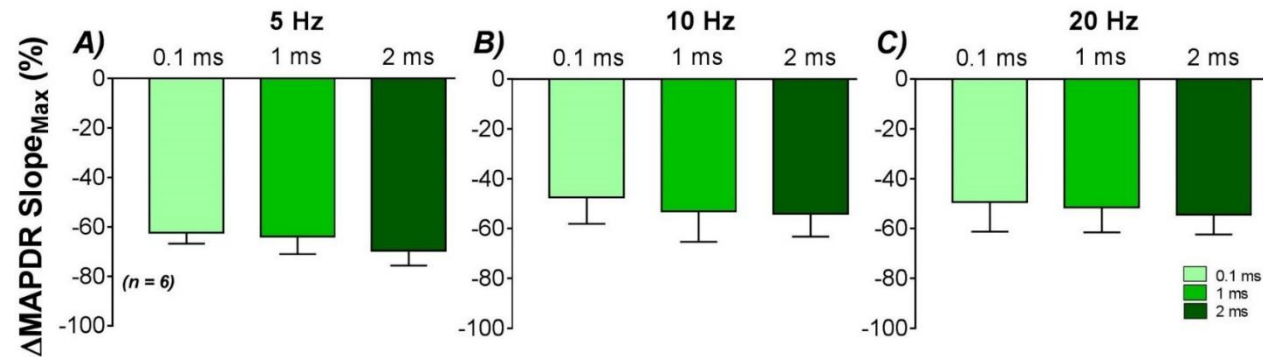


Figure 5.50 Effects of PW on percentage change of base MAPDR maximum slope by low voltage stimulation.

Monophasic action potential duration restitution maximum slope (MAPDR Slope_{Max}); n = 6, mean \pm SEM.

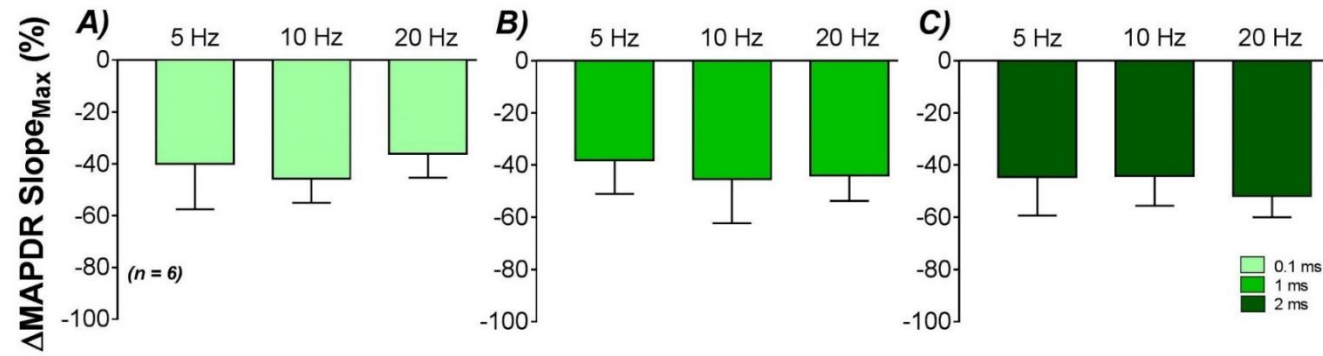


Figure 5.51 Effects of frequency on percentage change of apex MAPDR maximum slope by low voltage stimulation.

Monophasic action potential duration restitution maximum slope (MAPDR Slope_{Max}); $n = 6$, mean \pm SEM.

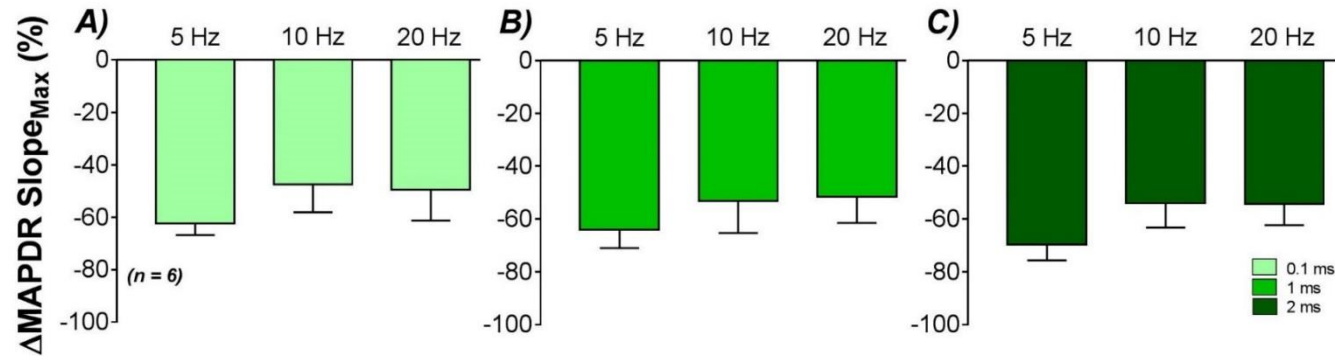


Figure 5.52 Effects of frequency on percentage change of base MAPDR maximum slope by low voltage stimulation.

Monophasic action potential duration restitution maximum slope (MAPDR Slope_{Max}); $n = 6$, mean \pm SEM.

5.7.3 Effect of low frequency low voltage stimulation on MAPDR slope

For the last RVNS strategy, the low frequency low voltage utilised voltage that reduced the heart rate less than 10% from baseline together with frequencies 1 Hz, 2 Hz, and 3 Hz. Effect of this stimulation approach was measured and compared with the others 2 approaches to establish impact of high amplitude voltage and high frequency on MAPDR curve. This low voltage low frequency stimulation shifted the restitution curve upward and to the left, as shown in figure 5.53. From figure, the maximum slope of VNS restitution was flatter than baseline restitution.

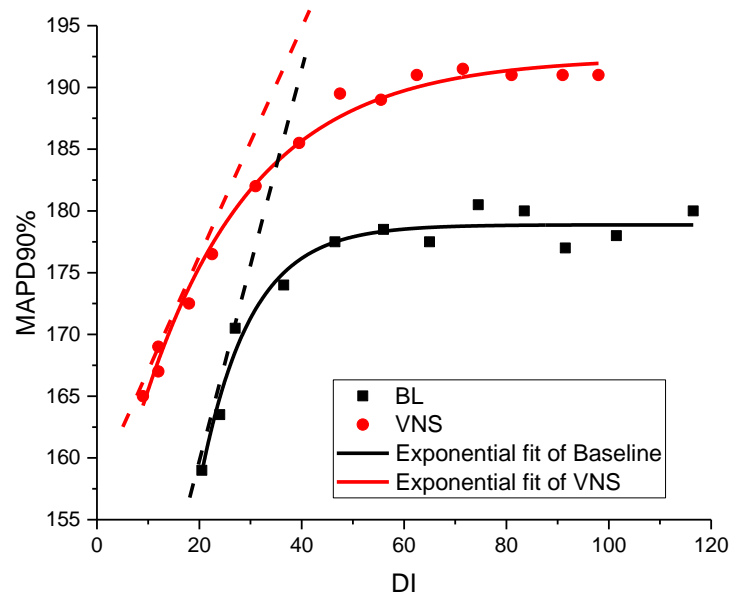


Figure 5.53 Baseline MAPDR and low frequency low voltage RVNS MAPDR

Baseline MAPDR was displayed in black and RVNS MAPDR was displayed in red. Baseline (BL), monophasic action potential duration at 90% repolarization (MAPDR90%), diastolic interval (DI), and vagus nerve stimulation (VNS)

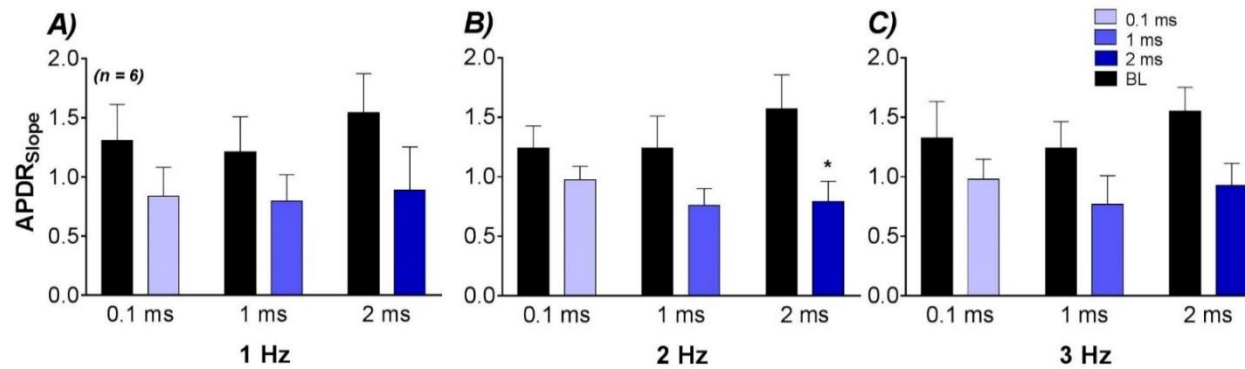


Figure 5.54 Effects of PW on apex APDR maximum slope by low frequency low voltage RVNS

Action potential duration restitution (APDR), milliseconds (ms); n = 6, mean ± SEM., Two-way ANOVA with Bonferroni post hoc test, * P < 0.05.

Results of apex MAPDR low frequency low voltage stimulation displayed an overall reduction of maximum slope by this very low strength parameter. For frequency 1 Hz stimulation of apex restitution, PW 0.1 ms flattened maximum slope from 1.3 ± 0.3 to 0.8 ± 0.2 (ns). PW 1 ms reduced maximum slope from 1.2 ± 0.3 to 0.8 ± 0.2 (ns) and a PW 2 ms decreased from 1.5 ± 0.3 to 0.9 ± 0.4 (ns), displayed in figure 5.54A. Frequency 2 Hz decreased apex maximum slope from 1.2 ± 0.2 to 1.0 ± 0.1 (ns) by PW 0.1 ms, from 1.2 ± 0.3 to 0.8 ± 0.1 (ns) by PW 1 ms, and from 1.6 ± 0.3 to 0.8 ± 0.2 ($P < 0.05$) by PW 2 ms, as shown in figure 5.54B. Effect of frequency 3 Hz is shown in figure 5.54C. PW 0.1 ms flattened slope from 1.3 ± 0.3 to 1.0 ± 0.2 (ns) while PW 1 ms decreased restitution slope from 1.2 ± 0.2 to 0.8 ± 0.2 (ns). Finally, PW 2 ms reduced maximum slope of apex restitution from 1.6 ± 0.2 to 0.9 ± 0.2 (ns). Apex MAPDRs were lowered than baseline by the very low strength RVNS. However, slope decreases were not statistically significant, which were similar to the low frequency stimulation MAPDR results.

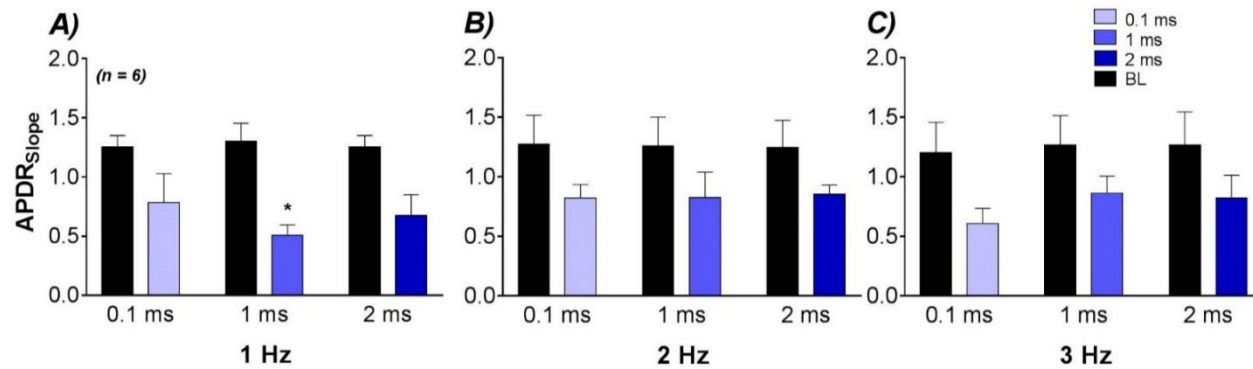


Figure 5.55 Effects of PW on base APDR maximum slope by low frequency low voltage RVNS

Action potential duration restitution (APDR), milliseconds (ms); n = 6, mean ± SEM., Two-way ANOVA with Bonferroni post hoc test, * P < 0.05.

The effects of low frequency low voltage stimulation on base restitution were measured. Similar response to the apex MAPDR was found, as shown in figure 5.55. From figure, the 1 Hz stimuli with PW 0.1 ms caused the maximum base restitution slope to reduce from 1.3 ± 0.1 to 0.8 ± 0.2 (ns). PW 1 ms significantly decreased the slope from 1.3 ± 0.2 to 0.5 ± 0.1 ($P < 0.05$) while 2 ms decreased the slope from 1.3 ± 0.1 to 0.7 ± 0.2 (ns), as displayed in figure 5.55A. Frequency 2 Hz flattened slope from 1.3 ± 0.2 to 0.8 ± 0.1 (ns) by PW 0.1 ms, from 1.3 ± 0.2 to 0.8 ± 0.2 (ns), and from 1.2 ± 0.2 to 0.9 ± 0.1 (ns), displayed in figure 5.55B. The 3 Hz stimuli decreased base restitution maximum slope from 1.2 ± 0.3 to 0.6 ± 0.1 (ns) by 0.1 ms, from 1.3 ± 0.2 to 0.9 ± 0.1 (ns) by 1 ms, and from 1.3 ± 0.3 to 0.8 ± 0.2 (ns) by 2 ms, showed in figure 5.55C. Even without any significant reduction, MAPDR responses to the very low strength RVNS demonstrated in figure 5.54 and 5.55 confirmed a potential to flatten maximum slope of ventricular restitution.

From the assessments of an effect of PW on both apex and base restitution slopes, there was no difference between the effects of different stimulation PW on the restitution slope flattening. Results are represented as effects of different stimulation frequency within the same PW in figure 5.56 for apex restitution and figure 5.57 for base restitution. From the figures, there was no significant difference between effects of different stimulation frequencies on slope flattening in both apex and base restitutions.

Percent change of apex restitution showed that a frequency of 1 Hz decreased apex slope 34.6 ± 13.3 % by 0.1 ms, 30.9 ± 11.3 % by 1 ms, and 46.1 ± 12.1 % by 2 ms, as shown in figure 5.58A. The 2 Hz stimuli flattened slope 17.6 ± 7.0 % by 0.1 ms, 16.7 ± 24.4 % by 1 ms, and 48.4 ± 9.7 % by 2 ms (figure 5.58B). With a stimulus frequency of 3 Hz, PW 0.1 ms decreased apex restitution slope 18.7 ± 8.7 %. PW 1 ms decreased the slope to 37.3 ± 14.8 % and 2 ms decreased 40.3 ± 7.3 %, figure 5.58C. For the effect on LV base restitution, frequency 1 Hz flattened base slope 36.9 ± 18.5 % by 0.1 ms, 57.6 ± 10.1 % by 1 ms, and 44.8 ± 15.9 % by 2 ms (shown in figure 5.59A). The 2 Hz stimuli caused the reduction 13.3 ± 25.3 % for 0.1 ms, 29.6 ± 18.0 % for 1 ms, and 20.8 ± 16.3 % for 2ms (figure 5.59B). With frequency 3 Hz, 0.1 ms flattened base slope 39.8 ± 12.8 %. PW 1 ms decreased slope 25.9 ± 11.8 % while 2 ms decreased 34.8 ± 9.4 %, as displayed in figure 5.59C. There was no difference between percent restitution slope flattening associated with different stimulation PW. Figure 5.60 presented percentage change of apex restitution as an effect of different stimulation frequency within the same PW whereas figure 5.61 illustrated the effect on base restitution. No difference between stimulation frequencies on both apex and base restitutions was observed.

MAPDR response to this low frequency low voltage stimulation displayed the same response level as observed by the low frequency stimulation in section 7.1. These 2 stimulation methods used the same frequency set and differed only at the voltage strength. On the other hand, both MAPDR data by low frequency were smaller than MAPDR response to the high frequency stimulation. This stimulation strategy displayed a potential to decrease restitution slope. However, the differences between effect of nerve stimulation on base restitution and apex restitution that was observed by the low frequency and the low voltage approaches were not seen in this low

frequency low voltage technique. The absence of base – apex difference by this stimulation suggested a role of either high strength voltage or high frequency required for nerve recruitment.

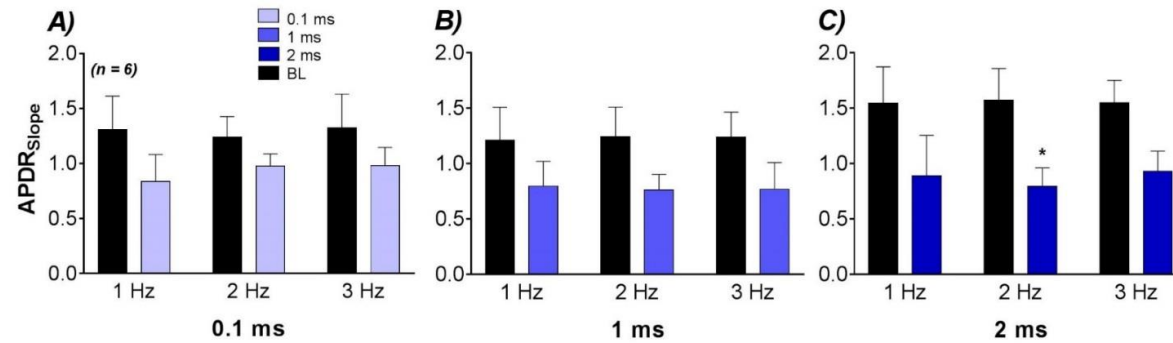


Figure 5.56 Effects of frequency on apex APDR maximum slope by low frequency low voltage RVNS

Action potential duration restitution (APDR), milliseconds (ms); $n = 6$, mean \pm SEM., Two-way ANOVA with Bonferroni post hoc test, * $P < 0.05$.

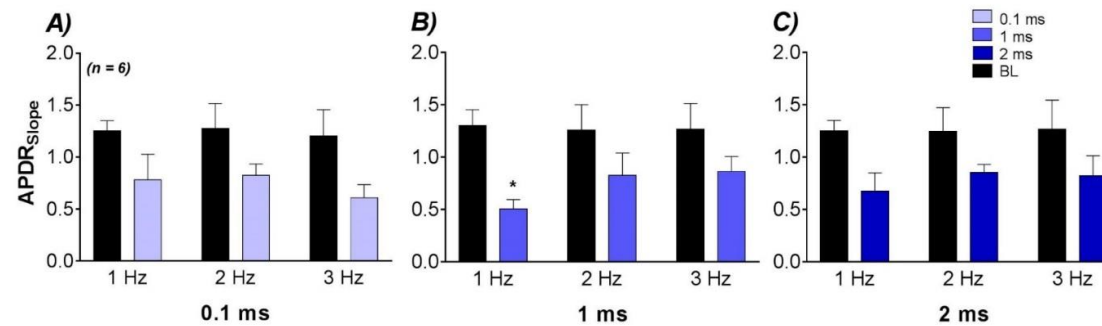


Figure 5.57 Effects of frequency on base APDR maximum slope by low frequency low voltage RVNS

Action potential duration restitution (APDR), milliseconds (ms); $n = 6$, mean \pm SEM., Two-way ANOVA with Bonferroni post hoc test, * $P < 0.05$.

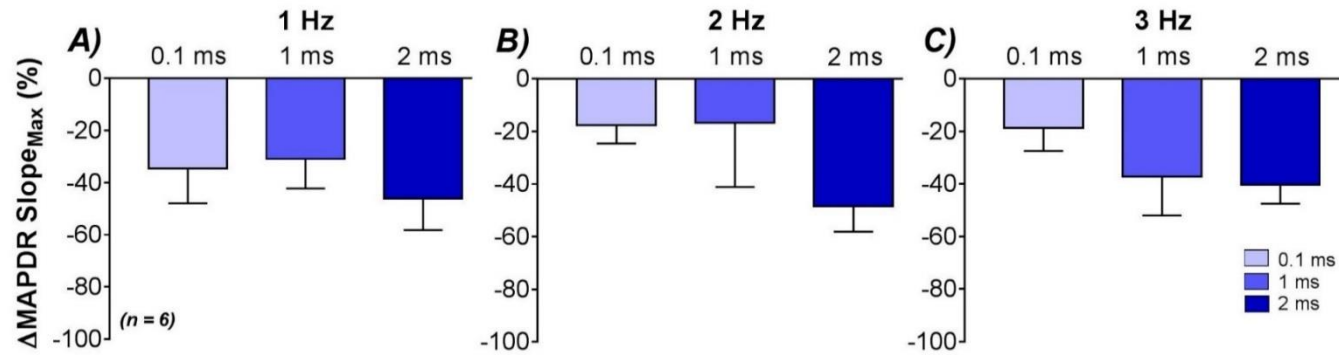


Figure 5.58 Effects of PW on percentage change of apex MAPDR maximum slope by low frequency low voltage stimulation.

Monophasic action potential duration restitution maximum slope (MAPDR Slope_{Max}); n = 6, mean ± SEM.

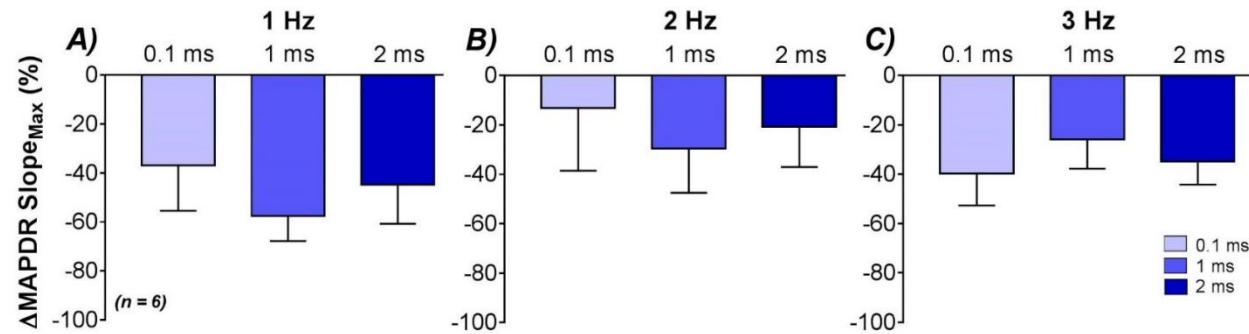


Figure 5.59 Effects of PW on percentage change of base MAPDR maximum slope by low frequency low voltage stimulation.

Monophasic action potential duration restitution maximum slope (MAPDR Slope_{Max}); n = 6, mean ± SEM.

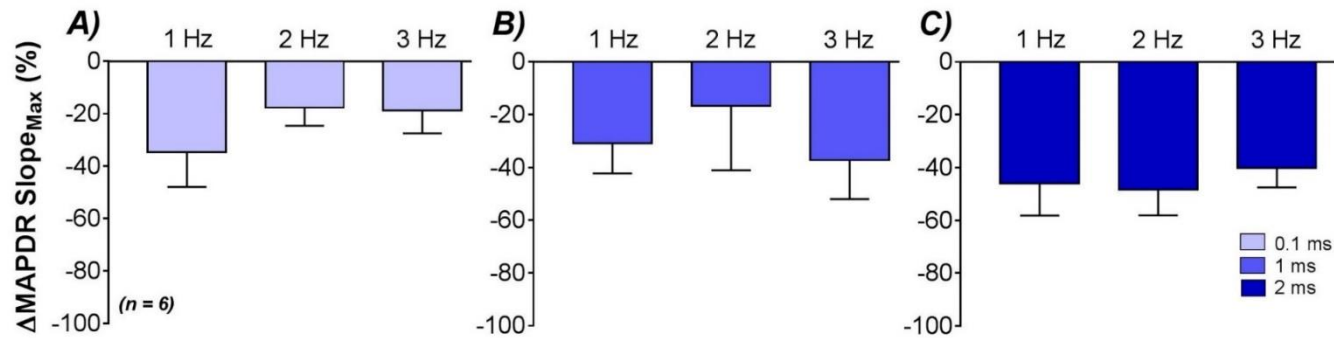


Figure 5.60 Effects of frequency on percentage change of apex MAPDR maximum slope by low frequency low voltage stimulation. Monophasic action potential duration restitution maximum slope (MAPDR Slope_{Max}); $n = 6$, mean \pm SEM.

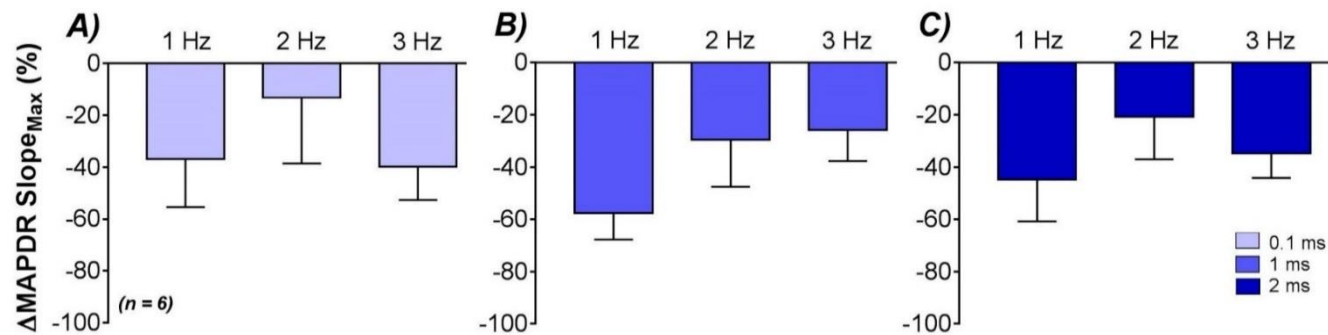


Figure 5.61 Effects of frequency on percentage change of base MAPDR maximum slope by low frequency low voltage stimulation. Monophasic action potential duration restitution maximum slope (MAPDR Slope_{Max}); $n = 6$, mean \pm SEM.

5.8 Discussion

5.8.1 RVNS parameters and anti – arrhythmic mechanism

The right vagus nerve was stimulated by extended stimulation parameters from the previous chapter. Ventricular electrophysiology responses to the different voltages, frequencies, and pulse widths in this chapter strongly supported the anti - ventricular arrhythmic effects of VNS (Zhang et al., 2016, Huang et al., 2015, Ng et al., 2007, Vanoli et al., 1991). In these current results, the protective effects were observed with and without heart rate (HR) reduction. The former was demonstrated by using of the voltage $80\% \Delta HR_{max}$, which impacted on muscarinic receptor activation of vagal stimulation at the atrial level (Herring and Paterson, 2001, Vanoli et al., 1991, Woolley et al., 1987). On the other hand, the voltage $10\% \Delta HR_{BL}$ decreased HR to a small extent, but exhibited a same level of anti-arrhythmic protection to the high strength voltage, which confirmed that vagal protection was independent to HR reduction (Gold et al., 2016, Shinlapawittayatorn et al., 2013, Vanoli et al., 1991). Responses of the heart to these 3 RVNS approaches (low frequency stimulation, low voltage stimulation, and low frequency low voltage stimulation) suggested the presence of 2 separate action pathways of vagal stimulation with i) predominantly HR reduction by muscarinic activation at the atrial level (Kalla et al., 2016a, Herring and Paterson, 2001) and ii) anti – arrhythmogenesis possibly by the nNOS – derived NO at the ventricular level (Stavrakis et al., 2013, Brack et al., 2011).

Results from this chapter also confirmed the hypothesis of the protective effect of low level VNS against ventricular arrhythmia induction and the hypothesis of an involvement of nNOS-derived NO with this mechanism. Although some data points of this chapter were not statistically different, the low level VNS displayed a potential to prolong ERP, increase VFT, and flatten MAPDR as part of the protection mechanisms. Repeating the investigation with a larger N number (than 6) might help confirm this effect.

5.8.2 RVNS parameters and vagal fibre recruitment

With an isolated innervated rabbit heart preparation, relation of vagus nerve and cardiac function was purely studied and was separated from the neuro – hormonal effect and the involvement of the higher centre of autonomic nervous system (Shivkumar and Ardell, 2016, Buckley et al., 2015, Ng et al., 2001). Stimulation of the right cervical vagus nerve of the rabbit produces only parasympathetic activation since there are no sympathetic efferent fibres innervated to the heart through the nodose ganglion in rabbit (Coote, 2013, Evans and Murray, 1954). The right vagal nerve was electrically stimulated to recruit efferent fibres in this action (Kalla et al., 2016a). These efferent fibres deliver basal parasympathetic tone to the heart (Yamakawa et al., 2015) and impact on the heart during activation by suppressing sympathetic tone at pre and post – synaptic levels with also direct action of vagal fibre on ventricular myocytes (Coote, 2013). The high amplitude voltage used by low frequency technique would evoke vagal cardiac effect provided by both myelinated and non-myelinated fibres (Woolley et al., 1987). In this process, evidence is produced of right vagal recruitment of an in - vivo swine model starting by low amplitude current firstly recruited the thick myelinated fibres (A fibre). Then, with an increasing current, the thin myelinated fibres (B fibres) were later recruited and slowed down the HR as a further effect (Tosato et al., 2006). However, a stable control of vagal HR modulation in this swine model was reported to be regulated by the non – myelinated fibres (C fibres), which were recruited by the high amplitude voltage (or current) (Tosato et al., 2006, Jones et al., 1995). Vagal C fibres were known to deliver parasympathetic tone to the heart while the B fibres were involved with the pulmonary bradycardia reflex and fired signal in a beat to beat manner (Jones et al., 1995). Jones et al. (1995) recruited the myelinated B fibres by voltage 5.0 ± 1.2 V and the unmyelinated C fibre by voltage 11.2 ± 0.9 V. Therefore, the voltages 6.00 ± 1.84 V to 8.17 ± 1.56 V ($80\% \Delta HR_{max}$) used by the low frequency stimulation this study was seemed to reduce HR via vagal B fibres recruitment.

The percentage increase of VFT and percentage decrease of MAPDR slope were more robust in the low voltage (with high frequency) stimulation. This results confirmed the HR independent cardio – protective effect of low level VNS (LVNS) (Katare et al., 2009). Ng et al. (2007) demonstrated a prolonged ERP, increased VFT, and flattened MAPDR slope by VNS that accompanied large HR drop. Brack et al. (2011) showed an attenuation of HR reduction and ERP prolongation with preserved increase in VFT and MADPR slope decrease by VNS during perfusion of muscarinic blockage (atropine) in the rabbit ventricle. In this current study, VFT increase and MAPDR slope decrease were found in all 3 parameter sets. With the low frequency stimulation of this study, the high strength voltage impacted on the HR effect as described previously (Ng et al., 2001). Together with the low frequencies (1 Hz, 2 Hz, and 3 Hz), this parameter set would be subjected to recruit both thick myelinated A fibres and thin myelinated B fibres during an excitation. In contrast, the low amplitude voltage ($< 2.42 \pm 0.26$ V for 20 Hz and $< 3.25 \pm 0.68$ V for 5 Hz) used by the other 2 approaches would be more likely to mainly recruit only the thick myelinated A fibres. However, with this subthreshold voltage level, small proportion of thin myelinated B fibres could be recruited and attributed to the vagal effect (Tosato et al., 2006, Middleton et al., 1950). In the study of HR vagal control in swine model, the VNS parameter that was used for maintaining the level of target HRs during nerve stimulation was stimulation frequency instead of voltage strength (Tosato et al., 2006). Modulation by increasing stimulation frequency displayed high percentage of the target HR/output HR. Frequency used were reported to provide an effective modulation of HR by frequencies between 20 – 25 Hz. Compared to results presented in this chapter, the frequency used was the same level to Tosato et al. (2006) but this chapter used the lower voltage strength. Voltage used was subjected to start recruitment of some population of the B fibres, which contributed to a relatively small HR effect. This RVNS technique minimised the HR reduction effect while still preserved cardio – protective effect of vagal B fibres by the modulation of high frequency used during stimulation. As a result, anti – arrhythmic mechanism of low strength stimulations in this study was likely to be mediated through the selective

recruitment of sub - population of vagal B fibres by the stimulation frequency, which could represent the vagal - nitrenergic fibres (Brack et al., 2011).

Impact of stimulation PW on ventricular EP was studied as it represented a recruitment duration of each activation. Due to the fact that this study used target HR as a reference and titrated stimulation voltage at each fixed PW [0.1 ms, 1 ms, and 2 ms] and fixed frequency to achieve the desire level, a pure response of stimulation PW was not properly investigated. From results, the shorter PW required higher amplitude of voltage than the longer PW to cause the same level of HR decrease. From the results, stimulation PW seemed to have a very small impact on ventricular EP parameters as changes caused by the 3 different PWs were not different. In addition, the EP parameter differences produced by different PWs were less than the differences generated by different frequencies.

5.8.3 Clinical relevance

Stimulation of vagus nerve had been translated to human clinical studies. In heart failure (HF) patients, nerve stimulation device was implanted and a relatively long follow up period (6 – 12 months) was allowed. The first pilot clinical study was performed with chronic heart failure patients (De Ferrari et al., 2011). Then, there were 3 main studies, the ANTHEM-HF (Premchand et al., 2014), the NECTAR-HF (Zannad et al., 2014), and the INOVATE-HF (Hauptman et al., 2012). The main inclusion criteria of these clinical studies was the New York Heart Association (NYHA) class II-III with LVEF < 35% (LVEF < 40% for ANTHEM-HF). Nerve stimulation parameters of all studies are summarised in the table 5.1, which are comparable to parameters used in this chapter.

Table 5.1 Summary of VNS stimulation parameters used by heart failure clinical study

Study	Strength	Frequency	Pulse width	Side	HR sensing
<i>INOVATE-HF</i>	4.1 ± 1.2 mA	1 – 3 Hz	-	Right	Yes
<i>ANTHEM-HF</i>	2.0 ± 0.6 mA	10 Hz	250 µs	Right or Left	No
<i>NECTAR-HF</i>	1.3 ± 0.8 mA	20 Hz	300 µs	Right	No

These clinical studies aimed to improve contractility function and reverse LV remodelling of the patients. Significant improvements of patients were reported at the 6 months follow-up in the INOVATE-HF and the ANTHEM-HF studies compared to baseline (Zannad et al., 2014, Premchand et al., 2014). However, with results from the NECTAR-HF, there were no significant changes between the control group and the treated (VNS) group at the 6 months endpoint (Hauptman et al., 2012). Of these human clinical studies, only 4 arrhythmias were reported during trial period. 2 atrial fibrillations were reported under the possibility to associate with the treatment procedure or system by De Ferrari et al. (2011). Then, 2 ventricular tachycardia were found in ANTHEM-HF (Premchand et al., 2014). There was no sudden cardiac death associated with lethal arrhythmias in all studies. These low incidence of arrhythmias was proposed to be an anti-arrhythmic effect of vagal activation. Data from this chapter provided a strong evidence to support the advantages of VNS on electrophysiology function. Voltage, frequency, and pulse width for the right vagus nerve stimulation of this study covered the range of parameters used in the clinical trials and produced promising ventricular electrophysiology responses.

The findings from this study provide information of the protective mechanism with regard to low level VNS in response to different voltage, frequency, and pulse width that were used to stimulate the nerve. Responses of the isolated innervated rabbit heart preparation were from the interaction between stimulation of the efferent vagus nerve at the cervical level and the heart *ex vivo*. Neuro-hormonal circulation was isolated from the study as well as interactions of the parasympathetic and sympathetic neurons at all 3 hierarchies (Ardell et al., 2016). Study of protective mechanisms with an *in vivo* model would be relevant because of an inclusion of the neuro-hormonal effect and the effect of neuron interaction that would represent the real physiologic condition but the isolated preparation goes some way to delineate the important downstream effects of direct nerve stimulation.

5.8.4 Limitations

Statistical comparison of both HR and ventricular EP results between 3 different stimulation techniques in this chapter was not performed due to the fact that each data set was collected from a different preparation. Within one preparation, data collection was recorded with HR reduction, ERP, VFT, and MAPDR that was stimulated by only one parameter set. Differences of baseline value between each stimulation approach were present, albeit subtle, as there was an effect of variation between each preparation.

Multiple comparisons by 2 way ANOVA with Bonferroni post hoc used in this study simultaneously compared co variant parameters, which were effects of frequency and pulse width. The multiple comparisons increased the threshold required to achieve a statistically significant level associated with the adjusted P value by the post hoc test. As a result, in some datasets, there were apparent differences that did not achieve significance at this higher threshold. A further investigation with a larger N number might potentially demonstrate the difference.

5.8.5 Next stage

Results from this chapter demonstrated differential responses of HR reduction and ventricular EP changes to a variety of vagal stimulation parameters; low versus high amplitude voltages, low versus high frequencies, and short, moderate, and long pulse widths. Next step of the study will be to focus on an impact of RVNS by different stimulation parameters on nitric oxide release in the rabbit left ventricle. Effect of voltage, frequency, and pulse width on the level of nitric oxide release will be investigated in the next chapter.

In addition, the growing evidence of the intrinsic cardiac autonomic nervous system indicated an important role of the neurons within the ganglionic plexuses (GPs) located in the heart (Wake and Brack, 2016, Pauziene et al., 2016). These local neurones comprise afferent, efferent, and interconnecting neurones that function as a first processing circuit (the little brain) within the area that it governs (Beaumont et al., 2016, Brack, 2015). He et al. (2013a) demonstrated prolongation of ventricular ERP and flattened of MAPDR slope by atrial GP stimulation, which led to the hypothesis about an involvement of this GP with the anti – arrhythmic effect of VNS. Functional data of GP stimulation and ventricular electrophysiology response are limited. As a result, the impact of intra – cardiac GP on vagal anti – arrhythmic effect should be further investigated.

This study was conducted by experimenting with a healthy rabbit model, in which vagal tone and cardiac function were in healthy conditions. Repeated study within HF (rabbit, swine, or canine) models would be required to investigate the VNS effect in the disease state.

Chapter 6 Effects of different right vagus nerve stimulation parameters on nitric oxide release in rabbit ventricular

6.1 Introduction

Nitric oxide (NO) is one of the neurotransmitters released during vagus nerve stimulation (VNS) which then modifies cardiac function (Herring and Paterson, 2009). Recent evidence demonstrated a co-localization of an NO production enzymes neuronal nitric oxide synthase (nNOS) with Choline Acetyltransferase (ChAT) within the neurons of intra-cardiac ganglionic plexus (GP) of the rabbit heart (Pauziene et al., 2016). NO was also found to be generated within cardiac myocytes and vascular endothelial cells (endothelial nitric oxide synthase: eNOS) (Förstermann et al., 1994). This gaseous molecule alters ionic currents of a variety of ion channels of the cardiac myocytes (Ziolo et al., 2008). At an organ level, NO was reported to be released during vagus nerve stimulation and involved with cardiac bradycardia (Herring and Paterson, 2001). With an anti-ventricular arrhythmic effect, Brack et al. (2007) demonstrated a reduction of a prolonged effective refractory period (ERP) and an increased ventricular fibrillation threshold (VFT) effects of vagal stimulation by a NO synthase inhibitor. These data suggested an important role of NO in the vagal protective effect against arrhythmogenesis and led to a novel development of technique for real time monitoring of fluorescence signals that measures changes of NO level from left ventricular epicardial surface of the beating heart (Patel et al., 2008). The innovative measurement method utilized fluorescence probe to generate NO dependent fluorescence signal, which was increased by VNS and correlated with prolonged ERP, increased VFT, and flattened restitution slope (Brack et al., 2011).

Data from the early stage of this study in chapter 4 demonstrated an increase of nitric oxide fluorescence (NOFL) signal related with altered electrophysiology (EP) variables [ERP, VFT, and MAPDR] following vagal activations. All changes were observed under the new set of stimulation parameters that extended area of investigation (voltage and frequency) from the previous finding of (Brack et al., 2011). The effects of right VNS on ventricular EP were then tested with the wider range of stimulation parameters of voltage, frequency, and pulse width (X, Y, and Z axis), which were presented in chapter 5. However, data on the effects of stimulation parameters on NO release are still required. Therefore, the NOFL signal changes corresponding to each parameter set were measured and correlated to electrophysiology data in this chapter.

6.2 Chapter objective

- 1) To investigate effects of right vagus nerve stimulation by different stimulation voltages on nitric oxide release in the left ventricle
- 2) To investigate effects of right vagus nerve stimulation by different stimulation frequencies on nitric oxide release in the left ventricle
- 3) To investigate effects of right vagus nerve stimulation by different stimulation pulse widths on nitric oxide release in the left ventricle

6.3 VNS parameters

The right vagus nerve was stimulated by using the same parameter configurations as used in chapter 5.

Stimulation aspect	Voltage (V)	Frequency (Hz)	Pulse width (ms)
<i>Low frequency</i>	80% ΔHR_{max}	1, 2, and 3	0.1, 1, and 2
<i>Low voltage</i>	10% ΔHR_{BL}	5, 10, and 20	0.1, 1, and 2
<i>Low frequency low voltage</i>	10% ΔHR_{BL}	1, 2, and 3	0.1, 1, and 2

6.4 Voltage response and frequency response curves of different RVNS parameters

NOFL experiments were performed in a different group of animals. Experiments started with voltage configurations and frequency response curve similar to EP experiments in chapter 4 and 5. Then, fluorescence technique was performed and the responses to different right VNSs were studied. Unlike EP experiment, right VNSs for NOFL study were performed with all parameter combinations (low frequency, low voltage, and low frequency low voltage) in the same heart. The voltages response and frequency response curves were tested in order to assess the HR reduction effects of right VNSs.

6.4.1 Low frequency stimulation

6.4.1.1 Voltage response curves

Previous data in this report demonstrated that there were differences in the voltage-response curves to vagal stimulus at different voltages and frequencies.

To investigate this with specific RVNS, voltage-response curves were recorded with 5 Hz stimulation frequency. Baseline heart rates, prior to stimulation, were stable at 168.2 ± 6.2 bpm to 165.3 ± 5.5 bpm, Figure 6.1A. Nerve stimulation at 0.1 ms pulse-width significantly reduced heart rate to 101.8 ± 5.9 bpm with a 20 V stimulus. At 2V there was a significant decrease in heart rate, and at a voltage of 3 or above there was no further significant reduction in heart rate. Similar effects were observed with a pulse width of 1 and 2 ms at 5 Hz (Figure 6.1B and C), but there was no significant further reduction in heart rate at voltages above 2.

6.4.1.2 Frequency response curves

From the voltage response curves section 4.1.1, voltages that produce HR drop around 80% of the maximum reduction of each PW were calculated. This voltage strength was classified as the high amplitude voltage that was used to recruit vagal fibres. As for the results, voltages at $80\% \Delta HR_{\max}$ were 4.25 ± 0.90 V for PW 0.1 ms, 5.50 ± 1.10 V for PW 1 ms, and 6.00 ± 0.98 V for PW 2 ms. Next, frequency response curves of all 3 PWs were established. During this stage, the high amplitude voltage was combined with low frequencies (1 Hz, 2 Hz, and 3 Hz) in order to investigate the effects of low frequency stimulation. With the frequency curves, the baseline HR of all PWs were stable with no significant differences between 3 stimulation frequencies (figure 6.2A – C for PW 0.1 ms, 1 ms, and 2 ms respectively), which ranged between 161.0 ± 5.9 bpm to 156.5 ± 5.0 bpm. With voltage $80\% \Delta HR_{\max}$, RVNS showed significant reduction of the HR in all PWs of frequency 3 Hz (figure 6.2 A – C). Maximum reductions were found by the 3 Hz stimulations of each stimulation PWs, which lowered HR to 124.9 ± 7.3 bpm ($P < 0.001$) by 0.1 ms, 115.9 ± 5.1 bpm ($P < 0.0001$) by 1 ms, and 116.4 ± 5.0 bpm ($P < 0.0001$) by 3 Hz. HR reduction of the low frequency stimulation frequency response curve showed a frequency dependent reduction. Frequency 3 Hz dropped HR more than 2 Hz and frequency 2 Hz also reduced HR more than 1 Hz, which effects were observed similarly in all PWs. Results from this step identified

voltage used for the following NOFL experiments and displayed effects of RVNS on HR reduction of these data set.

6.4.2 Low voltage stimulation

6.4.2.1 Voltage use

In contrast to low frequency stimulation, the low voltage stimulation utilized voltage that reduced HR around 10% from the baseline value ($10\% \Delta HR_{BL}$). This low amplitude voltage was introduced into stimulation scheme due to the usage of this strength in the low level VNS pre-clinical and human clinical studies. To identify the target voltage, frequency 20 Hz was used conjunction with each PW to stimulate right vagus. Voltage was titrated until stable HR value that lower than baseline about 10% was achieved, which were 1.74 ± 0.32 V for PW 0.1 ms, 1.30 ± 0.20 V for PW 1 ms, and 1.13 ± 0.16 V for PW 2 ms.

6.4.2.2 Frequency response curve

Frequency response curve of the low voltage stimulation was investigated and results were shown in figure 6.3A to C. Low amplitude voltage from section 4.2.1 were used together with high frequencies 5 Hz, 10 Hz, and 20 Hz in order to test the effects of high frequency stimulation on NO release. However, HR reduction effect of this low voltage stimulation was performed as a first step to assess effect of both low strength voltage and high frequency on HR decrease. From figure 6.3, baseline HRs were stable throughout the protocol and ranging between 159.4 ± 5.3 bpm to 156.0 ± 6.1 bpm. Right VNS decreased HR in all stimulation frequencies and all stimulation PWs (figure 6.3A – C). The lowest RVNS HR was observed by 20 Hz frequency stimulations of all PWs [(0.1 ms, 143.2 ± 7.1 bpm (ns)), (1 ms, 145.9 ± 5.5 bpm (ns)), and (2 ms, 144.1 ± 6.9 bpm (ns))] and there was no significant difference between effect of stimulation frequency within the

stimulation PW. Overall, HR reductions by this parameters were less than 10% from the baseline level in all stimulations.

6.4.3 Low frequency low voltage stimulation

6.4.3.1 Voltage use

For low frequency low voltage stimulation scheme, the $10\% \Delta HR_{BL}$ of each PW was configured under the same objective as the low voltage stimulation. However, to find an optimal voltage in this method, frequency 5 Hz was used instead of frequency 20 Hz used by the low voltage stimulation. As a result, voltage for low frequency low voltage stimulation were 2.22 ± 0.49 V for PW 0.1 ms, 1.49 ± 0.20 V for PW 1 ms, and 1.32 ± 0.20 V for PW 2 ms.

6.4.3.2 Frequency respond curves

Low strength voltages from section 4.3.1 were used to stimulate the right vagus with low frequencies 1 Hz, 2 Hz, and 3 Hz to test effect of both low voltage and low frequency on HR reduction of the RVNS. Frequency response curves of low frequency low voltage stimulation exhibited frequency dependent heart rate reduction in all stimulation PWs, as shown in figure 6.4A to C. From the results, baseline HR were between 158.2 ± 6.2 bpm and 155.1 ± 6.6 bpm. For RVNS, frequency 1 Hz stimulation did not significantly reduce HR from baseline. Higher frequency significantly decreased HR more than the lower frequency in all stimulation PWs (figure 6.4A – C). The lowest HR by RVNS was 140.8 ± 6.2 bpm by frequency 3 Hz and PW 0.1 ms (figure 6.4A). Even with frequency dependent HR reduction characteristic of these low frequency low voltage stimulation, all HR reductions were lower than 10% from baseline HR as an effect of the low amplitude voltage used in this method.

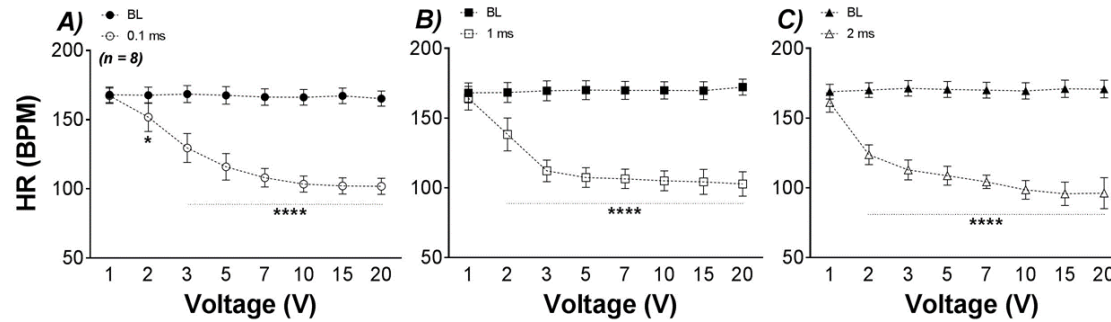


Figure 6.1 Voltage response curve of low frequency stimulation for NOFL technique

Voltage response curves of low frequency RVNS by PW 0.1 ms, 1 ms, and 2 ms at 5 Hz. Heart rate (HR), baseline (BL), beat per min (bpm), volt (V); n = 8, mean ± SEM., Two-way ANOVA with Bonferroni post hoc test, * P < 0.05, **** P < 0.0001.

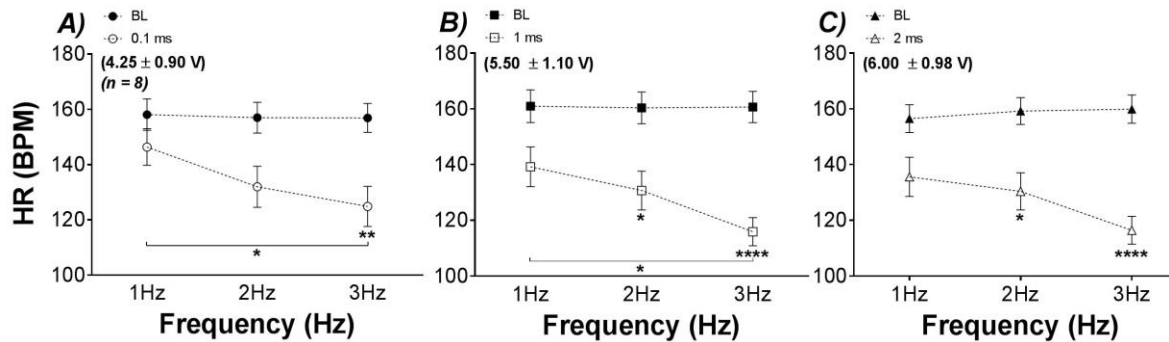


Figure 6.2 Frequency response curves of low frequency stimulation for NOFL technique

Frequency response curves of RVNS low frequency stimulation (80%ΔHR_{max} V with 1 Hz, 2 Hz, and 3 Hz) by PW 0.1 ms, 1 ms, and 2 ms. Heart rate (HR), baseline (BL), beat per min (bpm), volt (V); n = 8, mean ± SEM., Two-way ANOVA with Bonferroni post hoc test, * P < 0.05, ** P < 0.01, **** P < 0.0001.

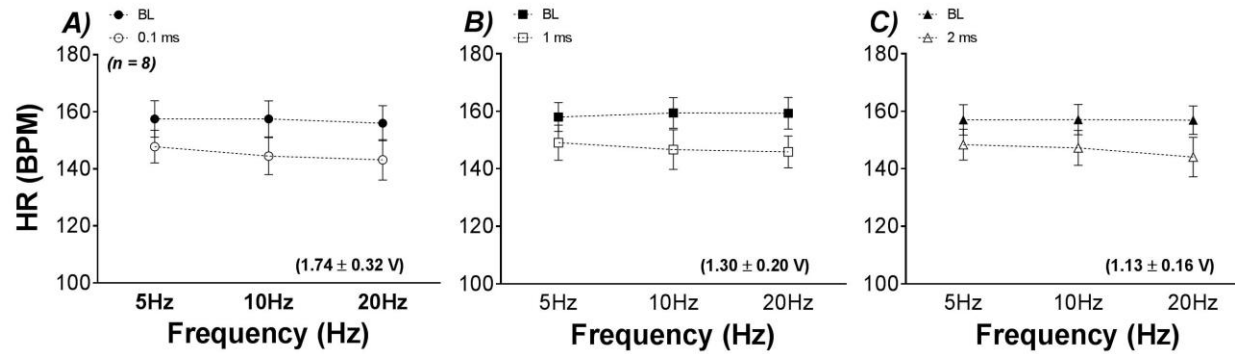


Figure 6.3 Frequency response curves of low voltage stimulation for NOFL technique

Frequency response curves of RVNS low frequency stimulation ($10\% \Delta \text{HR}_{\text{BL}}$ V with 5 Hz, 10 Hz, and 20 Hz) by PW 0.1 ms, 1 ms, and 2 ms. Heart rate (HR), baseline (BL), beat per min (bpm), volt (V); n = 8, mean \pm SEM.

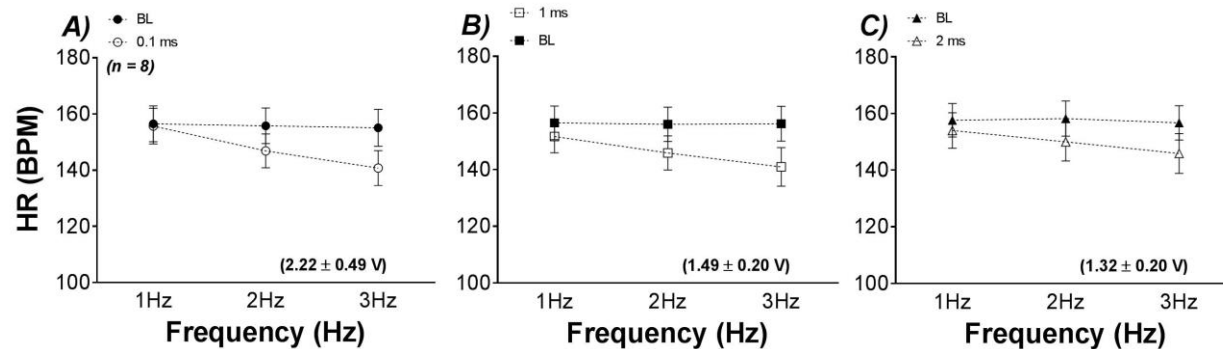


Figure 6.4 Frequency response curves of low frequency low voltage stimulation for NOFL technique

Frequency response curves of RVNS low frequency stimulation ($10\% \Delta \text{HR}_{\text{BL}}$ V with 1 Hz, 2 Hz, and 3 Hz) by PW 0.1 ms, 1 ms, and 2 ms. Heart rate (HR), baseline (BL), beat per min (bpm), volt (V); n = 8, mean \pm SEM.

6.5 Increase of nitric oxide fluorescence (NOFL) signal during right vagus nerve stimulation by a single bifurcated light guided system

6.5.1 Nitric oxide fluorescence (NOFL) signal increased by nerve stimulations

Following voltage response curves of all stimulation schemes, changes of NOFL signal during RVNS were studied during all stimulation parameter sets from the previous step. These sets of experiments were done in order to investigate the effect of RVNS on ventricular NO release. After dye loading and all functional parameters were stable, NOFL protocols were started. The recording and analysis of NOFL signal in this study was focused on F490 nm channel because of 2 reasons. Firstly, this channel gave the best representative changes of the fluorescence signal, which was also the channel with the largest magnitude of change of wavelengths measured (470-500nm) (Brack et al., 2011, Patel et al., 2008). Secondly, using F490 nm allowed the comparison of current results to the previous findings by Brack et al. (2011). Raw data recording by LabChart software, as shown in figure 6.5, illustrates a constant heart rate around 200 bpm. Fixing heart rate by constant pacing of the right ventricle allows a stable perfusion pressure and eliminated an effect of nitric oxide generated by endothelial nitric oxide synthase (eNOS) enzyme from the vascular system. As illustration, the low frequency approach caused increases of raw F490 NOFL signal as seen in figure 6.5. Changes of raw F490 NOFL signal by low voltage stimulation are shown in figure 6.6 while figure 6.7 displayed changes associated with low frequency low voltage stimulation. Unlike electrophysiology experiment, NOFL study stimulated the nerve by all 3 parameter sets in the same preparation. Protocol was randomly performed with a rest of the preparation between RVNS protocol. Then, baseline NOFL and RVNS NOFL were analysed offline and presented in a form of an increase of the signal in mV. Finally, NOFL results were related to changes of other functional parameters such as HR reduction and ventricular electrophysiology variables.

Increases of F490 NOFL signal by the 3 different stimulation protocols of this chapter are summarised and presented in table 6.1. All values from table 6.1 are illustrated as bar graphs associated with stimulation frequency of each protocol in figure 6.8 and bar graphs associated with stimulation pulse width in figure 6.9.

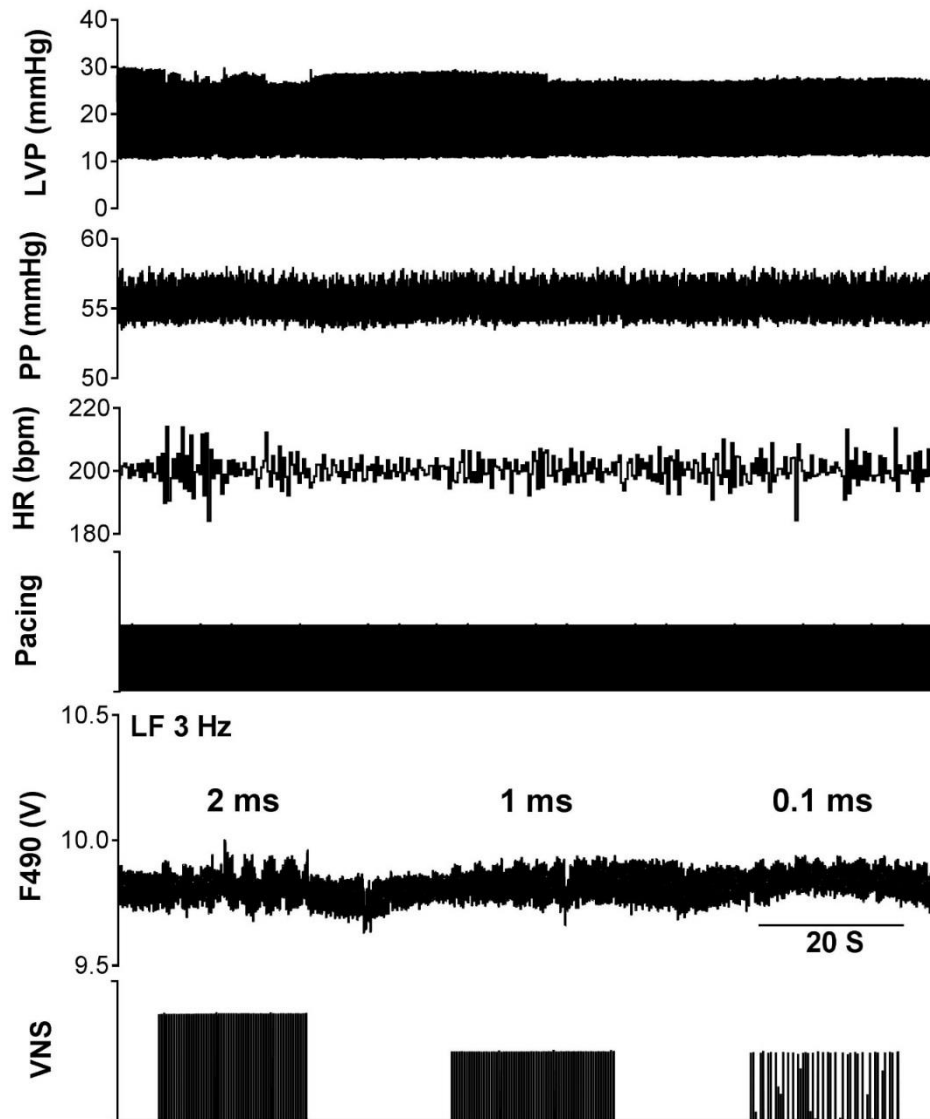


Figure 6.5 Increase of F490 nm NOFL signal during right vagus nerve stimulation by low frequency approach. Left ventricular pressure (LVP), perfusion pressure (PP), vagus nerve stimulation (VNS), volt (V), millimeter mercury (mmHg).

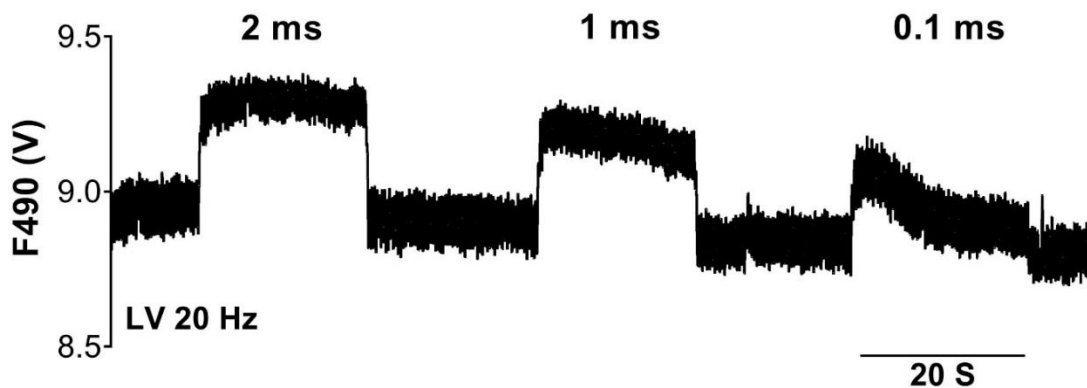


Figure 6.6 Increase of F490 nm NOFL signal by low voltage (LV) stimulation of the right vagus nerve.

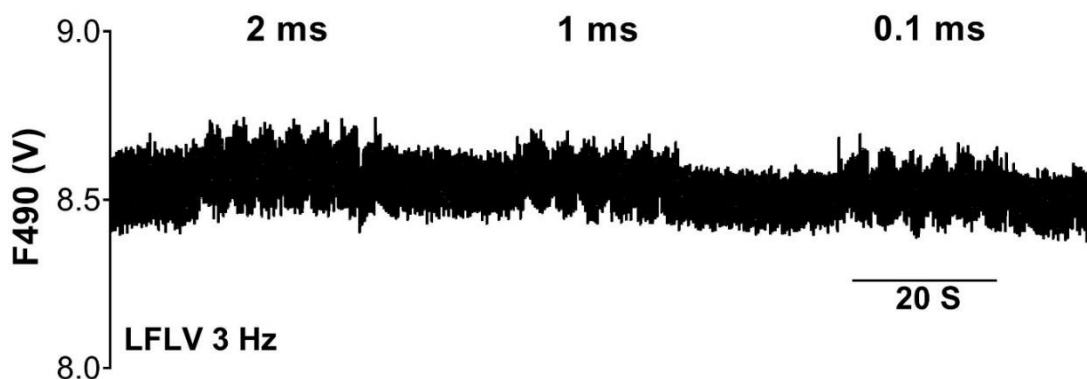


Figure 6.7 Increase of F490 nm NOFL signal by low frequency low voltage (LFLV) stimulation.

6.5.1.1 Effect of stimulation pulse width on NOFL signal changes

As shown in figure 6.8, effects of stimulation pulse width within the same stimulation frequency on NOFL increase were investigated. Briefly, there was no effect of different stimulation pulse width on signal increase within each stimulation frequency in all approaches (low frequency, low voltage, and low frequency low voltage). For signal increase from baseline by RVNS, low frequency stimulation increased signal by about 10 – 30 mV (NS). Differences between each pulse width were small and were not statistical significant (figure 6.8A). Next, the low voltage stimulation raised signal starting from 30 mV to maximum increase around 230

mV. The significant increases of signal from baseline were found by low voltage stimulation with all pulse widths at frequency 20 Hz ($P < 0.0001$) (figure 6.8B). As a final point, the low frequency low voltage stimulation produced very low increases of NOFL signal. Increases were ranging from around 4 mV to 20 mV with no statistical significant was observed by this stimulation method (figure 6.8C). Statistical comparison of these data was performed within all 3 stimulation approaches. Results of this section suggested a small impact of stimulation pulse width of the RVNS on the release of NO in the rabbit left ventricle.

6.5.1.2 Effect of stimulation frequency on NOFL signal changes

NOFL data were then re-arranged for an investigation of the effect of stimulation frequency within the same stimulation pulse width (figure 6.9). From the figures, there was no difference between effects of frequency on NOFL signal increase for the low frequency RVNS (figure 6.9A-C). In contrast, for low voltage stimulation significant differences were shown between NOFL signal increases by different stimulation frequencies. With pulse width 0.1 ms, frequency 20 Hz significantly increased signal more than 10 Hz ($P < 0.001$) and also more than 5 Hz ($P < 0.0001$), as displayed in figure 6.9D. With pulse width 1 ms (figure 6.9E), the 20 Hz significantly increased signal more than 10 Hz ($P < 0.0001$) and more than 5 Hz ($P < 0.0001$) similar to the pulse width 0.1 ms. For pulse with 2 ms, frequency 20 Hz increased signal more than 10 Hz ($P < 0.0001$). Frequency 10 Hz increased signal more than 5 Hz ($P < 0.05$) and frequency 20 Hz increased NOFL more than 5 Hz (0.0001), as shown in figure 6.9F. Finally, the low frequency low voltage stimulation showed differences between frequency 3 Hz and 1 Hz stimulations ($P < 0.01$) in both pulse width 0.1 ms and 2 ms (figure 6.9G and I, respectively). From these comparisons, NOFL results displayed a frequency dependent increase in RVNS stimulation approaches suggested an important role of stimulation frequency on NO release during the vagal activation.

6.5.1.3 Comparison between stimulation approaches

For the final evaluation of NOFL data, a brief comparison between all 3 RVNS approaches were performed and results showed that the low voltage stimulation caused the highest increase of signal more than other 2 approaches. Even at the lowest combination of the low voltage method (frequency 5 Hz and PW 0.1 ms), NOFL signal increase was still higher than all results of the other 2 approaches. Next, due to the fact that the low frequency stimulation and the low frequency low voltage stimulation used the same set of frequency but used different voltage strengths, comparison between these 2 methods reviewed effects of differences between high amplitude and low amplitude voltages on NOFL increase. With the pulse width 0.1 ms, differences between signal increase by the low frequency and the low frequency low voltage approaches were observed at frequency 1 Hz ($P < 0.0001$), 2 Hz ($P < 0.01$), and 3 Hz ($P < 0.01$) stimuli. With regard to pulse width 1 ms, differences were observed in frequency 1 Hz ($P < 0.05$), 2 Hz ($P < 0.01$), and 3 Hz ($P < 0.01$) stimuli. Finally, for pulse width 2 ms, differences were observed only in frequency 2 Hz stimulus ($P < 0.01$). Data displayed in this section demonstrated a small impact of the stimulation voltage on the increase of NO release in the rabbit ventricle by RVNS.

Table 6.1 Increase of nitric oxide (NOFL) signal by 3 different nerve stimulation strategies
n = 12, mean \pm SEM., Two-way ANOVA with Bonferroni post hoc test, ** P < 0.0001.**

<i>Stimulations</i>	<i>0.1 ms</i> (mV)	<i>1 ms</i> (mV)	<i>2 ms</i> (mV)
<i>Low frequency</i>			
1 Hz	15.7 \pm 4.7	11.6 \pm 2.9	18.8 \pm 7.1
2 Hz	16.2 \pm 3.9	21.4 \pm 3.9	25.5 \pm 5.4
3 Hz	15.0 \pm 2.8	28.4 \pm 8.7	31.9 \pm 7.5
<i>Low voltage</i>			
5 Hz	38.2 \pm 11.2	49.4 \pm 18.0	33.1 \pm 7.8
10 Hz	49.8 \pm 15.2	72.0 \pm 18.1	81.9 \pm 29.3
20 Hz	192.9 \pm 55.2 ****	233.2 \pm 57.5 ****	230.6 \pm 54.7 ****
<i>Low frequency low voltage</i>			
1 Hz	4.2 \pm 1.5	5.2 \pm 2.1	9.1 \pm 2.7
2 Hz	10.8 \pm 3.5	13.0 \pm 4.4	15.6 \pm 4.6
3 Hz	8.9 \pm 4.4	15.1 \pm 5.0	22.7 \pm 5.9

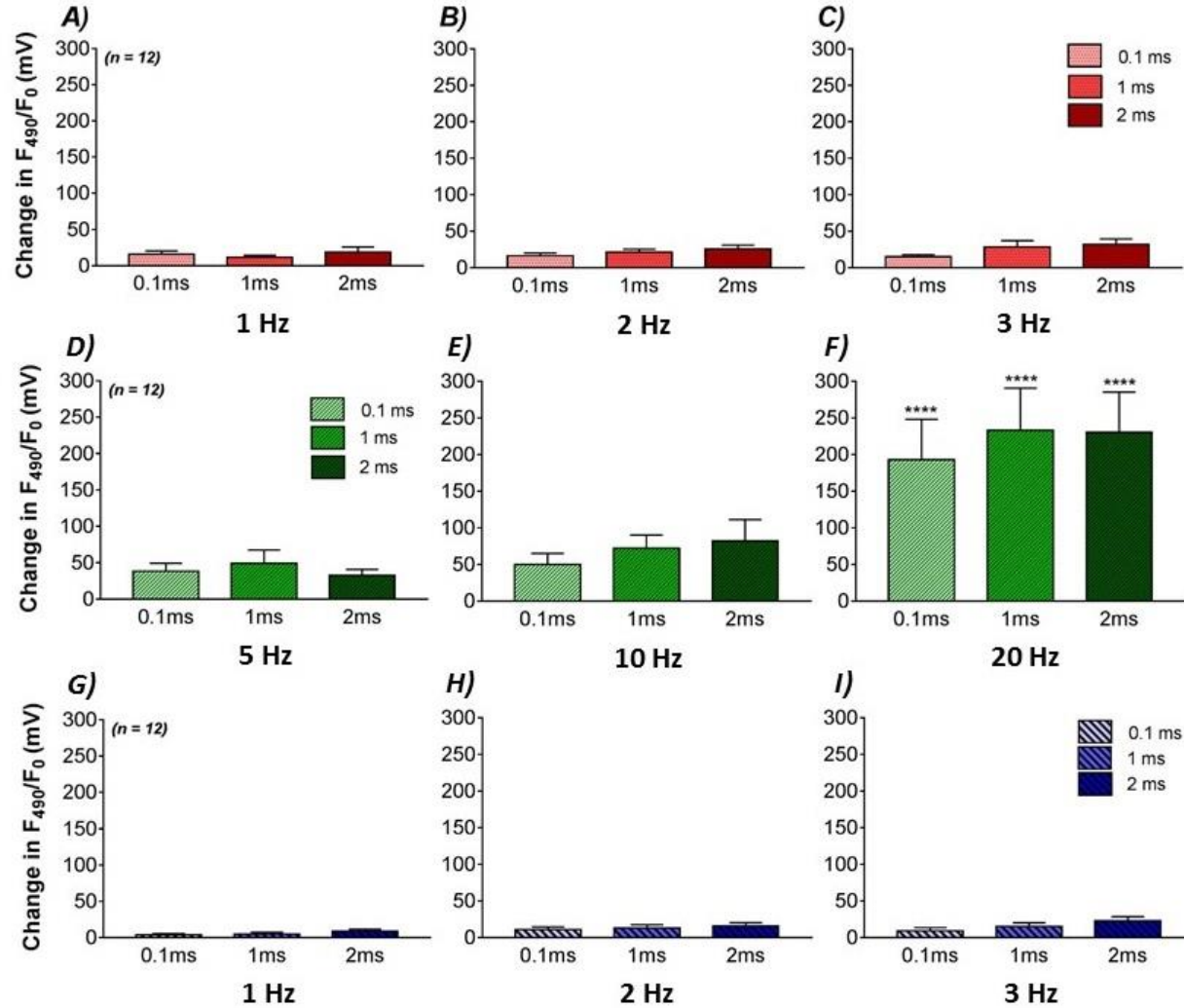


Figure 6.8 Effect of pulse width on increase of NOFL signal

$n = 12$, mean \pm SEM., Two-way ANOVA with Bonferroni post hoc test, **** $P < 0.0001$

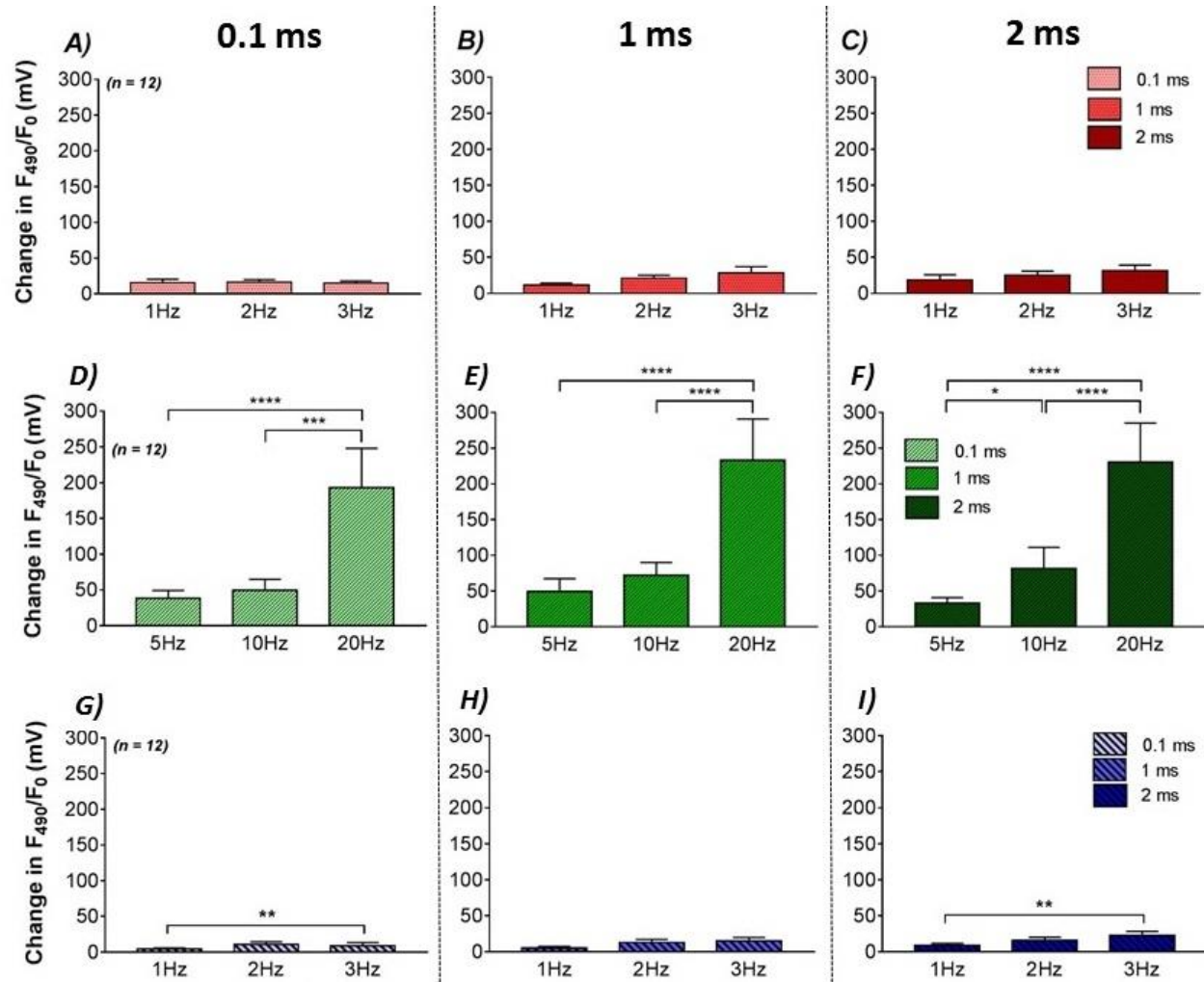


Figure 6.9 Effect of frequency on increase of NOFL signal

n = 12, mean \pm SEM., Two-way ANOVA with Bonferroni post hoc test, * P < 0.05, ** P < 0.01, *** P < 0.001, **** P < 0.0001

6.6 Changes of nitric oxide fluorescence (NOFL) signal and percentage change of other physiological parameters

From the previous section, RVNS illustrated a capability to increase NOFL signal from baseline. Level of signal elevations were varied according to the different voltage, frequency, and pulse width used during vagal activation. Nitric oxide released during nerve stimulation is known to alter cardiac function and cardiac electrophysiology. Therefore, it is necessary to consider the data of NOFL changes from the previous step of this chapter together with other physiological responses from right vagal stimulation in the previous chapter.

Firstly, changes of NOFL signal were displayed together with percentage heart rate reduction in figure 6.10. From the figure, the big change of NOFL signal was effected by high frequencies used in the low voltage strategy. This approach produced higher amount of signal increase particularly by the frequency 20 Hz. However, all percent HR drops of the low voltage scheme were lower than 10% from the baseline level. In contrast to HR decrease by the low voltage stimulation protocols, there was a high percentage of HR drop caused by high amplitude voltage used with the low frequency strategy. This method was seemed to have a small effect on NOFL signal elevation. Results of these 2 stimulation parameter sets confirmed a different role of voltage and frequency on cardiac function as voltage had a dominant effect in reducing heart rate while frequency was dominantly responsible for the increase in nitric oxide level in the ventricle with RVNS. With low frequency low voltage stimulation, NOFL signal was increased in a small level and overall percentage heart rate reduction was smaller than 10% from baseline HR.

In this comparison, there was no calculation of percent increase of effective refractory period because the overall level of ERP prolongation was very small (around 5% - 10%), which made an interpretation with the NOFL difficult.

Increases of NOFL signal compared to percent VFT increases are showed in figure 6.11. The low frequency stimulation increased the thresholds around 30% to

90% together with small increases of NOFL signal. In contrast, the higher level of NOFL signal increases and the higher percent of VFT increases were observed with the low voltage (high frequency) RVNS stimulation. This low voltage parameter set produced increases of threshold of approximately 60% to 130%. Finally, the lowest amount of NOFL signal increase was observed by the low frequency low voltage RVNS method. This last technique raised the VFT between 40% and 65%. From these data set, increase of VFT appears to be linked more with NO release in the ventricle during RVNS.

Finally, increases of NOFL signal compare to percentage MAPDR slope reduction are displayed in figure 6.12 for the apex restitution data and in figure 6.13 for the base restitution data. For the apex restitution, the low voltage (high frequency) approach produced higher level of maximum slope flattening more than other 2 approaches. For the base restitution results, similar responses of percentage slope flattening were observed with the low voltage (high frequency) stimulation causing the highest level of MAPDR slope reduction compared to the low frequency and the low frequency low voltage stimulations. When compared between the apex and the base restitutions, the base restitution results showed higher percentage MAPD slope reduction than the apex restitution with the low frequency and the low voltage approaches.

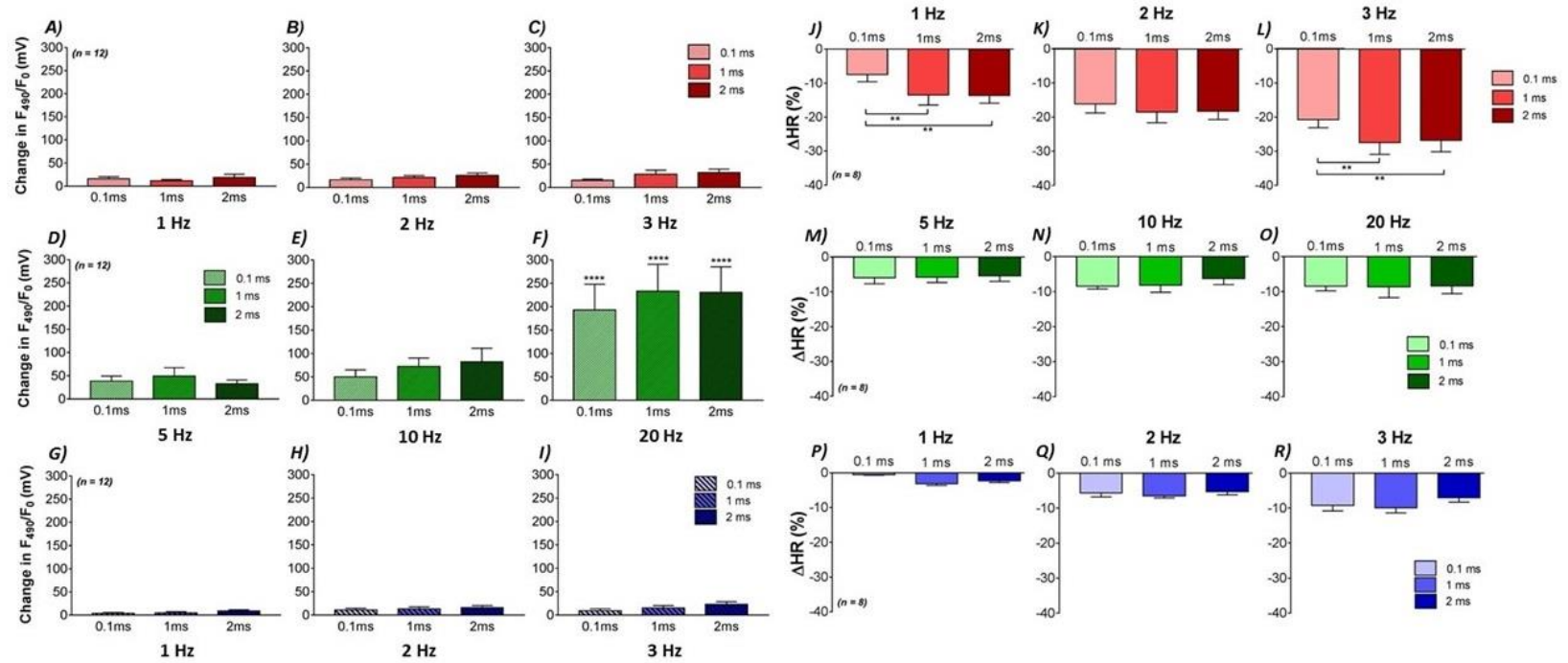


Figure 6.10 Increase of NOFL signal and percent heart rate reduction by low frequency stimulation (red), low voltage stimulation (green), and low frequency low voltage stimulation (blue); mean \pm SEM.

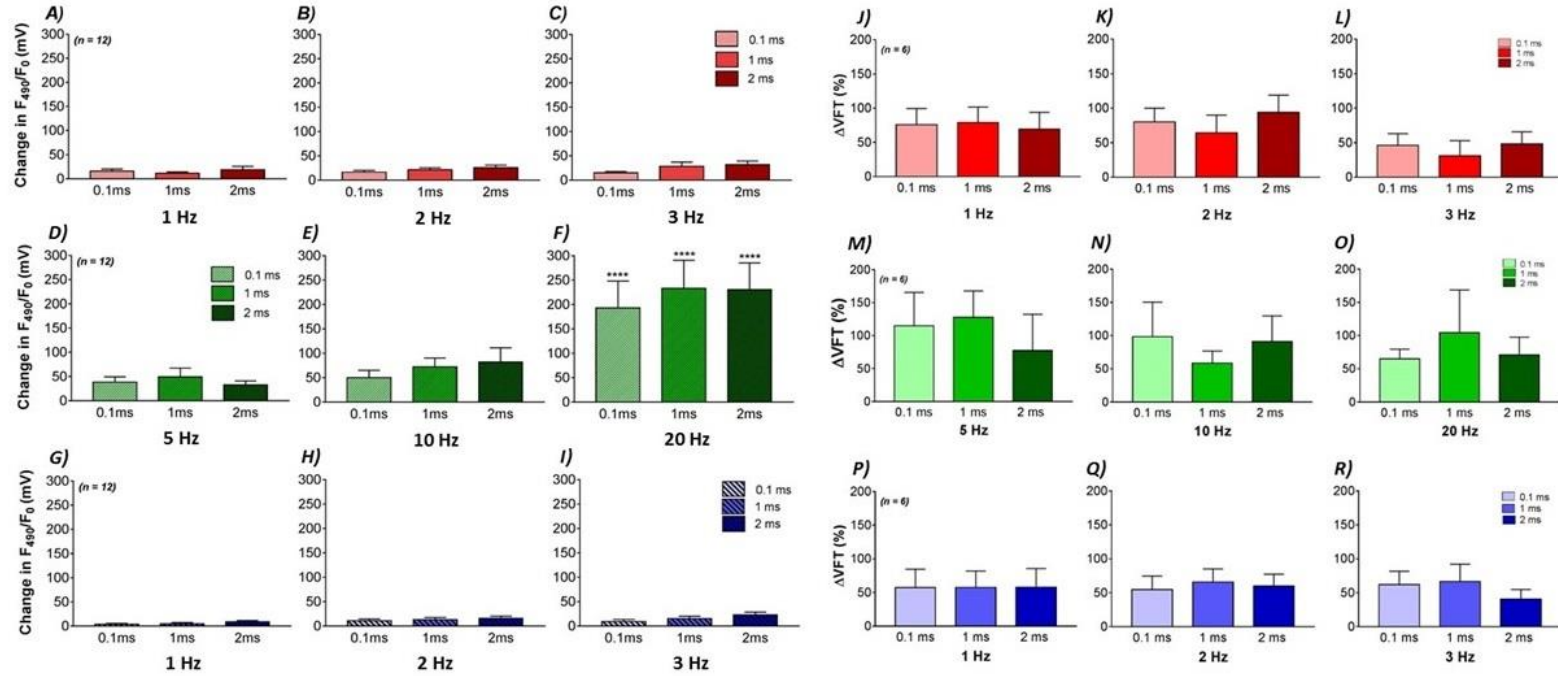


Figure 6.11 Increase of NOFL signal and percent ventricular fibrillation threshold increase by low frequency stimulation (red), low voltage stimulation (green), and low frequency low voltage stimulation (blue); mean \pm SEM.

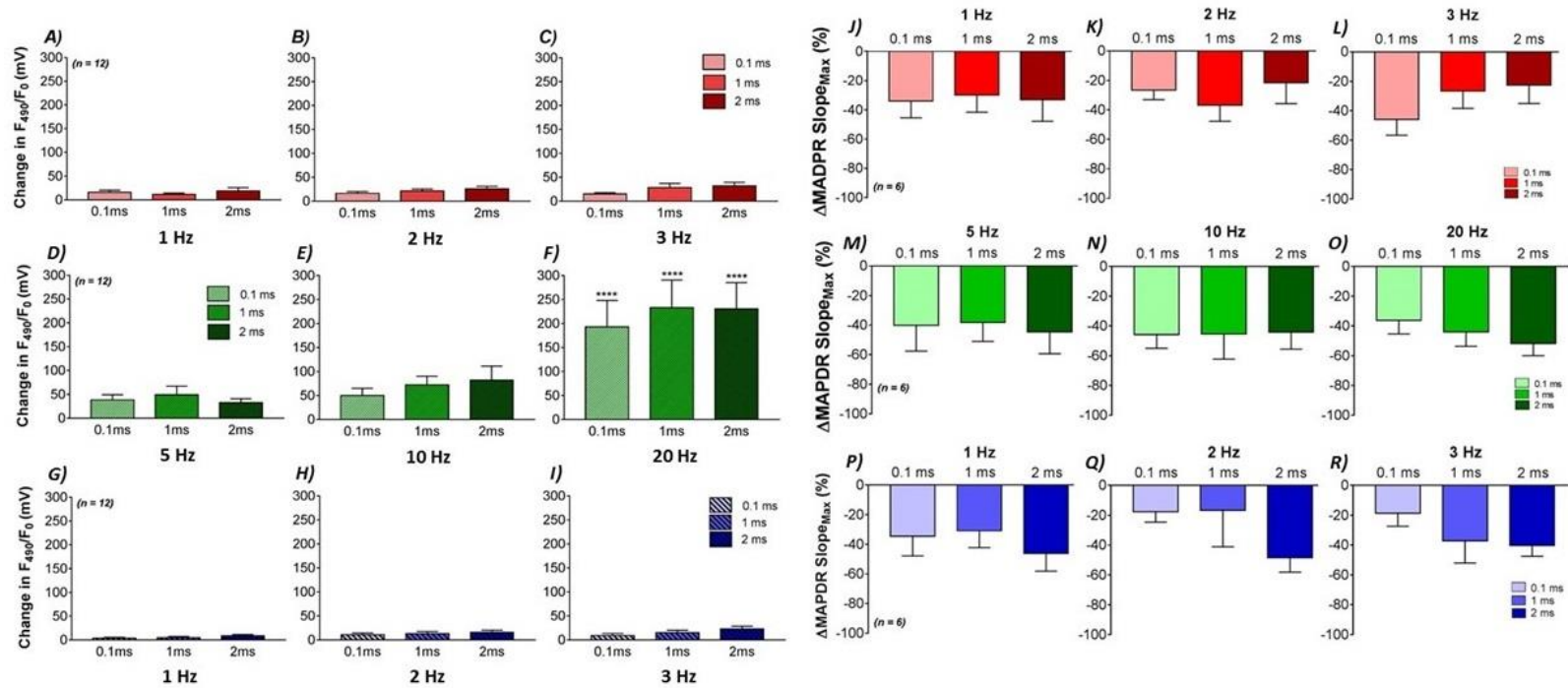


Figure 6.12 Increase of NOFL signal and percent maximum slope reduction of apex restitution by low frequency stimulation (red), low voltage stimulation (green), and low frequency low voltage stimulation (blue); mean \pm SEM.

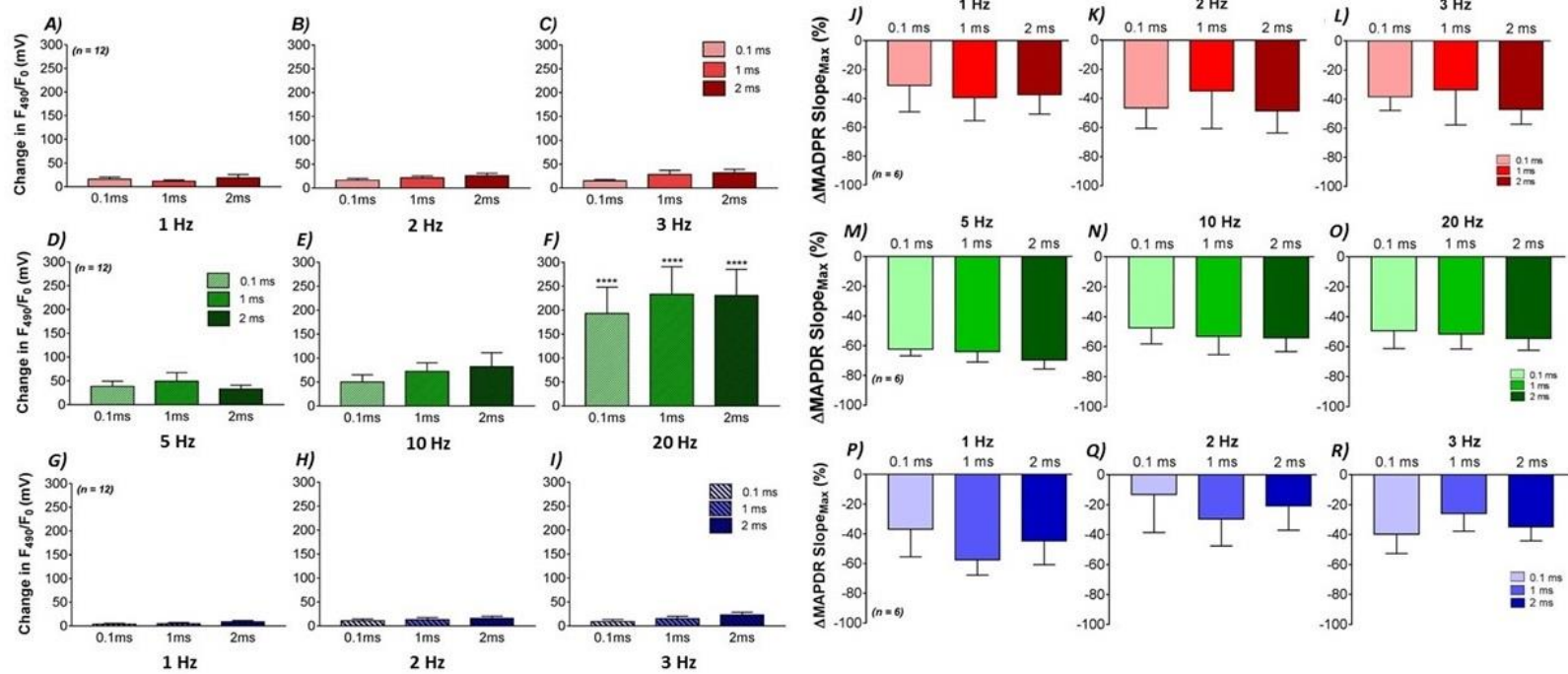


Figure 6.13 Increase of NOFL signal and percent maximum slope reduction of base restitution by low frequency stimulation (red), low voltage stimulation (green), and low frequency low voltage stimulation (blue); mean \pm SEM.

6.7 Discussions

6.7.1 Response of NOFL signal to right vagus nerve stimulation

Ventricular electrophysiology responses related to right vagus nerve stimulation were shown in chapter 5. The anti-arrhythmic mechanisms (prolonged ERP, increased VFT, and flattened restitution slope) are thought to involve the VNS-NO pathway, which was supported by the NOFL results of this chapter. In a canine model, stimulation of the right vagus with a very low strength reduced atrial fibrillation duration that was induced by acetylcholine, the effect of which was abolished by the NO synthase blocker (L-NAME) (Stavrakis et al., 2013). An increased of VFT was found together with increased NO content from coronary effluent from the rat heart that was perfused by Carbamylcholine. This cardio protection occurred through muscarinic and nicotinic (cholinergic) receptors activation because this protection could be prevented by atropine perfusion. Moreover, as the neuronal nitric oxide synthase inhibitor reversed the increases of effluent NO contents, NO which is involved with this mechanism in the rat was proposed to be derived from nNOS (Kalla et al., 2016a).

Using the single bifurcated light guide system with DAF-2 dye, fluorescence signal associated with NO release in rabbit ventricle was seen together with prolongation of ERP, increase of VFT, and flattening of the restitution slope (Brack et al., 2009). In rabbit heart, atropine perfusion inhibited vagal heart rate reduction but did not affect the anti-arrhythmic effects, which different from the response in the rat. Moreover, ganglionic blockade totally abolished vagal protective effect and also prevented increase of NO fluorescence signal (Brack et al., 2011). In addition, anatomical evidence of intrinsic cardiac neurones provides support for NO released by nNOS isoform in the heart to mediate vagal stimulation effects (Wake and Brack, 2016, Pauza et al., 2013) with the evidence of immunohistochemical staining of cell bodies and fibres of cardiac neurones displaying nNOS positive cells inside the rabbit ventricle (Pauziene et al., 2016). For rabbit model, as mentioned in the previous chapter, high strength voltage stimulation was seemed to alter heart rate through the vagal cholinergic fibres and muscarinic receptors activation. In contrast, the high frequency stimulation accompanied with a small heart rate reduction (<10% from baseline

HR) but produced higher NO release than the high amplitude voltage stimulation. These different responses between high strength voltage and high frequency of VNS suggested that high amplitude voltage and high frequency proceeded through the heart via a different type of vagus fibre. Many evidences supported that the vagal HR effect occurred through the cholinergic fibres and muscarinic receptors activation, which required the high amplitude voltage (Jones et al., 1998, Woolley et al., 1987, Ford and McWilliam, 1986). On the other hand, the use of high frequency attributed to the release of NO rather than decrease HR. These vagal NO effect was thought to be mediated by vagal nitrenergic fibres (Brack et al., 2011). Differences between response mechanisms of rat and rabbit models could be explained by different calcium handlings between the 2 species (Baczkó et al., 2016, Quinn and Kohl, 2016).

Changes of signal in this study were mainly observed with low voltage stimulation, which was in a frequency dependent manner similar to Brack et al. (2009). The NOFL increase in the current study was independent from heart rate reduction unlike the fluorescence data of previous study that accompanied large heart rate reduction (Brack et al., 2009). The simple explanation was the lower voltage amplitude used in the current study compared to the previous study. These results confirmed that the vagal protective action was independent from heart rate effect (Yamakawa et al., 2015). Furthermore, it suggested an important role of frequency use for stimulation with regard to nitric oxide release in the heart. High level of NOFL increase by low voltage technique was shown to produce a higher percent change of ventricular fibrillation threshold and higher percent reduction of restitution slope when compared to other parameter combinations.

To our knowledge, this was the first study that investigated an effect of stimulation pulse width on changes of NO in the rabbit ventricle. Previous studies used of stimulation duration were 0.1 ms (canine) (Stavrakis et al., 2013), 0.3 ms (canine) (Hamann et al., 2013), and 0.5 ms (swine) (Shinlapawittayatorn et al., 2013) together with frequency 20 Hz but only Stavrakis et al. (2013) provided evidence regard to involvement of NO with vagal protection. All studies reported anti-arrhythmic effects even with

differences of pulse width used suggested minimal effect of pulse width on vagal stimulation. In this study, 3 different durations were tested and the results showed no significant differences between fluorescence signal increases, which supports little impact of pulse width on vagal protection. For translating to the next stage, pulse width 0.1 ms would be recommended as it affects heart rate less than longer pulse widths but offers protection of the heart against arrhythmias involve with a nNOS-NO mechanism.

6.7.2 Source of nitric oxide

Kalla et al. (2016a) proposed that the release of nNOS-derived NO is at the upstream level of muscarinic receptor. Administration of carbamylcholine (CCh) to Langendorff perfused rat heart reduced heart rate, increase VFT, and flattened restitution slope, which specific nNOS inhibitor inhibited the VFT increased. NO content was measured from the coronary effluent by chemiluminescence assay. With this technique, there was a possibility that measured NO contents was a mixture of nNOS-derived NO from ganglionic plexuses and eNOS-derived NO from intact endothelial cells. In our group, using the bifurcated single light guide technique fluorescence signal is measured by activity of DAF-2 dye and NO inside the cardiac ventricular cell. Brack et al. (2011) denuded endothelium by using Triton-X, which lowered fluorescence signal from endothelial intact condition. However, the NOFL signal was elevated from endothelial denuded baseline by vagal activation suggested the measured NO signal was i) a mixture of nNOS-derived NO and eNOS-derived NO and ii) nNOS-derived NO was generated by intra-cardiac neurons during vagal stimulation. These functional data were supported by immunohistochemical evidence of nNOS positive staining of the intra-cardiac ganglionic plexus neurones (Pauziene et al., 2016, Saburkina et al., 2014).

6.7.3 DAF-2 specificity

DAF-2 DA dye was used to measure nitric oxide inside cardiac cell. This dye is suitable to measure nitric oxide generation inside the cell (von Bohlen und Halbach, 2003). DAF-2 dye is sensitive to peroxynitrite more than nitric oxide (von Bohlen und Halbach, 2003, Roychowdhury et al., 2002). Moreover, this dye also interacts with hydroascorbic acid and ascorbic acid (AA) (von Bohlen und Halbach, 2003, Zhang et al., 2002). Ascorbic acid is a water soluble antioxidant that was found maximally 9 mM in endothelial cells of human and from 1 – 10 mM in neurons. In addition, vitamin C is oxidized to dehydroascorbic acid (DHA), which reacts with DAF-2 and forms the DAF-2-DHAs. Fluorescence signals of DAF-2-DHAs is lower than fluorescence of DAF-2T (active isoform by the reaction between DAF-2 and NO) (Zhang et al., 2002). Since nitric oxide fluorescence by single light guided system measures fluorescence signal inside cardiac cells at an epicardium of left ventricle with an increasing of fluorescence signal by vagal stimulation under the condition of endothelial function disruption (Brack et al., 2011), the fluorescence signal recorded by this technique would be more likely to represent changes of the DAF-2T molecule (nNOS-derived NO from intra-cardiac neurons) rather than the DAF-2-DHAs (eNOS-derived NO from endothelial cell).

Peroxynitrite (ONOO^-) molecules are formed by the reaction between nitric oxide and superoxide ($\text{O}_2^{\bullet-}$) intracellularly. Study of DAF-2 fluorescence in glial cells employed a cell culture techniques, which allowed an accumulation of superoxide within specimens (Roychowdhury et al., 2002). In contrast, this study was done with Langedorff perfusion of the isolated innervated rabbit heart preparation, with well controlled pH, temperature, and other physiological environments to maintain stability of the beating heart. Superoxide generated inside cells would be rapidly removed by superoxide dismutase located in the mitochondria, cytoplasm, and extracellular compartments of the preparation (Pacher et al., 2007). Study in a beating swine heart illustrated a decrease of mitochondrial reactive oxygen species (ROS) by an intermittent low level vagal stimulation (Shinlapawittayatorn et al., 2013). This vagal ROS reduction effect suggests that the fluorescence signal recorded from the innervated preparation was unlikely to measure an activity of DAF-2 and peroxynitrite.

6.7.4 Limitations and future study

In this chapter, right vagus nerve stimulation displayed a potential to increase nitric oxide level in the rabbit ventricle. Increase in NO fluorescence signal by the current technique represented an increase of nitric oxide generated inside cardiac cells (Brack et al., 2011, Brack et al., 2009, Patel et al., 2008). The post ganglionic vagal efferent fibres were electrical stimulated at the cervical level, which was then processed by a network of intra-cardiac neurons before causing NO release in the ventricle (Hanna et al., 2017). However, the missing links between the post ganglionic vagal efferent fibre activation and how it triggers activity of neuronal nitric oxide synthase (nNOS) inside cardiac cells require further investigation.

The NO fluorescence measurement used in this study presented an increase of NO-related fluorescence signal compared to baseline fluorescence. The actual intra-cellular concentration of NO was not directly measured. Further investigation to correlate intra-cellular NO concentration with the amplitude of NOFL signal might allow the use of this fluorescence method to estimate an intracellular concentration of NO. Plotting intra-cellular NO concentration by using molecular techniques to measure nitrate or nitrite directly from the heart and linking it to fluorescence might enable an actual [NO] measurement.

In the ventricle, cholinergic nerves were shown to be more prominent in subendocardial than subepicardial regions (Kawano et al., 2003). Moreover, immunohistochemistry evidence displayed a co-localisation of ChAT and nNOS within the same neuron in human RAGP (Hoover et al., 2009). Therefore, there is a hypothesis that NO would be released throughout ventricular myocardium during VNS but the NOFL technique in this study was limited to measuring only signals from the epicardial surface. The DAF-2 fluorescent dye used in this technique was shown to interact with Nitrous Anhydrase (N_2O_3) (Planchet and Kaiser, 2006), and hence does not provide a direct measurement of the NO gaseous molecule.

NO released by the low frequency stimulation parameter set displayed a frequency-dependent release pattern but the electrophysiology response did

not. Therefore, it is possible that the vagal-NO anti-arrhythmic effect might represent a threshold effect rather than a linear response. Further study on this hypothesis should be done together with exploring downstream signalling pathways of this vagal-NO action. NO can act through either cGMP-dependent or cGMP independent (S-nitrosylation) pathways (Ziolo et al., 2008). Information with regard to vagal-NO mechanisms could lead to an optimisation of stimulation strength to provide beneficial effects to patients and identification of important signalling pathways whereby effective molecules and/or channels of this anti-arrhythmic effect could be developed.

Chapter 7 Development of DAF-2 optical mapping technique for measuring nitric oxide release in the rabbit ventricle

7.1 Introduction

Stimulation of the right vagus nerve with different stimulation parameters produced changes in ventricular electrophysiology. These anti-arrhythmic responses to varying strengths in VNS (chapter 5) were then correlated with nitric oxide (NO) releases in the left ventricle (LV) as a result of the different RVNS parameters (chapter 6). Electrophysiology results from this study strongly confirmed an anti – arrhythmic effect of vagal activation (Ng et al., 2007) even with the low intensity stimulation. Moreover, these data also provided evidence for an involvement of nNOS-derived NO with anti-arrhythmic effect of vagus nerve stimulation (VNS) (Kalla et al., 2016a, Brack et al., 2011).

Presence of heterogeneity of nerve innervation, ganglionic plexus, and ion channels within the left ventricle (LV) point to the possibility of regional heterogeneity in the response to VNS of physiological parameters in the heart (Wake and Brack, 2016, Pauziene et al., 2016, Saburkina et al., 2014, Szabó et al., 2005, Kawano et al., 2003, Berkels et al., 2000). Electrophysiological evidence from the monophasic action potential restitution (MAPDR) data from chapter 5 showed differential responses between the base and apex of the LV during VNS which also support this notion. The fluorescence technique used in chapter 6 for the measurement of NO release, was limited to recording changes of signal in a small area of the left ventricular (LV) epicardial surface at one time, and was not able to measure signal changes over a large area. Immunohistochemical data of rabbit heart innervation demonstrated positive staining of nNOS in neurones within the ganglionic plexuses across the LV (Pauziene et al., 2016). NO release during vagal stimulated could modify ion channel function, and distributions and expression of ion channels have been shown to be different between LV base and apex (Tamargo et al., 2010, Szentadrassy et al., 2005). These led to a relevant question as to the presence of heterogeneous release of NO during VNS and consequent heterogeneity in

the response of ion channels from different LV regions. Thus, measurements of the changes of NO release over a wide region of LV is necessary. This measurement of regional changes of NOFL signal during RVNS will provide important information of NO release characteristics and can be used to correlate with regional electrophysiological responses. In addition, the link between stimulation of the vagus nerve at cervical level to electrophysiological changes of cardiac myocardium in the beating heart can be directly related.

In this chapter, a new fluorescence method for measuring nitric oxide level was developed with an aim to capture changes of fluorescence signal associated with changes of NO level across the epicardial surface of the left ventricular free wall in the beating heart. This new technique was based on the successful NO fluorescence recording set up using the bifurcated single light technique (Patel et al., 2008). By building on the fluorescence property of DAF-2 DA dye (von Bohlen und Halbach, 2003) together with signal measurement of emitted light signal by photodetector of an optical mapping arrangement (Arora et al., 2003), the DAF-2 optical mapping technique was developed to measure NO release in the rabbit LV during RVNS.

7.2 Chapter objective

- 1) To develop an optical mapping technique that is able to measure changes of fluorescence signal associated with changes of nitric oxide level in the rabbit left ventricle

7.3 VNS parameters

RVNS parameters in this chapter were the same configurations as chapter 5 and

Stimulation aspect	Voltage (V)	Frequency (Hz)	Pulse width (ms)
<i>Low frequency</i>	80% ΔHR_{max}	1, 2, and 3	0.1, 1, and 2
<i>Low voltage</i>	10% ΔHR_{BL}	5, 10, and 20	0.1, 1, and 2
<i>Low frequency low voltage</i>	10% ΔHR_{BL}	1, 2, and 3	0.1, 1, and 2

7.4 Voltage response and frequency response curves of different RVNS parameters

7.4.1 Low frequency stimulation

7.4.1.1 Voltage response curves

To see how voltage intensity of each pulse width affected heart rate reduction, voltage response curve was performed as a first step. The voltage that caused the maximum heart rate reduction was defined by this protocol and the optimal voltage use by the low frequency stimulation was calculated in this step, similar to the description in earlier sections of this thesis. Response of HR reduction to voltage response curves by all 3 PWs (at frequency 5 Hz) displayed similar trend as baseline HRs were stable and the significant HR reduction were observed at 2 V by all 3 PWs (figure 7.1A-C). Baseline HR ranged between 180.2 ± 13.3 to 187.4 ± 12.7 bpm and the lowest HRs were 125.9 ± 18.6 bpm, 127.3 ± 19.1 bpm, and 120.7 ± 15.3 bpm for PW 0.1 ms, 1 ms, and 2 ms, respectively.

7.4.1.2 Frequency response curves

From the section 4.1.1, the optimal voltages were 6.29 ± 1.34 V for 0.1 ms, 6.57 ± 1.66 V for 1 ms, and 7.14 ± 1.55 V for 2 ms. Frequency response curves of this low frequency stimulation produced a frequency dependent HR reduction in all 3 PWs (figure 7.2 A-C). HR reduction were seen with frequency 1 Hz stimulation of all 3 PWs. Maximum reductions were at frequency 3 Hz stimulations (148.6 ± 16.6 bpm for 0.1 ms, 144.0 ± 17.6 bpm for 1 ms, and 141.1 ± 15.6 bpm for 2 ms).

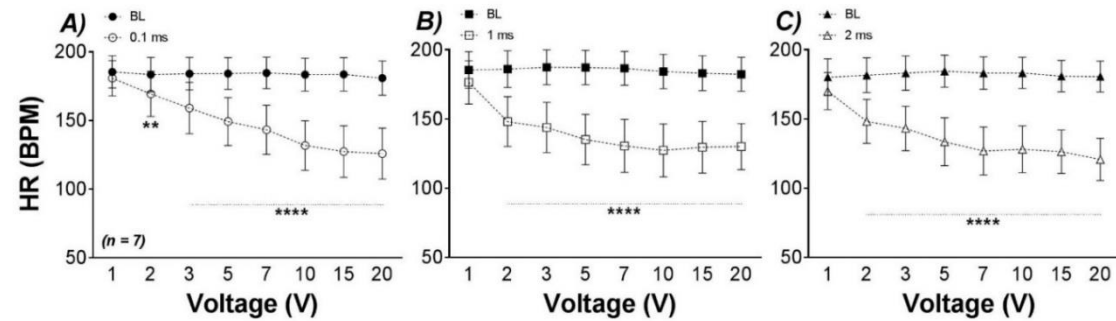


Figure 7.1 Voltage response curve of low frequency stimulation

Voltage response curves of low frequency RVNS by PW 0.1 ms, 1 ms, and 2 ms at 5 Hz. Heart rate (HR), baseline (BL), beat per min (bpm), volt (V); n = 7, mean \pm SEM., Two-way ANOVA with Bonferroni post hoc test, ** P < 0.001, **** P < 0.0001.

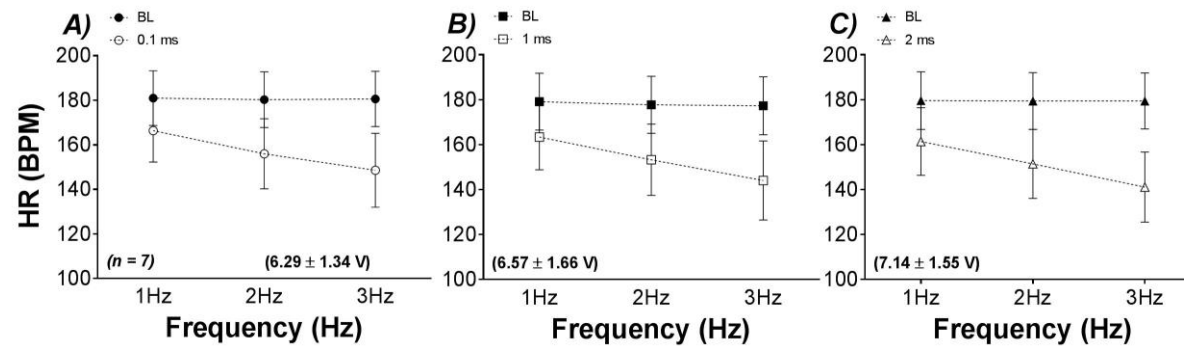


Figure 7.2 Frequency response curves of low frequency stimulation

Frequency response curves of RVNS low frequency stimulation by PW 0.1 ms, 1 ms, and 2 ms. Heart rate (HR), baseline (BL), beat per min (bpm), volt (V); n = 7, mean \pm SEM.

7.4.2 Low voltage stimulation

7.4.2.1 Voltage use

The voltages that reduced HR less than 10% at a frequency 20 Hz from the baseline value for the low voltage stimulation in this chapter were 2.18 ± 0.43 V, 0.91 ± 0.16 V, and 0.74 ± 0.14 V for PW 0.1 ms, 1 ms, and 2 ms, respectively.

7.4.2.2 Frequency response curves

Frequency response curves of the low voltage stimulation displayed HR reduction in all frequencies of all PWs (figure 7.3A-C). Baseline HR were between 156.0 ± 6.1 bpm to 159.4 ± 5.3 bpm and RVNS caused HR to drop to between 143.2 ± 7.1 bpm to 149.1 ± 6.1 bpm.

7.4.3 Low frequency low voltage stimulation

7.4.3.1 Voltage use

For this low frequency low voltage stimulation, the voltages that lower HR less than 10% from baseline by frequency 5 Hz were 2.54 ± 0.53 V, 1.24 ± 0.33 V, and 0.95 ± 0.21 V for PW 0.1 ms, 1 ms, and 2 ms, respectively.

7.4.3.2 Frequency response curves

Frequency response curves of low frequency low voltage stimulation exhibited frequency dependent HR reduction (figure 7.4A-C). Baseline HR of all PWs were stable between 155.1 ± 6.6 bpm to 158.2 ± 6.2 bpm. The lowest HR were found at frequency 3 Hz stimuli, which were 140.8 ± 6.2 bpm for 0.1 ms, 141.0 ± 6.9 bpm for 1 ms, and 145.9 ± 7.0 bpm for 2 ms.

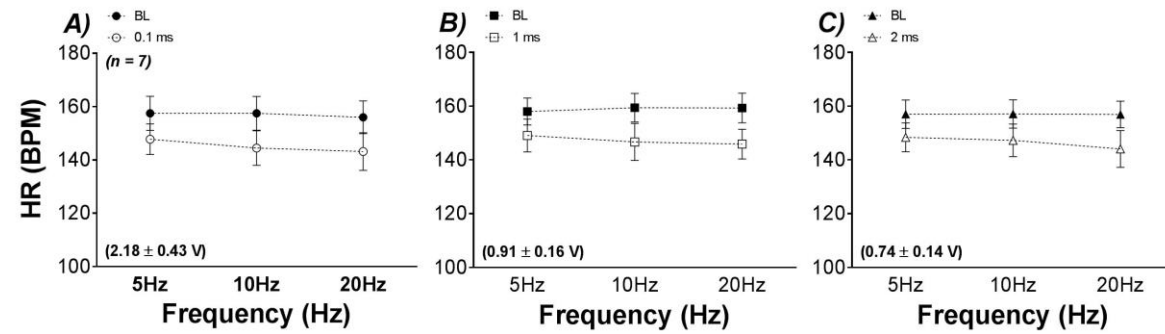


Figure 7.3 Frequency response curves of low voltage stimulation

Frequency response curves of RVNS low voltage stimulation by PW 0.1 ms, 1 ms, and 2 ms. Heart rate (HR), baseline (BL), beat per min (bpm), volt (V); n = 7, mean ± SEM.

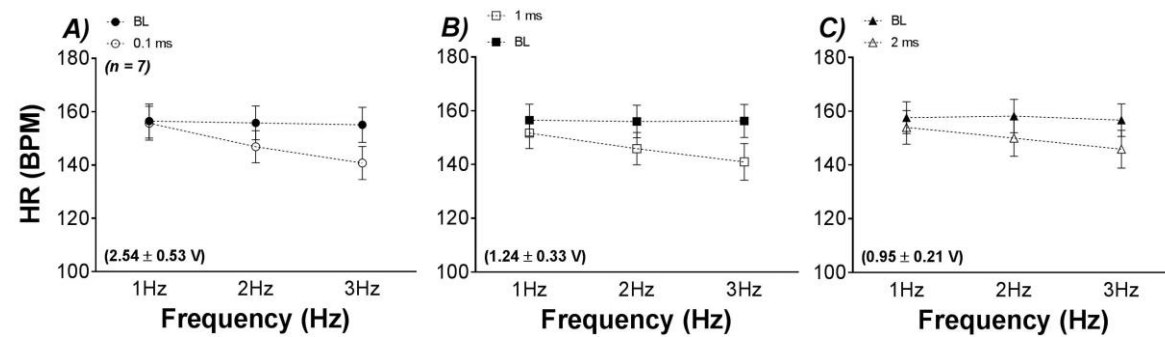


Figure 7.4 Frequency response curves of low voltage stimulation

Frequency response curves of RVNS low voltage stimulation by PW 0.1 ms, 1 ms, and 2 ms. Heart rate (HR), baseline (BL), beat per min (bpm), volt (V); n = 7, mean ± SEM.

7.5 NO fluorescence by DAF-2 DA optical mapping

7.5.1 Optical mapping apparatus

Components of the optical mapping equipment for measuring NO fluorescence signal are displayed in figure 7.5. The isolated innervated rabbit heart preparation was placed in the container A. The focus onto the recording camera was adjusted by varying the distance between the preparation (A) and the collector lens (B). Light (wavelength 470 nm) from the LED light source (D) was passed to the dichroic mirror in C which selectively reflected the wavelength below 510 nm to the preparation in A. After receiving an excitation light, emission light (wavelength 515 nm) was emitted from the cardiac cells associated with level of active form of DAF-2 dye, which activated at wavelength 495 nm (von Bohlen und Halbach, 2003). Emitted signal from the preparation was collected by the collector lens (B) and passed through the dichroic mirror (C) and the filter at F. At this stage, only wavelengths 510 nm to 560 nm were passed through the bandpass filter (F) to the photodetector in G. Photodetector (G) converts the light signal into electrical signal and sends it to the analysis software (Optiq). Focus adjustment and preparation alignment were performed under real-time monitoring by the video camera (E).

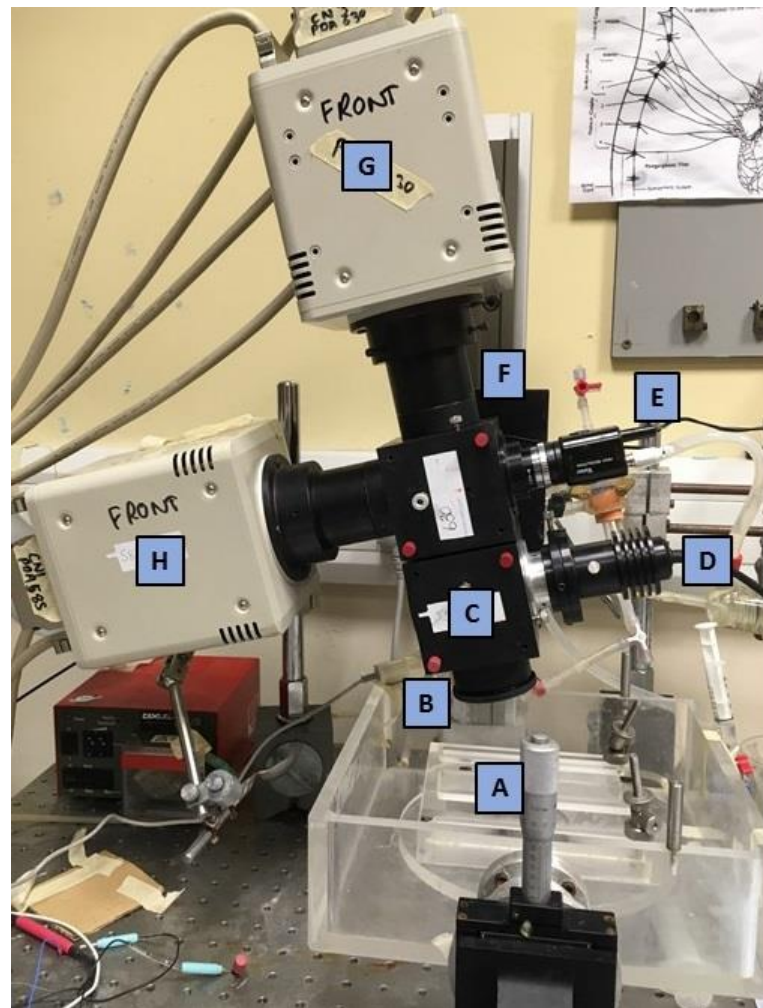


Figure 7.5 Optical mapping apparatus for measuring NO by DAF-2 DA dye. (A) preparation tray, (B) lens, (C) dichroic mirror, (D) LED light source, (E) video camera, (F) filter, (G) 1st photodetector, and (H) 2nd photodetector.

7.5.2 Response of isolated innervated rabbit heart to the excitation - contraction uncoupler

After obtaining the correct voltages for each stimulation, a pacing catheter was inserted into the right ventricle through an incision on pulmonary artery. Pacing threshold was obtained by increasing the pacing current until the heart beats in sync with the pacing rate, which was set to cycle length (CL) 300 ms (200 bpm). This (diastolic) threshold was doubled in value and used to ensure pacing capture. After that, the excitation – contraction uncoupler, 2,3-butanedione monoxime (BDM), was perfused into the preparation by mixing with the Tyrode's solution (Attin and Clusin, 2009). BDM stops the heart from

beating whilst electrical activity continues, as shown in figure 7.6. The heart responded to BDM by reducing the contraction as represented as reduction in left ventricular pressure (LVP) until no contraction, which is shown as a constant solid line of an LVP in figure 7.5. Perfusion pressure was constant throughout the procedure. Then, the DAF-2 DA dye (150 – 250 μ L) was delivered to the preparation through the right carotid artery under the same procedure as used in chapter 6 (described in detail in chapter 3). A waiting period of 60 – 75 minutes was allowed for the dye to be stabilised inside the cardiac cells.

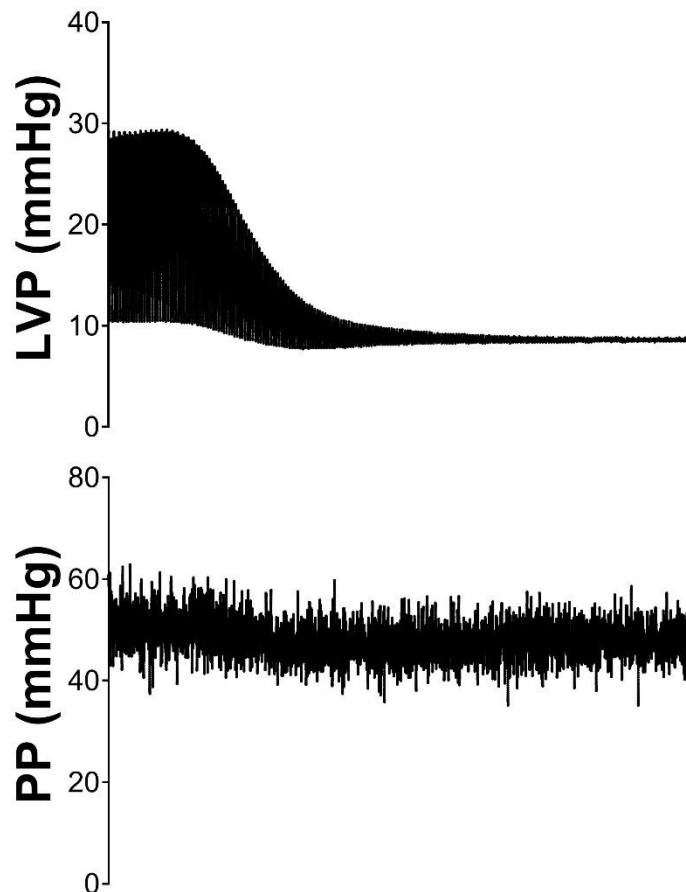


Figure 7.6 Response of the heart to BDM as loss of contraction represented by reduction of left ventricular pressure (LVP).

Then, the preparation was re-positioned to present the recording area of the LV as large as possible in the field of view of the optical mapping system. This step was performed together with focussing adjustment. The highest resolution image was obtained by adjusting the length between the preparation and the lens of the optic system. These processes were done under the monitoring by the video camera of the optical system. An example image of the LV free-wall that was optimally aligned with an optimal focus is shown in figure 7.7. During this step, the light source was turned on intermittently in order to help with alignment and to assure that the area of interest was in the correct light path.

Then, the recording protocol of the DAF-2 optical mapping was started. The heart was paced by the RV pacing catheter with a CL 300 ms. Baseline signal was recorded and followed by RVNS protocol. RVNS was performed with only one parameter set at a time and RV pacing was stopped between at the end of each set. Right vagus was removed from electrode and kept moist by applying Tyrode's solution during the break between each protocol.

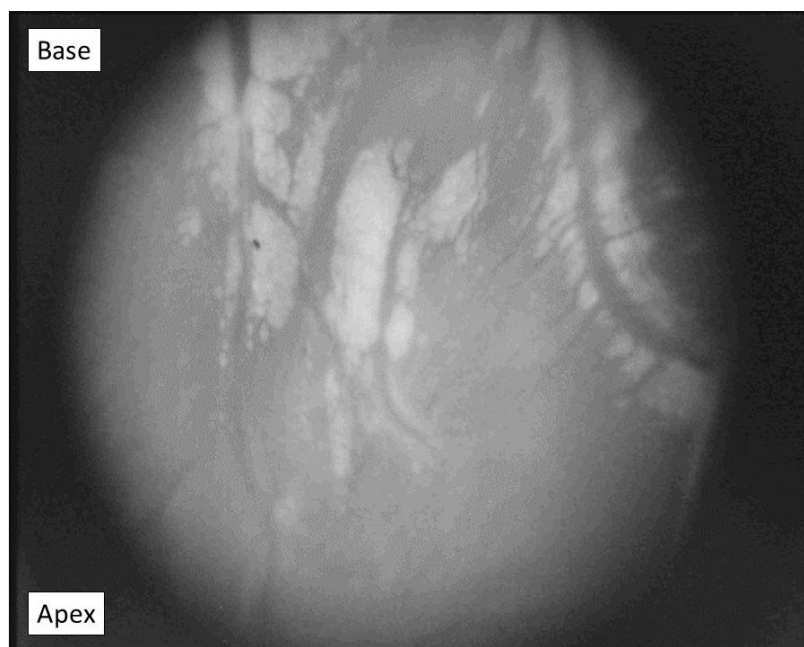


Figure 7.7 Left ventricular free-wall within the optimal focus length of an optical mapping system. Image was snap shot by the video camera of an optical mapping system.

7.5.3 Recording of NO fluorescence signal by optical mapping system

Results of DAF-2 optical mapping are represented in a 16 x 16 recording pixels (256 pixels), as shown in figure 7.8 and 7.9. Baseline fluorescence signal is shown in figure 7.8. Stimulation of the right vagus with frequency 20 Hz 1 ms and 1 V produced the fluorescence as displayed in figure 7.9. The X axis of each pixel represented the duration of recording for 10 seconds and the Y axis represented the amplitude of the recorded signal.

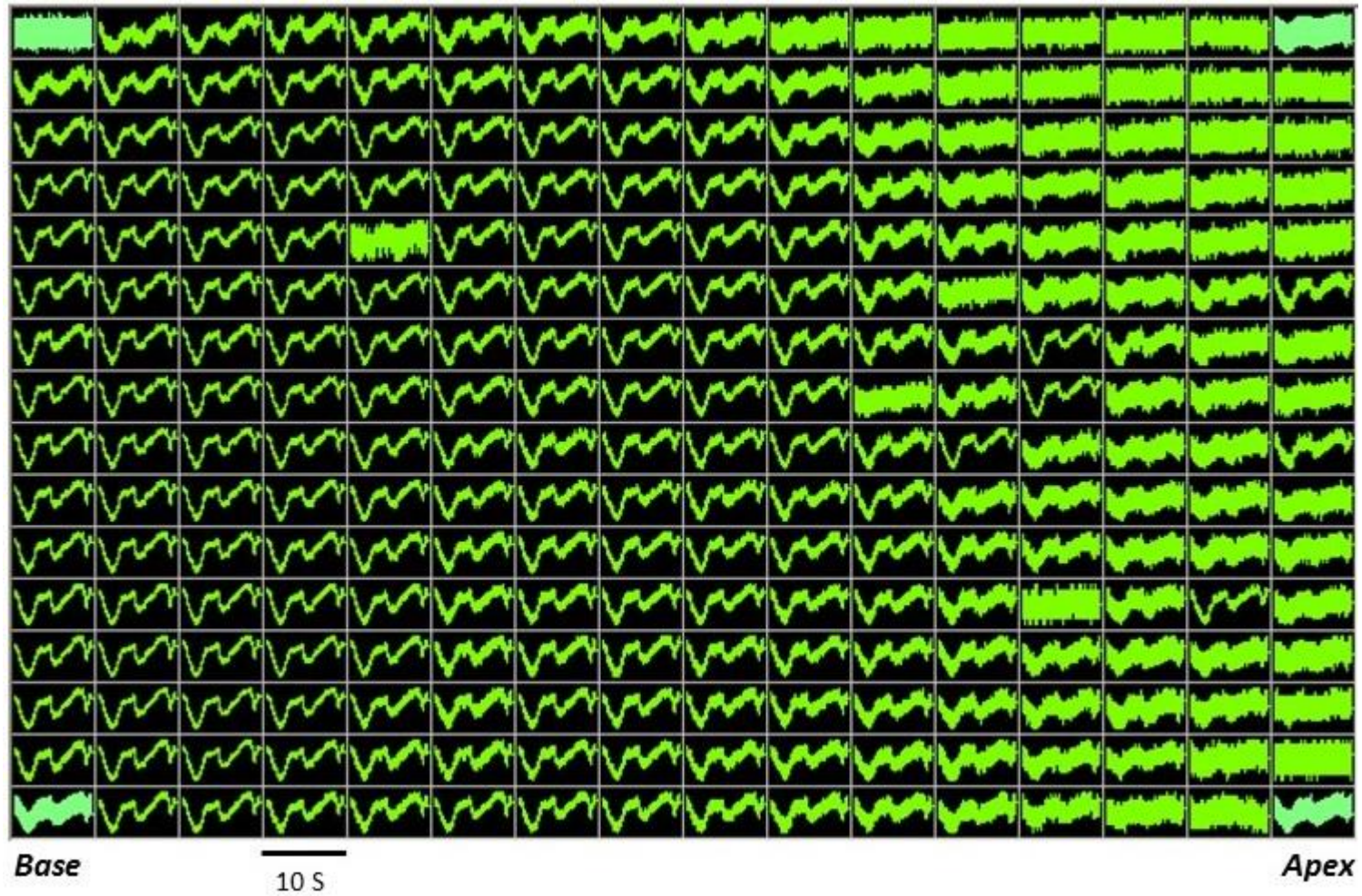


Figure 7.8 Fluorescence signal recorded by optical mapping system from the rabbit left ventricle during the baseline stage. Data represented as 16 x 16 (256) pixels. The X axis of each pixel was a 10 seconds time and the Y axis was an amplitude of the recorded signal.

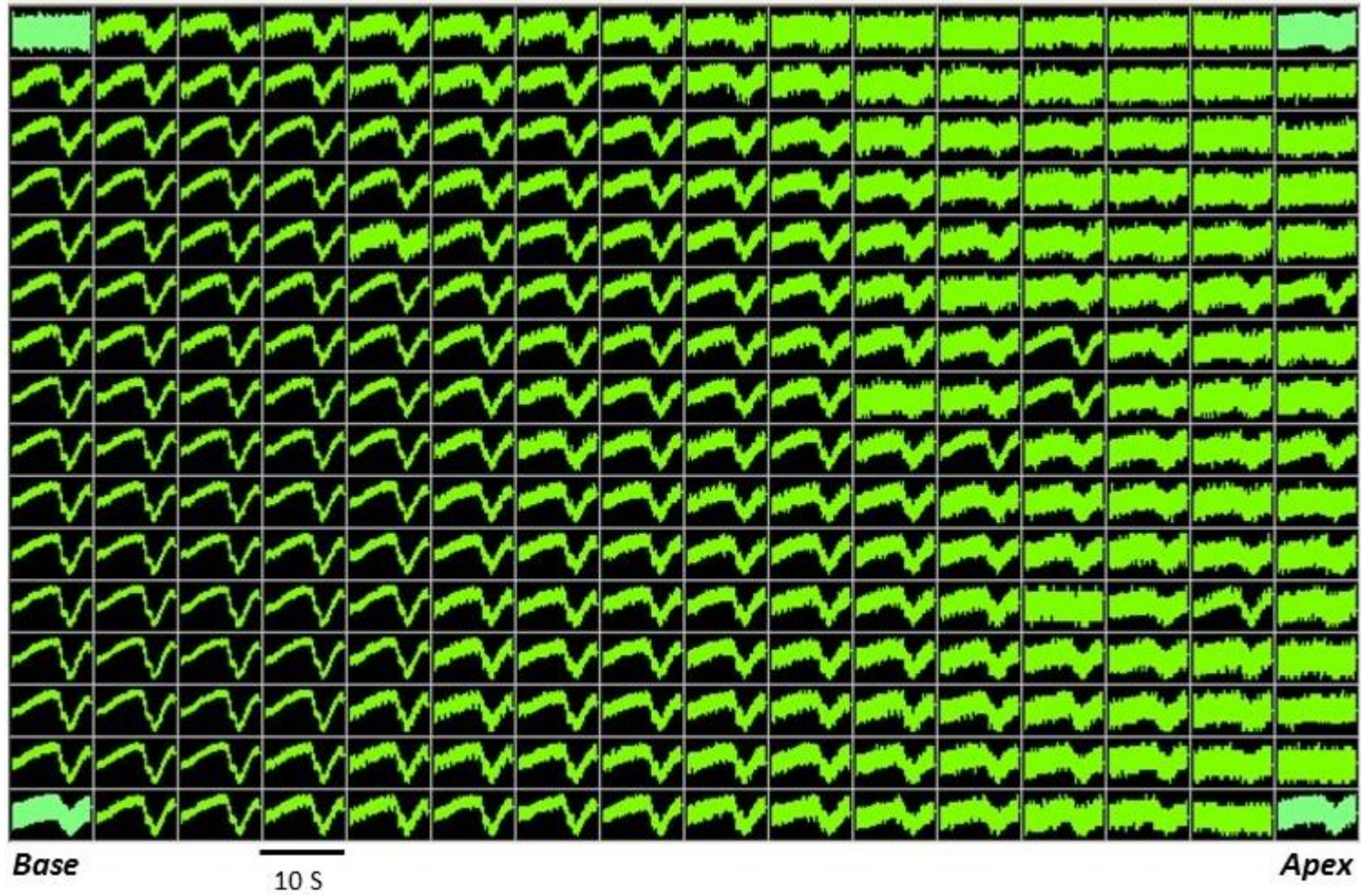


Figure 7.9 Fluorescence signal recorded by optical mapping system from the rabbit left ventricle during the RVNS by frequency 20 Hz pulse width 1 ms and voltage 1 V.

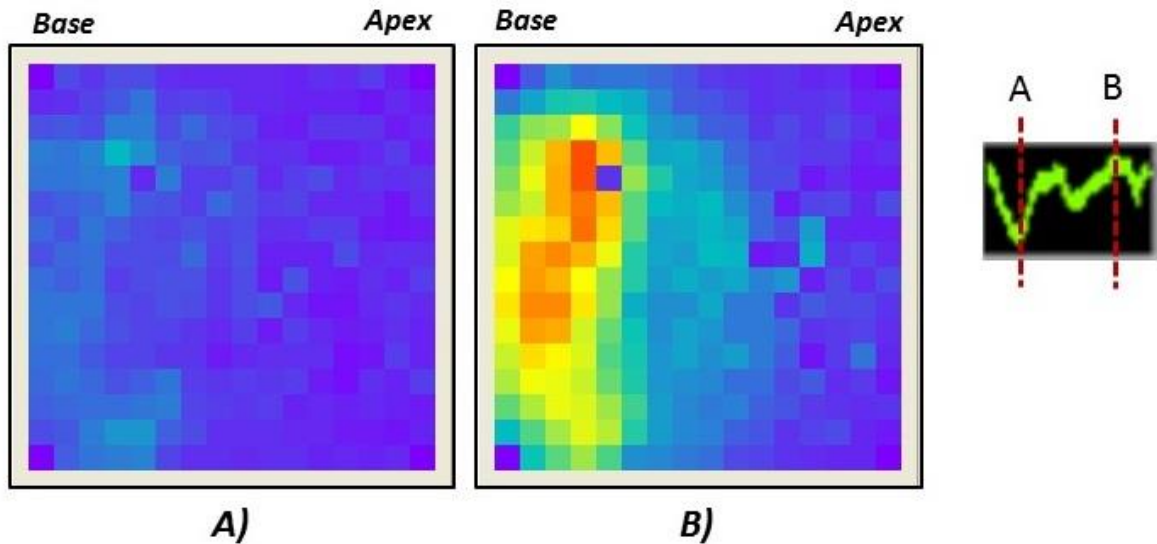


Figure 7.10 Representation of fluorescence signal change from figure 7.8 by a colour map. **A)** Colour mapping at the low amplitude signal within the recording 10 seconds pixel (the lowest point of a green tracing displayed in a small box) and **B)** colour mapping at the peak amplitude of the 10 seconds pixel (the highest point of a green tracing).

Within the recording area of the LV, optical mapping displayed the changes of fluorescence signal concurrently. Signals changed in a similar pattern in all pixels (figure 7.8 and 7.9). However, the recorded signal fluctuated within the pixel. By coding tracings of signal from figure 7.8 with the colour map (showed in figure 7.10), the changes of colour reviewed heterogeneity between the base and the apex of the LV as there was an increase in the amplitude of fluorescence at the base which was not present at the apex when compared between figure 7.10A (baseline level signal) and figure 7.10B (peak amplitude signal).

These results displayed a potential for using optical mapping technique to monitor changes of fluorescence signal from the rabbit heart. DAF-2 optical mapping was able to detect the fluorescence signal from the isolated innervated rabbit heart preparation. However, application of this technique is preliminary and its use requires further development and validation. The recorded signal was not of adequate quality due to low signal to noise ratio. Baseline signal during the control stage was not stable. Tracing of signal displayed a fluctuation unlike the signal that

recorded by the bifurcated single light guide system. As a result, results of this stage lead to a conclusion that the recorded signal was not a fluorescence signal of DAF-2T (active form of DAF-2). Adjustment of an optical system component is required with fine tuning in the optical and / or electronic arrangement to optimise the signal emitted from the preparation.

7.6 Discussions

7.6.1 Technical detail of optical mapping apparatus

Fluorescence technique for monitoring of NO release in the beating heart was first described in our group by Patel et al. (2008). The technique was used to investigate the nNOS-derived NO released during VNS to correlate with the anti-arrhythmic effect of vagus nerve stimulation (Brack et al., 2011). With this novel technique, NO level was indirectly measured by the fluorescence signal generated by reaction between NO and the DAF-2 DA dye. An active form of the dye (DAF-2T) is excited at wavelength 495 nm and emits signal at 515 nm (von Bohlen und Halbach, 2003, Leikert et al., 2001). With this technique, wavelength 490 ± 10 nm was reported to provide the highest temporal resolution fluorescence signal (Brack et al., 2009).

In this new development, the LED light source used for delivering the excitation light was at wavelength 470 ± 30 nm (figure 7.11). Output light 455 – 485 nm would be totally reflected to the preparation by the dichroic mirror. However, as mentioned previously, DAF-2T molecules are excited at wavelength 495 nm. By not receiving sufficient energy at the excitation wavelength, the DAF-2T molecules might not emit the fluorescence signal in a quantity that can be detect by the photodetector of the optical system, which would result in a poor signal to noise ratio which may be the reason behind the signals and results seen in this chapter. The mismatch between wavelength of output light from LED light source and the excitation wavelength of DAF-2T molecules at a current stage suggested that the

recorded signal in this chapter was not a quality fluorescence signal that represent DAF-2T fluorescence.

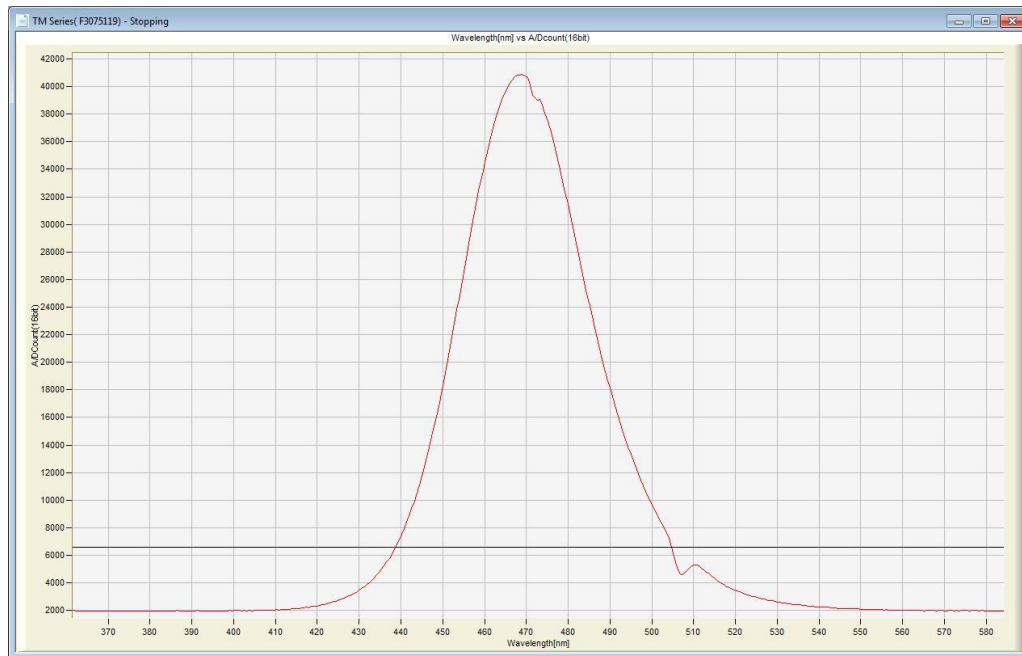


Figure 7.11 Wavelength profile of the 470 LED light head of optical system

7.6.2 Further development of DAF-2 optical mapping

Next development step should start with changing LED light to 490 nm. This LED head delivers wavelengths 475 – 505 nm, which covers the specific 495 nm excitation wavelength of the DAF-2T. Adjusting emission – detection wavelength of each component in the optic system in an optimal value will ensure that the fluorescence signal was emitted by DAF-2T. This should be the first important fundamental change to adapt for this new technique.

Then, a bespoke analysis software of the recoded signal should be developed. Recording was done by the embedded software of the optic mapping workstation, which was developed for mapping action potentials and Ca²⁺ signals. In this

study, results were presented in a form of changes of fluorescence signal tracing in 16 x 16 pixels, which was not particularly helpful. The analysis software that can measure amplitudes of signal of all 256 pixels will allow an investigation levels of signal change across the measured LV area. Comparison of changes of fluorescence amplitude between baseline and VNS of each pixel will allow the response to VNS of each sub-region of the LV to be seen more clearly, which can be related to the functional role of intra-cardiac ganglionic plexuses (Pauziene et al., 2016).

Finally, validation of the technique is required. As fluorescence signal from the heart can be emitted by many intra and extra cellular molecules, confirmation of NO fluorescence by applying both non-specific NO synthase inhibitor and specific NO synthase inhibitor will be required (Patel et al., 2008). Perfusion by NO donor sodium nitroprusside (SNP) will also be required. These pharmacological perfusion will lead to changes in fluorescence signal at baseline and under nerve stimulation condition. NO inhibitors should reduce signal from the baseline and should abolish signal increase during VNS. In contrast, SNP should gradually increase signal from the baseline.

In this new development, the optical mapping of DAF-2 DA fluorescence displayed a potential to monitor changes of fluorescence signal from the rabbit heart. So far, voltage and frequency configuration, dye loading, excitation - contraction uncoupler administration, focus adjustment and preparation alignment were successfully implemented. Optical system showed ability to record signal changes from the heart. However, more work is needed with regard to an optimal excitation wavelength together with the development of a specific analysis software.

Chapter 8 Conclusion

Electrical stimulation of the cervical vagus nerve protected the heart against arrhythmogenesis in pre-clinical models. Translation of vagus nerve stimulation (VNS) to treat heart failure (HF) in human clinical studies demonstrated mixed outcomes with regard to functional parameters by echocardiography. Previously in our group, functional studies confirmed the role of nitric oxide (NO) from the neural components in mediating the anti-arrhythmic action of VNS in the ventricle. The stimulus intensity used for stimulating the vagus in the previous NO study and other pre-clinical studies caused a significant heart rate (HR) reduction. In order to translate to clinical trial, activation parameters were titrated into a level that did not affect HR. This conflict related to vagal stimulation intensity led to questions regarding different effects of stimulation parameters (voltage, frequency, and pulse width) on many aspects of cardiac function, particularly ventricular electrophysiology and NO release from intra-cardiac neurones.

The results shown in this study provided fundamental data about the responses of the heart to different stimulation parameters related to protection against ventricular arrhythmias of VNS, which comprised of HR response, ventricular electrophysiology response, and associated NO release. With the data, VNS provided protective effects against ventricular arrhythmogenesis with prolonged effective refractory period (ERP), increased ventricular fibrillation threshold (VFT), and flattened monophasic action potential duration restitution (MAPDR) in all stimulation strengths. The impact of different pulse widths on ventricular electrophysiology was small and seemed to act in conjunction with the voltage on decreasing HR. Functional results demonstrated a dominant effect of high amplitude voltage on HR reduction and a dominant effect of high frequency on NO release in the left ventricle (LV). This major finding displayed the 2 distinct pathways of the vagal effect as the vagal-HR acts at the atria level involves with muscarinic receptor activation and vagal-NO acts at the ventricular level where it

may be independent of muscarinic activation. This outcome led to the proposal of VNS parameter configuration to optimize beneficial effect while minimize HR effect of vagal stimulation in the autonomic regulation therapy (ART) in HF.

Results from this work confirmed that the protective effect of VNS against ventricular arrhythmia initiation was independent to HR effect and also confirmed that the anti-arrhythmic action of VNS was dependent on NO release by the neural components within the intra-cardiac neuron hierarchy. The nNOS-derived NO was known to be involved with vagal protection in many facets. One of the critical advantages was to protect against ventricular arrhythmia initiation. This study demonstrated evidence of intracellularly increase of NO level of the LV myocytes during unilateral right cervical vagus stimulation suggesting an important role of intra-cardiac nervous system as a source of NO in this action.

In this study, the role of intra-cardiac ganglionic plexuses (GPs) was not studied. Clinical advancement of ART at this time was limited at the level of cervical vagus stimulation. However, growing evidence of both structural and functional suggested an important role related to local function of the heart that was modulated by specific GPs. A next step of this research should be to investigate responses of GPs to electrical stimulation in order to provide data in all relevant neural hierarchies. Moreover, of these GPs, identification of a specific GPs that modulate LV electrophysiology will narrow the target of developing a specific ART-HF treatment.

Current data of this study confirmed the vagal-NO anti-arrhythmic action by a range of electrical stimulation parameters. Next step of this evaluation should be to assess the protection pathway of this beneficial action as ventricular electrophysiology changes from NO are possibly mediated through the 2 distinct pathways; the cyclic guanosine monophosphate (cGMP)-dependent pathway and the cGMP-independent (S-Nitrosylation) pathway. Understanding details of the downstream vagal-NO protection pathway will enable novel pharmacological

treatment to be developed in addition to that of an electrical nerve stimulation approach.

Appendix

Poster presentations

- 1) Physiology 2016, 29th – 31st July 2016, Convention Centre Dublin, Ireland.
- 2) Midlands Academy of Medical Sciences Research Festival 2018, 23rd March 2018, Loughborough University, UK.
- 3) Frontier in Cardio Vascular Biology 2018, 20th – 22nd April 2018, Austria centre Vienna, Austria.

Journal publication

Reshma A. Chauhan, John Coote, Emily Allen, Pott Pongpaopattanakul, Kieran E. Brack, G. Andre Ng, Functional selectivity of cardiac preganglionic sympathetic neurones in the rabbit heart, *International Journal of Cardiology*, Volume 264, 2018, Pages 70-78.

References

- ANDO, M., KATARE, R. G., KAKINUMA, Y., ZHANG, D., YAMASAKI, F., MURAMOTO, K. & SATO, T. 2005. Efferent Vagal Nerve Stimulation Protects Heart Against Ischemia-Induced Arrhythmias by Preserving Connexin43 Protein. *Circulation*, 112, 164-170.
- ANTZELEVITCH, C. 2001. Transmural dispersion of repolarization and the T wave. *Cardiovascular Research*, 50, 426-431.
- ANTZELEVITCH, C., SICOURI, S., LITOVSKY, S. H., LUKAS, A., KRISHNAN, S. C., DI DIEGO, J. M., GINTANT, G. A. & LIU, D. W. 1991. Heterogeneity within the ventricular wall. Electrophysiology and pharmacology of epicardial, endocardial, and M cells. *Circulation Research*, 69, 1427-49.
- ARDELL, J. L., ANDRESEN, M. C., ARMOUR, J. A., BILLMAN, G. E., CHEN, P. S., FOREMAN, R. D., HERRING, N., O'LEARY, D. S., SABBAB, H. N., SCHULTZ, H. D., SUNAGAWA, K. & ZUCKER, I. H. 2016. Translational neurocardiology: preclinical models and cardioneural integrative aspects. *The Journal of Physiology*, 594, 3877-3909.
- ARMOUR, J. A. 2008. Potential clinical relevance of the 'little brain' on the mammalian heart. *Experimental Physiology*, 93, 165-176.
- ARMOUR, J. A., MURPHY, D. A., YUAN, B.-X., MACDONALD, S. & HOPKINS, D. A. 1997. Gross and microscopic anatomy of the human intrinsic cardiac nervous system. *The Anatomical Record*, 247, 289-298.
- ARORA, R., DAS, M. K., ZIPES, D. P. & WU, J. 2003. Optical Mapping Of Cardiac Arrhythmias. *Indian Pacing and Electrophysiology Journal*, 3, 187-196.
- ATTIN, M. & CLUSIN, W. T. 2009. Basic Concepts of Optical Mapping Techniques in Cardiac Electrophysiology. *Biological Research For Nursing*, 11, 195-207.
- BACZKÓ, I., JOST, N., VIRÁG, L., BŐSZE, Z. & VARRÓ, A. 2016. Rabbit models as tools for preclinical cardiac electrophysiological safety testing: Importance of repolarization reserve. *Progress in Biophysics and Molecular Biology*, 121, 157-168.
- BEAUMONT, E., WRIGHT, G. L., SOUTHERLAND, E. M., LI, Y., CHUI, R., KENKNIGHT, B. H., ARMOUR, J. A. & ARDELL, J. L. 2016. Vagus nerve stimulation mitigates intrinsic cardiac neuronal remodeling and cardiac hypertrophy induced by chronic pressure overload in guinea pig. *American Journal of Physiology - Heart and Circulatory Physiology*, 310, H1349-H1359.
- BERKELS, R., DACHS, C., ROESEN, R. & KLAUS, W. 2000. Simultaneous measurement of intracellular Ca²⁺ and nitric oxide: a new method. *Cell Calcium*, 27, 281-286.
- BOON, P., VONCK, K., REUCK, J. D. & CAEMAERT, J. 2001. Vagus nerve stimulation for refractory epilepsy. *Seizure*, 10, 448-455.
- BRACK, K., WINTER, J. & NG, G. A. 2013a. Mechanisms underlying the autonomic modulation of ventricular fibrillation initiation—tentative prophylactic properties of vagus nerve stimulation on malignant arrhythmias in heart failure. *Heart Failure Reviews*, 18, 389-408.

- BRACK, K. E. 2015. The heart's 'little brain' controlling cardiac function in the rabbit. *Experimental Physiology*, 100, 348-353.
- BRACK, K. E., COOTE, J. H. & NG, G. A. 2004. Interaction between direct sympathetic and vagus nerve stimulation on heart rate in the isolated rabbit heart. *Experimental Physiology*, 89, 128-139.
- BRACK, K. E., COOTE, J. H. & NG, G. A. 2006. The effect of direct autonomic nerve stimulation on left ventricular force in the isolated innervated Langendorff perfused rabbit heart. *Autonomic Neuroscience*, 124, 69-80.
- BRACK, K. E., COOTE, J. H. & NG, G. A. 2010. Vagus nerve stimulation inhibits the increase in Ca²⁺ transient and left ventricular force caused by sympathetic nerve stimulation but has no direct effects alone – epicardial Ca²⁺ fluorescence studies using fura-2 AM in the isolated innervated beating rabbit heart. *Experimental Physiology*, 95, 80-92.
- BRACK, K. E., COOTE, J. H. & NG, G. A. 2011. Vagus nerve stimulation protects against ventricular fibrillation independent of muscarinic receptor activation. *Cardiovascular Research*, 91, 437-446.
- BRACK, K. E., NARANG, R., WINTER, J. & NG, G. A. 2013b. The mechanical uncoupler blebbistatin is associated with significant electrophysiological effects in the isolated rabbit heart. *Experimental Physiology*, 98, 1009-1027.
- BRACK, K. E., PATEL, V. H., COOTE, J. H. & NG, G. A. 2007. Nitric oxide mediates the vagal protective effect on ventricular fibrillation via effects on action potential duration restitution in the rabbit heart. *The Journal of Physiology*, 583, 695-704.
- BRACK, K. E., PATEL, V. H., MANTRAVARDI, R., COOTE, J. H. & NG, G. A. 2009. Direct evidence of nitric oxide release from neuronal nitric oxide synthase activation in the left ventricle as a result of cervical vagus nerve stimulation. *The Journal of Physiology*, 587, 3045-3054.
- BRODDE, O.-E., BRUCK, H., LEINWEBER, K. & SEYFARTH, T. 2001. Presence, distribution and physiological function of adrenergic and muscarinic receptor subtypes in the human heart. *Basic Research in Cardiology*, 96, 528-538.
- BRODDE, O.-E. & MICHEL, M. C. 1999. Adrenergic and Muscarinic Receptors in the Human Heart. *Pharmacological Reviews*, 51, 651-690.
- BUCHHOLZ, B., DONATO, M., PEREZ, V., IVALDE, F. C., HÖCHT, C., BUITRAGO, E., RODRÍGUEZ, M. & GELPI, R. J. 2012. Preischemic efferent vagal stimulation increases the size of myocardial infarction in rabbits. Role of the sympathetic nervous system. *International Journal of Cardiology*, 155, 490-491.
- BUCKLEY, U., SHIVKUMAR, K. & ARDELL, J. L. 2015. Autonomic Regulation Therapy in Heart Failure. *Current heart failure reports*, 12, 284-293.
- CHEN, M., YU, L., LIU, Q., WANG, Z., WANG, S., JIANG, H. & ZHOU, S. 2015. Low level vagus nerve stimulation is a non-invasive approach for anti-atrial fibrillation via preventing the loss of connexins. *International Journal of Cardiology*, 179, 144-145.
- CHEN, P.-S., CHEN, L. S., FISHBEIN, M. C., LIN, S.-F. & NATTEL, S. 2014. Role of the Autonomic Nervous System in Atrial Fibrillation: Pathophysiology and Therapy. *Circulation Research*, 114, 1500-1515.

- CHO, Y., CHA, M.-J., CHOI, E.-K., OH, I.-Y. & OH, S. 2014. Effects of Low-Intensity Autonomic Nerve Stimulation on Atrial Electrophysiology. *Korean Circ J*, 44, 243-249.
- COOTE, J. H. 2013. Myths and realities of the cardiac vagus. *The Journal of Physiology*, 591, 4073-4085.
- COOTE, J. H. 2014. The Wanderer returns: myths and realities of the cardiac vagus. *Physiology News*, 2014, 32-37.
- DE FERRARI, G. M., CRIJNS, H. J. G. M., BORGGREFE, M., MILASINOVIC, G., SMID, J., ZABEL, M., GAVAZZI, A., SANZO, A., DENNERT, R., KUSCHYK, J., RASPOPOVIC, S., KLEIN, H., SWEDBERG, K. & SCHWARTZ, P. J. 2011. Chronic vagus nerve stimulation: a new and promising therapeutic approach for chronic heart failure. *European Heart Journal*, 32, 847-855.
- DE FERRARI, G. M., TUINENBURG, A. E., RUBLE, S., BRUGADA, J., KLEIN, H., BUTTER, C., WRIGHT, D. J., SCHUBERT, B., SOLOMON, S., MEYER, S., STEIN, K., RAMUZAT, A. & ZANNAD, F. 2014. Rationale and study design of the NEuroCardiac TherApy foR Heart Failure Study: NECTAR-HF. *European Journal of Heart Failure*, 16, 692-699.
- DICARLO, L., LIBBUS, I., AMURTHUR, B., KENKNIGHT, B. H. & ANAND, I. S. 2013. Autonomic Regulation Therapy for the Improvement of Left Ventricular Function and Heart Failure Symptoms: The ANTHEM-HF Study. *Journal of Cardiac Failure*, 19, 655-660.
- DIFRANCESCO, D. & BORER, J. S. 2007. The Funny Current. *Drugs*, 67, 15-24.
- DUCLAUX, R., MEI, N. & RANIERI, F. 1976. Conduction velocity along the afferent vagal dendrites: a new type of fibre. *The Journal of Physiology*, 260, 487-495.
- EVANS, D. H. L. & MURRAY, J. G. 1954. Histological and functional studies on the fibre composition of the vagus nerve of the rabbit. *Journal of Anatomy*, 88, 320-337.
- FEDOROV, V. V., LOZINSKY, I. T., SOSUNOV, E. A., ANYUKHOVSKY, E. P., ROSEN, M. R., BALKE, C. W. & EFIMOV, I. R. 2007. Application of blebbistatin as an excitation-contraction uncoupler for electrophysiologic study of rat and rabbit hearts. *Heart Rhythm*, 4, 619-626.
- FORD, T. W. & MCWILLIAM, P. N. 1986. The effects of electrical stimulation of myelinated and non-myelinated vagal fibres on heart rate in the rabbit. *The Journal of Physiology*, 380, 341-347.
- FÖRSTERMANN, U., CLOSS, E. I., POLLOCK, J. S., NAKANE, M., SCHWARZ, P., GATH, I. & KLEINERT, H. 1994. Nitric oxide synthase isozymes. Characterization, purification, molecular cloning, and functions. *Hypertension*, 23, 1121-31.
- FRANZ, M. R. 1999. Current status of monophasic action potential recording: theories, measurements and interpretations. *Cardiovascular Research*, 41, 25-40.
- FUKUDA, K., KANAZAWA, H., AIZAWA, Y., ARDELL, J. L. & SHIVKUMAR, K. 2015. Cardiac Innervation and Sudden Cardiac Death. *Circulation Research*, 116, 2005-2019.
- GARFINKEL, A., KIM, Y.-H., VOROSHILOVSKY, O., QU, Z., KIL, J. R., LEE, M.-H., KARAGUEUZIAN, H. S., WEISS, J. N. & CHEN, P.-S. 2000. Preventing ventricular

- fibrillation by flattening cardiac restitution. *Proceedings of the National Academy of Sciences*, 97, 6061-6066.
- GAUTHIER, C., LEBLAIS, V., KOBZIK, L., TROCHU, J. N., KHANDOUDI, N., BRIL, A., BALLIGAND, J. L. & LE MAREC, H. 1998. The negative inotropic effect of beta3-adrenoceptor stimulation is mediated by activation of a nitric oxide synthase pathway in human ventricle. *The Journal of Clinical Investigation*, 102, 1377-1384.
- GOLD, M. R., VAN VELDHUISEN, D. J., HAUPTMAN, P. J., BORGGREFE, M., KUBO, S. H., LIEBERMAN, R. A., MILASINOVIC, G., BERMAN, B. J., DJORDJEVIC, S., NEELAGARU, S., SCHWARTZ, P. J., STARLING, R. C. & MANN, D. L. 2016. Vagus Nerve Stimulation for the Treatment of Heart Failure The INOVATE-HF Trial. *Journal of the American College of Cardiology*, 68, 149-158.
- GRANT, A. O. 2009. Cardiac Ion Channels. *Circulation: Arrhythmia and Electrophysiology*, 2, 185-194.
- HAMANN, J. J., RUBLE, S. B., STOLEN, C., WANG, M., GUPTA, R. C., RASTOGI, S. & SABBAH, H. N. 2013. Vagus nerve stimulation improves left ventricular function in a canine model of chronic heart failure. *European Journal of Heart Failure*, 15, 1319-1326.
- HANNA, P., RAJENDRAN, P. S., AJIJOLA, O. A., VASEGHI, M., ANDREW ARMOUR, J., ARDELL, J. L. & SHIVKUMAR, K. 2017. Cardiac neuroanatomy - Imaging nerves to define functional control. *Autonomic Neuroscience*, 207, 48-58.
- HARVEY, R. D. & BELEVYCH, A. E. 2003. Muscarinic regulation of cardiac ion channels. *British Journal of Pharmacology*, 139, 1074-1084.
- HAUPTMAN, P. J., SCHWARTZ, P. J., GOLD, M. R., BORGGREFE, M., VAN VELDHUISEN, D. J., STARLING, R. C. & MANN, D. L. 2012. Rationale and study design of the INcrease Of Vagal TonE in Heart Failure study: INOVATE-HF. *American Heart Journal*, 163, 954-962.e1.
- HE, B., LU, Z., HE, W., HUANG, B., YU, L., WU, L., CUI, B., HU, X. & JIANG, H. 2013a. The effects of atrial ganglionated plexi stimulation on ventricular electrophysiology in a normal canine heart. *Journal of Interventional Cardiac Electrophysiology*, 37, 1-8.
- HE, B., LU, Z., HE, W., WU, L., HUANG, B., YU, L., CUI, B., HU, X. & JIANG, H. 2013b. Effects of low-intensity atrial ganglionated plexi stimulation on ventricular electrophysiology and arrhythmogenesis. *Autonomic Neuroscience*, 174, 54-60.
- HENNING, R. J. & SAWMILLER, D. R. 2001. Vasoactive intestinal peptide: cardiovascular effects. *Cardiovascular Research*, 49, 27-37.
- HERRING, N., DANSON, E. J. F. & PATERSON, D. J. 2002. Cholinergic Control of Heart Rate by Nitric Oxide is Site Specific. *Physiology*, 17, 202-206.
- HERRING, N. & PATERSON, D. J. 2001. Nitric oxide-cGMP pathway facilitates acetylcholine release and bradycardia during vagal nerve stimulation in the guinea-pig in vitro. *The Journal of Physiology*, 535, 507-518.
- HERRING, N. & PATERSON, D. J. 2009. Neuromodulators of peripheral cardiac sympatho-vagal balance. *Experimental Physiology*, 94, 46-53.

- HOOVER, D. B., ISAACS, E. R., JACQUES, F., HOARD, J. L., PAGÉ, P. & ARMOUR, J. A. 2009. Localization of multiple neurotransmitters in surgically derived specimens of human atrial ganglia. *Neuroscience*, 164, 1170-1179.
- HOOVER, D. B., SHEPHERD, A. V., SOUTHERLAND, E. M., ARMOUR, J. A. & ARDELL, J. L. 2008. Neurochemical diversity of afferent neurons that transduce sensory signals from dog ventricular myocardium. *Autonomic neuroscience : basic & clinical*, 141, 38-45.
- HUANG, J., QIAN, J., YAO, W., WANG, N., ZHANG, Z., CAO, C., SONG, B. & ZHANG, Z. 2015. Vagus nerve stimulation reverses ventricular electrophysiological changes induced by hypersympathetic nerve activity. *Experimental Physiology*, 100, 239-248.
- JONES, J. F., WANG, Y. & JORDAN, D. 1995. Heart rate responses to selective stimulation of cardiac vagal C fibres in anaesthetized cats, rats and rabbits. *The Journal of Physiology*, 489, 203-214.
- JONES, J. F. X., WANG, Y. & JORDAN, D. 1998. Activity of C fibre cardiac vagal efferents in anaesthetized cats and rats. *The Journal of Physiology*, 507, 869-880.
- JOYNER, M. J. 2016. Preclinical and clinical evaluation of autonomic function in humans. *The Journal of Physiology*, 594, 4009-4013.
- KALLA, M., CHOTALIA, M., COUGHLAN, C., HAO, G., CRABTREE, M. J., TOMEK, J., BUB, G., PATERSON, D. J. & HERRING, N. 2016a. Protection against ventricular fibrillation via cholinergic receptor stimulation and the generation of nitric oxide. *The Journal of Physiology*, 1-12.
- KALLA, M., HERRING, N. & PATERSON, D. J. 2016b. Cardiac sympatho-vagal balance and ventricular arrhythmia(). *Autonomic Neuroscience*, 199, 29-37.
- KATARE, R. G., ANDO, M., KAKINUMA, Y., ARIKAWA, M., HANDA, T., YAMASAKI, F. & SATO, T. 2009. Vagal nerve stimulation prevents reperfusion injury through inhibition of opening of mitochondrial permeability transition pore independent of the bradycardiac effect. *The Journal of Thoracic and Cardiovascular Surgery*, 137, 223-231.
- KATARE, R. G., ANDO, M., KAKINUMA, Y., ARIKAWA, M., YAMASAKI, F. & SATO, T. 2010. Differential regulation of TNF receptors by vagal nerve stimulation protects heart against acute ischemic injury. *Journal of Molecular and Cellular Cardiology*, 49, 234-244.
- KAWADA, T., YAMAZAKI, T., AKIYAMA, T., KITAGAWA, H., SHIMIZU, S., MIZUNO, M., LI, M. & SUGIMACHI, M. 2008. Vagal stimulation suppresses ischemia-induced myocardial interstitial myoglobin release. *Life Sciences*, 83, 490-495.
- KAWADA, T., YAMAZAKI, T., AKIYAMA, T., LI, M., ARIUMI, H., MORI, H., SUNAGAWA, K. & SUGIMACHI, M. 2006. Vagal stimulation suppresses ischemia-induced myocardial interstitial norepinephrine release. *Life Sciences*, 78, 882-887.
- KAWANO, H., OKADA, R. & YANO, K. 2003. Histological study on the distribution of autonomic nerves in the human heart. *Heart and Vessels*, 18, 32-39.
- KETTLEWELL, S., WALKER, N. L., COBBE, S. M., BURTON, F. L. & SMITH, G. L. 2004. The electrophysiological and mechanical effects of 2,3-butane-dione monoxime and cytochalasin-D in the Langendorff perfused rabbit heart. *Experimental Physiology*, 89, 163-172.

- LEIKERT, J. F., RÄTHEL, T. R., MÜLLER, C., VOLLMAR, A. M. & DIRSCH, V. M. 2001. Reliable in vitro measurement of nitric oxide released from endothelial cells using low concentrations of the fluorescent probe 4,5-diaminofluorescein. *FEBS Letters*, 506, 131-134.
- LI, S., SCHERLAG, B. J., YU, L., SHENG, X., ZHANG, Y., ALI, R., DONG, Y., GHAS, M. & PO, S. S. 2009. Low-Level Vagosympathetic Stimulation: A Paradox and Potential New Modality for the Treatment of Focal Atrial Fibrillation. *Circulation: Arrhythmia and Electrophysiology*, 2, 645-651.
- LI, S., ZHOU, X., YU, L. & JIANG, H. 2015. Low level non-invasive vagus nerve stimulation: A novel feasible therapeutic approach for atrial fibrillation. *International Journal of Cardiology*, 182, 189-190.
- LYMPEROPOULOS, A., RENGO, G. & KOCH, W. J. 2013. Adrenergic Nervous System in Heart Failure: Pathophysiology and Therapy. *Circulation Research*, 113, 739-753.
- M., N. J. & WEINONG, G. 2002. Heterogeneous Expression of Voltage - Gated Potassium Channels in the Heart: Roles in Normal Excitation and Arrhythmias. *Journal of Cardiovascular Electrophysiology*, 13, 406-409.
- MANTRAVADI, R., GABRIS, B., LIU, T., CHOI, B.-R., DE GROAT, W. C., NG, G. A. & SALAMA, G. 2007. Autonomic Nerve Stimulation Reverses Ventricular Repolarization Sequence in Rabbit Hearts. *Circulation Research*, 100, e72-e80.
- MASSION, P. B., FERON, O., DESSY, C. & BALLIGAND, J.-L. 2003. Nitric Oxide and Cardiac Function: Ten Years After, and Continuing. *Circulation Research*, 93, 388-398.
- MIDDLETON, S., MIDDLETON, H. H. & GRUNDFEST, H. 1950. SPIKE POTENTIALS AND CARDIAC EFFECTS OF MAMMALIAN VAGUS NERVE. *American Journal of Physiology-Legacy Content*, 162, 545-552.
- NG, G. A., BRACK, K. E. & COOTE, J. H. 2001. Effects of Direct Sympathetic and Vagus Nerve Stimulation on the Physiology of the Whole Heart – A Novel Model of Isolated Langendorff Perfused Rabbit Heart with Intact Dual Autonomic Innervation. *Experimental Physiology*, 86, 319-329.
- NG, G. A., BRACK, K. E., PATEL, V. H. & COOTE, J. H. 2007. Autonomic modulation of electrical restitution, alternans and ventricular fibrillation initiation in the isolated heart. *Cardiovascular Research*, 73, 750-760.
- OLSHANSKY, B., SABBAH, H. N., HAUPTMAN, P. J. & COLUCCI, W. S. 2008. Parasympathetic Nervous System and Heart Failure: Pathophysiology and Potential Implications for Therapy. *Circulation*, 118, 863-871.
- OSADCHII, O. E. 2012. Effects of ventricular pacing protocol on electrical restitution assessments in guinea-pig heart. *Experimental Physiology*, 97, 807-821.
- PACHER, P., BECKMAN, J. S. & LIAUDET, L. 2007. Nitric Oxide and Peroxynitrite in Health and Disease. *Physiological reviews*, 87, 315-424.
- PATEL, V., BRACK, K., COOTE, J. & NG, G. A. 2008. A novel method of measuring nitric-oxide-dependent fluorescence using 4,5-diaminofluorescein (DAF-2) in the isolated Langendorff-perfused rabbit heart. *Pflügers Archiv - European Journal of Physiology*, 456, 635-645.

- PAUZA, D. H., SABURKINA, I., RYSEVAITE, K., INOKAITIS, H., JOKUBAUSKAS, M., JALIFE, J. & PAUZIENE, N. 2013. Neuroanatomy of the murine cardiac conduction system: A combined stereomicroscopic and fluorescence immunohistochemical study. *Autonomic Neuroscience*, 176, 32-47.
- PAUZA, D. H., SKRIPKA, V., PAUZIENE, N. & STROPUS, R. 2000. Morphology, distribution, and variability of the epicardiac neural ganglionated subplexuses in the human heart. *The Anatomical Record*, 259, 353-382.
- PAUZIENE, N., ALABURDA, P., RYSEVAITE-KYGUOLIENE, K., PAUZA, A. G., INOKAITIS, H., MASAITYTE, A., RUDOKAITE, G., SABURKINA, I., PLISIENE, J. & PAUZA, D. H. 2016. Innervation of the rabbit cardiac ventricles. *Journal of Anatomy*, 228, 26-46.
- PINSKY, D. J., PATTON, S., MESAROS, S., BROVKOVYCH, V., KUBASZEWSKI, E., GRUNFELD, S. & MALINSKI, T. 1997. Mechanical Transduction of Nitric Oxide Synthesis in the Beating Heart. *Circulation Research*, 81, 372-379.
- PLANCHET, E. & KAISER, W. M. 2006. Nitric oxide (NO) detection by DAF fluorescence and chemiluminescence: a comparison using abiotic and biotic NO sources. *Journal of Experimental Botany*, 57, 3043-3055.
- PRECHTL, J. C. & POWLEY, T. L. 1990. The fiber composition of the abdominal vagus of the rat. *Anatomy and Embryology*, 181, 101-115.
- PREMCHAND, R. K., SHARMA, K., MITTAL, S., MONTEIRO, R., DIXIT, S., LIBBUS, I., DICARLO, L. A., ARDELL, J. L., RECTOR, T. S., AMURTHUR, B., KENKNIGHT, B. H. & ANAND, I. S. 2014. Autonomic Regulation Therapy via Left or Right Cervical Vagus Nerve Stimulation in Patients With Chronic Heart Failure: Results of the ANTHEM-HF Trial. *Journal of Cardiac Failure*, 20, 808-816.
- QU, Z., WEISS, J. N. & GARFINKEL, A. 1999. Cardiac electrical restitution properties and stability of reentrant spiral waves: a simulation study. *American Journal of Physiology-Heart and Circulatory Physiology*, 276, H269-H283.
- QUINN, T. A. & KOHL, P. 2016. Rabbit models of cardiac mechano-electric and mechano-mechanical coupling. *Progress in Biophysics and Molecular Biology*, 121, 110-122.
- RASTALDO, R., PAGLIARO, P., CAPPELLO, S., PENNA, C., MANCARDI, D., WESTERHOF, N. & LOSANO, G. 2007. Nitric oxide and cardiac function. *Life Sciences*, 81, 779-793.
- ROHR, S. 2004. Role of gap junctions in the propagation of the cardiac action potential. *Cardiovascular Research*, 62, 309-322.
- ROYCHOWDHURY, S., LUTHE, A., KEILHOFF, G., WOLF, G. & HORN, T. F. W. 2002. Oxidative stress in glial cultures: Detection by DAF-2 fluorescence used as a tool to measure peroxynitrite rather than nitric oxide. *Glia*, 38, 103-114.
- SABURKINA, I., GUKAUSKIENE, L., RYSEVAITE, K., BRACK, K. E., PAUZA, A. G., PAUZIENE, N. & PAUZA, D. H. 2014. Morphological pattern of intrinsic nerve plexus distributed on the rabbit heart and interatrial septum. *Journal of Anatomy*, 224, 583-593.
- SCHWARTZ, P. J. 2011. Vagal Stimulation for Heart Diseases: From Animals to Men – An Example of Translational Cardiology –. *Circulation Journal*, 75, 20-27.

- SHEN, M. J., CHANG, H.-C., PARK, H.-W., AKINGBA, A. G., CHANG, P.-C., ZHANG, Z., LIN, S.-F., SHEN, C., CHEN, L. S., CHEN, Z., FISHBEIN, M. C., CHIAMVIMONVAT, N. & CHEN, P.-S. 2013. Low-Level Vagus Nerve Stimulation Upregulates Small Conductance Calcium Activated Potassium Channels in the Stellate Ganglion. *Heart rhythm : the official journal of the Heart Rhythm Society*, 10, 910-915.
- SHEN, M. J., SHINOHARA, T., PARK, H.-W., FRICK, K., ICE, D. S., CHOI, E.-K., HAN, S., MARUYAMA, M., SHARMA, R., SHEN, C., FISHBEIN, M. C., CHEN, L. S., LOPSHIRE, J. C., ZIPES, D. P., LIN, S.-F. & CHEN, P.-S. 2011. Chronic Low-Level Vagus Nerve Stimulation Reduces Stellate Ganglion Nerve Activity and Paroxysmal Atrial Tachyarrhythmias in Ambulatory Canines. *Circulation*, 123, 2204-2212.
- SHENG, X., SCHERLAG, B. J., YU, L., LI, S., ALI, R., ZHANG, Y., FU, G., NAKAGAWA, H., JACKMAN, W. M., LAZZARA, R. & PO, S. S. 2011. Prevention and Reversal of Atrial Fibrillation Inducibility and Autonomic Remodeling by Low-Level Vagosympathetic Nerve Stimulation. *Journal of the American College of Cardiology*, 57, 563-571.
- SHINLAPAWITTAYATORN, K., CHINDA, K., PALEE, S., SURINKAEW, S., THUNSIRI, K., WEERATEERANGKUL, P., CHATTIPAKORN, S., KENKNIGHT, B. H. & CHATTIPAKORN, N. 2013. Low-amplitude, left vagus nerve stimulation significantly attenuates ventricular dysfunction and infarct size through prevention of mitochondrial dysfunction during acute ischemia-reperfusion injury. *Heart Rhythm*, 10, 1700-1707.
- SHIVKUMAR, K., AJIJOLA, O. A., ANAND, I., ARMOUR, J. A., CHEN, P.-S., ESLER, M., DE FERRARI, G. M., FISHBEIN, M. C., GOLDBERGER, J. J., HARPER, R. M., JOYNER, M. J., KHALSA, S. S., KUMAR, R., LANE, R., MAHAJAN, A., PO, S., SCHWARTZ, P. J., SOMERS, V. K., VALDERRABANO, M., VASEGHI, M. & ZIPES, D. P. 2016. Clinical neurocardiology defining the value of neuroscience-based cardiovascular therapeutics. *The Journal of Physiology*, 594, 3911-3954.
- SHIVKUMAR, K. & ARDELL, J. L. 2016. Cardiac autonomic control in health and disease. *The Journal of Physiology*, 594, 3851-3852.
- STAVRAKIS, S., HUMPHREY, M. B., SCHERLAG, B. J., HU, Y., JACKMAN, W. M., NAKAGAWA, H., LOCKWOOD, D., LAZZARA, R. & PO, S. S. 2015. Low-Level Transcutaneous Electrical Vagus Nerve Stimulation Suppresses Atrial Fibrillation. *Journal of the American College of Cardiology*, 65, 867-875.
- STAVRAKIS, S., SCHERLAG, B., FAN, Y., LIU, Y., MAO, J., VARMA, V., LAZZARA, R. & PO, S. 2013. Inhibition of atrial fibrillation by low-level vagus nerve stimulation: the role of the nitric oxide signaling pathway. *Journal of Interventional Cardiac Electrophysiology*, 36, 199-208.
- SZABÓ, G., SZENTANDRÁSSY, N., BÍRÓ, T., TÓTH, B., CZIFRA, G., MAGYAR, J., BÁNYÁSZ, T., VARRÓ, A., KOVÁCS, L. & NÁNÁSI, P. 2005. Asymmetrical distribution of ion channels in canine and human left-ventricular wall: epicardium versus midmyocardium. *Pflügers Archiv*, 450, 307-316.
- SZENTADRASSY, N., BANYASZ, T., BIRO, T., SZABO, G., TOTH, B. I., MAGYAR, J., LAZAR, J., VARRO, A., KOVACS, L. & NANASI, P. P. 2005. Apico-basal

- inhomogeneity in distribution of ion channels in canine and human ventricular myocardium. *Cardiovascular Research*, 65, 851-860.
- TAKEI, M., TSUBOI, M., USUI, T., HANAOKA, T., KUROGOUCHI, F., ARUGA, M., KATAGIRI, Y., OWA, M., KUBO, K. & KIYOSAWA, K. 2001. Vagal Stimulation Prior to Atrial Rapid Pacing Protects the Atrium From Electrical Remodeling in Anesthetized Dogs. *JAPANESE CIRCULATION JOURNAL*, 65, 1077-1081.
- TAMARGO, J., CABALLERO, R., GÓMEZ, R. & DELPÓN, E. 2010. Cardiac electrophysiological effects of nitric oxide. *Cardiovascular Research*, 87, 593-600.
- TOSATO, M., YOSHIDA, K., TOFT, E., NEKRASAS, V. & STRUIJK, J. 2006. Closed-loop control of the heart rate by electrical stimulation of the vagus nerve. *Medical and Biological Engineering and Computing*, 44, 161-169.
- UEMURA, K., ZHENG, C., LI, M., KAWADA, T. & SUGIMACHI, M. 2010. Early Short-Term Vagal Nerve Stimulation Attenuates Cardiac Remodeling After Reperfused Myocardial Infarction. *Journal of Cardiac Failure*, 16, 689-699.
- VANOLI, E., DE FERRARI, G. M., STRAMBA-BADIALE, M., HULL, S. S., FOREMAN, R. D. & SCHWARTZ, P. J. 1991. Vagal stimulation and prevention of sudden death in conscious dogs with a healed myocardial infarction. *Circulation Research*, 68, 1471-81.
- VON BOHLEN UND HALBACH, O. 2003. Nitric oxide imaging in living neuronal tissues using fluorescent probes. *Nitric Oxide*, 9, 217-228.
- WAKE, E. & BRACK, K. 2016. Characterization of the intrinsic cardiac nervous system. *Autonomic Neuroscience*, 199, 3-16.
- WEISS, J. N., CHEN, P.-S., QU, Z., KARAGUEUZIAN, H. S. & GARFINKEL, A. 2000. Ventricular Fibrillation: How Do We Stop the Waves From Breaking? *Circulation Research*, 87, 1103-1107.
- WINTER, J., BRACK, K. E., COOTE, J. H. & NG, G. A. 2014. Cardiac contractility modulation increases action potential duration dispersion and decreases ventricular fibrillation threshold via β 1-adrenoceptor activation in the crystalloid perfused normal rabbit heart. *International Journal of Cardiology*, 172, 144-154.
- WOOLLEY, D. C., MCWILLIAM, P. N., FORD, T. W. & CLARKE, R. W. 1987. The effect of selective electrical stimulation of non-myelinated vagal fibres on heart rate in the rabbit. *Journal of the Autonomic Nervous System*, 21, 215-221.
- YAMADA, M., INANOBE, A. & KURACHI, Y. 1998. G Protein Regulation of Potassium Ion Channels. *Pharmacological Reviews*, 50, 723.
- YAMAKAWA, K., RAJENDRAN, P. S., TAKAMIYA, T., YAGISHITA, D., SO, E. L., MAHAJAN, A., SHIVKUMAR, K. & VASEGHI, M. 2015. Vagal nerve stimulation activates vagal afferent fibers that reduce cardiac efferent parasympathetic effects. *American Journal of Physiology - Heart and Circulatory Physiology*, 309, H1579.
- YAN, C., MILLER, C. L. & ABE, J.-I. 2007. Regulation of Phosphodiesterase 3 and Inducible cAMP Early Repressor in the Heart. *Circulation research*, 100, 489-501.
- ZANNAD, F., DE FERRARI, G. M., TUINENBURG, A. E., WRIGHT, D., BRUGADA, J., BUTTER, C., KLEIN, H., STOLEN, C., MEYER, S., STEIN, K. M., RAMUZAT, A., SCHUBERT, B., DAUM, D., NEUZIL, P., BOTMAN, C., CASTE, M. A., ONOFRIO, A., SOLOMON, S. D., WOLD, N. & RUBLE, S. B. 2014. Chronic vagal stimulation

for the treatment of low ejection fraction heart failure: results of the neural cardiac therapy for heart failure (NECTAR-HF) randomized controlled trial. *European Heart Journal*.

- ZHANG, L., LU, Y., SUN, J., ZHOU, X. & TANG, B. 2016. Subthreshold vagal stimulation suppresses ventricular arrhythmia and inflammatory response in a canine model of acute cardiac ischaemia and reperfusion. *Experimental Physiology*, 101, 41-49.
- ZHANG, R., WUGETI, N., SUN, J., YAN, H., GUO, Y., ZHANG, L., MA, M., GUO, X., JIAO, C., XU, W., LI, T., LIU, H. & MA, Y. 2014. Effects of vagus nerve stimulation via cholinergic anti-inflammatory pathway activation on myocardial ischemia/reperfusion injury in canine. *International Journal of Clinical and Experimental Medicine*, 7, 2615-2623.
- ZHANG, X., KIM, W.-S., HATCHER, N., POTGIETER, K., MOROZ, L. L., GILLETTE, R. & SWEEDLER, J. V. 2002. Interfering with Nitric Oxide Measurements: 4,5-DIAMINOFLUORESCHEIN REACTS WITH DEHYDROASCORBIC ACID AND ASCORBIC ACID. *Journal of Biological Chemistry*, 277, 48472-48478.
- ZIOLO, M. T. 2008. The fork in the nitric oxide road: Cyclic GMP or nitrosylation? *Nitric Oxide*, 18, 153-156.
- ZIOLO, M. T., KOHR, M. J. & WANG, H. 2008. Nitric oxide signaling and the regulation of myocardial function. *Journal of Molecular and Cellular Cardiology*, 45, 625-632.